



PAULIUS KAVALIAUSKAS

**UTILIZATION OF
PHOTOGRAMMETRY
AND LASER SCANNING
TECHNOLOGIES FOR
AUTOMATED MONITORING
OF THE PROGRESS OF
CONSTRUCTION WORKS**

DOCTORAL DISSERTATION

K a u n a s
2 0 2 4

KAUNAS UNIVERSITY OF TECHNOLOGY

PAULIUS KAVALIAUSKAS

UTILIZATION OF PHOTOGRAMMETRY AND
LASER SCANNING TECHNOLOGIES FOR
AUTOMATED MONITORING OF THE
PROGRESS OF CONSTRUCTION WORKS

Doctoral dissertation
Technological Sciences, Civil Engineering (T 002)

2024, Kaunas

This doctoral dissertation was prepared at Kaunas University of Technology, Faculty of Civil Engineering and Architecture, Civil Engineering and Architecture Competence Centre during the period of 2018–2023.

Scientific Supervisor:

Prof. Dr. Andrius JURELIONIS (Kaunas University of Technology, Technological Sciences, Civil Engineering, T 002).

Edited by: English language editor Dr. Armandas Rumšas (Publishing House *Technologija*), Lithuanian language editor Aurelija Gražina Rukšaitė (Publishing House *Technologija*).

Dissertation Defense Board of Civil Engineering Science Field:

Prof. Dr. Darius PUPEIKIS (Kaunas University of Technology, Technological Sciences, Civil Engineering, T 002) – **chairperson**;

Dr. Vytautas BOCULLO (Kaunas University of Technology, Technological Sciences, Civil Engineering, T 002);

Assoc. Prof. Dr. Paris A. FOKAIDES (Frederick University, Cyprus, Technological Sciences, Civil Engineering, T 002);

Dr. Ignacio VILLALÓN FORNÉS (Kaunas University of Technology, Technological Sciences, Civil Engineering, T 002);

Assoc. Prof. Dr. Tatjana VILUTIENĖ (Vilnius Gediminas Technical University, Technological Sciences, Civil Engineering, T 002).

The official defense of the dissertation will be held at 10 a.m. on 8 May, 2024 at the public meeting of the Dissertation Defense Board of Civil Engineering Science Field in Rectorate Hall at Kaunas University of Technology.

Address: K. Donelaičio 73-402, LT-44249, Kaunas, Lithuania.

Phone (+370) 608 28 527; email doktorantura@ktu.lt

The doctoral dissertation was sent out on 8 April, 2024.

The doctoral dissertation is available on the internet at <http://ktu.edu> and at the library of Kaunas University of Technology (Gedimino 50, LT-44239, Kaunas, Lithuania).

© P. Kavaliauskas, 2024

KAUNO TECHNOLOGIJOS UNIVERSITETAS

PAULIUS KAVALIAUSKAS

AUTOMATIZUOTA STATYBOS EIGOS
STEBĖSENA TAIKANT FOTOGRAMETRIJOS
IR LAZERINIO SKENAVIMO METODUS

Daktaro disertacija
Technologijos mokslai, statybos inžinerija (T 002)

2024, Kaunas

Disertacija rengta 2018–2023 metais Kauno technologijos universiteto Statybos ir architektūros fakultete, Statybos ir architektūros kompetencijų centre.

Mokslinis vadovas:

prof. dr. Andrius JURELIONIS (Kauno technologijos universitetas, technologijos mokslai, statybos inžinerija, T 002).

Redagavo: anglų kalbos redaktorius dr. Armandas Rumšas (leidykla „Technologija“), lietuvių kalbos redaktorė Aurelija Gražina Rukšaitė (leidykla „Technologija“).

Statybos inžinerijos mokslo krypties disertacijos gynimo taryba:

prof. dr. Darius PUPEIKIS (Kauno technologijos universitetas, technologijos mokslai, statybos inžinerija, T 002) – **pirmininkas**;

dr. Vytautas BOCULLO (Kauno technologijos universitetas, technologijos mokslai, statybos inžinerija, T 002);

doc. dr. Paris A. FOKAIDES (Frederiko universitetas, Kipro respublika, technologijos mokslai, statybos inžinerija, T 002);

dr. Ignacio VILLALÓN FORNÉS (Kauno technologijos universitetas, technologijos mokslai, statybos inžinerija, T 002);

doc. dr. Tatjana VILUTIENĖ (Vilniaus Gedimino technikos universitetas, technologijos mokslai, statybos inžinerija, T 002).

Disertacija bus ginama viešame Statybos inžinerijos mokslo krypties disertacijos gynimo tarybos posėdyje 2024 m. gegužės 8 d. 10 val. Kauno technologijos universiteto Rektorato salėje.

Adresas: K. Donelaičio g. 73-402, LT-44249 Kaunas, Lietuva.

Tel. (+370) 608 28 527; el. paštas doktorantura@ktu.lt

Disertacija išsiųsta 2024 m. balandžio 8 d.

Su disertacija galima susipažinti interneto svetainėje <http://ktu.edu> ir Kauno technologijos universiteto bibliotekoje (Gedimino g. 50, LT-44239 Kaunas, Lietuva).

© P. Kavaliauskas, 2024

CONTENTS

ABBREVIATIONS AND GLOSSARY	7
LIST OF FIGURES.....	9
LIST OF TABLES	14
INTRODUCTION.....	16
1. LITERATURE REVIEW	21
1.1. Review of Construction Progress Monitoring Techniques.....	21
1.1.1. Building information modelling.....	21
1.1.2. Construction progress monitoring	28
1.1.3. Earthworks progress monitoring	32
1.1.4. As-planned vs. as-built construction	34
1.2. Identification of Potential Applications for Progress Monitoring	39
1.2.1. Construction phases.....	39
1.2.2. Practical applicability of data acquisition for construction progress monitoring	40
1.2.3. Scope definition for the methodology and experimental research	42
1.3. Chapter Conclusions	44
2. APPLICATION IN THE EARTHWORKS CONSTRUCTION.....	45
2.1. Description of the Research Object	45
2.2. Methods and Tools.....	46
2.3. Data Acquisition Workflows for Civil Construction.....	49
2.3.1. Traditional method	51
2.3.2. Ground control points-based approach.....	52
2.3.3. Real-time kinematic workflow	53
2.3.4. Post-processing kinematic workflow	54
2.4. Data Processing.....	56
2.5. Experimental Results of Earthworks Control	61
2.5.1. Volume estimation analysis.....	62
2.5.2. Control points accuracy assessment.....	65
2.5.3. Efficiency of automation	72
2.5.4. Real case approaches.....	75

2.6.	Chapter Conclusions	79
3.	APPLICATION IN BUILDING CONSTRUCTION	81
3.1.	Description of the Research Object	81
3.2.	Methods and Tools.....	82
3.3.	Data Capture Workflow for Structural Construction Monitoring	84
3.4.	Data Processing.....	87
3.4.1.	IFC and point cloud data alignment	88
3.4.2.	Automated object monitoring process.....	90
3.4.3.	Optimization	94
3.5.	Experimental Results of Construction Objects Monitoring.....	97
3.5.1.	Data alignment.....	97
3.5.2.	Evaluation of object detection	102
3.5.3.	Optimization	109
3.6.	Chapter Conclusions	113
4.	RESULTS AND DISCUSSION	115
4.1.	Impact of Automation on Monitoring Processes	115
4.1.1.	Accuracy.....	117
4.1.2.	Time and cost benefits.....	119
4.1.3.	Report and visualization	121
4.1.4.	Automation quality	122
4.1.5.	Health and safety	123
4.2.	Limitations	123
4.3.	Chapter Conclusions	124
5.	GENERAL CONCLUSIONS	126
6.	FURTHER WORK	129
7.	SANTRAUKA	130
	REFERENCES.....	172
	CURRICULUM VITAE	191
	ACKNOWLEDGMENT	192

ABBREVIATIONS AND GLOSSARY

AEC – architecture, engineering, construction.

AR – augmented reality is a combination of real-world environments and digital content.

Automated object detection – a method which automatically identifies structural objects in a point cloud by comparing data in an IFC model.

Average population – the average number of points in the specified volume in the point cloud. This metric indicates the density of points in the specified regions.

BIM – building information modelling is a construction management process based on a 3D digital model.

CAD – computer-aided design is a technology which replaces manual drafting.

CHP – a check point is a marker with known coordinates which is not used for photogrammetric data processing, but is intended to verify the accuracy of the results.

Classification of point cloud model elements – classifying points into separate categories based on their properties and allowing to identify objects in the point cloud accordingly.

CP – a control point is a marker with known coordinates that can be used as a check point or as a ground control point in the photogrammetry process.

Data noise – points in a point cloud that do not represent the actual geometric properties of the scanned environment due to reflective surfaces, moving objects, etc.

EPSG – *European Petroleum Survey Group* provides a database of standardized coordinate system information.

FM – facilities management.

GCP – ground control point is a marker with known coordinates, which is used for photogrammetric data processing.

GIS – geographic information system which analyzes and presents geographic data.

GNSS – *Global Navigation Satellite System* refers to the use of multiple satellite navigation systems, including GPS, which transmits positioning data to GNSS receivers for location determination.

GPS – *Global Positioning System* is a specific satellite navigation system which transmits positioning data to receivers on earth to determine a location.

GSD – the ground sample distance is the distance between pixel centers measured on the ground in a digital image.

ICP – iterative closest point algorithm used to align and register 3D point cloud sets.

IFC – *Industrial Foundation Classes* is an open and standardized file format for data exchange in the AEC industry.

LAS07 – the Lithuanian state elevation system, used together with the geoid model of the territory of the Republic of Lithuania LIT15G.

Laser scanning – a technology using laser beams to measure and represent a 3D environment. This is a general term which covers various laser scanning techniques.

LiDAR – *Light Detection and Ranging* refers to a laser scanning technology which uses laser pulses and is commonly used to acquire geospatial data over large areas.

LIT15G – the Lithuanian territorial geoid model used in geodetic and cartographic activities requiring information about the normal heights of points.

LitPOS – the Global Positioning System infrastructure for Lithuania.

LKS94 – a Lithuanian coordinate system using x and y axes in the 2D space.

MEP – mechanical, electrical, and plumbing.

PC – a point cloud consisting of a set of data points in 3D space defined by x , y , and z coordinates.

Photogrammetry – a photographic method used in surveying in order to take measurements.

Plane equation – represents a 3D plane in a Cartesian coordinate system. The equation is used to fit the plane to a 3D point cloud.

Plane limits – rejection of points that are outside the boundaries of a specific plane.

PPK – post-processing kinematic technology is used in surveying applications which records raw GPS data and corrects it later during data processing.

Point cloud alignment – adjustment of multiple point clouds to match each other in space.

Point cloud density – the space between points in a point cloud.

PTS – plain text file format.

RANSAC – random sample consensus is an algorithm used to fit models to data.

Redundant points – data points that contain duplicate or redundant information.

RFID – radio frequency identification is a wireless system for identifying tagged objects by using a reader.

RGBA – red, green, blue, and alpha color channel values.

RMSE – root mean square error is a statistical method for measuring the difference between values.

RTK – real-time kinematic technology is used in surveying applications to provide real-time positioning information.

SME – small and medium-sized enterprise.

Source point cloud – point cloud data obtained from laser scanner sensors.

Target point cloud – a point cloud created from the extracted vertices of the IFC elements.

TIN – triangulated irregular network is a spatial data structure for representing terrain.

TLS – terrestrial laser scanning involves the use of laser scanners mounted on a tripod.

Transformation matrix – a method that allows a point in one coordinate system to be expressed in another coordinate system.

TS – the total station is a measuring device used in land surveying and construction.

UAS – an unmanned aerial system consisting of several components which work together to control an unmanned aerial vehicle.

UAV – an unmanned aerial vehicle commonly known as a ‘drone’.

Voxel – a three-dimensional unit of data volume in a point cloud.

VR – virtual reality.

WiFi – wireless networking technology.

LIST OF FIGURES

Fig. 1. Research structure.....	18
Fig. 2. IFC4 data schema architecture. Reproduced from BuildingSMART International [14].....	22
Fig. 3. BIM used throughout the project lifecycle. Reproduced from PennState College of Engineering [22].....	24
Fig. 4. Summary of key factors for effective automated monitoring [105].....	31
Fig. 5. Number of studies on point cloud applications in the construction industry [116].....	32
Fig. 6. Main phases of construction execution.....	40
Fig. 7. Methodology and scope of experiments.....	42
Fig. 8. Testing site mesh model processed with <i>Bentley ContextCapture</i> software.....	46
Fig. 9. Testing site mesh model processed in the <i>Propeller Aero</i> platform.....	46
Fig. 10. Experimental research scheme.....	48
Fig. 11. Testing site sheme: a) site boundaries and CPs scheme. Blue boundaries indicate areas of traditional survey; b) self-made CP; c) <i>AeroPoint 1.0</i> base station.....	49
Fig. 12. Flight plans: a) at an altitude of 74 m; b) at an altitude of 100 m.....	50
Fig. 13. Stockpiles for volume estimation and random cross-section locations.....	52
Fig. 14. Post-processing kinematic (PPK) workflow for recording Global Positioning System (GPS) information.....	55
Fig. 15. PPK data acquisition timeline: a) data acquisition from a height of 74 meters; b) data acquisition from a height of 100 meters.....	56
Fig. 16. An example of imported TIN surfaces into photogrammetric software: a) reality mesh in <i>Trimble Stratus</i> platform; b) TIN surface imported into <i>Trimble Stratus</i> software.....	57
Fig. 17. Control points layout configuration for the ground control-based approach: a) 8 GCPs and 3 CHPs; b) 6 GCPs and 5 CHPs; and c) 5 GCPs and 6 CHPs.....	58
Fig. 18. Control points layout configuration for the Real-time kinematic approach: a) 5 GCPs and 3 CHPs; b) 3 GCPs and 5 CHPs.....	58
Fig. 19. Control points layout configuration for the Post-processing kinematic approach: a) 1 GCP and 10 CHPs; b) 1 GCP and 4 CHPs.....	59
Fig. 20. Example of the boundaries used for stockpiles volume calculation. Stockpile number 3: a) the view in <i>Trimble Stratus</i> platform; and b) the view in <i>ContextCapture</i> software with 50% mesh transparency. Stockpile number 15: c) the view in <i>Trimble Stratus</i> platform; and d) the view in <i>ContextCapture</i> software with 50% mesh transparency. Stockpile number 16: e) the view in <i>Trimble Stratus</i> platform; and f) the view in <i>ContextCapture</i> software with 50% mesh transparency.....	60
Fig. 21. Measurements of the coordinates of the control points in the photogrammetric model. The centers of the images show the x, y coordinates obtained with the GNSS receiver. Example of measurements on the <i>Trimble Stratus</i> platform: a) point No. 4; b) point No. 5; c) point No. 6; example of measurements in	

<i>Bentley Descartes</i> software with mesh transparency set to 50%: d) point No. 2; e) point No. 4; f) point No. 9	61
Fig. 22. Total volume comparison of 16 stockpiles obtained by different methods	64
Fig. 23. Total volume comparison of 5 stockpiles obtained by each method	64
Fig. 24. Vertical analysis of control points of 1 GCP-based PPK and 6 GCP-based GPS methods compared to ground-level survey measurements	69
Fig. 25. RMSE deviations of PPK and 6 GCPs-based methods	70
Fig. 26. Vertical datum analysis of UAV RTK approach	71
Fig. 27. RMSE deviations of RTK and smaller-scale PPK approaches	72
Fig. 28. Comparison of vertical datums results between all analyzed methods	72
Fig. 29. An example of a well-opened area for the installation of a base station. Reproduced from https://www.propelleraero.com/	75
Fig. 30. Dashed line represents the extended location where the GCP was installed	76
Fig. 31. Axes and building boundaries are imported into the photogrammetric model. View from the <i>Trimble Stratus</i> platform	77
Fig. 32. Visual assessment of x, y accuracy by comparing the as-built vs. as-planned	77
Fig. 33. Monitoring of work in progress compared to the design surface	78
Fig. 34. Earthworks control during the earthworks phase	78
Fig. 35. Example of transferring data points to CAD software	79
Fig. 36. Scanning location in <i>Piliamiestis A1</i> residential building	82
Fig. 37. Scanning locations in <i>Sqveras</i> office building	82
Fig. 38. Experimental research scheme	83
Fig. 39. Scan locations on the third floor of <i>Sqveras</i> building by using a <i>FARO Focus</i> laser scanner	85
Fig. 40. Scan path using <i>ZEB-GO</i> handheld laser scanner (<i>Piliamiestis A1</i> project)	86
Fig. 41. Workflow of data acquisition and pre-processing: a) mobile laser scanning workflow using the <i>ZEB-GO</i> scanner; b) static laser scanning workflow using the <i>FARO Focus</i> scanner; c) example of setting up a control point for georeferencing, <i>TOPCON GT</i> series robotic total station, and <i>FARO Focus</i> laser scanner	86
Fig. 42. Pre-processed IFC and point cloud data for further analysis: a) point cloud model obtained in <i>Sqveras</i> building; b) point cloud model obtained in <i>Piliamiestis A1</i> building; c) the corresponding IFC model of <i>Sqveras</i> building; d) the corresponding IFC model of <i>Piliamiestis A1</i> building	87
Fig. 43. Pipeline of IFC exploration	88
Fig. 44. The point cloud version obtained by extracting the vertices of IFC elements	89
Fig. 45. Pipeline of data alignment	89
Fig. 46. Selection of the reference points	90
Fig. 47. Automated object detection process	91
Fig. 48. Plane limits: a) distance calculation to all points; b) the process of discarding points that are outside the current plane	92
Fig. 49. A wall consists of 8 vertices and 12 faces	92
Fig. 50. Example of processing of wall face 0	93

Fig. 51. Example of a source point cloud point relationship to a face when the point belongs to a plane.....	93
Fig. 52. Example of a source point cloud point relationship to a face when the point does not belong to a plane.....	94
Fig. 53. Downsampling process when using 5 cm voxel size.....	95
Fig. 54. Face information of an IFC object, represented as a relationship between vertices.....	95
Fig. 55. IFC wall vertices in the as-built point cloud. IFC vertices are marked in green.....	96
Fig. 56. Example of face 1 separated into two triangles (green dots).....	96
Fig. 57. Example of face calculation results.....	96
Fig. 58. <i>Sqveras</i> 3 rd floor georeferenced point cloud data in <i>Open3D</i> module.....	98
Fig. 59. Spatial location of the source point cloud model compared to the target point cloud data after the transformation of the georeferenced data into zero-origin coordinates.....	99
Fig. 60. Spatial location of <i>Piliamiestis AI</i> point cloud data after coordinate transformation to zero origin.....	100
Fig. 61. Spatial location of <i>Sqveras</i> 1 st floor point cloud data after coordinate transformation to zero origin. The data obtained by using <i>FARO Focus</i> laser scanner was not that far aligned, and the data obtained by using <i>Leica</i> laser scanner was not aligned at all.....	100
Fig. 62. Alignment results: <i>Sqveras</i> 3 rd floor (<i>FARO Focus S70</i>).....	101
Fig. 63. Alignment results: <i>Piliamiestis AI</i> (<i>ZEB-GO</i> mobile laser scanner).....	101
Fig. 64. Alignment results: <i>Sqveras</i> 1 st floor (<i>Leica BLK360</i>).....	102
Fig. 65. Alignment results: <i>Sqveras</i> 1 st floor (<i>FARO Focus S70</i>).....	102
Fig. 66. Objects marked in green are detected and identified as built.....	103
Fig. 67. Global ID of a specific IFC object in <i>Bentley Descartes</i> software.....	105
Fig. 68. Method evaluation by removing objects in point cloud data.....	105
Fig. 69. Object detection in datasets 3 and 4 when there were missing objects in the point cloud.....	106
Fig. 70. Integration of source and target point cloud data: the case of <i>Sqveras</i> 3 rd floor where two columns and one wall were removed.....	106
Fig. 71. Example of the resulting point cloud in a cluttered environment: a) several columns were displaced and duplicated and had incompletely scanned surfaces; b) an obstruction caused a hole in the scanned surface, and redundant points were not removed; c) formwork was installed above the column, there were scaffolding and other items nearby.....	107
Fig. 72. Example of original and downsampled point cloud data.....	110
Fig. 73. The last two columns were not detected in the point cloud obtained with the <i>FARO Focus</i> laser scanner on the first floor of the <i>Sqveras</i> building.....	110
Fig. 74. There are no blue dots in the results visualization, which means that, after applying downsampling, all walls were detected.....	111
Fig. 75. Columns 1, 7 and 8 were not detected in the point cloud obtained with the <i>Leica BLK360</i> laser scanner on the first floor of the <i>Sqveras</i> building.....	111

Fig. 76. On the left side, the undetected column No. 1 is shown, whereas, on the right side, columns Nos. 7 and 8 went undetected	111
Fig. 77. Walls Nos. 9 and 11 were not detected.....	112
Fig. 78. Outcome of automated progress monitoring	116
Fig. 79. Comparison of automated construction monitoring technologies compared to the traditional approach.....	117
Fig. 80. Cross-sections of random stockpiles	118
Fig. 81. Data acquisition time of automated vs. traditional approaches	119
Fig. 82. Efficiency in relation to the scale of project.....	120
Fig. 83. Example of visualization and report of earthworks control.....	121
Fig. 84. Example of visualization and report of structural construction progress monitoring	121
Fig. 85. Multiple cycle slips from satellites (image from https://www.propelleraero.com/ support team).....	124
86 pav. Eksperimentų metodika ir apimtis	137
87 pav. Eksperimentinio tyrimo vietos fotogrametrinis modelis, gautas naudojant Bentley ContextCapture programinę įrangą.....	138
88 pav. Eksperimentinio tyrimo schema.....	139
89 pav. Bandymo aikštelės schema ir kontroliniai taškai: a) aikštelės ribos ir kontrolinių taškų išdėstymo schema (mėlynose ribose buvo atlikta žemės tūrių analizė), b) savadarbis kontrolinis taškas, c) AeroPoint 1.0 bazinė stotis	140
90 pav. 2D fotogrametrijos skrydžių planai: a) 74 m aukštyje, b) 100 m aukštyje	141
91 pav. Žemės atsargų krūvos tūriui įvertinti ir atsitiktinės skerspjuvių vietos	142
92 pav. PPK darbo eiga GPS informacijai įrašyti.....	143
93 pav. Bendras 16 krūvų tūrio palyginimas	145
94 pav. Bendras 5 krūvų tūrio palyginimas	146
95 pav. PPK ir ŽKT pagrįstų metodų RMSE nuokrypiai	147
96 pav. RTK ir PPK metodų RMSE nuokrypiai mažos apimties tyrimuose.....	148
97 pav. Visų analizuotų metodų vertikaliųjų atskaitos taškų rezultatų palyginimas	148
98 pav. Ašys ir pastato ribos importuotos į fotogrametrinį modelį	149
99 pav. Vizualinis x, y tikslumo įvertinimas	150
100 pav. Praktinio panaudojimo būdai: a) vykdomų darbų stebėjimas lyginant su projektiniu paviršiumi, b) žemės darbų apimčių kontrolė.....	150
101 pav. Eksperimentinio tyrimo schema.....	151
102 pav. Duomenų gavimo darbo eiga: a) mobilus lazerinis skenavimas, b) statinis lazerinis skenavimas, c) kontrolinis taškas, TOPCON GT serijos robotizuotas tacheometras ir FARO Focus lazerinis skeneris	153
103 pav. IFC ir 3D taškų debesies modeliai paruošti tolesnei analizei: a) Sqveras pastato 3D taškų debesies modelis, b) Piliamiestis A1 3D taškų debesies modelis, c) Sqveras pastato IFC modelis, d) Piliamiestis A1 IFC modelis	154
104 pav. 3D taškų debesies versija, gauta išfiltravus IFC elementų viršūnes	155
105 pav. Automatizuotas objektų aptikimo procesas	156
106 pav. Plokštumos riba: a) atstumo iki visų taškų skaičiavimas, b) taškų, esančių už plokštumos, atmetimas	157

107 pav. IFC objekto paviršiaus informacija, vaizduojama kaip ryšys tarp viršūnių	157
108 pav. Taškų sumažinimo procesas naudojant 5 cm vokselio dydį	158
109 pav. Sqveras trečiojo aukšto geografiškai nukreiptas 3D taškų debesies modelis Open3D modulyje	158
110 pav. Erdvinė šaltinio ir tikslinio 3D taškų debesies vieta po koordinacių transformacijos	159
111 pav. Sulygiavimo rezultatai: a) Sqveras trečias aukštas, b) Piliamiestis A1, c) Sqveras pirmas aukštas (Leica BLK360), d) Sqveras pirmas aukštas (FARO Focus S70)	159
112 pav. Objektai pažymėti žaliai buvo identifikuoti kaip pastatyti	160
113 pav. Rezultatų ataskaitos pavyzdys	161
114 pav. 3D taškų debesies modelis atspindintis sudėtingą statybos aplinką: a) kelios kolonos buvo pasislinkusios ir susidubliavusios, b) dėl kliūčių nuskenuotame paviršiuje atsirado skylė, c) virš kolonų buvo sumontuoti klojiniai	161
115 pav. Visų duomenų rinkinių objektų aptikimo rezultatai	162
116 pav. Objektų aptikimo rezultatai po duomenų sumažinimo	163
117 pav. Automatizavimo įtaka statybos darbų pažangos stebėjimui	164
118 pav. Automatizuotų statybos eigos stebėjimo technologijų palyginimas su tradiciniu metodu.....	165
119 pav. Atsitiktinių žemės krūvų pjūviai	166
120 pav. BO fotogrametrijos ir tradicinio metodo duomenų gavimo laikas	167
121 pav. Efektyvumas atsižvelgiant į projekto mastą.....	167

LIST OF TABLES

Table 1. Main features of the software used in the experiment.....	47
Table 2. Main data acquisition equipment used in the experiment	49
Table 3. Control points measurement information	53
Table 4. 74-meter height PPK flight information	55
Table 5. 100-meter height PPK flight information.....	56
Table 6. Report of conventionally calculated stockpile quantities	62
Table 7. Comparison of each stockpile volume obtained by all analyzed methods.	63
Table 8. CPs measurement information for the UAV 5 GCPs-based method	65
Table 9. CPs measurement information for the UAV 6 GCPs-based method	65
Table 10. CPs measurement information for the UAV 8 GCPs-based method	66
Table 11. Control points measurement information for the UAV PPK method	66
Table 12. Control points measurement information for the UAV RTK method.....	66
Table 13. Control point measurement information for the additional ground-level survey and the smaller-scale UAV PPK method	67
Table 14. Root mean square error (RMSE) deviations for 11 control points.....	68
Table 15. RMSE deviations for GCPs and CHPs separately	68
Table 16. Differences of vertical reference points of UAV GCPs-based photogrammetric model from GNSS receiver measurements.....	68
Table 17. RMSE deviations excluding control point No. 8.....	70
Table 18. RMSE deviations of GCPs and CHPs excluding control point No. 8.....	70
Table 19. RMSE deviations of the RTK method for 8 control points.....	70
Table 20. RMSE deviations of the RTK method excluding control point No. 10 ...	71
Table 21. RMSE deviations obtained by the PPK method in winter conditions.....	71
Table 22. UAV data capture information for 36 ha area	72
Table 23. Data capture efficiency for 5549.55 m ² area	73
Table 24. Data processing information of analyzed methods	74
Table 25. The main parameters of laser scanners used in the experiment	83
Table 26. Brief description of datasets	84
Table 27. Details of analyzed point cloud models.....	87
Table 28. Fragment of <i>Sqveras</i> 3 rd floor scan data obtained with <i>FARO</i> laser scanner	97
Table 29. Representation of <i>Sqveras</i> 3 rd floor scan data in <i>Open3D</i> module.....	98
Table 30. Transformation of <i>Sqveras</i> 3 rd floor scan data coordinates to zero origin	99
Table 31. Automated tracking report listing 0's and 1's along with global IDs	104
Table 32. Object detection in cluttered construction environment.....	107
Table 33. Object detection results for all datasets	108
Table 34. Point cloud (PC) data reduction information.....	109
Table 35. Object detection results for all datasets after applying downsampling ..	112
36 lentelė. Eksperimente naudojama duomenų gavimo įranga	140
37 lentelė. Žemės krūvų tūrio palyginimas.....	145
38 lentelė. RMSE nuokrypiai 11 kontrolinių taškų	147
39 lentelė. RMSE nuokrypiai vertinant žemės kontrolinius taškus ir patikros taškus	147

40 lentelė. Duomenų gavimo efektyvumas 0,55 ha plote.....	148
41 lentelė. Pagrindiniai eksperimente naudotų lazerinių skenerių parametrai	152
42 lentelė. Informacija apie 3D taškų debesies modelius	154
43 lentelė. 3D taškų debesies modelių informacija	162

INTRODUCTION

Problem statement and research relevance

The construction industry plays an important role in the any country's economy; however, during the last decades, this sector was one of the least digitized. The transformation of the construction industry through digitalization was defined by the term *Construction 4.0*, and the industry started to rapidly adopt new digital technologies, tools, and practices so that to improve the efficiency, quality, and sustainability of construction projects. As the need for housing [1] and infrastructure [2] has been growing due to an increasing global population and the climate change, the construction industry has to adopt novel practices along with new workflows in order to continue support human activities in a more sustainable and efficient way.

Despite the rapid digitization of the construction industry, this progress has been heterogeneous between the countries. For example, Northern and Western European countries are advancing faster than Central or Eastern European countries. By digitizing the construction sector, Europe aims to leverage advanced technologies such as *Building Information Modelling* (BIM), *Unmanned Aerial Systems* (UAS), laser scanning technologies combined with machine learning and computing to improve the efficiency of construction processes, reduce waste, and improve quality throughout the whole life-cycle of built assets. Moreover, digitalization can make design decisions more transparent, help to solve complex issues for higher sustainability standards, promote innovation, and increase safety [3, 4].

Among digital innovations, BIM implementation has been in the spotlight for the past decade, but, in parallel, the importance of technologies such as *Unmanned Aerial Vehicle* (UAV)-based photogrammetry and 3D laser scanning has been on the rise. These technologies allow for more accurate measurement of quantities and identification of potential waste. In this way, materials can be used more efficiently, and the impact on the environment can be reduced, thus improving the sustainability of construction. In addition, laser scanning technologies can be used to monitor the construction process, which can help prevent errors and ensure that the construction project is carried out according to the plan. This can help reduce the need for rework and reduce time and resources. UAVs can be utilized on construction sites to enhance the monitoring of the construction progress, identify potential risk factors, and improve quality control and safety measures. They play a crucial role in minimizing the risk of accidents at construction sites. By replacing human labor in perilous and hard-to-reach areas like heights or hazardous equipment, these technologies effectively reduce the reliance on manpower and ensure the comprehensive safety of construction sites. In addition, UAVs are being increasingly used to gather data from construction sites, thereby allowing efficient and accurate monitoring of the construction process.

Construction progress monitoring is an important component of project management due to helping to identify and address issues that may arise during the construction process in a timely manner and ensuring that up-to-date information is available to make the necessary decisions and deliver the project on time and within

the budget [139]. Construction companies across various industries are actively employing 3D laser scanning and photogrammetry in their operations. Bridges, roads, and other infrastructure assets, building structures, as well as non-functional areas are scanned to assess the situation. Applications include topographic measurements, road surface and pavement profiling, volume calculations, bridge damage assessments, and more. These methodologies are applied to survey the ‘as-is’ condition of buildings, brownfield sites and infrastructure prior to design, and then the same sites are resurveyed for progress monitoring and analysis [135].

To monitor construction progress, UAV-based photogrammetry is widely used to control the quantities of earthworks, while laser scanning is more common in building construction projects. While the advancements in technology have led to the increased use of these technologies for monitoring construction progress, they also encounter several challenges. These include the mistrust associated with new technologies, integration complexities with other technologies, such as BIM, and insufficient levels of automation. The constant change and occluded environment of construction sites often make it difficult obtain high-quality data. Under such conditions, data obtained by laser scanning or photogrammetry often contains noise and outliers, and the surface of objects is not fully captured, which poses challenges for data alignment and object identification.

The analysis and development of an automated construction monitoring methodology in the real construction environment can significantly enhance the efficiency, productivity, and image growth of the construction sector, thereby contributing to the realization of European goals towards digitization of construction.

Aim of the research

This research aims to investigate the application of photogrammetry and laser scanning techniques for construction progress monitoring, encompassing tasks from earthworks control to building object monitoring, and to propose an automation methodology for the monitoring process focused on the integration of building information model and laser scanning data.

Research objectives

To achieve the goal of developing an automated construction progress monitoring methodology, several specific objectives were identified:

1. To analyze the existing literature and investigate data acquisition tools, technologies, and methods used for construction progress monitoring.
2. To conduct experiments and analyze various advanced UAV-based photogrammetric workflows, thereby providing observations that compare the efficiency and reliability of different methods for monitoring the progress of earthworks.
3. To capture spatial data of building structures within the construction environment by using different laser scanning techniques and create pilot datasets from the acquired data.

4. To develop a methodology for aligning and integrating 3D point cloud data and the corresponding BIM model in the *Industrial Foundation Classes* (IFC) format.
5. To develop an automated process for monitoring as-built versus as-planned objects, with a particular focus on object detection within noisy and occluded construction environments, as well as for representing as-built structures.

Research methodology

Considering the defined research objectives, this section outlines the research approach adopted to investigate these objectives.

To accomplish these goals, it is essential to comprehend the concept of BIM technology, the various geometry capture technologies available, the integration possibilities between these technologies, and the impact and challenges they present in the context of construction progress monitoring. An extensive literature review on these technologies, tools and methods was conducted.

Based on the findings of the literature review and practical observations, in terms of construction progress monitoring, it was established that the application of photogrammetry is more effective for earthworks management, while the use of laser scanning technologies is more applicable in the building construction phase. For this reason, two experiments were conducted in the study: progress monitoring in the earthwork phase, and progress monitoring in the building construction phase (Figure 1).

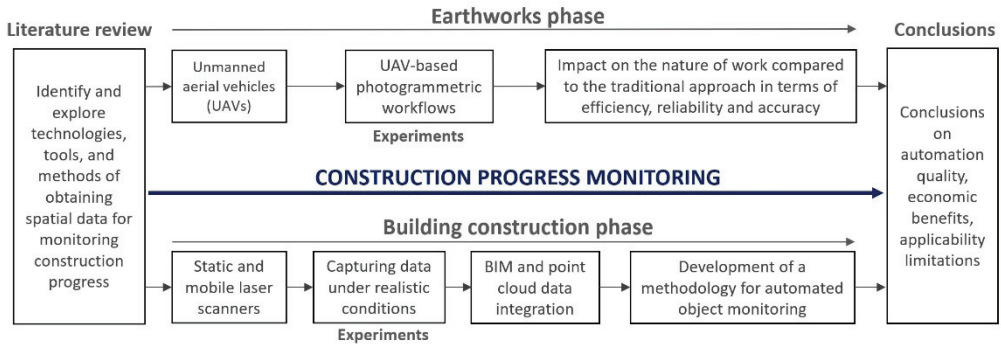


Fig. 1. Research structure

In the construction process, it is difficult to control the progress of earthworks, measurements are often carried out manually, or the progress is estimated by prediction. At this stage of construction, the introduction of UAVs simplified this process. However, UAV-based photogrammetry involves various workflows and methodologies which can determine the efficiency and reliability of the progress monitoring process. This was investigated through experiments to demonstrate the impact of different workflows on the nature of work compared to the traditional approach in terms of efficiency, reliability, and accuracy.

In the building construction phase, the application of laser scanning technologies for progress monitoring was investigated. In modern construction, laser scanning and BIM technologies are already in practical use. However, the integration of these technologies with each other and their application to automated

monitoring of construction progress is not developed enough. At this stage, the geometric data of building structures was captured in the construction environment by using laser scanning technologies. By using the obtained data, a methodology was developed that enables extraction of BIM data, calculating the plane equation of the faces, and performing a point-to-plane distance estimation [139]. This allows the integration of IFC and point cloud data and automatic identification of building objects in a point cloud based on the corresponding IFC model.

This thesis focuses on the technological rather than the managerial aspects of the construction progress monitoring workflow.

Scientific novelty

The novelty of the research is based on the use of photogrammetry and laser scanning technologies to monitor the progress of construction in a constantly changing construction environment:

1. The accuracy and reliability of advanced real-time kinematic and post-processing kinematic UAV-based photogrammetric techniques have been determined and compared to the conventional practice by using a ground-based GNSS receiver.
2. A novel method has been proposed which integrates laser scanning data with an IFC model to automatically detect objects in a point cloud based on the provided IFC.
3. An object detection process has been developed by calculating the plane equation of the face of each IFC element and determining the point-to-object relationship, which allows the identification of incompletely scanned objects.

In this context, the scientific novelty lies in the seamless integration of 3D laser scanning data with the IFC model for automated detection of construction objects. Object detection by comparing the 3D point cloud to the IFC model sets it apart from other studies. In addition, the process allows the identification of incompletely scanned objects, which distinguishes the proposed method as a contribution to object detection in occluded environment under real construction conditions.

Defended statements

1. In the process of monitoring construction progress, automated UAV-based photogrammetric workflows provide efficiencies for large-scale projects over 925 m² in terms of accuracy, reliability and time compared to the traditional methods.
2. The process of integrating IFC and point cloud data by extracting vertices from IFC elements ensures the possibility of data alignment and automatic detection of construction objects compared to the provided IFC data.
3. The proposed model enables the extraction of IFC data, calculating the plane equation of the object faces, and performing a point-to-plane distance estimation, which allows automatic detection of building objects in an occluded environment when the surface is incompletely scanned, or the obtained reality data is of poor quality.

Practical value

The proposed methodology can significantly improve the efficiency of construction progress monitoring by ensuring that reliable and most up-to-date information is available to support decision-making which is necessary to deliver the project goals on schedule and within budget, thereby saving time and cost. The automation of this process could contribute to the European goals for the digitization of the construction sector by reducing labor and time requirements, thereby improving the overall safety of construction sites and the overall efficiency of construction processes.

Scope and thesis structure

This thesis investigates the use of photogrammetry and laser scanning technologies in the construction phase. The application of these technologies for monitoring the construction progress of earthworks and building structures is being examined. The thesis structure is organized in the following order. The introductory part presents the essence of the work, followed by literature review in Chapter 1. Experimental research on the application of photogrammetry in the earthworks phase is presented in Chapter 2, and research on the application of laser scanning in the construction phase is presented in Chapter 3. Chapter 4 presents the results and discussion, followed by general conclusions, literature sources and a list of publications on the topic of the dissertation. The volume of the thesis consists of 194 pages, 121 figures and 43 tables.

Publications and conferences

Two scientific publications on the topic of the dissertation have been published in international journals indexed by *Clarivate Analytics Web of Science*:

1. ISPRS international journal of geo-information, 2021, Vol. 10 (6), p. 399. *Geometric Accuracy of 3D Reality Mesh Utilization for BIM-Based Earthwork Quantity Estimation Workflows.*
2. Buildings (Basel), 2022, Vol. 12(10), p. 1754. *Automation of Construction Progress Monitoring by Integrating 3D Point Cloud Data with an IFC-Based BIM Model.*

The research results contributing during these doctoral studies have been presented at two international scientific conferences:

1. Advanced Construction and Architecture: proceedings of 1st international scientific conference, 23–25 September 2020, Kaunas, Lithuania. *3D reality mesh utilization for BIM-based earthwork quality estimations.*
2. 3rd Baltic Conference of Young Researchers in Architecture, Landscape Architecture, Urbanism and Civil Engineering, 24 November 2022, Kaunas, Lithuania. *Integrating BIM and 3D Point Cloud Data for Construction Monitoring Automation.*

1. LITERATURE REVIEW

This chapter consists of a literature review on the topics covered in this thesis. Knowledge of BIM, spatial data capturing technologies and the possibilities of using these technologies in the construction progress monitoring process is required for the further progress of the final work.

In this thesis, detailed analysis of BIM does not fall into the scope of research. However, it is necessary to understand this technology as it is the core of construction digitization, and it can serve as an integral part of photogrammetry and laser scanning technology in terms of automation of construction progress monitoring. Therefore, this chapter first reviews the main aspects of BIM related to research objectives, such as the benefits of using BIM in construction management and the level of adaptability and readiness for monitoring the construction progress. The following is a review of construction progress monitoring methodologies in the earthworks and building construction phases by focusing on the application of photogrammetry and laser scanning technologies. These technologies have developed in parallel with BIM and, together, have an important role in the automation of the construction progress monitoring process. Finally, this chapter reviews and identifies the potential applications of progress monitoring methods in the construction phase from a practical perspective.

1.1. Review of Construction Progress Monitoring Techniques

1.1.1. Building information modelling

The industry's driving force has traditionally been based on time, cost, and quality. In addition, industries, including the construction sector, have been facing stricter requirements for sustainability. BIM was developed as a collaborative process to reduce waste, improve efficiency, and optimize construction project management throughout the project life cycle [5, 6]. This process is based on information exchange operations and supported by a variety of tools and technologies. It requires collaborative workflows to be defined and optimized [7]. In new construction projects, this process creates information from design to construction and can capture the as-is condition of the building, thereby providing a basis for maintenance.

The term *BIM* was already being mentioned in the academic community as early as in the 1990s, and the popularization and practical use in real projects began after 2000 [8, 9]. The term was first introduced by *Autodesk* and later adopted by software vendors such as *Bentley* and *Graphisoft* [10]. Although BIM originated from a technological process, from a business process perspective, the term is more commonly defined as *Building Information Management* rather than *Building Information Modelling* [11]. Two decades after the term began to be popularized, some construction professionals still have misconceptions about what BIM is, such as assuming that it is a single 3D model. The purpose of BIM is much broader, and it includes processes such as coordinating and sharing up-to-date information among

project participants, coordinating different design disciplines, controlling quantities and costs, recording, and analyzing safety issues, and more [12].

In the BIM process where several organizations collaborate in the project, it is important to use compatible tools. In 1994, the development of IFC as an open data model standard was initiated to meet BIM interoperability needs for the industry [13]. IFC is an open and standardized digital description intended to enable data exchange between various hardware and software tools to ensure an efficient BIM process [14]. The architecture of the IFC scheme was described by Clemen and Gründig [15]. The schema consists of four layers, where each layer refers to entities in the same or lower layer(s). The resource layer contains geometry and topology information. The Core layer includes concepts such as the object, group, process, or relationship, and they are specialized by the Resource level. Entities at the Core layer or above have a globally unique ID and history information. The Interoperability layer includes schemas for use in multiple disciplines and defines shared building elements such as a beam, a column, or a wall. The Domain layer entity definitions are not allowed to refer to any other domain, and those definitions are commonly used for information exchange and sharing. The architecture of the IFC schema is shown in Figure 2.

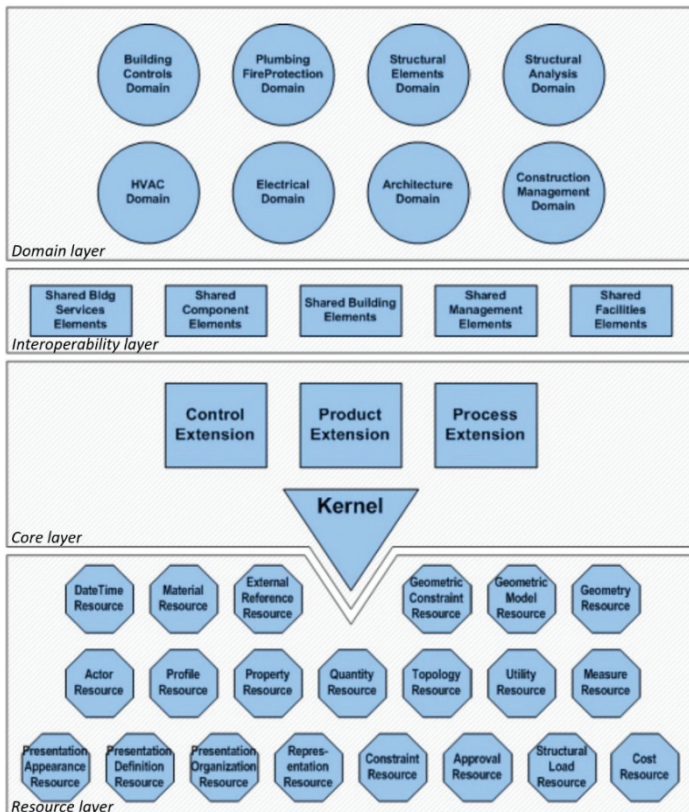


Fig. 2. IFC4 data schema architecture. Reproduced from BuildingSMART International [14]

In the BIM process, the IFC data model enables all participants in a construction project to exchange information in a common data environment, thereby improving construction and management processes [16].

Although the intent of IFC is data interoperability between different BIM software applications [17], this is where the issues arise. IFC data exchange interoperability issues were analyzed by Lai and Deng [18]. When using IFC, data is often lost when exchanging and sharing data, for example, objects are missing, or their geometry is represented incorrectly. Data loss can be caused by software tools not able to correctly interpret multiple objects from different disciplines, or by using different methods to represent the same geometry and other parameters when importing and exporting data, which may result in inaccuracies.

Over the past century, construction project management has evolved from the incremental approach to the integrated approach. The incremental approach is based on the principle of an individual craftsman when everything was done by one person, and each new stage of the project was carried out only after the previous one had been completed [19]. Today's projects are complex, with ever-increasing sustainability requirements, and they involve large numbers of participants with narrow expertise who are operating in a coherent manner. The benefits of using BIM in managing such projects are eminently significant. The main benefits of BIM, as identified by Glick and Guggemos [20], are the fact that this technology allows for a three-dimensional representation of the building, integrates information generated by specialists, allows information to be stored centrally, quickly updated, and accessed by several stakeholders, thus reducing the amount of waste, and improving the overall efficiency of the project. Bryde et al. [21] found that the most commonly reported benefits of using BIM in construction project management are related to cost reduction, time savings, and project control throughout its life cycle, while negative benefits were mostly directed towards the use of BIM software.

In construction management, BIM plays an important role throughout the project life cycle. For example, creating a 3D model of existing conditions by using BIM software and laser scanning, photogrammetry or other surveying techniques can provide tangible benefits such as providing environmental documentation for future use, assisting with future modelling and coordinating 3D design, and providing an accurate representation of the completed works [22]. Figure 3 illustrates the uses of BIM in the planning, design, construction, and operation phases, including the generation of accurate quantity take-offs and cost estimates, engineering systems and sustainability analysis, emergency management, and more.

PLAN	DESIGN	CONSTRUCT	OPERATE
Capture Existing Conditions			
Author Cost Estimate			
Author 4D Model			
Analyse Program Requirements			
Analyse Site Selection Criteria			
Author Design			
Review Design Model(s)			
Analyse Structural Performance			
Analyse Lighting Performance			
Analyse Energy Performance			
Analyse Engineering Performance			
Analyse Sustainability Performance			
Coordinate Design Models			
Author Construction Site Logistics Model			
Author Temporary Construction Systems Model			
Fabricate Products			
Layout Construction Works			
Compile Record Model			
			Monitor Maintenance
			Monitor System Performance
			Monitor Assets
			Monitor Space Utilization
			Analyse Emergency Management

Fig. 3. BIM used throughout the project lifecycle. Reproduced from PennState College of Engineering [22]

The use of BIM is not limited to construction projects, and it is also being applied in infrastructure. BIM has been attracting the attention of researchers due to its potential in terms of economic advantages [23, 24]. However, the core value of the BIM technology is that it can improve the construction process by increasing the level of collaborative integration at different stages, thereby increasing the overall productivity of the construction industry [25].

Providing transparent project cost-benefit information to relevant stakeholders is essential in the decision-making process. Recently, Biancardo et al. [26] introduced a framework for integrating cost-benefit analysis into BIM as a combination of the already existing design and infrastructure planning tools with process automation. The proposed method can be useful to prepare a project with an up-to-date archive of information that could produce results based on cost-benefit analysis which reflect the interests of stakeholders. Cantisani et al. [27] presented a study that implemented a benefit-cost analysis in a road project by using geometrical, environmental and microsimulation methods. The approach proposed by the authors focuses on the phases of programming, design, realization, and facility management, and it considered the 7 dimensions of BIM, specifically, 3D geometrical information, scheduling, cost analysis, sustainability, and maintenance. However, BIM success depends on many factors, such as the project size, BIM proficiency of the project team members, communication, and other organizational external factors, and therefore the actual return and investment will vary from project to project [28].

The integration of a three-dimensional model with planning information, defined as BIM 4D, has gained much potential to improve construction processes

and is very important for onsite planning as it allows for the effective detection of inconsistencies and thus facilitates communication between decision-makers [29]. Logistics management has a significant impact on the project cost, time, and safety. Bortolini et al. [30] proposed a logistics planning and control model in a BIM 4D environment based on the Lean Production principles and BIM functionalities. According to the authors, the proposed method can be practically used as a reference for companies delivering engineer-to-order prefabricated building systems. Tak et al. [31] introduced an onsite crane operation management framework for multiple concurrent mobile crane operations in a BIM 4D environment that provides motion controlling, time and cost analyses, safety monitoring, clash detection and spatiotemporal site analysis. The method proposed by the authors could facilitate site planning and provide alternative scenarios for construction execution.

Over the last decade, the importance of sustainable building projects has been growing, and today, the world, and the construction sector in particular, is being pushed further towards sustainable growth [32]. Sustainable development is largely constrained by practices in the construction industry, which is a significant producer of waste and other emissions, and, as a result, the construction sector is forced to adopt innovative solutions to use cleaner construction technologies that could reduce the use of resources [33]. In construction, sustainability covers topics such as construction waste, energy consumption, thermal performance, the lifecycle cost of buildings, and more [34].

Recently, Kang et al. [35] presented a framework for applying the BIM technology to enhance the efficiency of construction waste management. The authors of this study used the BIM technology in combination with Internet of Things (IoT) solutions, which enabled response to user activities such as waste quantification, demolition process planning, the optimal disposal route selection, and the waste management strategy. Guerra et al. [36] applied the BIM 4D technology to improve construction waste reuse and recycling planning by focusing on the management of concrete and drywall waste streams.

BIM-based technologies can be adopted in most areas related to the sustainability of construction. Recently, several studies have been conducted on the application of BIM tools for facilities management and maintenance [37, 38, 39, 40]. Li et al. [41] developed a BIM-enabled building lifecycle management system. Laine et al. [42] emphasized the importance of thermal performance analysis as it has significant implications for building life cycle costs and other environmental factors. They argued that BIM facilitates the monitoring of thermal performance at various stages of construction. Although there are many ways to integrate BIM and sustainability practices in construction, Olawumi and Chan [43] identified the key benefits, such as improving the simulation of building performance and energy consumption, facilitating multi-design alternatives, and significantly improving the overall quality and efficiency of the project.

The integration of BIM and other technologies can significantly expand the application boundaries. For example, the integration of the BIM model and sensor data into digital twin technology allows simulating the behavior and performance of the building in different scenarios and thus evaluating the performance of the

building [44]. Recently, Panya et al. [45] presented a study which integrated BIM, *Virtual Reality* (VR), and *Augmented Reality* (AR) technologies. The system proposed by the authors is intended to reduce the rework of design changes by exporting the BIM model to the Unreal game engine and integrating the aforementioned technologies.

Despite the advantages of BIM, the implementation of this technology requires significant technical knowledge and increases the operating costs for companies in the short term. The cost of new BIM applications, staff training, and getting the technology up and running effectively is a major investment decision for organizations [46]. BIM maturity and capability levels vary across Architecture, Engineering, Construction and Facilities Management (AEC/FM) organizations [47]. Large companies have more human and financial resources for BIM implementation, and therefore BIM is being more commonly used in large organizations than in small and medium-sized enterprises (SMEs). In addition, large companies are more likely to be working on large and complex projects and are more likely to be requested to use BIM [48]. A study by Saka et al. [49] revealed that the major factors determining the use of BIM by SMEs in developing economies are client requirements, contractual conditions, and project costs. Vidalakis et al. [50] agreed that the adoption of BIM by SMEs is highly cost-dependent, and, given that SMEs tend to have a low level of knowledge and understanding of BIM, the identified factors encourage a wider adoption of BIM, such as knowledge sharing with other companies and industry initiatives.

The USA is an extensive country which is an influential player in the production of BIM technologies. It is considered one of the pioneers of the application of these technologies in construction. There, in the early 2000s, the National 3D–4D BIM program in the public sector was launched [51]. However, since then, the adoption of BIM has grown significantly worldwide, especially in the more developed countries [52]. In North America, Europe or Asia, BIM development has been rapid, while in the Middle East and South America the pace of development has generally been slower [53]. Several studies have been conducted exploring the level of BIM adoption in the construction practice in the United Kingdom [54], France [55], Australia [56, 57], Pakistan [58], as well as some other countries. Due to reasons such as the country level of development or uneven government incentives, the BIM adoption in practice and BIM adoption strategies tend to vary between countries. For example, the study conducted by Herr and Fischer [59] revealed that the adoption of BIM in the AEC industry in China differs from foreign practices and focuses on linear workflows rather than collaborative work. According to the authors, the BIM adoption in China is uneven and over-reported, and, while adoption is encouraged through government guidelines and policies, practical standards and guidelines are not yet well developed. The study reported that the actual benefits of BIM are far harder to attain than those officially reported by companies. The benefits are related to close cooperation with foreign clients, the use of BIM in construction process management and prefab production, while, in all other cases, 2D drawings are typically used, and interdisciplinary cooperation remains somewhat limited.

Although the United States is considered the most mature country in the field of BIM implementation, most European countries have been rapidly advancing and becoming leaders in adapting these technologies [60]. However, in a study by Charef et al. [61], the results revealed that not all European countries are advanced in BIM adaptation, and, in some countries, BIM implementation at the national level did not yet exist at the time of the research. The authors highlighted early adopter countries such as Denmark, Finland, or the UK, which have already been using BIM technologies for more than a decade, while some European countries such as Lithuania or Poland are still catching up. In general, the level of BIM adaptation in Europe is not high. According to the data published by the European Commission, BIM 3D is used by 29% of construction companies in Europe, while the use of BIM 4D reaches only 6% [48].

Currently, the ever-increasing pressure to lower emissions and avoid waste of resources is forcing European countries to apply BIM in public procurement. Due to the prominently large scale of projects and public control, the public construction sector exerts a strong influence on design and construction service providers and therefore drives BIM adaptation forward [62]. In 2014, Directive 2014/24/EU was announced in the European Union, which recommends the use of electronic tools in public works contracts and design tenders [63]. It has recently been estimated that the public sector accounts for 20–30% of all construction costs in Europe and USA [64], thus providing important business opportunities for the private sector. It is thus one of the main incentives for companies to adopt and implement BIM. However, currently, the AEC industry's readiness to adopt BIM varies considerably due to factors such as the organizational approach or regional and cultural aspects, and therefore different countries may need different strategies to promote the use of BIM [65].

Considering the trends of Europe and other continents, Lithuania is not an exception regarding the influence of the public sector on the construction sector. The public sector in Lithuania occupies a large share of investments in the construction industry. It is considered an influential client of construction projects. In 2019, about 44 percent of investments in the country's construction sector were public sector investments. Therefore, Lithuania aims to implement the BIM strategy through the strengthening of the public sector by developing digital tools, improving the supply chain, and thus ensuring the leadership of the public sector [66]. Contributing to the implementation of these goals by focusing on the creation of digital tools, the Ministry of Environment of the Republic of Lithuania launched the BIM-LT project involving the country's major universities and public sector companies in the project implementation process. In 2022, the government-approved resolution on the mandatory application of BIM methods in the public sector entered into force which required the application of BIM methods when implementing high-value objects. The published document indicates that the calculated construction prices and investment amounts, from which it would be mandatory to apply BIM methods, will be gradually reduced every two years [67].

Although most construction companies agree on the importance of BIM and the benefits that this technology can provide [68], the adoption of this technology

still remains somewhat limited. Walasek and Barszcz [69] described the main barriers related to BIM adoption, such as interoperability, compliance with user requirements, changing work processes, legal issues, training, and creation of new roles and responsibilities. Meanwhile, Chan et al. [70] identified barriers related to stakeholder resistance to change, insufficient organizational support, and lack of BIM industry standards.

The BIM technology for monitoring the construction progress is still at an early stage of development in terms of practical use. Using BIM to track the construction progress requires manual work. Process automation can be achieved through the adoption of more advanced technologies such as BIM 5D, which is based on the integration of model, data, sharing and software tools, and the integration of the project model and attribute information can provide timely construction information, e.g., the project construction progress, construction design drawings, and some other information [71]. However, the level of adaptation of such technologies is very low in Europe, and these technologies are being more commonly used in large and BIM-mature companies. In addition, with the use of BIM 5D technologies, the progress of works is often inspected and entered into the system manually, and the automation of this process requires the integration of technologies such as laser scanning or photogrammetry. The integration of BIM with 3D laser scanning and photogrammetry technologies for progress monitoring offers great potential of streamlining the monitoring process, and it is already entering the construction market. Yet, at the moment, only the development stage has been achieved. However, so far, the monitoring of the construction progress through the integration of these technologies has limitations, such as insufficiently effective as-is data acquisition, the application accuracy requirements are not clear, and the monitoring process itself is not sufficiently automated [72].

1.1.2. Construction progress monitoring

As construction projects are becoming more complex, the effectiveness of monitoring construction progress becomes critical to project management, which, in turn, requires timely and accurate information [73, 74]. The availability of up-to-date information is a critical decision aid to achieve the project goals on schedule and within budget, for example, it can prevent errors and rework, thereby reducing waste of materials and resources [75, 76].

Although advanced technology is within the reach of most construction companies, the traditional methods such as visual inspection, the use of foreman's daily reports, or the use of a plumb line and gauge are still often used to monitor progress today, which is time-consuming and error-prone [77, 78]. Typically, collecting data and updating schedules based on the actually existing construction conditions takes 20–30% of the time each day [79]. Ineffective monitoring of the construction progress is partly responsible for the fact that more than 53% of construction projects get behind schedule and more than 66% are over budget [80]. Improving progress monitoring to be effective requires automating this process, and using the BIM technology alone will limit the automation process, as it first requires the effective acquisition of as-built data. Existing construction site data in the point cloud or reality mesh formats can be efficiently captured by using laser scanning or

photogrammetry methods and contribute to the advancement of the progress monitoring process, such as automatic BIM geometry extraction from the point cloud [81], earthworks construction estimation [82, 83], monitoring of building zones [84], and more. Point cloud datasets obtained at different times can be compared with each other as the work progresses, comparing the difference over time, or the obtained data can be compared with the designed BIM model. Enabling these technologies opens up new opportunities to improve the efficiency of monitoring the work progress by automating the process. For example, when using a 3D laser scanner, captured and processed as-is data can be integrated into BIM, and the existing data can be checked against the designed model to detect deviations [85].

However, obtaining accurate point cloud data is time-consuming, and it also requires technical expertise and manual work [86]. Several accuracy assessment studies have been conducted to compare point cloud data obtained by using photogrammetry and laser scanning techniques [87, 88]. Casella et al. [89] analyzed the accuracy of UAV-based photogrammetry by comparing five different software packages and various configurations, such as different ground control points (GCPs) to check points (CHPs) ratios. The accuracy of photogrammetry based on GCPs strongly depends on their placement strategy, such as the number of GCPs or their placement location [90]. Martínez-Carricondo et al.'s [91] study suggests that, for maximum accuracy, GCPs should be placed around the edges and inside the study area. Such placement of control points (CPs) in the territory reduces the efficiency of data collection in terms of time and does not ensure the avoidance of errors. Cryderman et al. [92] analyzed the accuracy of UAV-based photogrammetry for estimating earthworks. The authors evaluated the accuracy of UAV-based photogrammetry compared to the conventional GNSS RTK approach by estimating stockpiles and concluded that the methods are at least equivalent in terms of accuracy. However, when using the photogrammetric method, accuracy is challenged by topographical conditions, such as vegetated terrain [93]. In general, the accuracy of a photogrammetric model can be affected by several reasons, such as the camera settings, image resolution, a high contrast, a uniform feature-free surface, the image format and compression level, and other reasons [94, 95].

Martínez et al. [96] analyzed the accuracy of UAV-based photogrammetry for building surveying applications. The authors performed GNSS and PPK workflows by using various UAS configurations to evaluate the impact on the point cloud accuracy. The drawback of this study stems from the fact that the proposed method was not evaluated under complex construction conditions and would be difficult to apply inside a building. Close-range photogrammetry can be used to capture geometry inside a building, but the accuracy of this technology can be greatly affected by several factors, such as the camera calibration and network configuration, the quality of the camera and the captured images, the shooting distance, or the surface properties of the material [97, 98].

Laser scanning is considered one of the most accurate and efficient technologies for capturing geometric data in construction environments, especially when it comes to point cloud data integration with BIM [72]. However, obtaining

accurate and high-quality data requires technical knowledge of the technology and understanding of its limitations in terms of accuracy and performance. For example, obstacles or blind spots in the scanning path, or surface reflection due to material properties have a significant impact on the quality and accuracy of the obtained data, and it should be considered that the processing time may take much longer than expected so that to obtain high-resolution data [99]. Static laser scanners are not as flexible as cameras for data acquisition in terms of obstructions. Combining close-range photogrammetry with the *Terrestrial Laser Scanning* (TLS) technology can improve the accuracy of the obtained results, since the photogrammetry method allows free movement around obstructing objects [100]. However, using two methods instead of one makes the whole process of data acquisition and processing less efficient. In this case, a more efficient way to obtain as-is data while reducing occlusion could be the mobile laser scanning technology [101]. This technology allows flexible movement in the occluded construction environment but is limited by a relatively short scanning range and insufficient accuracy for engineering applications [102, 103, 104].

In previous studies, point clouds and reality meshes obtained by the laser scanning and photogrammetry methods helped to improve construction progress monitoring processes by automating them and overcoming the limitations inherent to the traditional approaches. However, despite the best of efforts, the unsolved challenges remain related to the occluded construction environment, point cloud density and noise filtration, and the complexity of the methods, etc., which hinders the development of an effective automated progress monitoring methodology [105, 106].

Qureshi et al. [105] conducted an interview-based qualitative analysis and developed a framework for effective automated monitoring. The authors identified the 3D scanner, site imaging, site video, and tracking & sensing as the main categories for automated monitoring and provided a summary of critical factors based on their research (Figure 4). Both the laser scanning and photogrammetry categories address aspects related to occlusion. Omar and Nehdi [107] analyzed the main automated construction data collection technologies and provided insights into the advantages and limitations of each technology. The study found that, compared to photogrammetry, laser scanning offers advantages in terms of the point cloud accuracy, the processing speed, and the range distance for capturing as-is data in building construction.

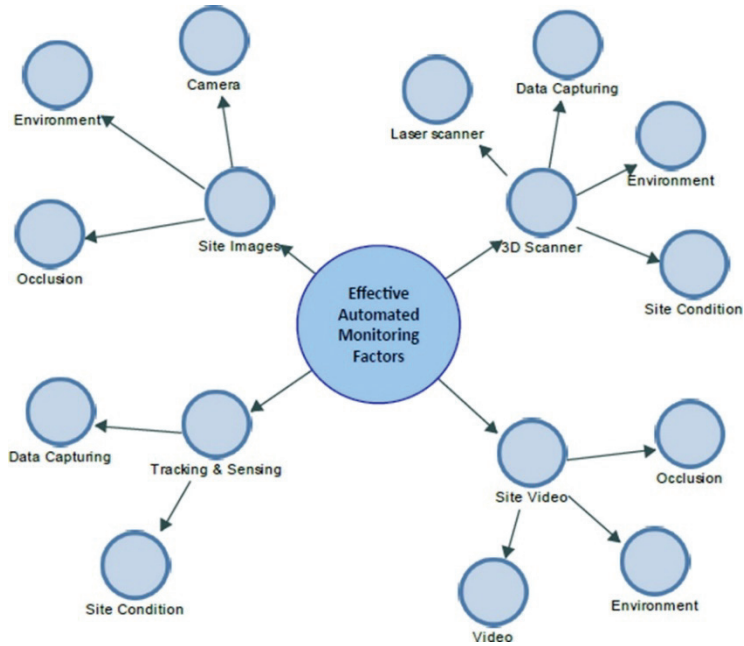


Fig. 4. Summary of key factors for effective automated monitoring [105]

Numerous researchers have applied photogrammetry and laser scanning technologies for the development of automated construction progress monitoring frameworks. Turkan et al. [77] proposed an automated approach combining time-stamped laser scans and 4D schedule information based on the object recognition technology. The method requires converting the 3D *Computer Aided Design (CAD)* model into a triangulated mesh format, and, based on the number of recognized objects, it shows the progress in percentage values. In the study by Reja et al. [108], the progress monitoring report is also based on percentages. The proposed method directly integrates the as-designed BIM model with the point cloud data and calculates the progress based on the number of points in both models by using the point intensity as the main parameter. The main drawback of this method is that it has not been sufficiently tested in an occluded construction environment. Another study by Zhang and Arditi [109] also used a methodology to calculate progress based on the percentage of completion. The proposed method integrated a point cloud obtained from a laser scanner with a 3D model in the .dgn format and compared the number of points associated to the faces of the object. The experiments of this study were carried out under laboratory conditions, and the factors of real construction were not evaluated.

Golparvar-Fard et al. [110] proposed an automated approach for construction progress monitoring based on photogrammetry and an IFC-based BIM model. The authors used a color-coded scheme which marks changed and unchanged IFC elements in red and green, while those elements whose progress is not reported remain grey. ElQasaby et al. [111] combined a 3D object recognition technology with 5D BIM data to track construction progress. The authors proposed an approach which uses color coding to display the condition of each element based on its

recognition and scheduling status. The system has limitations such as it is only available through the *Autodesk Revit* platform; also, the color coding system incorrectly identified several columns due to occlusion.

Pučko et al. [112] developed a method for automated continuous progress monitoring by using small, low-precision scanning devices that can be attached to safety helmets. Based on the comparison of as-built and as-designed BIM data, deviations from the schedule are identified by listing items that are built ahead of schedule or not built on time. To improve progress monitoring based on the comparison of as-planned and as-built, Braun et al. [113] proposed a methodology which combines point clouds, semantic data, and computer vision. The authors used a machine learning-based object detection method which verifies element categories by comparing them against the predicted data from a digital model. The main limitation of this method is that it uses image data that can only be used due to the photogrammetric process and the camera pose estimation, which makes the laser scanning technology unsuitable.

1.1.3. Earthworks progress monitoring

Earthworks control is an important factor that must be considered to estimate the optimal construction cost on a construction site. It is important from the design of engineering structures to the construction stage [114]. Over the past 30 years, earthworks monitoring processes have evolved significantly from the use of settlement plates and gauges [115] to the application of 3D point clouds. In general, the application of point clouds in the construction industry has been analyzed by a number of researchers. Wang and Kim [116] presented the most researched application areas of point clouds in the past fifteen years (Figure 5). Based on the data provided, the main application areas are 3D model reconstruction and geometry quality control, followed by construction progress monitoring and other areas.

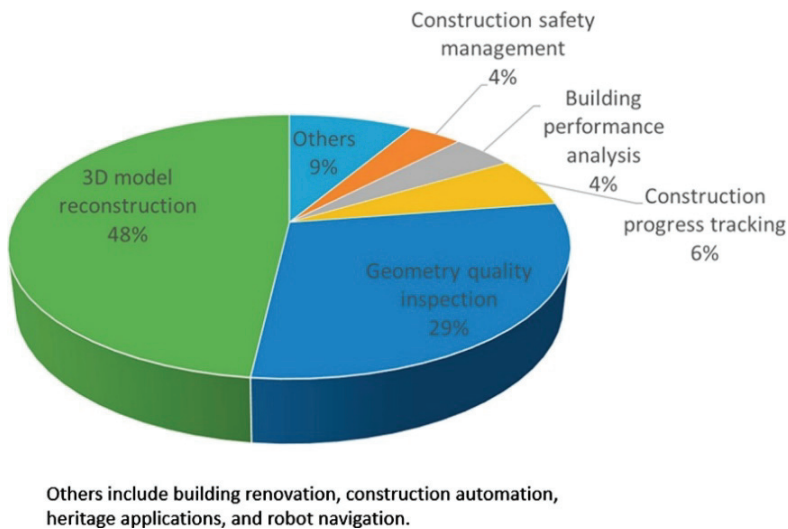


Fig. 5. Number of studies on point cloud applications in the construction industry [116]

For the monitoring of the progress of construction earthworks, point cloud applications provide a number of benefits. For example, Chae et al. [118] investigated the automation of earthworks by capturing the earthwork environment with a laser scanner and using the obtained information to remotely control an unmanned excavator. Kwon et al. [118] also developed an unmanned and remotely controlled earthworks excavation system that allows real-time fusion of two models acquired by a 3D laser scanner and a Stereovision system. In another study, Al-Hanbali et al. [119] presented an earthworks monitoring method using a helicopter-based *Light Detection And Ranging* (LiDAR) system and a land-based mobile mapping system. The system proposed by the authors was tested in a large-scale civil engineering project and compared to the traditional earthworks monitoring approaches. It was found to provide advantages, such as efficiency and reduction of the risk of overspending the budget. The obtained accuracy of the method reached 8–9 cm RMS. Kim et al. [120] proposed a UAV-based point cloud and BIM integration process for earthworks monitoring. The method was applied to a housing construction project to monitor the as-planned earthwork design and to create an earthwork execution plan. However, this would be difficult to achieve in practice as earthmoving solutions are constantly changing. Another study on the application of a point cloud to BIM was presented by Cho et al. [121] in which the authors proposed a method for automatic earthwork volume calculation based on a digital elevation model.

Recently, with the rapid development of 5G, digital twins, artificial intelligence and other technologies, researchers have been applying them to improve construction progress monitoring systems. For example, You et al. [122] presented an earthwork monitoring system for an unmanned bulldozer based on 5G technology. A communication system was developed for real-time data transmission between the unmanned bulldozer and the digital construction platform, thus ensuring safe and efficient construction. More studies on the capabilities of automated earthworks, focusing on excavation, were presented in [123, 124]. In a recent study, Rogage et al. [125] proposed a digital twin framework for monitoring earthworks during the construction phase of infrastructure projects. The system is composed of components such as IoT and BIM data, a programming interface and artificial intelligence. It can predict equipment utilization rates and productivity, detect the time spent on various tasks and visualize earthworks. Another study by Kamari and Ham [126] presented a vision-based stockpile volume computation method which automatically detects and segments objects in point cloud models by using the deep learning approach and performs 3D semantic segmentation. Although the method has potential for automating volumetric calculations, there are several limitations, such as poor performance in low-light conditions or adverse effects due to environmental changes and occlusion.

Unmanned aerial vehicles are not completely new to the construction industry, but their application in earthwork construction monitoring has only become more popular in recent years. The level of data obtained by UAVs is not inferior to data collected by traditional approaches on the ground, but, with the use of UAVs, up to 30 times greater distance can be covered in a day, thus making this technology a key

tool for monitoring the progress of earthworks in large-scale projects [127]. The effectiveness of drones is particularly evident when calculating the volume of the earthwork or monitoring specific areas at risk of landslides [128, 129].

Recently, several studies have been conducted on the topic of using unmanned aerial vehicles to monitor the progress of earthworks construction [130, 131, 132]. Akgul et al. [133] conducted a study on earthwork volume calculation comparing the traditional method using a GNSS receiver with a UAV-based photogrammetry technology in road projects. The results of the study showed that, in large projects, the use of a UAV provides much more efficient data acquisition while ensuring sufficient accuracy. In addition, a much higher density of UAV-measured points can provide more reliable results than the use of the traditional GNSS approach. Another study by Moon et al. [87] compared a UAV-based photogrammetry method with the terrestrial laser scanning technology for earthworks. In the conducted study, the data acquisition time using photogrammetry was four times faster compared to TLS, and, although the accuracy of photogrammetry was lower, it was sufficient for earthworks. Seong et al. [134] compared fixed-wing and rotary-wing UAVs with the objective to estimate the volume of earthworks. Although both methods used different ground sample distance (GSD) values in the experiment, the results showed that the difference between the calculated amounts was not significant. In addition, it was observed that, with an increase in the size of the GSD, the volume of earthworks increases. The UAV-based surveying technology provides time and cost advantages for monitoring the progress of earthworks construction. However, different aerial photogrammetry methods have different workflows and may have a significant error in the calculation result of the volume of earthworks, which may be caused by various factors [114, 135]. Kim et al. [120] emphasized the importance of the photogrammetry process and identified several factors affecting the photogrammetry accuracy, such as image overlapping rates, surface materials, or low image resolution. They highlighted GCPs as the most influential factor. Kavaliauskas et al. [135] analyzed different workflows for UAV-based photogrammetry, including a method based on GCPs, *Post-Processing Kinematic* (PPK) and *Real-Time Kinematic* (RTK). The conducted study compared the influence of the aforementioned factors on data accuracy considering different UAV-based photogrammetry methods and highlighted the effectiveness and reliability of the PPK approach for earthworks monitoring. Park and Jung [136] performed earthwork volume calculations by using a UAV-based LiDAR system and UAV-based photogrammetry. After calculating the volume at the survey site, the results calculated by the UAV-based laser scanning technology showed a slightly larger difference from the GNSS survey results compared to the UAV-based photogrammetry. Although UAVs with LiDAR are suitable for monitoring the progress of earthworks and have some advantages, such as the ability to penetrate foliage, this technology is currently not a popular choice in the construction industry due to its relatively high cost and a lower accuracy compared to UAV-based photogrammetry methods [127].

1.1.4. As-planned vs. as-built construction

Over the past decade, the interest of researchers in the topic of construction progress monitoring has been growing annually, while mainly focusing on

technologies such as BIM, laser scanning, or photogrammetry [137]. Monitoring the progress of construction earthworks often only involves the calculation of volumes and is therefore a relatively simple process, while monitoring building structures requires more effort, as various building elements must be identified from the point cloud by comparing the as-built point cloud data with the corresponding as-designed BIM model [116]. When automating the monitoring of construction progress, it is important to consider the following steps, such as capturing the existing building data, and performing as-planned and as-built data alignment and integration into a single model [138, 139]. It is also important that the obtained point cloud data should meet the quality requirements for the application area. The efficiency and accuracy of as-built data capture depends on the method used and the experience of the engineer performing the measurements, which can influence under- or over-quality of the data. Rebolj et al. [86] examined point cloud quality requirements for the automation of building progress monitoring based on the identification of building elements. The research results showed that the quality of the point cloud data obtained by photogrammetry may not meet the efficiency requirements, as some type(s) of elements may remain unidentified or misidentified.

As previously reviewed, one of the most reliable methods in terms of accuracy is to capture as-is building data from a terrestrial laser scanner in the form of point clouds, but there has also been considerable research into photogrammetry, mobile laser scanning, and other techniques to automate progress monitoring based on efficiency requirements, cost, and the nature of the application. Masood et al. [140] proposed a low-cost and low-labor monitoring approach for multi-building construction site by using crane-mounted cameras and photogrammetry techniques. The study aimed to align as-is point cloud data of construction site with the as-designed model by converting 3D alignment to 2D. By using a point-to-point *Iterative Closest Point* (ICP) algorithm, the authors first aligned the xy projections and then the yz projections of the top and façade of the building. Although the method offers automated alignment, it has drawbacks, such as the cameras do not cover the full construction site, point cloud and BIM model scales are slightly inconsistent, or irregular building shapes may affect alignment accuracy.

Data alignment is a critical process for monitoring the construction progress based on as-built point cloud data and the as-designed BIM model. The well-known classical ICP method can be used to align this type of data [141, 142]. This method is generally used to co-register two point clouds, and it performs best when the source point cloud is close enough to the target point cloud. The ICP algorithm is designed to find the optimal rigid transformation that can refine the alignment, by assuming that point clouds are already roughly aligned, and it iteratively approximates the correspondences between points by searching for the closest distance between them, thereby improving the alignment results incrementally. Research studies have introduced several variations based on ICP, such as Sparse ICP [143, 144] and Go-ICP [145], to address the more difficult task of global registration. Fontana et al. [146] tested ICP, *Generalized-ICP* (G-ICP), *Normal Distributions Transform* (NDT) and *Probabilistic Point Cloud Registration* (PPCR) algorithms for local registration problems and a TEASER++, Fast Global

Registration and simple Random Sample Consensus (RANSAC)-based approach for global registration problems.

He et al. [147] proposed an ICP algorithm based on the point cloud geometric features such as density, curvature, or surface normal. Their algorithm uses these features to search for matches between the point clouds. Bosché [148] and Bueno et al. [149] used a plane-based registration approach to solve the coarse registration problem by extracting planes from a laser scanning point cloud and from a 3D mesh model. Typically, the as-built point cloud model is in a different coordinate system is compared to the BIM model, which makes the alignment of the datasets challenging [150, 151]. Kaiser et al. [152] presented an automatic co-registration approach for aligning photogrammetric point clouds and images with the BIM model when coarse alignment is not required. To calculate the transformation parameters, the authors extracted 3D lines from the images and mapped them with planes extracted from the IFC model by using the building model as a reference for co-registration. However, the proposed method has several limitations, such as the factor that high-quality textured images are required to extract the lines, and uniform white walls have a negative impact on feature point detection.

Registration of BIM models and point cloud data presents additional challenges, as the data is presented as a completely different file structure [139]. Previous studies tended to focus more on the laser scanned point cloud alignment with BIM models expressed in 3D CAD or triangulated mesh formats [109, 153]. However, with the recent development of construction technologies, studies comparing IFC with laser scanning and photogrammetric point clouds are more relevant for automated object detection from the perspective of progress monitoring. For example, Krijnen and Beetz [154] presented an IFC schema extension to integrate point cloud data obtained from laser scanning with an IFC model.

After data alignment, another important process for progress monitoring is the automated identification of objects based on captured as-built data against the as-designed model. There are several possible options to execute this process, such as comparing the point cloud to the BIM model [155, 156], or converting the point cloud to the BIM model [157, 158]. The latter option is more complex as it typically requires segmentation and classification of point cloud model elements, and also often requires the application of machine learning, deep learning, as well as other sophisticated approaches [159, 160, 161].

Mahami et al. [162] proposed a construction progress monitoring method using close-range photogrammetry and computer vision. To generate the as-built BIM model, the authors converted the point cloud to a triangular surface mesh, and, by using this mesh model, generated a CAD model that could be compared to the as-planned model. Macher et al. [163] presented a framework for 3D reconstruction of building interior structures from point clouds. For the integration into BIM software, the walls and slabs from the point cloud were generated in the IFC format, by using .obj (Wavefront) as the transition format from the point cloud to IFC. Another approach of IFC reconstruction from point clouds was presented by Bassier et al. [164]. The study was based on the reconstruction of the wall geometry from unstructured point cloud data. Although Scan-to-BIM methods look promising, they

still require significant manual intervention and are sensitive to occlusion and noise in the data [165].

Bariczova et al. [166] presented a wall geometry verification method using TLS point cloud data and an IFC model. The proposed approach compares the as-designed model with the as-built point cloud data by performing detailed segmentation and verifies the structural elements by deriving the geometry from the IFC file. In another study, Erdélyi et al. [167] also used regression models and detailed segmentation and proposed a methodology to verify building elements – such as walls and columns – by comparing photogrammetric and TLS point cloud data with the as-planned IFC model. Meyer et al. [168] presented a voxel-based approach for indoor construction progress monitoring, which compares the TLS point cloud data and the BIM model. Another study by Ibrahimkhil et al. [106] proposed a construction progress monitoring methodology comparing as-planned BIM and as-built BIM models. In the study, the authors used mobile laser scanning to capture as-is data and extracted the objects of interest from the resulting point cloud. The point cloud was aligned with the as-designed BIM model to create an as-built BIM model. An as-built BIM model was created by aligning the point cloud data with the as-designed BIM model by using an Autodesk Revit software tool. Kavaliauskas et al. [139] used TLS and mobile laser scanning technologies to acquire data and performed automated object identification by extracting the vertices of IFC elements and thus obtaining the as-designed point cloud data which was compared with the as-built point cloud data.

Several construction progress monitoring studies have been conducted, focusing on the comparison of the building model with the point cloud data obtained by photogrammetry approaches. For example, Tuttas et al. [169] captured images of the entire construction site by using hand-held terrestrial cameras to validate BIM components against the resulting point cloud data to assess whether the building elements have actually been built or not. Another study by Tuttas et al. [170] investigated hand-held camera and UAV-based photogrammetry approaches by focusing on data capture techniques and as-built point cloud data as-designed BIM model co-registration. Recently, Meyer et al. [171] proposed a geometric BIM verification method for indoor construction by using an *Apple iPhone*, *DJI Inspire 2 UAV*, and a *Sony Alpha* hand-held camera. The accuracy of the latter methods was found to be sufficient to verify the building elements, but not when millimeter-level accuracy is required. However, in some cases, the deviations were too large due to insufficient measurement, and the process itself requires extensive effort to make accurate and reliable measurements.

Several studies have been conducted focusing on UAV-based approaches for construction progress monitoring by comparing UAV photogrammetric data with the BIM models of buildings. Anwar et al. [172] proposed a framework based on volumetric comparison between a BIM-based *Autodesk Revit* model and a 3D model in the .obj format generated from UAV data. In the presented approach, the UAV was flown at heights of 20, 30 and 50 meters while using different camera angle settings to capture images of a single-story residential apartment building. However, due to the data quality, data acquisition altitude, as well as some other factors, errors

could not be avoided, and the average accuracy of measuring the control points was found to be about 12 centimeters in all the studied cases. Another study by Qu et al. [173] used a UAV-based oblique photogrammetry approach for automated construction progress monitoring in a construction project of a triangular column structure 70-meter high chimney building by flying at an altitude of 100 meters. However, the proposed automated process suffers from several drawbacks, such as the occurrence of holes in the photogrammetric model due to geometric distortion or the need for manual intervention for geometric corrections. In addition, when comparing the as-built photogrammetric model to the as-planned BIM-based model, there are challenges to compare the planes inside the exterior structures, because the UAV camera cannot capture them due to occlusions. Although the application of UAVs inside a building is limited, future developments in autonomous indoor UAV technology have potential for automating indoor construction progress monitoring in terms of safety and efficiency [127, 171].

Recent studies have investigated the feasibility of automatically updating the as-planned BIM model to reflect the as-is conditions of the building by using laser scanning and parametrization techniques. Yang et al. [174] proposed an *Autodesk Revit*-based BIM model generation approach for steel structures using *Dynamo*. However, the study has several limitations, such as the fact that the point cloud segmentation process is carried out manually, and the study only covered four common types of structural components. In another study, Wang et al. [175] presented a parametric BIM generation method for *Mechanical, Electrical, and Plumbing* (MEP) elements by automating the process of detecting and modelling regular and irregular MEP elements. The drawback of this method is that if the directions of the MEP components are not aligned beforehand with the main directions of the building, detection challenges may arise. Rausch and Haas [176] proposed an automated parametric approach focusing on updating the shape and pose of BIM elements from laser scanned point clouds. The presented work focused on automatic BIM updating to fit the as-built geometry of concrete foundations.

Researchers have conducted a number of studies on effective construction progress monitoring by using diverse and complex methodologies with multiple concepts and technologies based on computer vision [177], vision-based deep learning [178], machine learning [179], and other technologies. For example, Gordon et al. [180] proposed a Scan-to-BIM methodology for the automated detection of BIM elements by using photogrammetry and laser scanning with the *Apple iPhone 12 Pro*. In order to determine the possible locations of BIM elements, the authors used the currently existing statistical and computer vision techniques. The quality of the output of this method was affected by occlusion, noise, and missing data. Data noise can be caused by various measurement errors [181]. However, one of the main challenges for object detection is occlusion. Braun and Borrmann [182] observed that the use of deep learning or machine learning techniques has the potential to improve object detection in construction environments through image analysis, but this approach necessitates a significant number of images to be labelled, which is a manual and time-intensive task. Therefore, the authors proposed an automatic labeling methodology based on

information obtained from the photogrammetry process and object information extracted from the BIM model. Nevertheless, there is a noticeable gap between computer vision techniques for indoor object detection and outdoor structure monitoring related to occlusion, lighting conditions, and camera movement [183].

Several other point cloud-based object recognition approaches have been introduced. They use automated segmentation and classification, such as automatically segmenting static and mobile laser scanning point clouds and creating 3D surfaces [184], voxel-based segmentation of 3D point clouds, where a huge amount of training data is not required, which allows to significantly save time for creating labeled datasets, thus providing a significant advantage over the deep learning and machine learning techniques [185], as well as some other approaches [186, 187, 188].

1.2. Identification of Potential Applications for Progress Monitoring

In the course of the literature review, it is important to define the scope of construction progress monitoring and to determine the data acquisition tools and methods that will be used for experimental research. Next, by extracting the most relevant information and considering its practical applicability, the literature review aims to provide clarity and understanding in choosing the right tools and methodology for research experiments.

1.2.1. Construction phases

The construction process consists of several phases required to complete the project. However, the understanding of construction stages can be somewhat ambiguous. For example, some stakeholder-run and scientific studies consider construction phases as pre-construction, construction, and post-construction [189, 190]. The pre-construction phase includes initiation, planning, bidding, specifications, scheduling, etc. The construction phase is conducted when construction is executed to meet the project goals, and it includes all aspects of construction. Meanwhile, post-construction is considered as the closing phase of the project. Construction phases can also be divided into design, operation and management and other phases [191].

This thesis investigates the monitoring of construction progress during the construction phase. In order to effectively manage complex construction projects, it is necessary to divide them into phases based on the construction process. Since the construction phase includes all aspects related to construction execution, this phase can be divided into several phases, such as earthworks, structural construction, MEP, completion, and other phases depending on the nature of the works [192, 193]. Based on a general approach, earthworks, structural works, MEP and finishing works can be named as the main phases of construction execution (Figure 6).

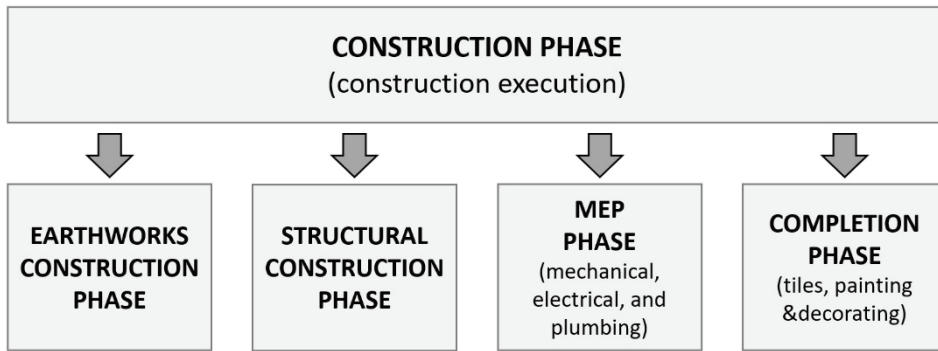


Fig. 6. Main phases of construction execution

1.2.2. Practical applicability of data acquisition for construction progress monitoring

There are several different data acquisition technologies that can be used for automated construction progress monitoring, such as the *Geographic Information System* (GIS), the *Global Positioning System* (GPS), barcodes, *Radio Frequency Identification* (RFID), laser scanning, photogrammetry, videogrammetry, etc., but all these technologies can be divided into four main categories, such as laser scanning, site images, site videos, and tracking and sensing [105].

However, the results obtained by videogrammetry are greatly influenced by factors such as the camera quality, the video quality, the lighting conditions, and other factors, and the approach itself does not ensure sufficient accuracy compared to laser scanning or photogrammetry [194, 195].

A tracking and sensing technology, such as RFID, is more time-saving compared to the traditional visual inspection, but it is relatively expensive and runs into challenges, such as RFID systems being not very accurate; also, object recognition problems arise if several tags need to be detected at the same time, or if certain materials (such as metal and concrete) cause interference [196, 197].

For construction progress monitoring, photogrammetry is a cost-effective and efficient approach to obtain reasonably accurate point cloud data [137], while laser scanning is considered one of the most reliable methods to ensure the accuracy [72]. Advanced computer vision and machine learning techniques can be integrated to improve the results, but these are complex methods with some limitations, such as the need to manually label images or objects, along with many other factors that affect the performance of these approaches [183].

The application of as-is construction data in the form of a point cloud is widely studied in the scientific community. Most studies investigated point cloud data, by applying it to 3D modelling, geometry inspection, and then to construction progress monitoring [116]. However, all of these mentioned application methods are interrelated and are important for improving construction progress monitoring. Collecting as-is information in the form of a point cloud is a practical and promising approach in the construction industry. Compared to the traditional approaches, a significantly larger amount of data is acquired within a much shorter timespan, and the geometry of the obtained data can be compared with the as-planned 3D model.

Therefore, such data has great potential to improve the effectiveness of progress monitoring through automation.

Various technologies, such as photogrammetry, terrestrial laser scanning, total stations (TS), or GPS receivers, can be used to control earthworks. TS is considered to be one of the most accurate methods for making measurements in construction and is usually used in practice for precise measurements of buildings, roads, bridges, and other measurements where millimeter-level accuracy is required. TLS in earthworks can achieve a similar accuracy and a significantly more time-efficient data acquisition efficiency compared to TS, while the GPS-RTK receiver may have a slightly lower accuracy [78]. However, TLS is not a popular solution for earthwork monitoring in building construction projects because it is a relatively expensive technology, the time efficiency of data acquisition can be greatly affected by the ground conditions due to the line of sight, and the accuracy can be negatively affected by the vertical angle of the instrument due to uneven ground. UAV-based LiDAR systems do not provide higher accuracy for earthworks while being more expensive. Meanwhile, in the construction phase, UAV-based photogrammetry is cost-effective, and the data accuracy is comparable to the traditional earthwork survey approaches.

Despite being relatively expensive, TLS is practically the most reliable way to capture structural data for building construction, as the accuracy of the data is of particular importance here. However, this technology is not efficient in terms of time and when bypassing line-of-sight obstacles. UAV-based photogrammetry has limitations in terms of accuracy and obstacles in capturing data inside a building, which makes the technology difficult to apply in practice. In the future, autonomous UAV technologies could be applied to capture building interior data. However, in general, when using photogrammetry indoors, limitations, such as lighting conditions, remain. A mobile scanning technology could be practically used to monitor the construction progress, improving time and occlusion avoidance factors, but it would result in a lower data accuracy.

Monitoring the MEP progress by using point clouds obtained from photogrammetry or laser scanning is not practical for several reasons. At this construction phase, for example, laser scanning can provide information on the location and orientation of MEP components, but it is necessary to ensure that the data is accurate, which can be a time-consuming process. Also, obtaining accurate data requires good access to the objects to be scanned, and certain locations may be difficult to access or even completely inaccessible at this phase of construction. Additionally, progress monitoring during this phase is limited by occlusion, where the view of one pipe, for instance, is blocked by other pipes, and small components, elbows, T-connections, or partially hidden objects may thus not be detected [156]. Therefore, laser scanning or photogrammetry methods for monitoring progress during the MEP phase may be impractical.

During the completion phase of indoor construction, progress monitoring by using photogrammetry or laser scanning approaches also has several challenges that may reduce benefits of this process. During this construction phase, most of the work is related to aesthetic improvements, the space can be cluttered with various

objects, occupied by furniture, or finishing materials, which makes it challenging to capture all surfaces and obtain detailed and accurate as-is data. In addition, the reflection and texture of certain materials, a low resolution, or the lighting conditions can also affect the accuracy of the data, and the as-designed BIM model is required to be very detailed [198]. Capturing as-is data under such conditions can be time-consuming and can increase the cost, which is bound to make the monitoring process inefficient and impractical.

1.2.3. Scope definition for the methodology and experimental research

As mentioned above, the construction phase can be divided into four major groups of works, such as earthworks, structural construction, MEP, and finishing works. Photogrammetry and laser scanning in the form of a point cloud are among the approaches with the greatest potential for data acquisition and for improving the efficiency of construction progress monitoring. Currently, the application of these technologies in MEP and finishing works is very limited and may provide little practical benefit. Therefore, the scope of this thesis is limited to monitoring the progress of earthworks and structural construction by applying point cloud data derived from UAV-based photogrammetry and laser scanning. Data capture techniques were used for the experiments based on practical application. Considering the practical application of technologies for monitoring progress in the construction phase, the methodology and scope of the experiments are shown in Figure 7.

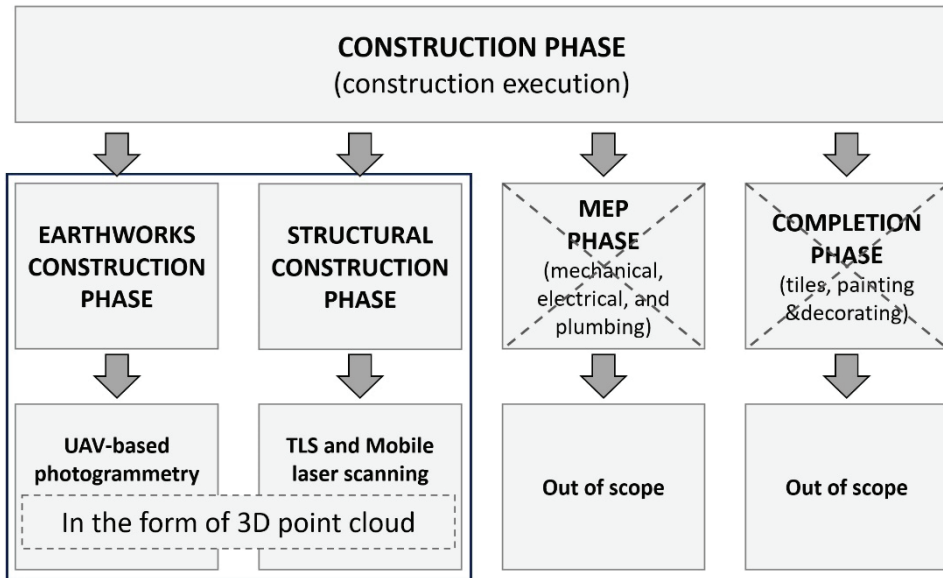


Fig. 7. Methodology and scope of experiments

As shown in Figure 7, the scope of this study consists of two major categories of works in the construction phase: earthworks and structural construction. MEP and completion works were not considered in this research.

Earthworks control is an important process during the construction execution, which can have a significant impact on the cost of the entire construction project. However, in practice, the process of earthworks is still often controlled by counting the waybills of the incoming and outgoing quantities, visual inspection, or, to some extent, by performing manual measurements. It is not uncommon for disagreements to arise between the contractor and subcontractors regarding the quantities of work performed. In addition, manual measurement can be unsafe in many cases, as a worker has to climb into trenches and onto slopes. Considering the practical applicability, UAV-based photogrammetry is used for the progress monitoring experiment in this construction phase.

Another important phase is the construction of building structures. Although nowadays almost every construction has the as-planned BIM model, but the monitoring of work progress is also often done manually. In this construction phase, the most appropriate way is to monitor the progress by comparing the as-built data with the as-planned model. Since the identification of structural elements requires accurate data, the TLS technology was used in the experiment considering its practical applicability. Additionally, a mobile laser scanning technology has been tested, which may also be a practical option when a lower accuracy is acceptable.

Based on previously published studies, this thesis examines automated construction progress monitoring by using photogrammetry and laser scanning techniques during the construction phase. In the construction phase, these technologies are practically applied in earthworks management and building construction. For works such as MEP or finishing works, the application of these technologies in real construction conditions has no practical significance. There is a general opinion that, during the construction phase, it is most effective to use UAVs to monitor the progress of earthworks, and to use static laser scanners to monitor the construction progress of the building. This is because earthworks construction projects are typically large-scale, and, in building construction, data accuracy is of particular importance. In terms of cost-effectiveness, UAV-based photogrammetry is a popular choice for earthworks management. Previous studies examined various UAV-based photogrammetry techniques, such as PPK and RTK, and used a variety of UAVs ranging from standard to modified unmanned aerial systems. However, there is a lack of research considering the practical applicability and comparison with the traditional methods in terms of efficiency, reliability and accuracy. Therefore, this thesis explores different advanced photogrammetry workflows and uses such UAVs which are being widely used in the industry. This allows evaluating the performance of different workflows and comparing the impact on the traditional nature of work under real construction conditions. On the other hand, in building construction, the main challenges arise from the constantly changing environment and occlusion at construction sites. Obtaining accurate, high-quality data under these conditions is challenging, and point cloud data often contains noise, outliers, or missing information. First, it poses challenges for data alignment. In addition, under such conditions, the ability to capture the full surface of the object with a laser scanner is limited, which makes the object detection process challenging. Based on the challenges mentioned in previous studies, the present thesis undertakes to

develop a methodology which shall allow to align and integrate the scan data with an IFC model and automatically identify objects in a 3D point cloud even when they are not fully scanned, or when the data contains noise and outliers.

1.3. Chapter Conclusions

1. A number of studies conducted show that the application of 3D point cloud data in the construction industry, including integration into the BIM technology, has grown over the past decade and is still a popular topic among the researcher community. There is a general consensus that photogrammetry and laser scanning technologies using point cloud data contribute to more effective monitoring of the construction progress. However, it has been recognized that the level of automation of this process is limited due to the ever-changing construction environment, and the problem of occlusion still remains a major challenge.
2. In construction, works are divided into many different categories, depending on their nature, and therefore the construction process requires clear understanding of its phases. The construction phase typically consists of work categories, such as earthworks, structural construction, MEP and completion works. Effective monitoring of the construction progress during the construction phase is critical to the successful completion of a construction project.
3. UAV-based photogrammetry can be a cost-effective and efficient way to obtain reasonably accurate point cloud data during the earthworks construction phase. Meanwhile, laser scanning is considered one of the most reliable methods for ensuring accuracy in the structural construction phase. Both approaches can produce data in the 3D point cloud format. However, the use of these techniques in the MEP and completion phases has several limitations that may provide only limited practical benefits to the progress monitoring process. According to the above-mentioned aspects, the methodology and scope of the experiments have been defined.
4. Earthworks management during construction is an important aspect in determining the most cost-effective construction method. This consideration is significant throughout the construction phase. The reported accuracies of UAV-based photogrammetry approaches are similar to those of the conventional methods using GNSS receivers. However, further investigation is still needed in terms of reliability and efficiency under different workflows.
5. BIM is generally underutilized for earthworks in building construction projects. Therefore, point cloud to point cloud comparison or point cloud to digital elevation model comparison methods are commonly used to automate the progress monitoring process. Meanwhile, BIM, especially IFC models, are widely used in building construction. Here, progress monitoring requires a comparison between IFC and a 3D point cloud, which is a challenge due to the alignment and integration of data from different structures.

2. APPLICATION IN THE EARTHWORKS CONSTRUCTION

In this thesis, construction progress monitoring experiments shall be conducted by analyzing UAV-based photogrammetry and 3D laser scanning technologies. Although these technologies are based on point clouds, their workflows, methods, tools and practical applications differ and are used to monitor different types of work during the construction phase. Accordingly, experimental research objects, methods and tools are described in separate chapters to facilitate the reader's understanding. Chapter 2 presents the research of construction progress monitoring when using the UAV-based photogrammetry technology for earthworks management, and describes the research object, methods, tools, experimental results, and conclusions of the chapter. Meanwhile, Chapter 3 proposes a methodology for monitoring the building construction progress by applying 3D laser scanning and BIM technologies. In Chapter 3, the research object, methods, tools, results and conclusions are presented for the case of the laser scanning experiment.

This chapter explores traditional and UAV-based photogrammetry workflows for automated progress monitoring during the construction phase of earthworks. A research article with the methodology and results of this experimental study has been published by Kavaliauskas et al. [135] in a scientific journal. Part of the experimental research results have been presented at a scholarly conference [199].

2.1. Description of the Research Object

In the case of construction progress monitoring based on UAV photogrammetry, different data acquisition workflows were analyzed, and the accuracy and efficiency of data acquisition were compared. Considering the findings of the literature review, UAV-based photogrammetry in construction can be most effectively applied in monitoring the progress of earthworks. Therefore, in this case, the tested site was a 36 ha (ca. 89 acres) quarry in Lithuania, in Trakai District, which contained gravel and crushed stone stockpiles with an approximate height of up to 5 m (Figure 8). This site was selected for the research due to its relatively large scale to assess the efficiency and accuracy of data acquisition. The research required several UAV flights and safety considerations. Therefore, it was considered that the site was not in operation at the time of the investigation.



Fig. 8. Testing site mesh model processed with *Bentley ContextCapture* software

Additionally, the UAV-based photogrammetry approach was tested for progress monitoring in a real industrial building construction project. The construction site was located in Kaunas City and covered an area of approximately 16 ha (ca. 39.5 acres). The project included the construction of a factory, which also required a substantial amount of earthwork, as shown in Figure 9. The area of this site was smaller compared to the main study at the quarry site, but the calculations of the quantities of earthworks were more complex and more concentrated. This research object was intended as a follow-up study to explore the practical benefits of UAV-based photogrammetry for automated construction progress monitoring.



Fig. 9. Testing site mesh model processed in the *Propeller Aero* platform

2.2. Methods and Tools

This experiment explores three different automated data acquisition workflows using UAVs based on their practical applicability in construction. The automated workflows were compared with each other and with the traditional approach used in the current practice. First, measurements were made by using a traditional method that was used as a baseline for evaluating automated approaches, considering the impact on the nature of the work in terms of accuracy, reliability, and time.

In the experimental study, a ground-level survey with a GNSS-RTK receiver was considered as the traditional approach. Data processing in this case was performed with *Autodesk Civil 3D* software. Meanwhile, UAV-based photogrammetric workflows, such as Post-processing kinematic, Real-time

kinematic, and based on GCPs were used for automated data collection. This study relied on photogrammetric workflows rather than on comparing photogrammetric software. Many photogrammetric software tools have already been explored and compared in scientific studies. Therefore, professional and advanced photogrammetry software was selected for the study, which was based on the analyzed workflows. Data from RTK and GCPs-based workflows was processed by using *Bentley ContextCapture* software, and the *Bentley Descartes* software tool was used for data analysis. It is worth noting that *Bentley ContextCapture* software has since been renamed, and it is currently called *Bentley iTwin Capture Modeler*. Meanwhile, the data obtained during the PPK workflow was processed and analyzed on the *Trimble Stratus* and *Propeller* platform. The main features of the software used in the experiment are presented in Table 1.

Table 1. Main features of the software used in the experiment

No	Software	Main features
1	Autodesk Civil 3D	Civil engineering and infrastructure design: <ul style="list-style-type: none"> • Allows creation of detailed surface models representing the existing terrain. • Integration of survey data. • Earthworks calculations such as cut-and-fill volumes.
2	Trimble Stratus, powered by Propeller	Cloud-based platform for analyzing UAV data in construction: <ul style="list-style-type: none"> • UAV data integration. • 3D visualization of construction site conditions and construction progress. • Earthworks calculations such as cut-and-fill volumes.
3	Bentley ContextCapture	Reality modeling from photographs and/or point clouds: <ul style="list-style-type: none"> • Allows creation of highly detailed 3D models. • Terrain, building and infrastructure modeling for engineering and construction projects.
4	Bentley Descartes	Reality modeling data processing software: <ul style="list-style-type: none"> • Processing, editing and vectorization of raster images for use in CAD and GIS applications. • Allows working with reality data, such as raster, scalable terrain models, point clouds and reality meshes. • A volume calculation tool for comparing two meshes or a mesh and an element.

Each method was analyzed by performing two flights at 74 m and 100 m altitudes. The height of data acquisition was chosen based on the lower and upper limits according to the manufacturers' recommendations and practical applicability. The altitude of the flight depends on several factors, such as the type of terrain, the specifications of the camera, the purpose for which the data will be used, etc. Determining the flight altitude requires consideration of the terrain elevation and various obstacles, such as cranes, transmission towers, or tall buildings. For monitoring the progress of earthworks, it is fundamentally important to choose the optimal flight height. Flying at low altitude results in a smaller *Ground Sample*

Distance (GSD), which results in higher resolution images. GSD represents the distance between the center points of each pixel on the ground, which also corresponds to the real-world size of one pixel in the images. A photogrammetric model cannot be more accurate than the size of each pixel. For example, when collecting data with a *DJI Phantom 4RTK* from a height of 30 m, a GSD of 0.82 cm/px is obtained, which means very high resolution images. Although high-resolution images are available that can produce a more detailed photogrammetric model, in practice, UAV-based photogrammetry is unlikely to achieve an accuracy higher than 2 cm horizontally. In addition, when flying at a low altitude, especially for large-scale projects, more effort is required to ensure a sufficient photo overlap, a significantly larger amount of data is obtained, and a slower flight speed must be set. This affects the efficiency of data acquisition without substantially improving the accuracy of the data. Meanwhile, when flying above 100 m height with the same UAV, the quality of the photos can already have a greater negative impact on the accuracy of the photogrammetric model. More details about the flight altitudes and other flight parameters used in this study are given in Chapter 2.3.

The experimental study consists of seven data sets which were analyzed by comparing the accuracy of the control points and the estimation of quantities, considering the efficiency of the earthworks control process and the reliability of the data. The experimental scheme is shown in Figure 10.

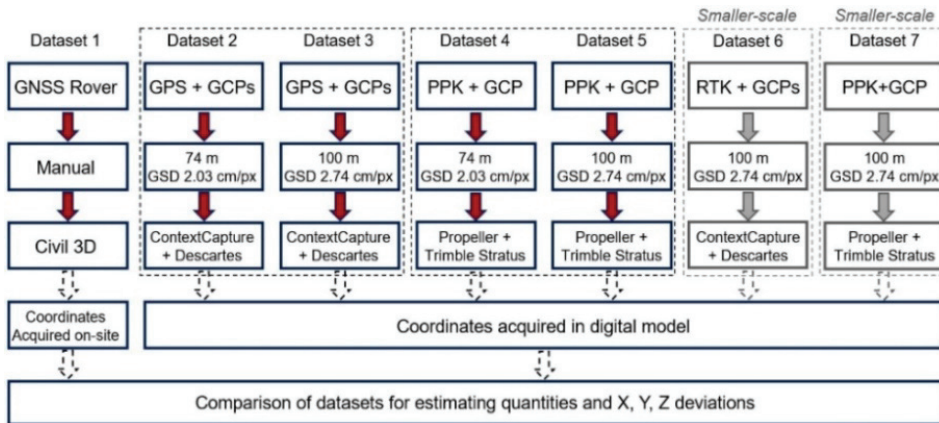


Fig. 10. Experimental research scheme

Control points are used to determine the scale of the photogrammetric model. They have a critical influence on the model accuracy. During the experimental study, 11 markers were used, which were placed in the test area to serve as ground control points to establish the scale and check the accuracy of the model. The boundaries of the researched area and the layout of the control points are shown in Figure 11a. The assessment of the earth volume was carried out within the boundaries marked in blue. In the experiment, 0.6×0.6 m control points made of plywood with a black and white checkerboard pattern were used (Figure 11b). In addition, the PPK method used *Propeller Aeropoint 1.0* smart control points that served as base stations (Figure 11c).

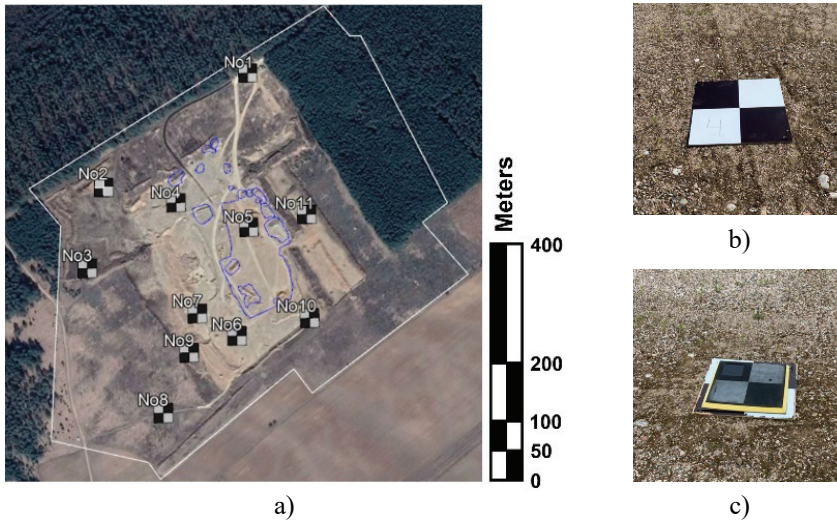


Fig. 11. Testing site scheme: a) site boundaries and CPs scheme. Blue boundaries indicate areas of traditional survey; b) self-made CP; c) *AeroPoint 1.0* base station

During the experiment, a GNSS-RTK receiver and three unmanned aerial vehicles were used to acquire the real earth surface data. These measuring devices were chosen based on their practical applicability. A GNSS receiver is commonly used for earthwork measurements in construction where millimeter-level accuracy is not required. Meanwhile, *DJI Phantom 4 RTK* is one of the most popular UAVs used in the construction industry for the mapping and surveying purposes due to their relatively low cost along with the ability to obtain reasonably accurate data. In the experiment, the *DJI Phantom 4 PRO* aircraft was also tested, which does not have an on-board RTK technology, and its price is approximately three times lower compared to the *DJI Phantom 4 RTK* version. The measuring devices that were used in the experiment are listed in Table 2.

Table 2. Main data acquisition equipment used in the experiment

No	Device	Device name	Main features
1	GNSS receiver	Trimble SPS985	RTK fixed
2	Unmanned aircraft	DJI Phantom 4 RTK	On-board RTK technology, 20 MP camera, mechanical shutter speed
3	Unmanned aircraft	DJI Phantom 4 RTK	On-board RTK technology (RTK disabled), 20 MP camera, mechanical shutter speed
4	Unmanned aircraft	DJI Phantom 4 Pro	Global positioning system, 20 MP camera, mechanical shutter speed

2.3. Data Acquisition Workflows for Civil Construction

In this experimental study, separate data acquisition devices were used for each data acquisition workflow. First, the earth surface was measured manually by using a conventional GNSS-RTK receiver which is described in more detail in

Chapter 2.3.1. This was followed by flights using three different workflows and separate UAVs for each workflow to capture the ground surface data. A *DJI Phantom 4 PRO* unmanned aircraft was used to measure the ground surface based on the layout of the GCPs. This method is further described in Chapter 2.3.2. Two *DJI Phantom 4 RTK* unmanned aircrafts were used: one for the RTK approach, and the other aircraft for the PPK method with the RTK mode turned off. The RTK workflow is further described in Chapter 2.3.3, whereas the PPK approach is described in Chapter 2.3.4.

Each of the different UAV-based data acquisition methods was tested by using the same flight and camera settings. The optimal flight parameters were set based on previous studies [89, 90] and practical experience. With each approach, two flights were carried out at 74 m and 100 m above the ground level. The flight altitude significantly affects the possible flight speed and also the size of GSD. For the UAVs used in the experiment, capturing images from a height of 74 m yields a GSD of 2.03 cm/px, whereas capturing images from a height of 100 m yields a GSD of 2.74 cm/px. Regardless of the flight altitude, all the flight plans were set on a 2D photogrammetry nadir pattern for automated data acquisition (Figure 12a, b). In all cases, the image capture overlap was set to 80% for the frontal overlap and 70% for the side overlap, while the UAVs flight speed was set to 5.8 m/s. All UAVs used in the experiment had built-in cameras. When capturing data, the gimbal was set at an angle of 90° , the photo ratio was 3:2, and the distance shooting mode was selected. Capturing the surface of the ground by setting the gimbal at 90° is a common practice. Capturing straight-down images ensures the optimal ground coverage, minimizes distortion, and simplifies geometric calculations during photogrammetry processing. Other settings were as follows: camera sensor width 13.2 mm, sensor height 8 mm, focal length 8.8 mm, image width 5472 px, and image height 3648 px. The flights were conducted in the summer time under clear skies and sunny conditions. Since it was bright and sunny, the automatic shooting mode was being used. An additional, smaller-scale survey was conducted under winter conditions. The quarry was inactive during the experiments, which ensured that the ground base was not moved during the data capture.

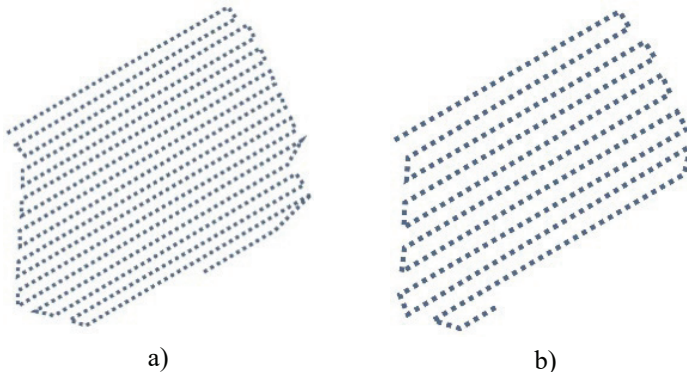


Fig. 12. Flight plans: a) at an altitude of 74 m; b) at an altitude of 100 m

2.3.1. Traditional method

Although various technologies such as photogrammetry, laser scanning, total stations, or GPS receivers can be used to control earthworks, the most common practice for earthworks in building construction projects is the use of a GPS or GNSS receiver. The main difference between GNSS and GPS is that GNSS allows the use of more navigation satellites, and it is therefore considered more accurate. In this experiment, a *Trimble SPS985* GNSS receiver with the RTK fixed precision type was being used. This measurement system uses the *Lithuanian POsitioning System* (LitPOS), which is the *Global Navigation Satellite System* infrastructure for Lithuania. At the time the experiment was being conducted, 26 LitPOS GNSS permanent reference stations were providing data for real-time and post-processing applications and were covering the entire territory of Lithuania [200]. These stations provide real-time calculated and error-corrected data from GNSS satellites.

Typically, the earth surface is measured manually by capturing x , y , z data points every few meters depending on surface curvatures. In this case, in the areas containing a flat surface, the distance between the measurement points ranged approximately between 10 to 15 m, while, when measuring stockpiles, the data points were captured every 1 to 5 m. In this way, 1108 x , y , z data points were captured in the measured area of 5549.55 m². By using this traditional approach, the data capture took approximately 6 hours. Considering the travel and rest time, it can be assumed that the ground-level survey of an area of this size can potentially take a full working day. A similar data capture time efficiency was obtained in a study by Abd-Elmaaboud et al. [78].

The measured area included 16 stockpiles of various sizes (Figure 13). The stockpile volumes varied from less than 100 m³ to more than 3000 m³, with a total volume of more than 10000 m³. The measured flat earth base and stockpile surfaces were later processed in *Civil 3D* software for further comparison with the data generated by automated workflows. Figure 13 also shows random locations of the cross-sections where the accuracy of the photogrammetric data and manual measurements will be evaluated.

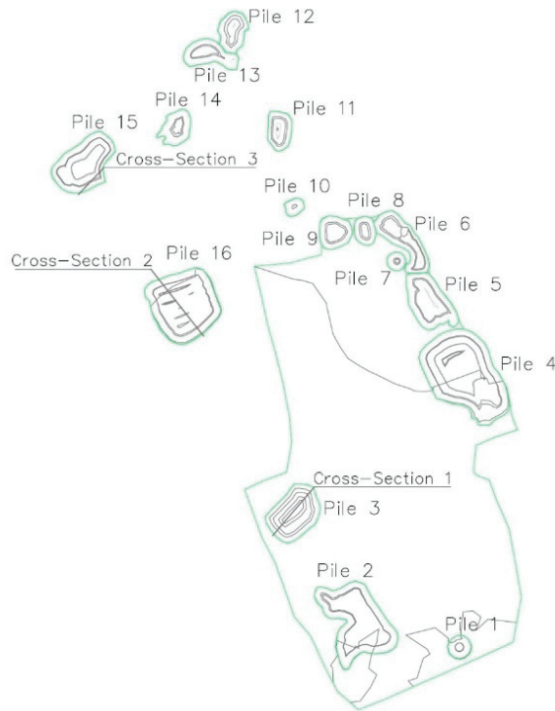


Fig. 13. Stockpiles for volume estimation and random cross-section locations

All horizontal x , y measurements in the experiment were performed in the *European Petroleum Survey Group* (EPSG) projection 3346 – *Lithuanian Coordinate System* (LKS-94). Vertical point measurements were performed in the *Lithuanian State Elevation System* (LAS07) by using the *Lithuanian Territorial Geoid Model* (LIT15G). Automated photogrammetric surveys using UAVs were also performed in the same coordinate systems, as the accuracy in this type of measurement is highly dependent on data alignment based on the coordinate system.

2.3.2. Ground control points-based approach

In this stage of the experiment, a *DJI Phantom 4 PRO* unmanned aircraft was used to capture the earth surface data. These aircraft do not have an integrated GNSS RTK antenna which would allow the system to directly geotag the positioning coordinates, by making use of ground control points critical to the accuracy of the reality model. GPS units built into drones are not highly accurate, and they may incur deviations of approximately up to 3–9 m from the actual x , y , z location being recorded. In this case, the placement of control points is particularly important to ensure the accuracy of the measurement, as the images obtained by the UAV need to be anchored to the ground. It is necessary to ensure that the number of the control points is sufficient, and that they are placed on the edges and inside the investigated area [90, 91]. However, implementing such a layout strategy under real construction conditions can be difficult and often impossible due to various obstacles, moving

traffic, or a built-up area. With these considerations in mind, 11 control points were placed at more or less random locations (Figure 11a).

However, the photogrammetric software vendor’s recommendations for placement distances between GCPs were being followed. For this type of survey, the recommended distance between control points is 20,000 pixels. In this experiment, two data acquisition flights were performed at 74 m and 100 m above the ground, which resulted in GSD values of 2.03 cm/px and 2.74 cm/px, respectively. Therefore, considering the pixel size, the recommended distance is approximately 400 m when flying at an altitude of 74 m, and approximately 550 m when flying at an altitude of 100 m. In the case of this experiment, the distances between control points fell within the recommended limits.

This approach used standard black and white checkerboard pattern control points that were measured by using the previously described traditional method by using a GNSS-RTK receiver. Control points measurement information is provided in Table 3.

Table 3. Control points measurement information

CP No.	Northing, m	Easting, m	Elevation, m	H. Precision, m	V. Precision, m
1	6050236.702	556234.258	162.661	0.008	0.013
2	6050043.436	555982.149	159.556	0.008	0.013
3	6049904.339	555953.424	159.463	0.008	0.014
4	6050013.152	556105.802	157.799	0.009	0.015
5	6049966.717	556230.278	156.111	0.009	0.016
6	6049781.284	556206.660	155.857	0.010	0.018
7	6049821.187	556140.183	152.670	0.010	0.018
8	6049656.291	556080.627	157.837	0.010	0.017
9	6049755.716	556125.198	157.208	0.011	0.016
10	6049807.246	556330.669	158.154	0.010	0.014
11	6049985.528	556330.097	155.408	0.010	0.015

2.3.3. Real-time kinematic workflow

Real-time kinematic workflows are widely available with the current drone technology, but questions remain as to how this technology differs from other UAV-based workflows in terms of time efficiency, the accuracy of data obtained, and the reliability of the method itself. RTK-enabled UAVs differ from the conventional aircrafts, such as the *DJI Phantom 4 PRO*, in that the RTK technology allows for accurate tracking of their positions and recording of GPS information during real-time kinematic processing. With this technology, the aircraft records GPS information and geotags images by recording the GPS location at the center of the image, thus facilitating accurate geospatial referencing. With the RTK method, fewer ground control points are required as the base station on the ground sends raw GPS data to the aircraft, thus determining its position relative to the base station. The GPS unit installed in the aircraft combines this information and, by making corrections, refines the position of the aircraft. However, this process has an important consideration that must be taken into account. This workflow requires

maintaining a constant connection between the base station and the UAV while the aircraft is gathering data, as the loss of the RTK signal makes the acquired data unreliable.

In this experiment, a *DJI Phantom 4 RTK* aircraft was used to capture data, and an aircraft radio controller with a LitPOS network RTK service was used as a base station to investigate the RTK workflow. The flight parameters of the aircraft were set according to other UAV-based workflows used in the experiment; also, the main camera settings, the flight height and speed were identical. This approach also uses control points previously located and measured by GNSS reception. Aspects of ground control point placement are evaluated later in the data processing phase. Except for the use of the base station, the data acquisition workflow remained largely unchanged until this stage of the experiment.

2.3.4. Post-processing kinematic workflow

The main difference between the Post-processing kinematic and the Real-time kinematic approaches is the processing workflow of how the base station data is processed for correction and accuracy. When using the PPK workflow, the GPS unit on the aircraft geotags the x, y, z coordinates of each image, while the base station records the position data with more accurate triangulation (Figure 14). The PPK workflow in this study was based on the *Propeller Aeropoint 1.0* smart GCPs, whereas the data collection and processing guidelines were developed by *Propeller Aerobotics Pty Ltd*. These Aeropoint GCPs are used as base stations to record GPS information. Based on the recommended guidelines at the time the experiment was being conducted, the PPK workflow in this experiment consisted of the following steps:

- 1) First, Aeropoint base stations were placed in the studied area. If the area falls into the Propeller Correction Network, then, the base stations can be processed and corrected automatically. In this case, this correction network was not supported in Lithuania, and therefore it was necessary to know the x, y, z coordinates of at least one base station. These base stations were placed on previously measured standard control points so that the coordinates of all base stations were known and could later be verified. The base stations were activated to gather GPS data and remained active for at least 45 minutes as required by the technology providers.
- 2) The UAV flight was launched approximately 15 minutes after the last base station was activated. The flight time must not be less than 10 minutes, and, if the survey area is too small, the flight mission should be paused at some point, and the aircraft should hover for the required time. In this case, the survey area was large enough that the flight times would exceed the recommended minimum data acquisition time.
- 3) After completing the UAV survey, the base stations must be disconnected from the GPS data acquisition process before being lifted off the ground. Once this was done, the automatic wireless networking technology (WiFi) signal search was immediately activated, and the data upload to the cloud-based platform began.

- 4) The next step is to upload the images obtained by the UAV to the same cloud-based platform. After uploading the images, the two GPS data sets were matched by using photo timestamps and post-processed by correcting the less accurate UAV onboard GPS data and providing accurate geotags for the images, thereby reconstructing the exact flight path.
- 5) After uploading the data from the aircraft and the base stations, it was necessary to specify the coordinates of one base station. After several settings and data checks, the final data processing was further done automatically on the cloud-based platform.

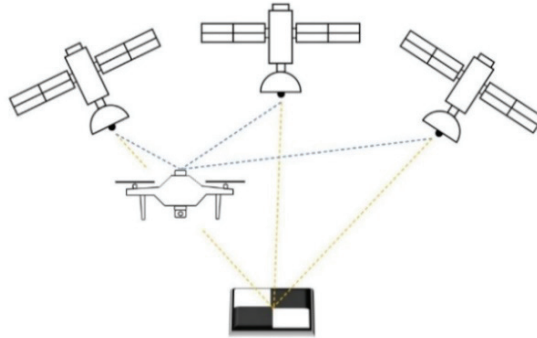


Fig. 14. Post-processing kinematic (PPK) workflow for recording Global Positioning System (GPS) information

As with the RTK approach, a *DJI Phantom 4 RTK* aircraft was also used to analyze the PPK workflow. Although the aircraft model is the same, it must be considered as a different device. The only difference in the flight settings compared to the RTK workflow is that the aircraft's RTK mode was disabled for the PPK workflow. This means that this experiment used an RTK aircraft with the RTK mode disabled. As in the other cases, when analyzing the PPK workflow, data was collected from heights of 74 m and 100 m. Flying at a lower altitude significantly increased the data collection time. With one battery, depending on the weather conditions, the aircraft can fly for approximately 20 minutes. Accordingly, the 74 m-high UAV survey required two flights of 18 and 19 minutes each, and resulted in 883 images in total. The details of this flight are listed in Table 4. Meanwhile, the 100 m altitude flight significantly reduced the data acquisition time as well as the amount of data acquired (Table 5). In all the analyzed cases, the flight time was the same, regardless of the workflow used in the experiment.

Table 4. 74-meter height PPK flight information

Flight number	Start date and time	End date and time	Number of images	Flight duration	GPS quality
Flight 1	9 July 2020, 12:29	9 July 2020, 12:48	450	19 min	100.00%
Flight 2	9 July 2020, 12:51	9 July 2020, 13:09	443	18 min	100.00%

Table 5. 100-meter height PPK flight information

Flight number	Start date and time	End date and time	Number of images	Flight duration	GPS quality
Flight 1	9 July 2020, 13:19	9 July 2020, 13:36	392	17 min	100.00%

The base stations used in the experiment record GPS data from satellites, and therefore environmental interference can affect the reliability of the data obtained. For this reason, it is fundamentally important to follow their placement guidelines. Since these smart base stations were placed on a part of the previously measured standard GCPs, those GCPs were selected for the placement of the base stations while taking into account that they were in an open area so that the GPS signal would be clear. The main considerations were to place the base stations on a flat surface and at an angle of 15° in an unobstructed open area. It is also highly important not to go far so that to see all active base stations, especially the one whose coordinates are known and will be used as the ground control point. If the base station is moved during the operation, the data may become unreliable. The timeline of 36 ha area data acquisition when using the PPK approach is shown in Figure 15a, b.

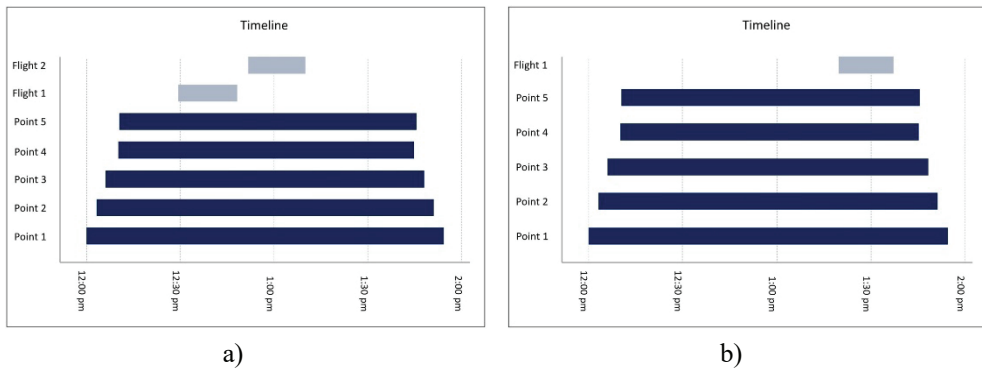


Fig. 15. PPK data acquisition timeline: a) data acquisition from a height of 74 meters; b) data acquisition from a height of 100 meters

2.4. Data Processing

The processing and analysis of the obtained 3D point cloud data was performed by using modern software solutions. First, the data from the traditional workflow was processed, and then the resulting surface model was imported into photogrammetric software for accuracy analysis and comparison. The surface model obtained by using the traditional workflow was used as a baseline for comparison with the photogrammetric models.

The manually measured x, y, z data points using the GNSS receiver were processed in the *Autodesk Civil 3D 2021* engineering software. Based on the imported data points, the software generated a *Triangulated Irregular Network* (TIN) surface. To calculate the volumes, the ground base surface and the surfaces of each stockpile are created separately. After creating the surfaces in the *Civil 3D*

software, the volume of the stockpiles was calculated by using the Volume Dashboard tool. This calculation method is widely used to control the quantities of earthworks. After the stockpile volumes had been calculated, the same TIN surfaces were imported into photogrammetric software to create cross-sections for accuracy analysis. An example of the imported TIN surfaces into photogrammetric software is presented in Figure 16a, b.



Fig. 16. An example of imported TIN surfaces into photogrammetric software: a) reality mesh in *Trimble Stratus* platform; b) TIN surface imported into *Trimble Stratus* software

The data acquired by the *DJI Phantom 4 PRO* aircraft was processed by using *Bentley ContextCapture 10.17.00.39* desktop software. Since this aircraft does not have an RTK antenna, the generation of the photogrammetric model was based on ground control points. This approach requires a sufficient number of them, and, for this reason, different layout schemes were used for data processing to determine how the number of GCPs affects the accuracy of the model. During data processing, GCPs were assigned to a certain number of 11 known points previously measured by the GNSS receiver, and the remaining known points were used as check points. Three layout configurations were used: 8 GCPs and 3 CHPs, 6 GCPs and 5 CHPs, and 5 GCPs and 6 CHPs (Figure 17a–c). GCPs were used in data processing to obtain an accurate photogrammetric model, and CHPs were used to verify the obtained accuracy. Processing was performed by using the default triangulation and reconstruction settings in the software. After the photogrammetric model had been generated, volume calculations and accuracy assessment were further analyzed with *Bentley Descartes 10.07.00.15* software.

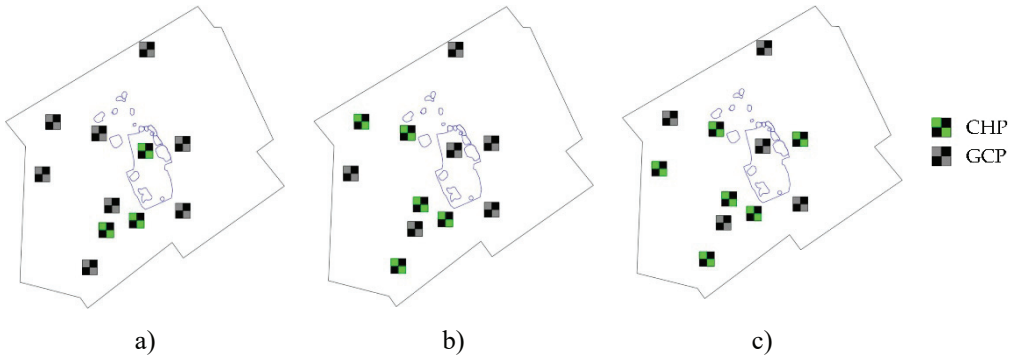


Fig. 17. Control points layout configuration for the ground control-based approach: a) 8 GCPs and 3 CHPs; b) 6 GCPs and 5 CHPs; and c) 5 GCPs and 6 CHPs

The RTK survey data was also processed by using *Bentley ContextCapture* software, and the resulting photogrammetric model was further analyzed with *Bentley Descartes* software. The data processing procedure was essentially the same as the previously described ground control points-based approach, but, since RTK technology requires fewer GCPs, layout schemes with fewer GCPs were used to generate the photogrammetric model. In this case, two layout configurations were employed; they were using 3 and 5 GCPs. Due to human error, part of the area was not captured during data collection, which resulted in fewer check points to assess the accuracy. The layout configurations of GCPs and CHPs for RTK data processing are shown in Figure 18a, b.

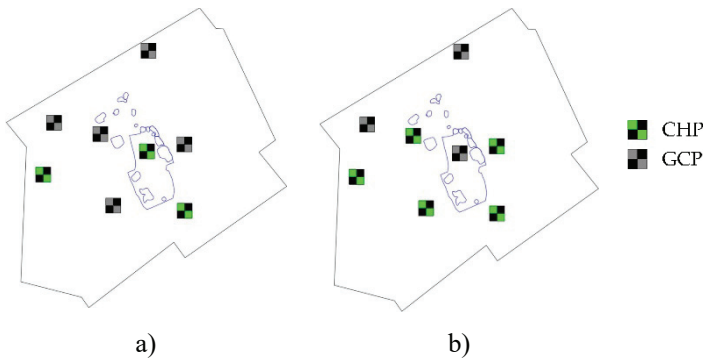


Fig. 18. Control points layout configuration for the Real-time kinematic approach: a) 5 GCPs and 3 CHPs; b) 3 GCPs and 5 CHPs

The UAV data obtained by the PPK approach was processed on the cloud-based *Propeller* platform which is integrated with the *Trimble Stratus* software and provides a complete UAV data processing and analysis solution. Data processing used GPS data recorded by five *Aeropoint 1.0* base stations, which were automatically matched to image data by using image timestamps and then post-processed to correct the less accurate UAV-derived GPS data. A single *Aeropoint* base station serves as a ground control point and can be sufficient for most quarries or construction sites of up to 60 ha, provided that there are no significant elevation

changes on the site being surveyed. All other *Aeropoint* base stations function as validation checkpoints to verify the PPK data. In this case, during data processing, one *Aeropoint* base station was selected as the ground control point, while the other four base stations acted as checkpoints to confirm the accuracy of the PPK data. In the processing software, it was mandatory to specify the coordinates of the selected ground control point. All the coordinates of the base stations were known as the base stations were placed on the same markers which had been previously measured by the GNSS receiver and used to analyze all other workflows. Therefore, one ground control point (control point number 4 as in Figure 11a) was selected for data processing, and the remaining ten known points were used to evaluate the accuracy of the model. The layout configuration of GCPs and CHPs for PPK data processing is shown in Figure 19a. An additional experiment was conducted in winter to observe the influence of weather conditions on the accuracy results. The data was obtained in a smaller area, as changes had occurred in another part of the study site. In this small-scale experiment, five *Aeropoint* base stations were used for data processing and accuracy assessment, one of which served as GCP, and the remaining four contributed as CHPs (Figure 19b).

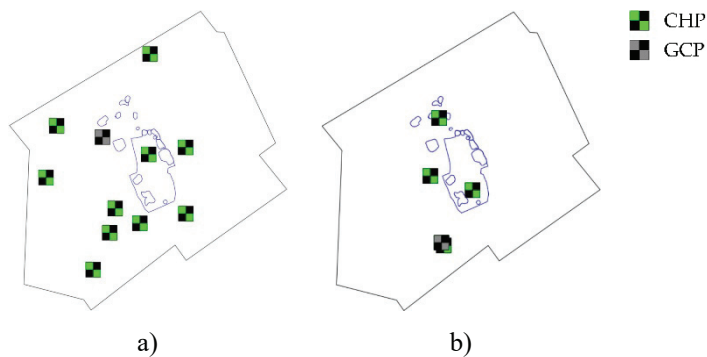


Fig. 19. Control points layout configuration for the Post-processing kinematic approach: a) 1 GCP and 10 CHPs; b) 1 GCP and 4 CHPs

The accuracy of the methods analyzed in the experiment was evaluated by comparing the calculated volumes of the stockpiles and the deviations of the x , y , z coordinates of the control points. First, volume calculations and control point measurements were performed by using a traditional method employing a GNSS receiver. Then, photogrammetric models were generated, and the volumes of the same stockpiles were calculated. The results obtained by all analyzed photogrammetric workflows were compared against the results obtained by adopting the traditional approach.

In the photogrammetric models, stockpiles were calculated by importing stockpile boundaries calculated with *Civil 3D* software (Figure 20a–f). Some parts of the piles sometimes had vegetation, which caused some challenges when calculating the volumes in the photogrammetric model. Manual measurements of data points on the earth’s surface are denoted by advantages in this case, as the actual situation is evaluated on site, and the GNSS receiver can penetrate through

the vegetation and capture the earth's surface data 'as-is'. Meanwhile, photogrammetric models can perform automatic ground extraction by removing vegetation and other objects, while leaving only the earth terrain in the model. However, this process is not always error-free, and it thus requires additional review after the extraction has been completed. In the experiment, the vegetation was removed manually, and the data points in those areas were adjusted to match the ground surface in order to obtain greater accuracy.

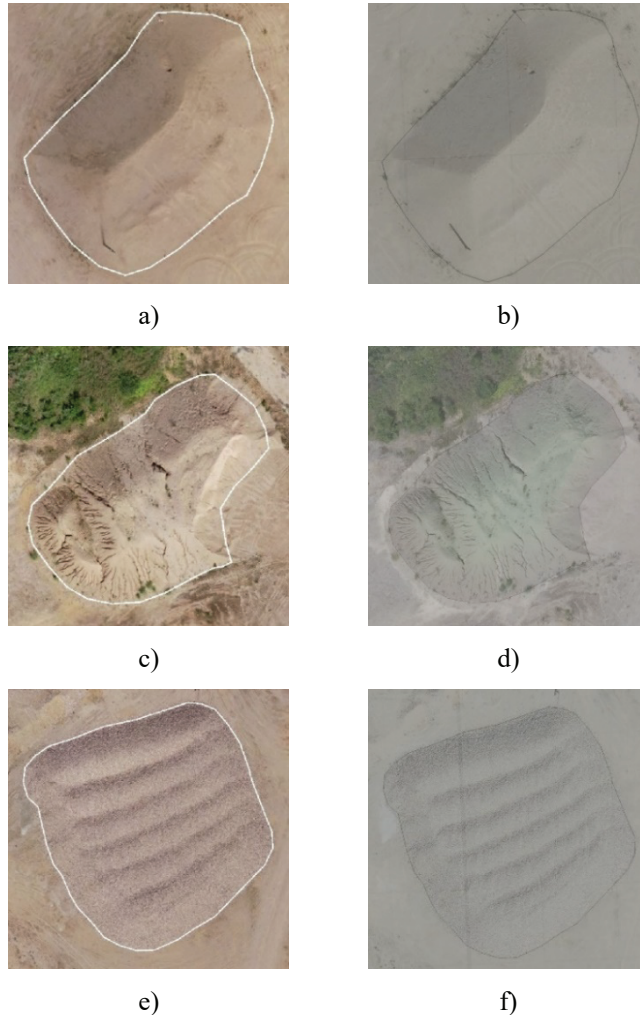


Fig. 20. Example of the boundaries used for stockpiles volume calculation. Stockpile number 3: a) the view in *Trimble Stratus* platform; and b) the view in *ContextCapture* software with 50% mesh transparency. Stockpile number 15: c) the view in *Trimble Stratus* platform; and d) the view in *ContextCapture* software with 50% mesh transparency. Stockpile number 16: e) the view in *Trimble Stratus* platform; and f) the view in *ContextCapture* software with 50% mesh transparency

The accuracy of the x , y , z data points was evaluated by measuring the marked control points on the photogrammetric model and comparing the difference with the measurements obtained by the traditional approach. In photogrammetric models, the software provides an automatic report of the control point accuracy. However, for a more reliable assessment of accuracy, the marked control points were measured manually by using a cursor (Figure 21a–f). In the figure, the centers of the images show the x , y coordinates obtained with the GNSS receiver and compared with the coordinates obtained from the photogrammetric model. Due to the limited resolution of the images, the precise measurement of the x , y values may be affected. Pre-processing can help improve the image quality, including resolution adjustment, noise reduction, etc. However, in this case, the data was acquired under sunny weather conditions and was considered to be of sufficient quality. Image pre-processing can be time consuming, and its use in practice where time is of essential value would not be reasonable. For the above reasons, data pre-processing was not considered in this experiment. In addition, the main focus of the study was emphasized z -value analysis.

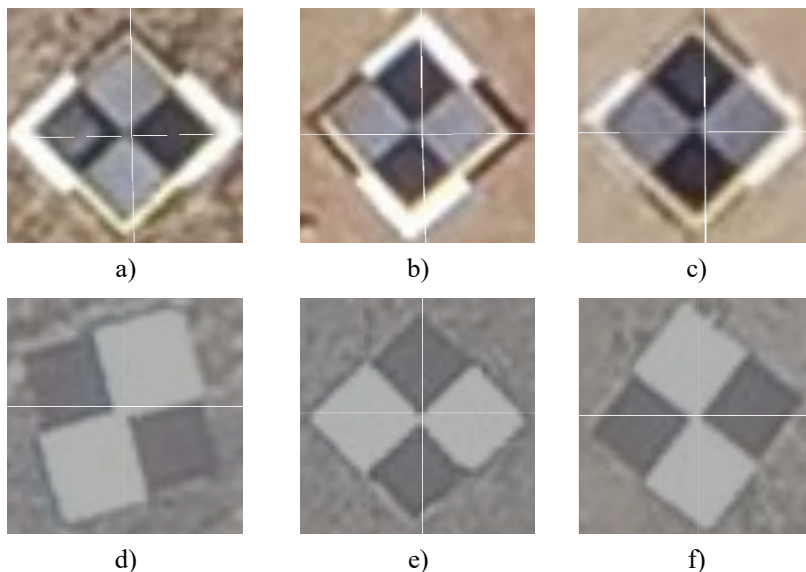


Fig. 21. Measurements of the coordinates of the control points in the photogrammetric model. The centers of the images show the x , y coordinates obtained with the GNSS receiver. Example of measurements on the *Trimble Stratus* platform: a) point No. 4; b) point No. 5; c) point No. 6; example of measurements in *Bentley Descartes* software with mesh transparency set to 50%: d) point No. 2; e) point No. 4; f) point No. 9

2.5. Experimental Results of Earthworks Control

The results of the study are presented in the following way: Chapter 2.5.1 and Chapter 2.5.2 evaluate the accuracy of the analyzed approaches, Chapter 2.5.3 examines the automation efficiency of the methods, and Chapter 2.5.4 provides examples of cases of real use.

2.5.1. Volume estimation analysis

The accuracy of the methods analyzed in the experiment was evaluated by comparing the stockpile volume results calculated by each method and the difference in the x, y, z coordinates between the eleven known points.

The volume estimation was analyzed by examining 16 stockpiles of various sizes. First, the analyzed stockpiles were measured by using a *Trimble GNSS* receiver, and their volume was calculated by using *Civil 3D* software. The total estimated volume of 16 stockpiles was 10532.18 m³. A report of the volume calculation results for each stockpile is given in Table 6. These measurements were used as a baseline to evaluate the accuracy of the UAV-based photogrammetric approaches.

Table 6. Report of conventionally calculated stockpile quantities

Name	2D area, m ²	Net, m ³
Pile 1	87.66	91.95
Pile 2	790.59	1407.86
Pile 3	427.14	832.19
Pile 4	1107.03	3046.91
Pile 5	390.47	623.28
Pile 6	316.83	475.5
Pile 7	55.60	48.22
Pile 8	102.60	115.7
Pile 9	177.34	242.96
Pile 10	53.27	36.21
Pile 11	160.91	255.4
Pile 12	184.48	228.59
Pile 13	217.71	255.57
Pile 14	166.90	175.31
Pile 15	493.98	1185.39
Pile 16	817.04	1511.13
Total	5549.55	10532.18

After establishing a baseline for accuracy assessment by using a ground-level survey, volumes within the same boundaries were calculated in the photogrammetric models. In the processing of the data obtained by the GCPs-based approach, three control point layout schemes were used, of which, the configuration of 6 GCPs provided the most reliable results of the photogrammetric model. This model was further used for the stockpile volume estimation analysis, while the remaining photogrammetric models processed by using 5 and 8 GCPs layout configurations were discarded from further calculations. The results obtained by using these layout schemes are described in more detail in Chapter 2.5.2.

During the acquisition of data from a height of 74 m by using the RTK method, the RTK signal was lost, and the data became unreliable for further analysis and was therefore discarded. Meanwhile, the data obtained from a height of 100 m was reliable, but, due to a flight planning error, not all of the studied area was captured. For these reasons, the RTK method was further investigated on a smaller

scale basis, including five stockpiles totaling at approximately 3800 m³ in volume for accuracy assessment. Table 7 shows a comparison of each stockpile volume obtained by all the methods considered in the experiment, including the results of a full-scale survey of 16 stockpiles and the results of the small-scale survey obtained by the RTK method consisting of 5 stockpiles.

Table 7. Comparison of each stockpile volume obtained by all analyzed methods

Pile No.	GNSS receiver	PPK approach		6 GCPs-based approach		RTK approach
	Ground-level, m ³	74 meters height, m ³	100 meters height, m ³	74 meters height, m ³	100 meters height, m ³	100 meters height, m ³
1	91.95	96.95	94.57	95.09	94.95	–
2	1407.86	1285.00	1254.00	1280.17	1273.18	–
3	832.19	791.00	775.00	797.65	791.79	800.72
4	3046.91	3210.00	3187.00	3119.22	3003.53	–
5	623.28	598.00	582.00	650.09	639.56	–
6	475.50	421.00	413.00	430.66	411.46	–
7	48.22	51.65	49.17	50.80	49.10	–
8	115.73	117.00	114.00	114.65	114.44	–
9	242.96	239.00	236.00	236.13	229.00	237.29
10	36.21	35.15	32.82	36.35	36.00	35.31
11	255.40	236.00	230.00	226.56	223.05	–
12	228.59	210.00	194.00	219.38	219.19	–
13	255.57	266.00	266.00	267.28	253.86	–
14	175.31	157.00	153.00	161.34	154.25	–
15	1185.39	1101.00	1094.00	1060.42	1053.92	1068.88
16	1511.13	1511.00	1499.00	1512.46	1492.87	1526.81

Examination of the results for each stockpile shows that, in most cases, the differences between the photogrammetric methods and the ground-level survey results are negligible. In some stockpiles, the differences were more significant, for example, in stockpile No. 2, a larger volume was estimated by the traditional method, while stockpile No. 4 had a larger volume in three out of four cases as determined by the photogrammetric approaches. However, when examining each stockpile separately, no correlation was found between the results obtained by different methods. Figure 22 and Figure 23 show the comparison of the total quantities obtained by each method.

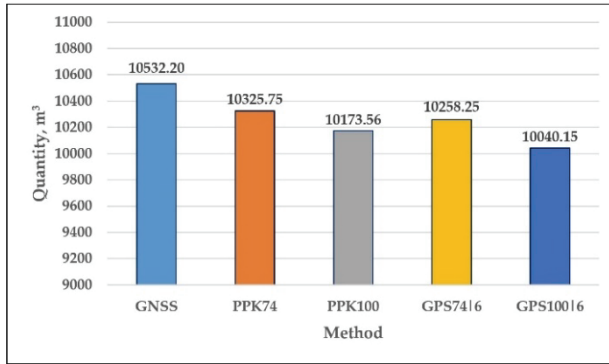


Fig. 22. Total volume comparison of 16 stockpiles obtained by different methods

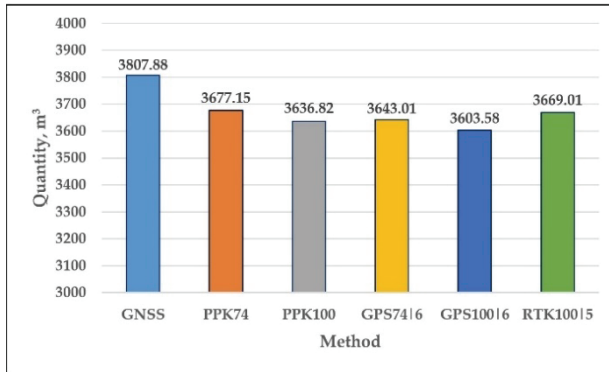


Fig. 23. Total volume comparison of 5 stockpiles obtained by each method

When analyzing the total quantities, a correlation between the different approaches can be observed. Ground-level survey results provided the largest volume when analyzing the full-scale survey, as well as when analyzing smaller-scale results. When comparing the photogrammetric methods, a correlation was observed between the calculated results depending on the GSD value. The height from which the images were captured had a relatively small effect on the obtained results, and, when analyzing all methods in a full-scale study as well as in a small-scale experiment, the difference between the results obtained from different heights did not exceed 1.44% on average. Although the difference was not significant, it was observed that the results calculated by using the higher resolution images produced larger volumes.

For the ground-level survey, the total calculation results for 16 stockpiles differed by 1.96–4.67% from the UAV-based approaches, while in the 5-stockpile small-scale survey, the traditional estimates differed by 3.43–5.36% from the photogrammetric results. When comparing the UAV photogrammetric methods with each other and regardless of the flight height, the difference between the obtained results was 0.65–2.76% in the full-scale survey, and 0.17–2% in the small-scale survey. The PPK results from the 74 meter-high survey were the closest to the ground-level survey results, with a difference of 1.96% for the 16-stockpile survey and 3.43% for the 5-stockpile survey.

2.5.2. Control points accuracy assessment

The accuracy of the control points was evaluated by comparing the deviation of the x, y, z coordinates obtained in the photogrammetric models from the measurements obtained by the GNSS receiver. The information of the points measured by the GNSS receiver is presented in Table 3. The information of the same points measured in the photogrammetric models obtained by the UAV GCPs-based method and the PPK method is presented in Tables 8–11. Since the RTK method captured a smaller area and not all known points were included in the photogrammetric model, the accuracy of this method was evaluated by comparing fewer control points (Table 12). Also, an additional smaller-scale study was conducted under winter conditions by using the PPK workflow. In this case, 5 control points were used, which were re-measured by the GNSS receiver at other locations unrelated to the previous measurements. The ground-level survey and photogrammetric measurement information for these points is given in Table 13.

Table 8. CPs measurement information for the UAV 5 GCPs-based method

CP No.	5 GCPs-based 74 m height			5 GCPs-based 100 m height		
	Northing, m	Easting, m	Elevation, m	Northing, m	Easting, m	Elevation, m
1	6050236.701	556234.259	162.677	6050236.703	556234.255	162.695
2	6050043.431	555982.135	159.570	6050043.445	555982.142	159.573
3	6049904.347	555953.455	160.203	6049904.398	555953.411	159.576
4	6050013.147	556105.792	157.605	6050013.142	556105.785	158.040
5	6049966.716	556230.287	156.121	6049966.718	556230.279	156.137
6	6049781.295	556206.677	155.624	6049781.339	556206.672	155.742
7	6049821.185	556140.202	152.521	6049821.195	556140.210	152.157
8	6049656.238	556080.624	158.929	6049656.314	556080.621	157.359
9	6049755.709	556125.182	157.224	6049755.715	556125.199	157.216
10	6049807.246	556330.677	158.159	6049807.246	556330.668	158.172
11	6049985.544	556330.127	155.877	6049985.514	556330.097	155.030

Table 9. CPs measurement information for the UAV 6 GCPs-based method

CP No.	6 GCPs-based 74 m height			6 GCPs-based 100 m height		
	Northing, m	Easting, m	Elevation, m	Northing, m	Easting, m	Elevation, m
1	6050236.703	556234.257	162.682	6050236.702	556234.258	162.662
2	6050043.401	555982.133	159.564	6050043.416	555982.138	159.568
3	6049904.338	555953.413	159.466	6049904.337	555953.408	159.470
4	6050013.119	556105.788	157.800	6050013.141	556105.774	157.859
5	6049966.712	556230.288	156.132	6049966.716	556230.277	156.127
6	6049781.313	556206.672	155.885	6049781.325	556206.649	155.884
7	6049821.194	556140.204	152.703	6049821.186	556140.210	152.710
8	6049656.282	556080.681	157.989	6049656.304	556080.611	157.780
9	6049755.708	556125.191	157.224	6049755.716	556125.198	157.207
10	6049807.247	556330.669	158.166	6049807.246	556330.669	158.156
11	6049985.528	556330.110	155.434	6049985.526	556330.097	155.432

Table 10. CPs measurement information for the UAV 8 GCPs-based method

CP No.	8 GCPs-based 74 m height			8 GCPs-based 100 m height		
	Northing, m	Easting, m	Elevation, m	Northing, m	Easting, m	Elevation, m
1	6050236.699	556234.258	162.679	6050236.704	556234.254	162.675
2	6050043.434	555982.142	159.577	6050043.441	555982.154	159.579
3	6049904.342	555953.412	159.458	6049904.349	555953.422	159.472
4	6050013.147	556105.800	157.815	6050013.139	556105.798	157.828
5	6049966.713	556230.268	156.177	6049966.717	556230.265	156.117
6	6049781.310	556206.653	155.912	6049781.311	556206.665	155.880
7	6049821.187	556140.182	152.685	6049821.183	556140.187	152.702
8	6049656.300	556080.641	157.841	6049656.298	556080.604	157.816
9	6049755.698	556125.177	157.328	6049755.715	556125.197	157.209
10	6049807.246	556330.677	158.165	6049807.248	556330.670	158.170
11	6049985.536	556330.092	155.433	6049985.525	556330.099	155.437

Table 11. Control points measurement information for the UAV PPK method

CP No.	PPK 74 m height			PPK 100 m height		
	Northing, m	Easting, m	Elevation, m	Northing, m	Easting, m	Elevation, m
1	6050236.696	556234.219	162.697	6050236.752	556234.249	162.724
2	6050043.456	555982.113	159.573	6050043.478	555982.139	159.579
3	6049904.378	555953.411	159.510	6049904.373	555953.436	159.460
4	6050013.165	556105.786	157.799	6050013.171	556105.800	157.762
5	6049966.746	556230.242	156.084	6049966.726	556230.275	156.055
6	6049781.309	556206.621	155.860	6049781.303	556206.684	155.842
7	6049821.211	556140.154	152.685	6049821.197	556140.191	152.668
8	6049656.276	556080.618	157.861	6049656.275	556080.672	157.910
9	6049755.714	556125.178	157.182	6049755.711	556125.228	157.192
10	6049807.233	556330.654	158.182	6049807.213	556330.702	158.179
11	6049985.560	556330.067	155.380	6049985.523	556330.130	155.386

Table 12. Control points measurement information for the UAV RTK method

CP No.	3 GCPs-based RTK 100 m height			5 GCPs-based RTK 100 m height		
	Northing, m	Easting, m	Elevation, m	Northing, m	Easting, m	Elevation, m
1	6050236.690	556234.246	162.669	6050236.694	556234.252	162.662
2	6050043.439	555982.150	159.571	6050043.437	555982.150	159.567
3	6049904.355	555953.417	159.453	6049904.367	555953.425	159.474
4	6050013.145	556105.796	157.833	6050013.153	556105.805	157.832
5	6049966.687	556230.258	156.091	6049966.733	556230.267	156.106
7	6049821.181	556140.163	152.662	6049821.191	556140.180	152.691
10	6049807.179	556330.666	158.162	6049807.236	556330.617	158.256
11	6049985.532	556330.113	155.412	6049985.539	556330.116	155.421

Table 13. Control point measurement information for the additional ground-level survey and the smaller-scale UAV PPK method

CP No.	Ground-level survey			PPK 100 m height		
	Northing, m	Easting, m	Elevation, m	Northing, m	Easting, m	Elevation, m
1	6050066.107	556169.741	156.523	6050066.145	556169.744	156.482
2	6049871.842	556259.675	154.222	6049871.845	556259.67	154.190
3	6049722.953	556182.283	156.363	6049722.97	556182.271	156.348
4	6049730.563	556176.176	155.965	6049730.576	556176.162	155.978
5	6049910.055	556146.170	152.203	6049910.095	556146.167	152.187

In practice, placing GCPs according to the correct layout scheme can be difficult or even outright impossible for a variety of reasons, such as moving traffic, human movement, dense built-up environments, and other various obstacles. In the course of data acquisition, GCPs cannot be moved and must be visible in the images captured by the UAV. A sufficient number of GCPs and their correct placement is especially important when the aircraft does not support the RTK mode. Accordingly, in order to evaluate the GCPs-based method, different layout schemes of the ground control points were used in the experiment. The markers were placed according to the recommended distance requirements of not exceeding 20000 pixels between them, but the placement locations were random. The markers were used for different data processing schemes by using them as ground control points and check points. The deviations of x, y, z measurements obtained by photogrammetric methods compared to the ground-level survey measurements were calculated by using the *Root Mean Square Error* (RMSE) statistical method. The RMSE values were obtained by squaring the differences between the conventionally measured and the photogrammetrically measured points, adding them and dividing that by the number of used points, and calculating the square root of the obtained result:

$$RMSE = \sqrt{\frac{\sum(y_i - y_p)^2}{n}}, \quad (1)$$

where: y_i is the actual value of each ground control point measured by the GNSS receiver; y_p is the predicted value of the corresponding ground control points obtained from the photogrammetric model; n is the total number of ground control points.

The results of the x, y, z deviations of the UAV GCPs-based and PPK approaches for all the control points, without evaluating GCPs and CHPs separately, are presented in Table 14. In this case, 11 control points were analyzed, where part of these points was set as GCPs and the rest as CHPs. During data processing, coordinates are manually specified for the ground control points, and a photogrammetric model is generated based on them. Meanwhile, the check points do not affect the generation of the photogrammetric model and are intended to evaluate the accuracy. The results of GCPs and CHPs x, y, z deviations are presented in Table 15.

Table 14. Root mean square error (RMSE) deviations for 11 control points

Method	x, m	y, m	z, m
5 GCPs-based GPS 74 m	0.017	0.017	0.434
5 GCPs-based GPS 100 m	0.026	0.011	0.256
6 GCPs-based GPS 74 m	0.018	0.020	0.050
6 GCPs-based GPS 100 m	0.015	0.014	0.030
8 GCPs-based GPS 74 m	0.010	0.010	0.047
8 GCPs-based GPS 100 m	0.010	0.009	0.021
1 GCP-based PPK 74 m	0.023	0.028	0.026
1 GCP-based PPK 100 m	0.026	0.024	0.038

Table 15. RMSE deviations for GCPs and CHPs separately

Method	GCPs			CHPs		
	x, m	y, m	z, m	x, m	y, m	z, m
5 GCPs-based GPS 74 m	0.008	0.018	0.237	0.023	0.017	0.547
5 GCPs-based GPS 100 m	0.004	0.003	0.022	0.035	0.015	0.346
6 GCPs-based GPS 74 m	0.040	0.09	0.018	0.026	0.028	0.071
6 GCPs-based GPS 100 m	0.010	0.07	0.012	0.022	0.020	0.043
8 GCPs-based GPS 74 m	0.005	0.008	0.016	0.018	0.014	0.085
8 GCPs-based GPS 100 m	0.007	0.009	0.023	0.016	0.008	0.014
1 GCP-based PPK 74 m	0.013	0.016	0.000	0.023	0.029	0.028
1 GCP-based PPK 100 m	0.019	0.002	0.037	0.027	0.025	0.038

The obtained results showed that the UAV GCPs-based method using 5 ground control points for data processing resulted in several abnormal z-values. This could have happened for various reasons, such as an insufficient number of GCPs, an incorrect placement scheme, or software-related issues. GCPs were manually specified in the software based on the measurements obtained by the GNSS receiver. However, measurement with a GNSS receiver does not ensure millimeter-level accuracy, and the error of each measured data point can vary by several centimeters. Inaccurate specification of the coordinates of several GCPs in the software can determine the accuracy of the entire photogrammetric model. Therefore, expertise and software knowledge are required to ensure the accuracy of a photogrammetric model when using a GCPs-based workflow. Table 16 shows the z-value differences of each control point of the photogrammetric model from ground level-survey measurements.

Table 16. Differences of vertical reference points of UAV GCPs-based photogrammetric model from GNSS receiver measurements

CP No.	UAV 5 GCPs-based		UAV 6 GCPs-based		UAV 8 GCPs-based	
	74 meters height, m	100 meters height, m	74 meters height, m	100 meters height, m	74 meters height, m	100 meters height, m
1	-0.016	-0.034	-0.021	-0.001	-0.018	-0.014
2	-0.014	-0.017	-0.008	-0.012	-0.021	-0.023
3	-0.740	-0.113	-0.003	-0.007	0.005	-0.009

4	0.194	-0.241	-0.001	-0.060	-0.016	-0.029
5	-0.010	-0.026	-0.021	-0.016	-0.066	-0.006
6	0.233	0.115	-0.028	-0.027	-0.055	-0.023
7	0.149	0.513	-0.033	-0.040	-0.015	-0.032
8	-1.092	0.478	-0.152	0.057	-0.004	0.021
9	-0.016	-0.008	-0.016	0.001	-0.120	-0.001
10	-0.005	-0.018	-0.012	-0.002	-0.011	-0.016
11	-0.469	0.378	-0.026	-0.024	-0.025	-0.029

In the case of the 5 GCPs-based approach, half of all the vertical points differed from the GNSS receiver measurements by more than 10 cm, and about a quarter of the points differed within the range of 20–50 cm. Meanwhile, in the case of the 6 GCPs-based method, a greater difference was observed only at control point number 8. This was not unexpected as the marker was placed on the edge of the study area. When using 8 GCPs, the overall accuracy of the photogrammetric model was similar to that with 6 GCPs, but the difference between the control point z-values was inconsistent. For example, control point No. 8 deviation from the ground-level survey was very small even though the CP was placed on the edge, while several other control points had deviations of 5.5 cm, 6.6 cm, and 12 cm, which are relatively significant deviations in terms of accuracy. Moreover, considering the exclusion of this CP from the calculations, it would not affect the accuracy significantly in this case. Based on the results obtained, the 5 and 8 GCPs-based methods were discarded in further analysis. For further analysis, 1 GCP-based PPK and 6 GCP-based GPS methods were investigated. The vertical deviations of each point for these methods are shown in Figure 24.

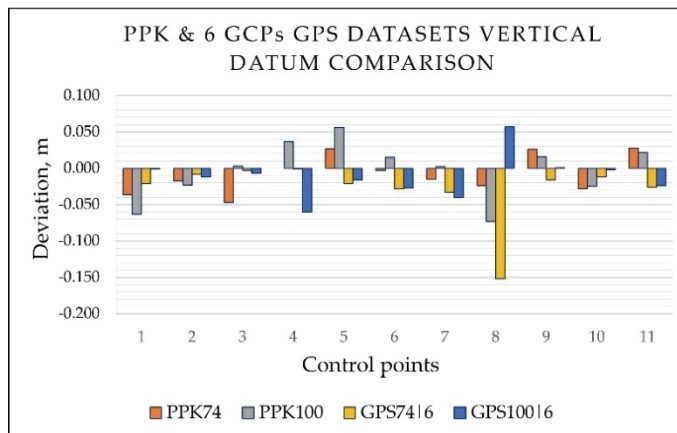


Fig. 24. Vertical analysis of control points of 1 GCP-based PPK and 6 GCP-based GPS methods compared to ground-level survey measurements

Vertical datum analysis showed that, in both PPK and GCPs-based approaches, the largest deviation was observed when comparing CP No. 8 which was located at the edge of the surveyed area. In the case of the PPK workflow, a maximum deviation of 7.3 cm was observed when the data was captured at 100 m. Meanwhile, for the 6 GCP-based approach, the largest deviation was 15.2 cm when

the data was captured at a height of 74 m. This control point was used as a check point and did not affect the accuracy of the photogrammetric model. However, the addition of these CP values to the calculations skews the overall accuracy of the results. For this reason, CP No. 8 was eliminated from the calculations, and the accuracy was re-evaluated. x, y, z deviations excluding CP No. 8 are given in Table 17. The deviation RMSE values for GCPs and CHPs are shown in Table 18.

Table 17. RMSE deviations excluding control point No. 8

Method	x, m	y, m	z, m
6 GCPs-based GPS 74 m	0.018	0.012	0.020
6 GCPs-based GPS 100 m	0.015	0.014	0.026
1 GCP-based PPK 74 m	0.023	0.029	0.026
1 GCP-based PPK 100 m	0.027	0.020	0.033

Table 18. RMSE deviations of GCPs and CHPs excluding control point No. 8

Method	GCPs			CHPs		
	x, m	y, m	z, m	x, m	y, m	z, m
6 GCPs-based GPS 74 m	0.004	0.009	0.018	0.028	0.016	0.022
6 GCPs-based GPS 100 m	0.001	0.007	0.012	0.023	0.021	0.039
1 GCP-based PPK 74 m	0.013	0.016	0.000	0.024	0.030	0.028
1 GCP-based PPK 100 m	0.019	0.002	0.037	0.028	0.021	0.032

Re-estimation of the results without CP No. 8 showed a significant improvement in the accuracy of the results for the 6 GCPs-based approach, whereas the differences were less significant for the PPK method. The obtained results are visually represented in Figure 25. The results showed that, in the photogrammetric models, the deviations of the x and y values from the GNSS receiver measurements did not exceed 3 cm, and the z values did not exceed 4 cm.

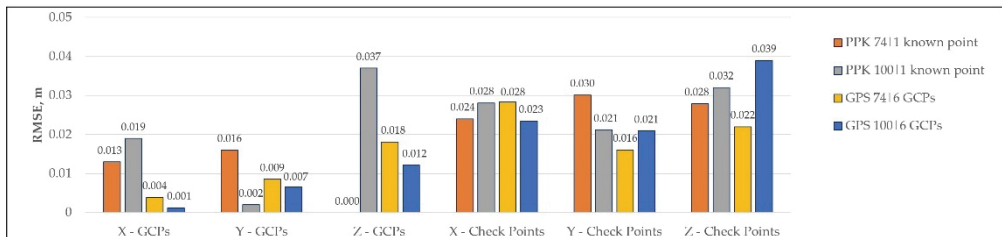


Fig. 25. RMSE deviations of PPK and 6 GCPs-based methods

To evaluate the accuracy of the RTK method, datasets obtained at a height of 100 meters with 3 and 5 GCPs processing schemes were analyzed. In this case, since a smaller area was captured, 8 control points were analyzed to evaluate the accuracy. The results of the x, y, z deviations are presented in Table 19.

Table 19. RMSE deviations of the RTK method for 8 control points

Method	x, m	y, m	z, m
3 GCPs-based RTK 100 m	0.027	0.013	0.016
5 GCPs-based RTK 100 m	0.013	0.020	0.039

When testing the RTK workflow, the deviation of CPs from the ground-level survey was negligible when using the 3 GCPs processing scheme. However, with the 5 GCPs processing scheme, the difference in the z values was significantly larger. Analysis of vertical points (Figure 26) revealed a deviation of 10.2 cm at control point No. 10. Since a smaller area was captured by using the RTK workflow, this resulted in CP No. 10 being located on the edge of the survey area. A control point placed at the very edge may give unreliable measurement and may affect the overall accuracy calculation. Elimination of this control point from the calculations significantly improved the overall accuracy (Table 20).

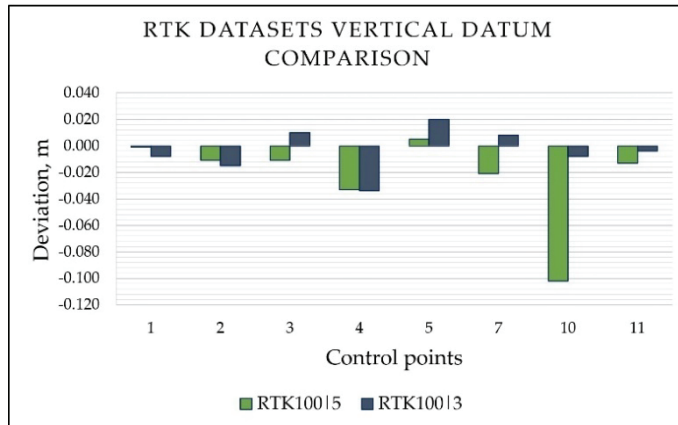


Fig. 26. Vertical datum analysis of UAV RTK approach

Table 20. RMSE deviations of the RTK method excluding control point No. 10

Method	x, m	y, m	z, m
3 GCPs-based RTK 100 m	0.014	0.014	0.017
5 GCPs-based RTK 100 m	0.013	0.009	0.017

Additionally, a smaller-scale PPK workflow experiment was conducted under winter conditions. In this case, five control points were used, which were re-measured by the GNSS receiver and were unrelated to the previous measurements. For data processing and accuracy assessment, the 1 GCP and 4 CHPs layout scheme was used. The RMSE deviation values obtained in this comparison between the PPK approach and the ground-level survey are shown in Table 21. The deviation results for GCPs and CHPs for these smaller-scale PPK and RTK methods are shown in Figure 27. Although a smaller number of control points were analyzed, the results showed that the deviations of the z-values did not exceed 3 cm.

Table 21. RMSE deviations obtained by the PPK method in winter conditions

Method	x, m	y, m	z, m
1 GCP-based PPK 100 m	0.026	0.009	0.026

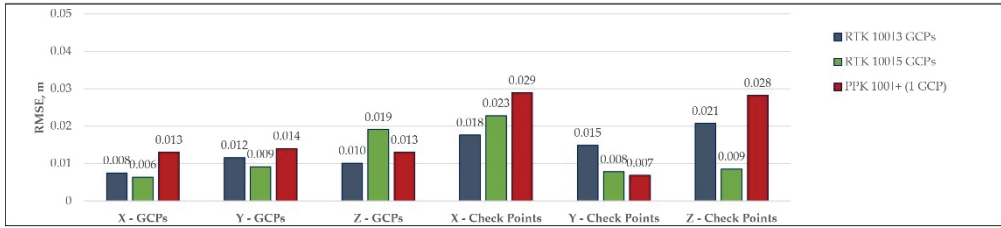


Fig. 27. RMSE deviations of RTK and smaller-scale PPK approaches

Summarizing on the results of all the methods, the z-values pose more accuracy issues than the x- and y-values. The x and y deviations in all the analyzed cases did not exceed 3 cm. Meanwhile, the z deviations when using ground control point-based workflows had issues in most cases and required detailed analysis. However, the results of the z values of GCPs and CHPs obtained in the experiment did not exceed 4 cm, and the overall accuracy of x, y, z was approximately in the range of 2–3 cm. A summary of vertical datum results among all the analyzed methods is presented in Figure 28.

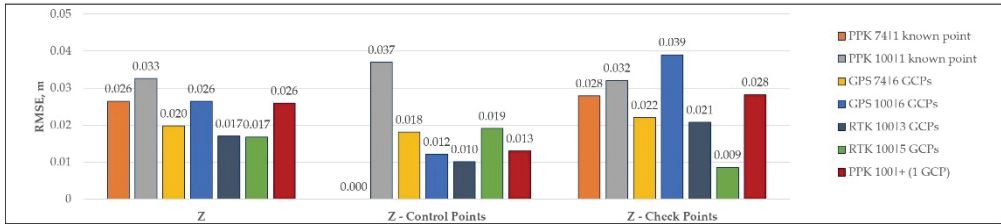


Fig. 28. Comparison of vertical datum results between all analyzed methods

2.5.3. Efficiency of automation

The traditional approach with a GNSS receiver required approximately 6 hours to measure the area of 5549.55 m². The data points were measured at every 1–15 m depending on the curvature of the terrain. In this way, 1108 x, y, z data points were captured in the studied area. Meanwhile, unmanned aerial vehicles required 17 minutes to capture an area of 36 ha from a height of 100 m, and 37 minutes from a height of 74 m. The 36 ha area data capture information is provided in Table 22. The flight altitude had a negligible effect on the data accuracy, but had a significant effect on the flight time and the data size. The flight time at a height of 74 m was 54% longer, and the amount of the data obtained was 55% larger compared to the flight at a height of 100 m.

Table 22. UAV data capture information for 36 ha area

Flight time	Area	Flight height	No of images	Data size
37 min	36 ha	74 m	883	3.22 GB
17 min	36 ha	100 m	392	7.18 GB

However, the analyzed UAV-based workflows had specific requirements to consider. In addition to the flight, a significant part of the data acquisition time is spent preparing for the flight. For example, GCPs-based approaches required

approximately 45 minutes to locate the markers for GCPs measurements. The markers required the placement to be at least 20000 pixels apart between the ground control points and had to be measured manually with a GNSS receiver. On the other hand, the PPK method required only one ground control point for an area of this size, but the *Aerpoint 1.0* base stations used in the workflow had to remain on the ground while recording GPS data for at least 45 minutes. As a result, the overall survey time, including the UAV flight and preparation, increased to approximately one hour. A comparison of the data collection efficiency of the 5549.55 m² area is presented in Table 23.

Table 23. Data capture efficiency for 5549.55 m² area

Data acquisition method	Survey area	Flight height	Acquisition time	No. of data points
GNSS-RTK receiver	5549.55 m ²	Ground-level	6 hours	1108
UAV-based photogrammetry	5549.55 m ²	74 m	1 hour	Millions
UAV-based photogrammetry	5549.55 m ²	100 m	1 hour	Millions

The recommended operating temperature of the UAVs used in the experiment is between 0 and +40 °C. At low temperatures, the battery may discharge faster, but the data acquisition speed is not affected by the temperature within the specified range. Meanwhile, the operating temperature of the GNSS receiver used in the experiment is specified in the manufacturer’s technical specifications from –40 to +65 °C. However, it should be noted that the specified operating temperature of the GNSS receiver battery is down to –20 °C. The data acquisition time with UAV photogrammetry techniques is greatly affected by the lighting conditions and the flight altitude. In cloudy weather or under flight altitude restrictions, data acquisition can take significantly longer, as the photogrammetry process requires high-quality images. In addition, it is not recommended to use the UAV in rain, fog, or with wind speeds exceeding 10 m/s.

Ground-level survey data was processed by using engineering CAD software. Here, data is processed to calculate specific results, such as to conduct volume calculations, and this operation requires advanced software skills. In this case, data processing together with the calculation of stockpile volumes took approximately 6 hours of manual work. GCPs-based UAV data was processed by using desktop photogrammetric software. In this case, data processing required software skills and manual intervention to prepare images for model generation. In addition, generating photogrammetric models in desktop applications required high-powered computer hardware, which, due to being so resource-intensive, limited the performance of other tasks at the time of processing. Meanwhile, the data obtained through the PPK workflow was processed on a cloud-based platform. In the case of the PPK workflow, the GPS data from the base stations was uploaded via wi-fi automatically, and, when uploading the images to the platform, the main important task was to manually enter the x, y, z coordinates of one known point and assign it to the

selected ground control point. Here, data preparation for photogrammetric model generation was straightforward, and it required minimal software skills. The generation of photogrammetric models, regardless of the software used in the experimental study, took approximately 6–10 hours. Photogrammetric models are generated automatically, and human intervention is not required at that time. Cloud-based processing does not require powerful computing equipment, and the computer could be used without performance limitation for other tasks during photogrammetric model generation. Data processing information for all the analyzed methods is presented in Table 24. Once the photogrammetric models had been generated, volume measurements were obtained within minutes. However, the photogrammetric desktop application required skills to calculate quantities, and, on a cloud-based platform, calculations can be performed by any construction participant without the need for a surveyor. Also, a detailed report together with visualization can be automatically generated after stockpile volumes or other measurements have been taken.

Table 24. Data processing information of analyzed methods

Method	Processing software	Processing time, hours	Remarks
Ground-level survey	Engineering CAD software	6	Data was specifically processed to produce volume results
UAV-based approach	Desktop application	8–10	High-powered computer hardware and software required
UAV-based approach	Cloud-based platform	6–8	Automated data processing process. Minimal manual intervention

The results obtained by all the analyzed methods were similar in terms of accuracy. However, in addition to the accuracy of the photogrammetric model and the efficiency of data acquisition and processing, it is also highly important to consider the reliability of the workflow. For example, when testing the GCPs-based approach, the data produced abnormal results depending on the GCP processing scheme. Also, the CP located on the edge of the studied area distorted the accuracy of the results, and data re-processing was thus required to evaluate the accuracy of the model. When using a GCPs-based approach, images are stitched together by incorporating data from the GCPs and, first, the camera positions are calculated, which could have been the cause of inaccuracy. Therefore, a sufficient number of ground control points and accurate coordinates for data processing is very important. Although a sufficiently accurate photogrammetric model was obtained during the experiment, the conducted tests showed that additional efforts and expertise were needed to ensure the reliability of the data when the workflow was based on ground control points.

An RTK-based UAV workflow requires fewer control points, which thus allows less time to be spent on flight preparation. This method is considered more accurate because the camera positions are corrected in real time. However, when testing this workflow, during a flight at 74 m altitude, there were gaps in the RTK signal that were not noticed. The lost signal made the data unreliable, and the

obtained data was not analyzed further. Despite the high accuracy of the data, the problem of signal loss is common, and, when a signal loss is observed, a re-flight is required.

When testing the PPK workflow, a single ground control point was used for data processing. Since only one GCP is needed, it makes the data acquisition process much more efficient. During the PPK experiment, the results were stable in all cases, no corrections had to be made, and no issues occurred. In addition, the control point located at the edge of the study area did not significantly affect the overall accuracy of the model. The PPK method does not correct geotags to images immediately, but rather calculates based on the actual geometries of the satellites when available. This ensures that satellite geometry errors are corrected, and that signal gaps can be filled later by PPK calculations. In addition, the analyzed method used a smart base station as a ground control point. This ensured that point tuning after geotags would not correct the point tuning of the absolute position, and that the x , y , z position in relation to the earth's surface would be adjusted by using a known point. During the experiment, the PPK method demonstrated stable and reliable results.

2.5.4. Real case approaches

Since the analyzed PPK workflow demonstrated high reliability, the technology was further tested in a real industrial building construction project. The construction site covered an area of approximately 16 ha and required a substantial amount of earthwork.

The use of UAV-based PPK technology in the project began immediately after earthworks began and continued throughout the construction phase. Since the survey area of the factory construction site was about 16 ha, it was sufficient to use only one *Aeropoint* base station as a ground control point based on the experimental research results. As check points, five additional base stations were used, which were placed in the territory of the construction site in order to obtain information about the accuracy of the obtained photogrammetric model. However, this workflow has limitations because *Aeropoint* base stations must be in a broadly open area, as shown in Figure 29.

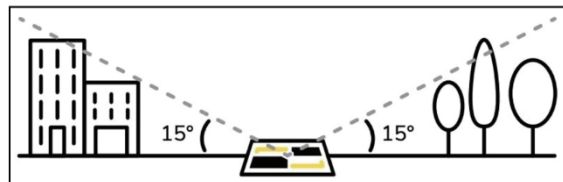


Fig. 29. An example of a well-opened area for the installation of a base station. Reproduced from <https://www.propelleraero.com/>

In this construction site, there were no eligible open areas for the installation of an *Aeropoint*, as there were obstacles such as buildings, trees, and high-power electricity towers around the site. In addition, the UAV must fly over the base station during data collection. To bypass this limitation, the flight area was simply extended to a location suitable for placing the base station (as shown in Figure 30). Another restriction in this location was not for a specific workflow, but for the

general use of unmanned aircrafts, as the flight height was limited by the authorities to a height of 30 m above the ground. Initially, several flights were made at a height of 30 meters, where each flight consumed approximately three and a half batteries, and the flight time for surveying the area was about 70 minutes in total. When high-rising equipment, such as cranes, appeared on the construction site, it became necessary to carry out flights at a more elevated height. Since the flight height at the survey area was restricted, permission from the authorities was required to carry out flights at a higher altitude. The process of obtaining the permit was not complicated, and, after obtaining the permit, further flights were carried out at a height of 60 m. The flight at a height of 60 m only consumed one and a half batteries and took approximately 30 minutes of the flight time in total. The accuracy of the obtained data in relation to the flight height in this case was not analyzed in detail, but no significant effect was observed.



Fig. 30. Dashed line represents the extended location where the GCP was installed

In order to effectively monitor the progress of the earthworks, flights were conducted continuously once or twice a week during the entire construction phase of the earthworks. Therefore, a solid ground control point with known x , y , z coordinates was established, on which, the base station was always placed, thus eliminating the need for the arrival of a surveyor.

First, to plan and control the progress of the earthworks, the axes and building boundaries were imported into the photogrammetric model in the CAD format, as shown in Figure 31. The x and y accuracy of the photogrammetric model was assessed by visually comparing the design drawings in the LKS-94 coordinate system, by superimposing them on the photogrammetric model. For example, axes were exported from design CAD drawings and imported into the *Propeller* platform for comparison. Since the CAD drawings and the photogrammetric model were in the same coordinate system, it was possible to compare the work done in the photogrammetric model with the design drawings. In the example presented in Fig.

32, the location of the column installation was visually assessed. In the photogrammetric model, the center of intersection of the axes visually corresponded to the center of the column. In this way, it is possible to visually check whether the photogrammetric model is correctly aligned in the x and y coordinate system, and, at the same time, to follow the progress of the construction work and control the location of the installation of structures.

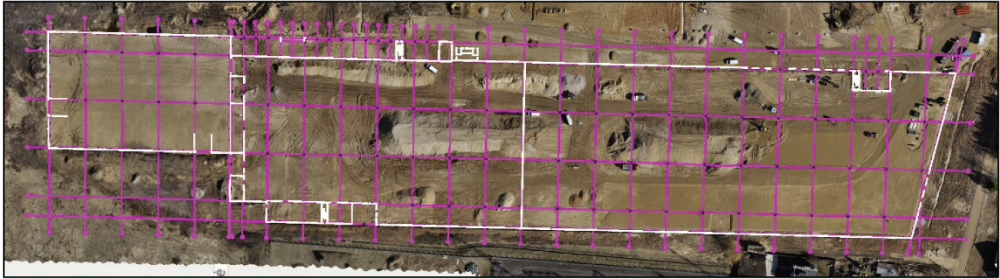


Fig. 31. Axes and building boundaries are imported into the photogrammetric model. View from the *Trimble Stratus* platform

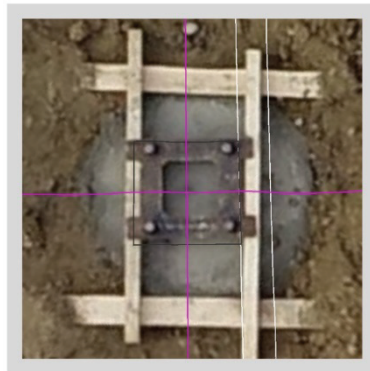


Fig. 32. Visual assessment of x, y accuracy by comparing the as-built vs. as-planned

One example of the use of the photogrammetry technology for earthworks control was the control of the earth leveling process. Ground leveling was carried out by using GPS-equipped bulldozers, and construction managers could simply control the process from a computer without the need for a surveyor. The as-designed surface mesh in the LandXML format was imported into the photogrammetry software, where the progress of the work could be monitored by comparing the current state with the as-designed data (Figure 33).

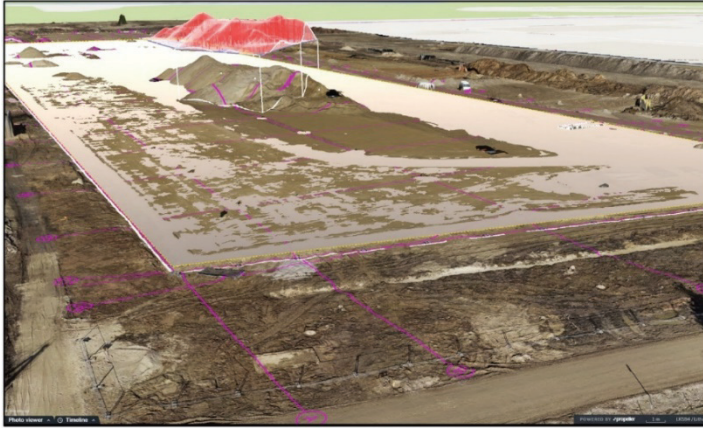


Fig. 33. Monitoring of work in progress compared to the design surface

Throughout the earthworks phase, this UAV-based photogrammetry method was used to plan and manage the earthworks volumes (an example is shown in Figure 34). In most cases, this was done by construction managers without the need for a surveyor. Since the reality data on the construction site was captured weekly, it helped to effectively control the progress of earthworks. Automated quantity reports were documented and used for self-control and control of the subcontractors' work. Earth volume reports were also used to agree on the quantities with the construction technical supervisor.

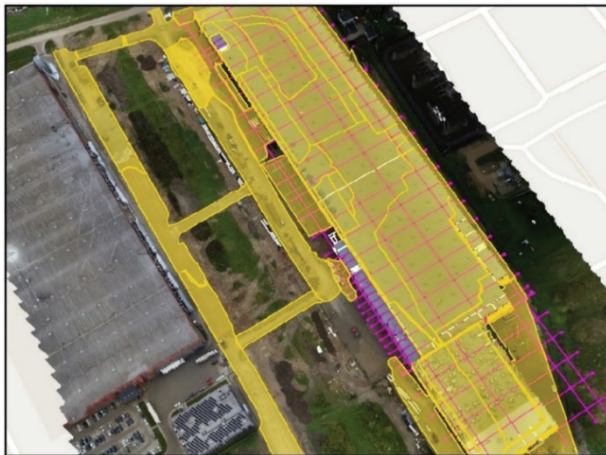


Fig. 34. Earthworks control during the earthworks phase

If needed, the x , y , z point data can be easily transferred and imported for use in the engineering CAD software. This can be useful for surveyors who are used to working in a 'more traditional' way, as it provides the same type of data without having to walk around the site. Figure 35 shows the transfer of z -coordinates of points to CAD software. However, it has been observed that some construction professionals still question the reliability of drone data.

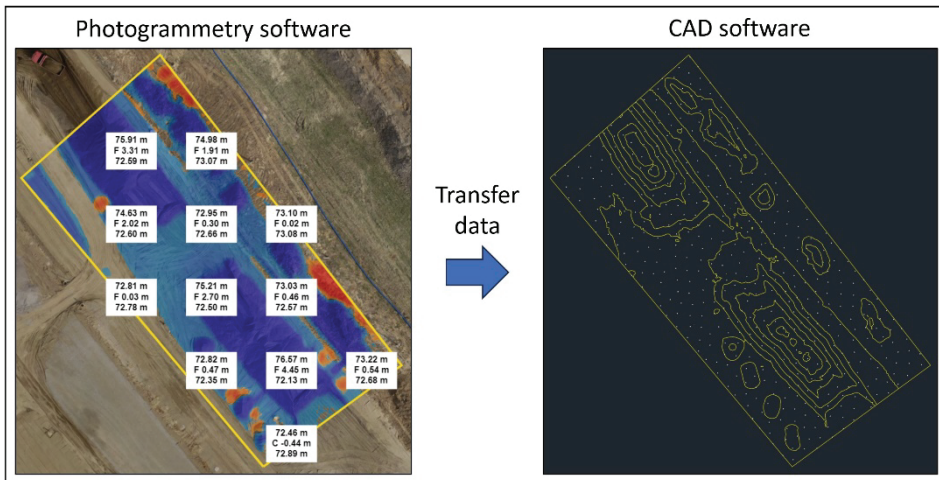


Fig. 35. Example of transferring data points to CAD software

Overall, this automated workflow significantly improved the earthworks management process and received positive feedback from construction managers. By using a constantly updated reality model, construction managers can better feel the scope of work and can import the necessary CAD designs for further earthworks management without the need for surveyors. In addition, there have been cases where real-world data captured by drones has helped avoid disagreements over unclear scopes of work with subcontractors.

2.6. Chapter Conclusions

1. During the experiment, *DJI Phantom 4* series unmanned aerial vehicles, which are widely used in the construction industry for earthworks control, were tested, and GCP-based, Real-time kinematic and Post-processing kinematic workflows were analyzed in a 36 ha quarry. The analyzed workflows were compared with the traditional ground-level survey in terms of accuracy, efficiency, and data reliability.
2. The study found that the accuracy of the data obtained by the UAVs was very similar to the results obtained by a ground-level survey when measured with a GNSS receiver. When comparing the x, y, z coordinates between the GNSS receiver measurements and the results obtained by the UAVs, the difference was approximately up to 3 cm RMSE. For 16 stockpiles with a total volume of 10532.18 m³, the difference between the photogrammetric and the traditional calculations was 1.96–4.67%.
3. It was found that, when the UAV captured data from a height of 74 m, the flight time was 54% longer, and the amount of data obtained was 55% higher, compared to capturing data from a height of 100 m. The height of the data capture reduces the image resolution, but, during the experiment, the flight altitude had a negligible effect on the accuracy of the obtained results. However, regardless of the flight height, data acquisition with the UAV was approximately 6 times faster than with the GNSS receiver. Meanwhile, the PPK workflow was

the most efficient for data acquisition, as it required only one ground control point for the entire study area.

4. In the experiment, the accuracy results of all the analyzed UAV-based photogrammetric methods were similar and close to the ground-level survey results. However, methods based on GCPs required additional efforts to assess the accuracy of the data, as abnormal values were obtained, and data re-processing was required. Data reliability in GCPs-based workflows is difficult to assess and may lead to erroneous results. During the experiment, the PPK-based approach demonstrated the most reliable results, as the data was stable, and no issues occurred.

3. APPLICATION IN BUILDING CONSTRUCTION

This chapter explores the application of laser scanning and BIM technologies for automated progress monitoring during the structural construction phase. A research article with the methodology and results of this experimental study was published by Kavaliauskas et al. [139] in a scientific journal. Part of the experimental research results were presented at the conference [201].

3.1. Description of the Research Object

3D laser scanning is typically used in building construction environments or where millimeter-level accuracy or penetration through vegetation is required. In the construction of buildings, the IFC model is usually used, according to which, works are carried out, and their progress is monitored. In order to create a construction monitoring automation methodology, two different types of buildings with an IFC model were selected for the experiment. The scanning was carried out at the construction sites of the office building *Sqveras* and the residential house project *Piliamiestis AI*. As-is point cloud data was captured on the analyzed floors of the buildings separately, and it did not cover full-scale scanning of buildings. These objects were chosen for the study because they represented a typical construction environment. Since the analyzed objects are similar compared to other typical construction objects, the developed methodology could be more easily applied in practice.

In the *Sqveras* project, laser scanning was performed on the first and third floors of an office building. The structural design was the same in both analyzed floors of the building. The structures of the building were monolithic, the floor area covered approximately 600 m², and each floor had standard structures, such as columns, beams, and walls. On the third floor, the building structures were clearly visible, i.e., not covered by construction materials or other construction equipment. On the first floor, the construction environment was occluded: formwork was installed above the columns, there was scaffolding and other items nearby, and part of the surfaces of the structures were cluttered with building materials. This reflected the real-world construction environment, where work is overlapping and continuous, and scanning without obstructions can be a challenge.

The scanned area in the *Piliamiestis AI* project contained brickwork and monolithic structures consisting of slabs, walls, and beams. The total floor area covered 450 m², no construction work was being carried out at the time of scanning, and the environment was clear without obstructions. The locations analyzed in the experiment are shown in Figures 36 and 37.

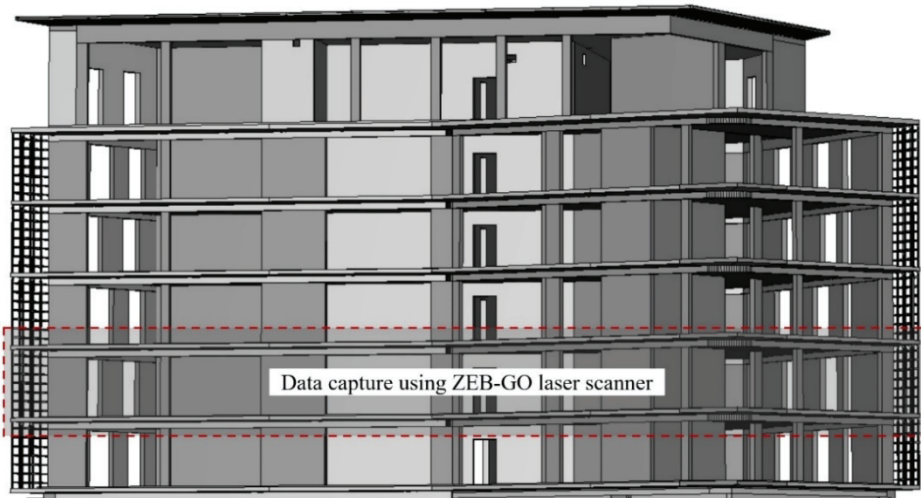


Fig. 36. Scanning location in *Pilamiestis A1* residential building

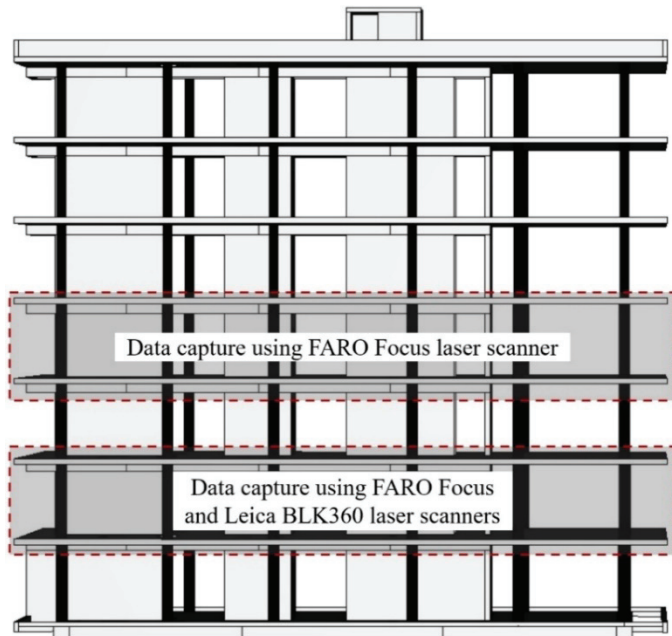


Fig. 37. Scanning locations in *Sqveras* office building

3.2. Methods and Tools

This experimental research examines the application of a 3D point cloud derived from laser scanner sensors for the monitoring of the construction progress by automatically identifying as-built structural objects based on the comparison with the as-planned IFC model. The research methodology consists of three experiments performed under different conditions. In the experiments, six data sets were analyzed, each consisting of as-is point cloud data and an IFC file corresponding to

the scanned location. The as-is data was captured on construction sites in two different buildings by using three laser scanners with different technical parameters. From the obtained data, a methodology was developed for point cloud data alignment with the IFC model and automated identification of objects in the point cloud compared to IFC. The experimental research scheme is presented in Figure 38.

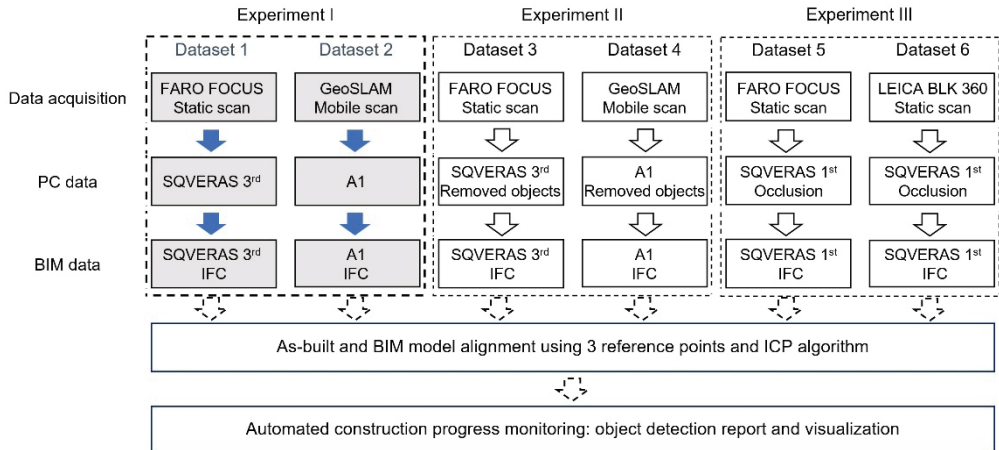


Fig. 38. Experimental research scheme

The geometry of the building’s structures was captured by using static laser scanners *FARO Focus S* and *Leica BLK360*, and a handheld laser scanner *ZEB-GO*. All these devices are different in terms of technical parameters such as the scanning range, the scanning speed, accuracy, etc. However, data accuracy was not analyzed in this research. Previous studies have shown that static *Terrestrial Laser Scanners* (TLS) can achieve millimeter-level accuracy when measuring vertical structures compared to the total station measurements [78]. In this study, the parameters declared by the manufacturer were taken into account, and further accuracy assessment was not performed. The main technical parameters of the devices used for data acquisition are presented in Table 25.

Table 25. The main parameters of laser scanners used in the experiment

Device name	Device type	Distance accuracy	Scanning range, m	Scanning speed, pts/sec
FARO Focus S70 laser scanner	Static / TLS	1 mm	70	1000000
Leica BLK360 laser scanner	Static / TLS	4 mm at 10 m 7 mm at 20 m	60	360000
ZEB-GO laser scanner & ZEB-DL2600 data logger	Mobile / handheld	10–30 mm	30	43000

First, the data was obtained in a relatively clean construction environment by using a high-quality *FARO Focus* laser scanner. The declared accuracy of this scanner reached up to 1 mm and was the highest among the scanners used in this experiment. Therefore, the data obtained by this scanner in an orderly environment was used to develop the initial automated object identification methodology. In

parallel, the data obtained by the mobile ZEB-GO laser scanner was used to verify the object identification process. After obtaining successful results, a number of objects were removed from this point cloud data to evaluate whether the developed process successfully identifies the missing objects. Finally, scanning was performed with a high-quality *FARO Focus* scanner and a lower spec, but significantly cheaper *Leica BLK360* scanner in an occluded construction environment. Each dataset consisted of laser scanner point cloud data and the corresponding IFC model. A brief description of the data sets is given in Table 26.

Table 26. Brief description of datasets

Dataset No.	Brief description
Dataset 1	Consists of an as-built point cloud acquired from the third floor of the office building and the corresponding IFC model. Point cloud data was obtained by using a <i>FARO Focus S70</i> static laser scanner in a clean environment. The resulting point cloud was georeferenced to the global coordinate system.
Dataset 2	Consists of as-built point cloud data acquired from the residential building and the corresponding IFC model. Point cloud data was obtained by using a <i>ZEB-GO</i> mobile laser scanner in a clean environment.
Dataset 3	Consists of modified data from Dataset 1. One wall and two columns were removed from the point cloud. The IFC model was not modified.
Dataset 4	Consists of modified data from Dataset 2. Two walls and two columns were removed from the point cloud. The IFC model was not modified.
Dataset 5	Consists of as-built point cloud acquired from the first floor of the office building and the corresponding IFC model. Point cloud data was obtained by using a <i>FARO Focus S70</i> static laser scanner in an occluded environment. Redundant points due to noise were not removed in the point cloud model.
Dataset 6	Consists of as-built point cloud acquired from the first floor of the office building and the corresponding IFC model. Point cloud data was obtained by using a <i>Leica BLK 360</i> static laser scanner in an occluded environment. Redundant points due to noise were not removed in the point cloud model.

Pre-processing of the scan data, such as the point cloud registration, removal of redundant points, or file format conversion, was performed by using *Leica Cyclone*, *Autodesk ReCap* and *GeoSLAM Hub* software, depending on the output scan data format of the laser scanner. Later, the automated object detection process was developed in the *Python* environment.

3.3. Data Capture Workflow for Structural Construction Monitoring

In the experimental study, scanning was performed by using three laser scanners with different technical specifications. First, scanning was performed in an orderly environment where the structures were clearly visible in the line of sight. This was the environment on the third floor of the *Sqveras* office building and the *Piliamiestis AI* residential building. In this case, the *FARO Focus* laser scanner was used for scanning in the *Sqveras* building, and the *ZEB-GO* handheld laser scanner was used in the *Piliamiestis AI* building. Subsequently, scanning was performed in

an occluded environment where the structures were covered with various building materials and equipment. Such an environment was considered on the first floor of the *Sqveras* building. Here, the scanning was performed with the same high-spec *FARO Focus* laser scanner and a relatively low-spec *Leica BLK360* scanner.

A special effort was made to obtain high-quality data for the third floor of the *Sqveras* building, as this data was intended for the development of the methodology. First, seven control points were installed on the walls and columns. Control points were made by printing a black-and-white checkerboard pattern on an A4-sized sheet of paper. By using these control points and a *TOPCON GT* series robotic positioning system, the point cloud model was then georeferenced in the *LKS-94* coordinate system and the *LAS07* elevation system. A full-floor environmental scan was performed from sixteen locations (Figure 39). To obtain a single point cloud model, this data from individual scans were imported into *Autodesk ReCap* software, where registration was performed. The methodology of automatic object identification was based on the alignment and spatial association of point cloud data with the point cloud data extracted from the vertices of IFC objects. Considering this, it was enough to know the x, y, z coordinates of each point. Therefore, the *Plain Text File* (PTS) format, which is a simple text file containing the x, y, z coordinates of each point, was chosen for further data processing. Since the manufacturer's scan output data formats are often specific and can only be processed by using the software provided by the manufacturer, in all cases, the point cloud data was imported into *Autodesk* software and then exported into the PTS format.

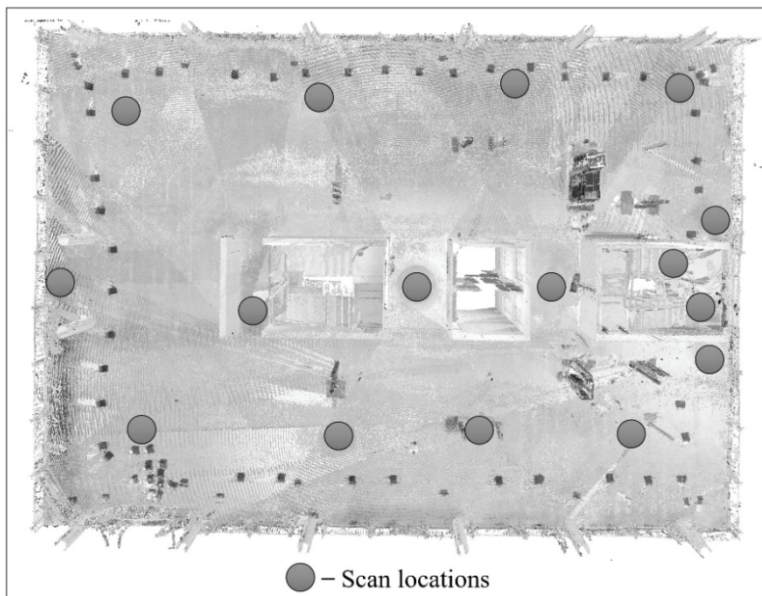


Fig. 39. Scan locations on the third floor of *Sqveras* building by using a *FARO Focus* laser scanner

The scans performed on the first floor of the *Sqveras* building and in the *Piliamiestis A1* building were not georeferenced, as the IFC files were coordinated

in the local coordinate system, which complicates data alignment. Whereas static scanning required multiple scan locations, data acquisition using the mobile scanning technique required a single continuous scan looping around the scan area (as shown in Figure 40). Scan registration using the *Leica BLK360* scanner was performed in the *Leica Cyclone* software provided by the manufacturer, and, in the case of mobile scanning, in the *GeoSLAM Hub* platform. However, in all the cases, the point cloud data was imported into *Autodesk ReCap* software for the conversion to the PTS format. The workflow of data acquisition and pre-processing, as well as the equipment used, is presented in Figure 41.

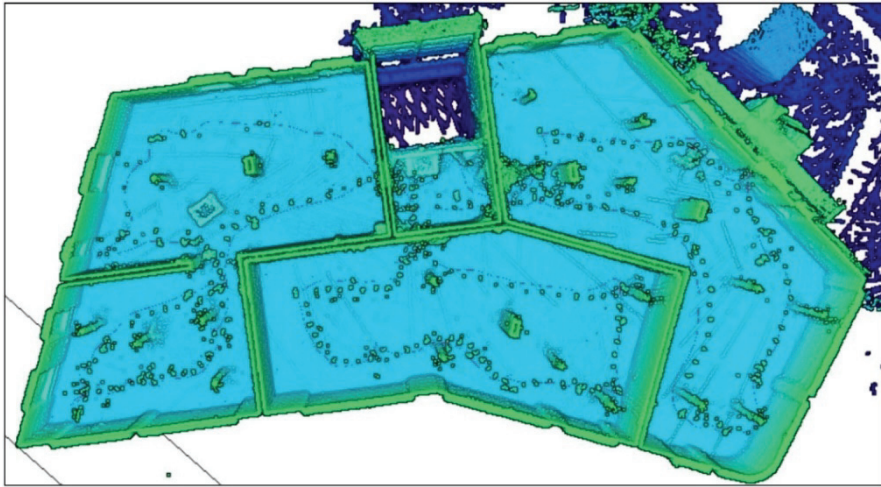


Fig. 40. Scan path using *ZEB-GO* handheld laser scanner (*Pilamiestis A1* project)

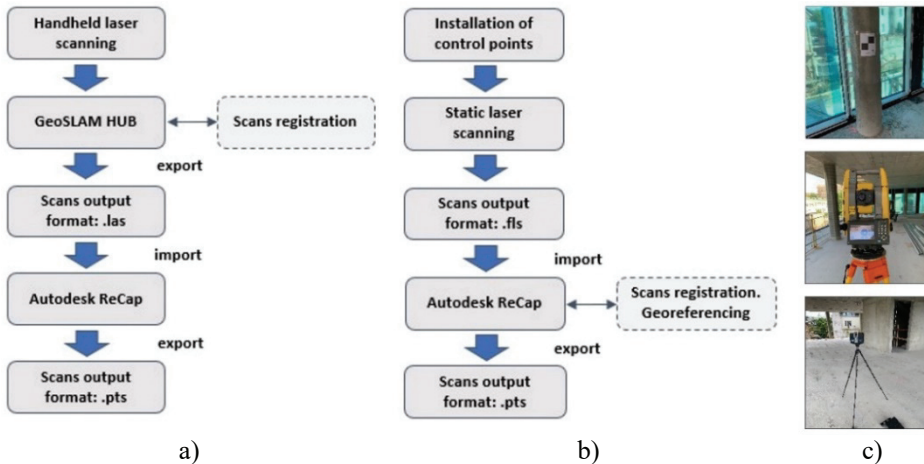


Fig. 41. Workflow of data acquisition and pre-processing: a) mobile laser scanning workflow using the *ZEB-GO* scanner; b) static laser scanning workflow using the *FARO Focus* scanner; c) example of setting up a control point for georeferencing, *TOPCON GT* series robotic total station, and *FARO Focus* laser scanner

3.4. Data Processing

The main focus of the research was the automated detection of vertical objects, such as walls and columns, in a point cloud by comparing the geometry of the point cloud with the IFC model. In this case, the detection of the ceiling and floor planes was not analyzed. The obtained point cloud data was pre-processed by removing the redundant points, and, for better visualization, the upper slab was removed in both the point cloud model and the IFC model. The pre-processed data for further analysis is shown in Figure 42. Only the ground floor point cloud data of the *Sqveras* building was minimally pre-processed, thus leaving out most of the unnecessary, noise-induced points for methodology validation. The details of point cloud models prepared for further analysis are given in Table 27.

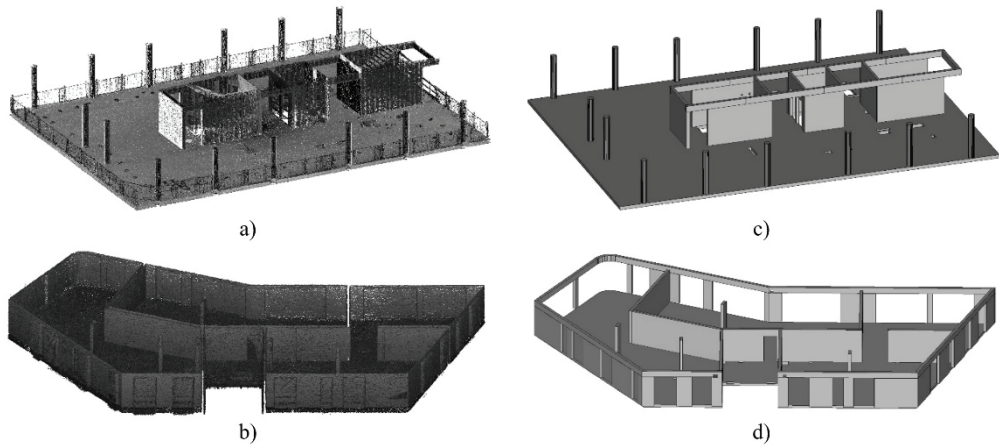


Fig. 42. Pre-processed IFC and point cloud data for further analysis: a) point cloud model obtained in *Sqveras* building; b) point cloud model obtained in *Piliamiestis A1* building; c) the corresponding IFC model of *Sqveras* building; d) the corresponding IFC model of *Piliamiestis A1* building

Table 27. Details of analyzed point cloud models

Point cloud data	Acquisition date	Average population	No. of points	Data size
SQVERAS 3rd floor (FARO Focus S70)	2 July 2019	1438.78 pts/m ³	9451351	758 MB
PILIAMIESTIS A1 (ZEB-GO)	24 December 2021	521.48 pts/m ³	12510712	677 MB
SQVERAS 1 st floor (FARO Focus S70)	2 July 2019	2211.69 pts/m ³	13882774	1007 MB
SQVERAS 1 st floor (Leica BLK360)	4 June 2019	726.60 pts/m ³	12990132	903 MB

As-is point cloud data reconstruction can be based on 3D model geometry reconstruction, where the model only contains geometric information, or the reconstruction process can also include semantic information and object recognition from the point cloud model [117]. In this experimental study, only the geometric

information of the point cloud data was required. Automated object recognition in this case was based on the comparison of the point cloud and the IFC model, where semantic information of the object identified in the point cloud model can be directly extracted from IFC. The research methodology at this stage was based on the automatic identification of objects in the point cloud model that are built or not built, and the semantic information was needed to determine the relationship of the identified object with the IFC object. Accordingly, the IFC model was simplified by removing redundant elements and element assemblies and leaving only the model of the scanned area without the ceiling plane. The models were originally created in *Tekla Structures 2017* software and exported into the IFC format, selecting the *IFC2X3* scheme with the default settings. Removal of the unnecessary elements of the IFC model was done in *Simplebim 8.2 SR1* software and then saved again in the IFC format.

3.4.1. IFC and point cloud data alignment

To perform the process of tracking built and not built objects, the as-built and as-designed data models had to be aligned first. However, IFC and point cloud files have different data structures that are not directly comparable. For example, IFC files contain a structured list of building elements (e.g., slabs, beams, walls, columns), wherein each element is characterized by its properties, such as vertices, lines, faces, and their spatial coordinates (x, y, z). Meanwhile, point cloud files contain a set of points representing the geometry of the objects captured during the scan. These data points are accompanied by their spatial coordinates but have no information regarding their semantic representation (e.g., column, wall, beam).

Consequently, two alternatives for aligning different types of data were considered at this stage. One option considered was converting point cloud data to IFC data. However, this is a complex process which requires detailed and comprehensive understanding of the structure and nuances of the IFC schema. Another alternative for data alignment was to convert IFC data to point cloud data. The latter option only required the understanding of storing and retrieving vertices of IFC elements, and it was therefore selected for further analysis.

To perform the automated alignment, the IFC file format was first explored, and an extraction process was conducted to obtain feature vertices of the IFC elements. The pipeline of IFC exploration process is depicted in Figure 43. This extraction process produced a point cloud version of the IFC data as shown in Figure 44.

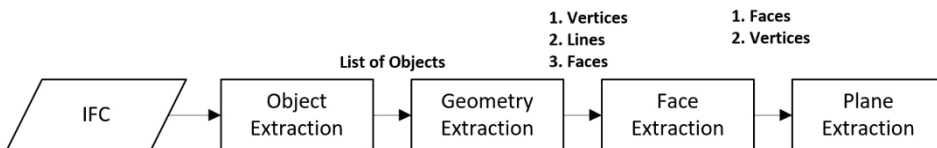


Fig. 43. Pipeline of IFC exploration

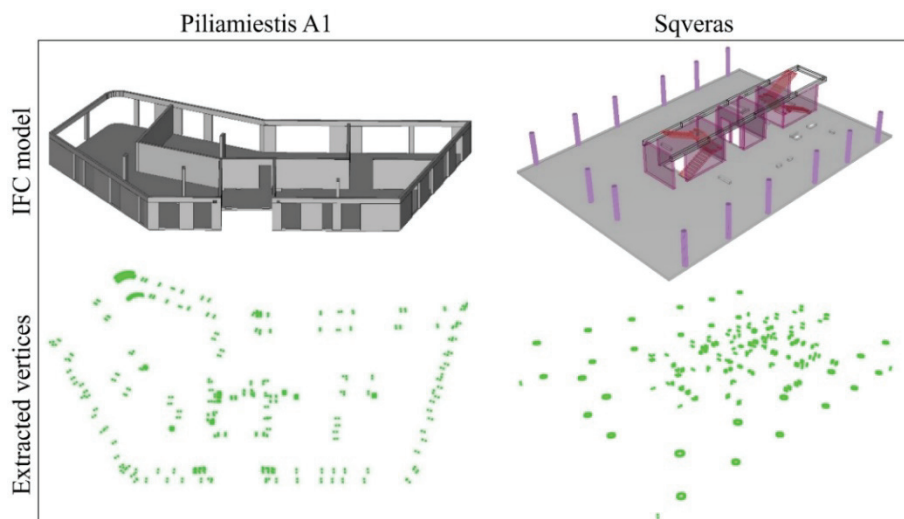


Fig. 44. The point cloud version obtained by extracting the vertices of IFC elements

The reading of the IFC format and the extraction of the geometry information was performed by using the open-source IFC toolkit (*IfcOpenShell*) in conjunction with the *Python* programming language. *IfcOpenShell* (<http://www.ifcopenshell.org>, accessed on 14 July 2022) is an open-source software library released under the LGPL license for reading, writing, and modifying IFC files [139]. The extracted geometry information for each IFC object was represented as a set of faces, lines, and vertices along with their corresponding relationships. Specifically, to create a point cloud, only the x, y, z spatial coordinates of the object vertices were required.

After obtaining the point cloud by extracting the vertices from each IFC object, alignment of the as-built and as-designed data was performed. The pipeline of data alignment is shown in Figure 45. For the alignment, the well-known *Iterative Nearest Point* (ICP) algorithm was applied. The ICP algorithm is a widely used automated alignment technique that operates on two different sets of point clouds, where one is considered as the source point cloud and the other as the target point cloud. In the present context, the source point cloud corresponded to the data acquired from the laser scanner sensors, while the target point cloud represented the point cloud created from the extracted vertices of the IFC elements.

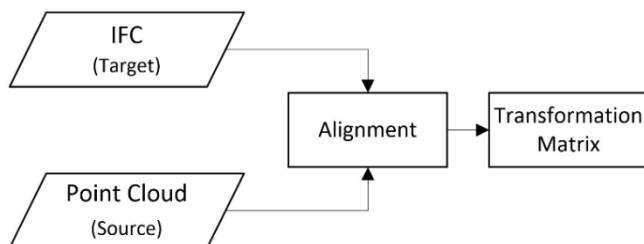


Fig. 45. Pipeline of data alignment

In order to achieve accurate alignment results, a coarse registration must first be performed, which will provide the correct parameters for the transformation. The

ICP algorithm operates by assuming that the point clouds are initially roughly aligned and aims to determine the optimal rigid transformation for refining the alignment. This process involves iteratively searching for the nearest distances between points to approximate the correspondences, thereby enhancing the alignment with each iteration.

Typically, data alignment by using the ICP approach relies only on point cloud information. In this study, user input was required to initiate the alignment process by selecting three pairs of reference points in the source and target point clouds, which provided a reasonably accurate and efficient alignment process. Figure 46 illustrates the selection of these reference points. The ordering of the reference points in each set is maintained, with the first reference point in the source point cloud corresponding to the first reference point in the target point cloud, and so forth. The reference points are color-coded, with the first point depicted in yellow, the second in magenta, and the third point in orange. Through this procedure, an initial transformation matrix was calculated, which was subsequently applied to the source data to achieve the initial alignment.

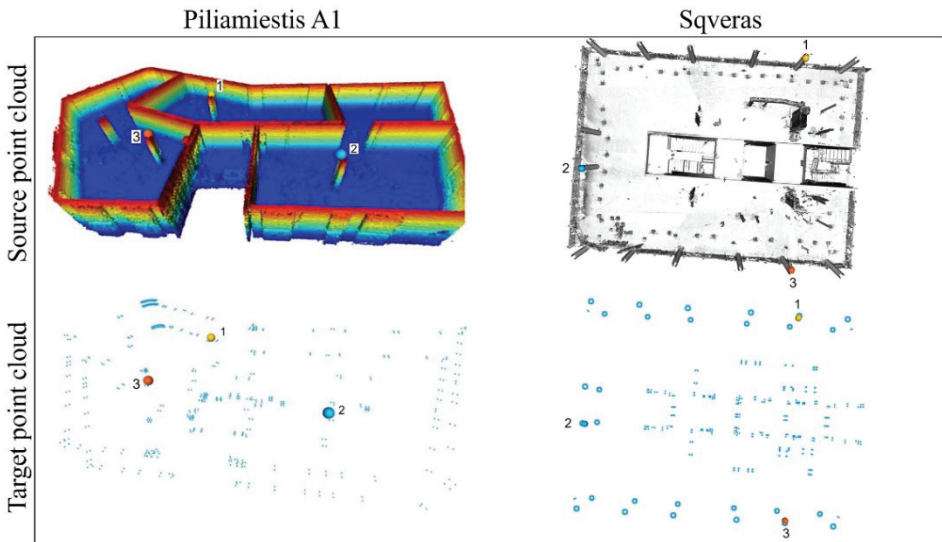


Fig. 46. Selection of the reference points

Following the initial alignment, a point-to-point ICP algorithm was employed to align all data points within the source and the target point clouds. The transformation matrix obtained from this process was utilized to perform the final alignment of the source data, which subsequently enabled the execution of the object monitoring process by comparing the as-built and as-planned states.

3.4.2. Automated object monitoring process

After aligning the source point cloud obtained from the laser scanner sensor with the target point cloud obtained from the vertices of the IFC elements, a process was implemented to automatically compare the actual construction with the as-

planned design for the purpose of identifying built and not built construction objects. The automated object detection process is shown in Figure 47.

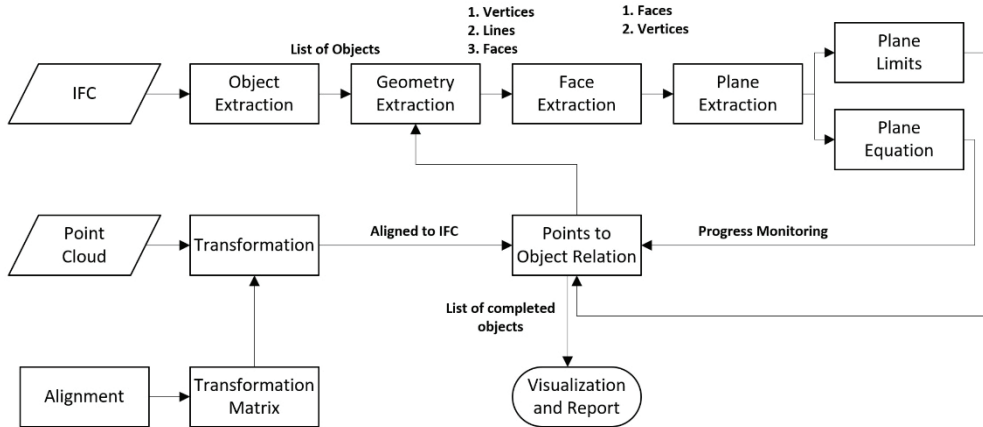


Fig. 47. Automated object detection process

As shown in Figure 47, the whole process consists of several tasks. The compared point cloud model has no semantic information and cannot determine which object it represents. In order to determine exactly what object was recognized in the point cloud, an object extraction process was performed. As previously stated, IFC files include a structured list of building objects. An object extraction process was used to examine IFC files and extract object identifiers. The main geometric attributes of IFC objects, such as vertices, lines and faces, were extracted through the geometry extraction process. Face information in IFC objects is represented as a relationship between vertices; therefore, only face and vertex information was extracted in the face extraction process. Also, since the entire process was performed in a three-dimensional environment, it facilitated the identification of the plane (e.g., (x, y) , (x, z) or (y, z)) to which each face belonged. This was achieved in the course of the plane extraction process by examining the axis where the plane extended further.

In order to verify whether the object under construction had already been built compared to the IFC model, a methodology was adopted which compared how many points in the point cloud were close to the faces of each IFC object. This task is known as point-to-plane distance estimation. In order to calculate the distance from the point to the plane, it was first necessary to calculate the equation of the face plane. The faces of an IFC object are represented as mesh triangles, thereby simplifying the calculation of the plane equation, which required only three points:

$$ax + by + cz + d = 0. \quad (2)$$

This equation represents a 3D plane in the Cartesian coordinate system. Here, x , y , z , are coordinates defining any point in 3D space, and a , b , and c are coefficients representing the normal vector to the plane. The vector (a, b, c) is perpendicular to the plane, and its direction determines the orientation of the plane. Meanwhile, d is a constant term, and it affects the position of the plane in 3D space in the direction of

the normal vector. Knowing the values of a , b , c and d allows us to describe the 3D plane and its relationship to other entities in the environment. This equation was used for the task of fitting a plane to a set of 3D points. The distance from points to the plane was calculated by using the plane equation encompassing all points, irrespective of whether they fell within the specific plane boundaries (as illustrated in Figure 48a). Therefore, the process involved discarding points lying beyond the confines of the current plane (as shown in Figure 48b).

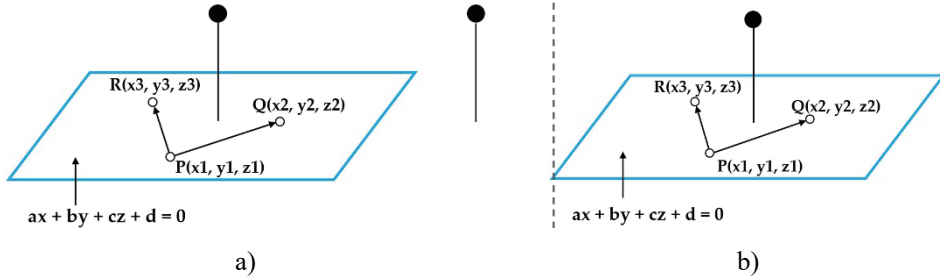


Fig. 48. Plane limits: a) distance calculation to all points; b) the process of discarding points that are outside the current plane

Figure 49 shows an example of an elementary wall. Typically, such a wall consists of 8 vertices, and each face in the plane can be composed of two triangles, which can also be considered faces, as shown in the example.

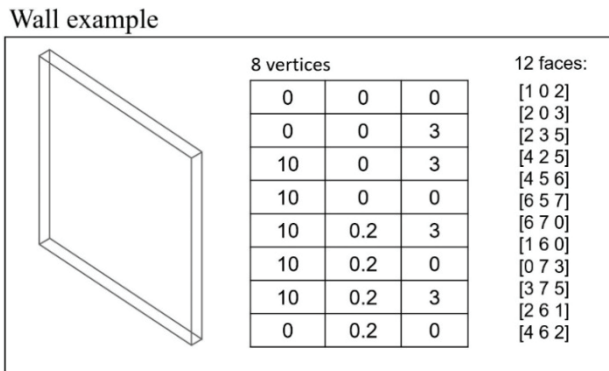


Fig. 49. A wall consists of 8 vertices and 12 faces

Finally, based on point-to-object relation, an object detection process was performed where each object was analyzed separately, and plane-to-point distance estimation was performed for each face of each object. A point was considered associated with a face if its distance to the face fell below a predefined threshold, and the initial output of this process consisted of a set of faces and the corresponding number of points associated with each face of each object. An example of determining whether a source point cloud point belongs to an IFC face is shown in Figures 50–52. The final result of the monitoring process was a list of objects detected in the point cloud model, and categorized as either built or not built, along with the identification of these objects by object identifiers extracted from the IFC file.

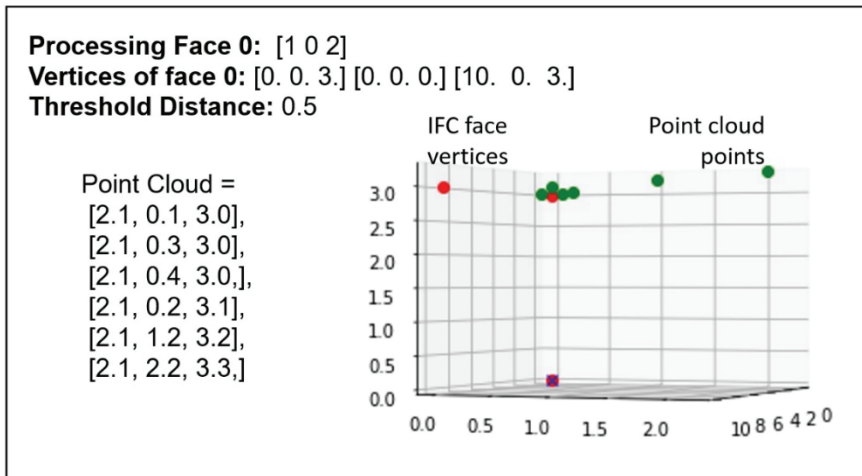


Fig. 50. Example of processing of wall face 0

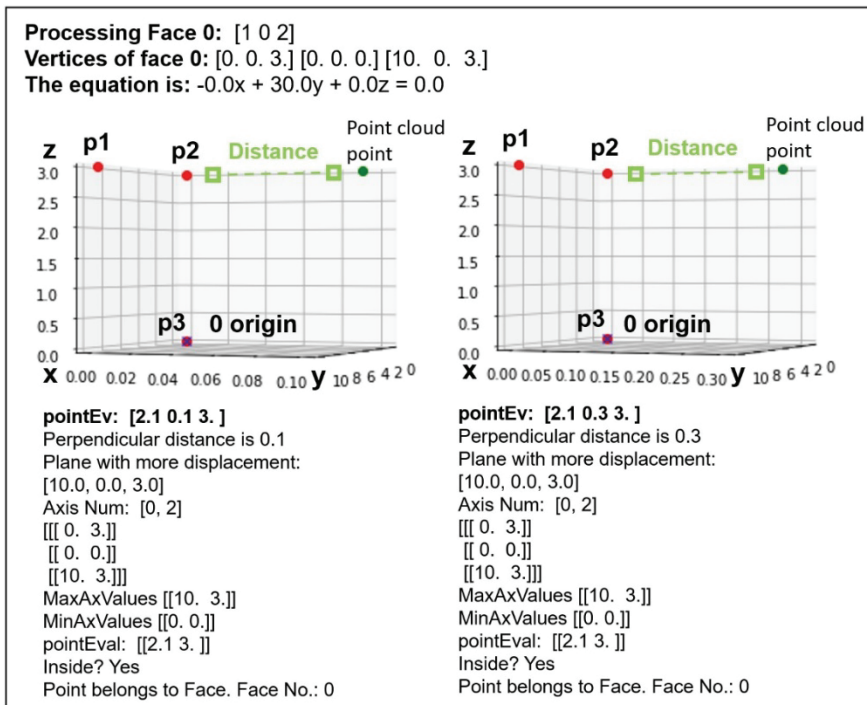


Fig. 51. Example of a source point cloud point relationship to a face when the point belongs to a plane

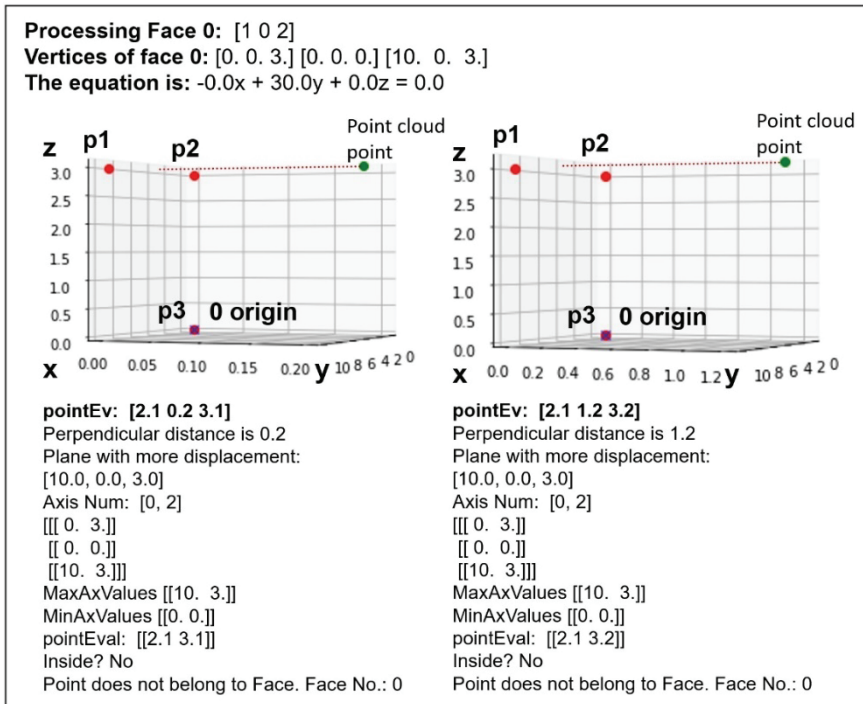


Fig. 52. Example of a source point cloud point relationship to a face when the point does not belong to a plane

3.4.3. Optimization

Point cloud data has value because it allows for a reasonably accurate geometric representation of the shape of the target environment. However, dealing with point cloud data presents certain challenges, such as a large amount of data, which can lead to higher computational costs for data processing or visualization. Also, the data density of point clouds is often higher than a given application requires. Reducing the density of the point cloud would also reduce the amount of the data, thus allowing for more efficient data management.

In this experimental study, the size of the point cloud data was reduced by implementing a sub-sampling technique, specifically, by using a feature provided by *Open3D* (`open3d.geometry.voxel_down_sample`). *Open3D* is a *Python* library for 3D data processing. The Downsampling function in the *Open3D* library is used to reduce a 3D point cloud by using a voxel grid. The downsampling process was performed by using a voxel size of 5 cm (as depicted in Figure 53), which allowed a significant reduction in the amount of data. The voxel size is a parameter which defines the size of the voxel grid used for data reduction. Points in the same voxel are downsampled to a single point. This approach aimed to alleviate the computational burden associated with dense point cloud data.

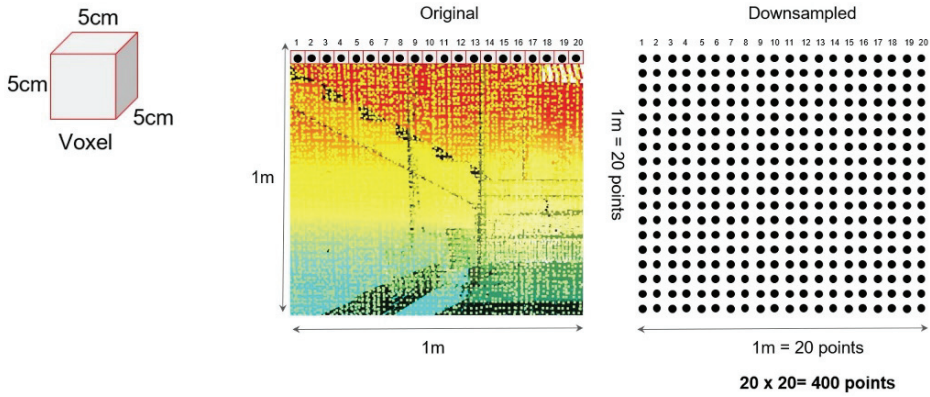


Fig. 53. Downsampling process when using 5 cm voxel size

Furthermore, in order to optimize the process, the determination of the relationship between the point and the face was carried out by processing one triangle for each face. Based on the wall example shown in Figure 54, each face of the IFC object was found to be composed of two triangles forming a mesh, and the entire wall was composed of 6 faces containing 12 triangles. This optimization method was based on experimental observations during the point-to-plane distance estimation process. During the experiment, it was observed that, when determining the relationship between points and the face of an IFC object, an equal number of points was associated with triangles belonging to the same face (as shown in Figures 55–57). Based on this finding, only one triangle per face was processed to optimize the object detection process.

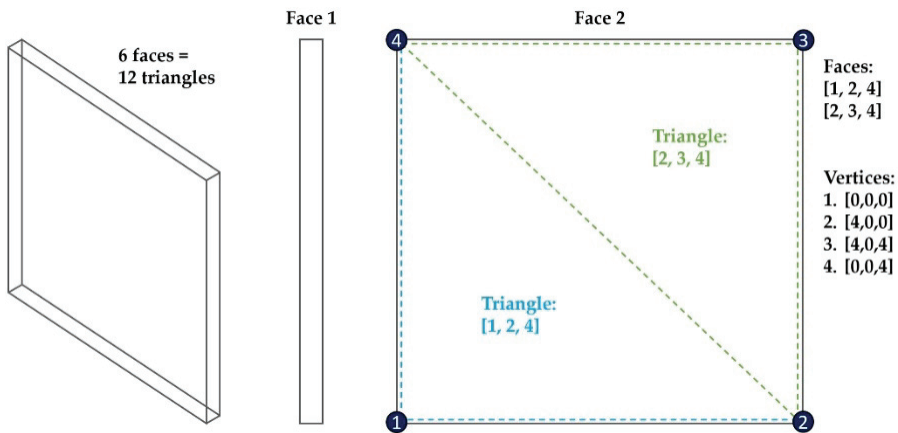


Fig. 54. Face information of an IFC object, represented as a relationship between vertices

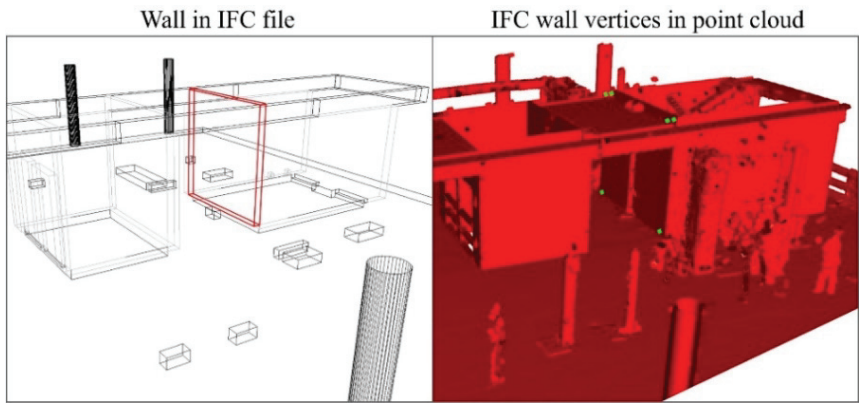


Fig. 55. IFC wall vertices in the as-built point cloud. IFC vertices are marked in green

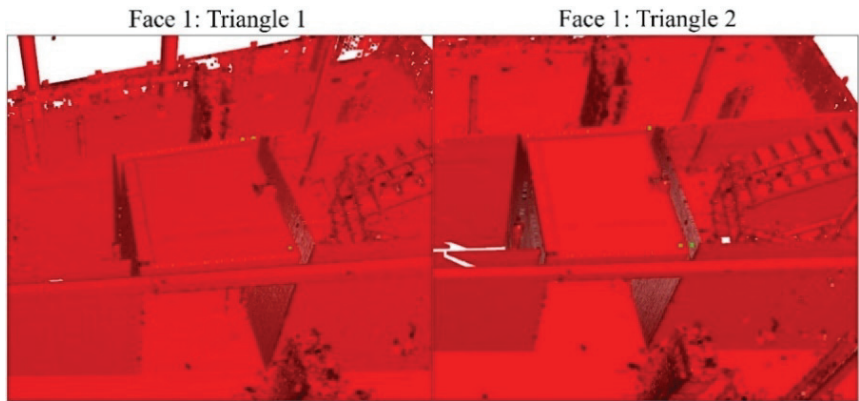


Fig. 56. Example of face 1 separated into two triangles (green dots)

Face 1: T1_T2

Face 1: T1 and T2

Results:

- Face 1. Triangle 1 [661. 0.]
- Face 1. Triangle 2 [661. 0.]
- Face 2. Triangle 1 [98138. 0.]
- Face 2. Triangle 2 [98138. 0.]
- Face 3. Triangle 1 [314. 0.]
- Face 3. Triangle 2 [314. 0.]
- Face 4. Triangle 1 [80769. 0.]
- Face 4. Triangle 2 [80769. 0.]
- Face 5. Triangle 1 [57345. 0.]
- Face 5. Triangle 2 [57139. 0.]
- Face 6. Triangle 1 [46638. 0.]
- Face 6. Triangle 2 [47166. 0.]

Fig. 57. Example of face calculation results

3.5. Experimental Results of Construction Objects Monitoring

The results of the study are presented in the following way: Chapter 3.5.1 analyzes the specifics of data alignment, Chapter 3.5.2 explores the process of object detection and evaluates the proposed methodology under various construction conditions, and Chapter 3.5.3 examines the aspects of the optimization process.

3.5.1. Data alignment

The scan data can provide several columns of information, such as the x, y, z coordinates, the red, green, blue, and alpha (RGBA) color channel values, the scan angle, the intensity values, the timestamps, and some other parameters. Table 28 shows a fragment of the scan data from the third floor of the *Sqveras* building where the data had been georeferenced. This data allows us to understand what information is used in the data alignment process and where challenges arise. For example, the *FARO Focus* laser scanner provided the x, y, z spatial coordinates of the points in the 3D shape, RGBA color data, and normal vector information, which is used to represent the surface orientation of each point. However, the proposed alignment process only uses information from the first three columns, which are the x, y, and z values. Since the methodology proposed in this study only required geometry information, other information, such as the RGBA color channel was not considered. In addition, the obtained scan data shows that the values of the georeferenced coordinates are very large.

Table 28. Fragment of *Sqveras* 3rd floor scan data obtained with *FARO* laser scanner

3D spatial coordinates of the points, m			Color information, channel value				Normal vector's component, unit vectors		
x	y	z	R	G	B	A	x	y	z
494492.728	6084293.186	39.630	227	226	226	226	-0.522	0.836	-0.166
494491.433	6084292.959	39.052	179	179	179	179	0.015	-0.015	-0.999
494492.682	6084293.141	40.323	222	222	222	222	-0.796	0.604	0.012
494491.070	6084293.245	39.804	221	221	221	221	0.758	0.651	0.011
494492.027	6084292.790	39.045	23	23	23	23	0.195	-0.014	-0.980
494492.196	6084292.896	39.310	217	216	216	216	-0.045	0.015	0.998
494492.316	6084293.162	39.055	141	141	141	141	-0.045	0.015	-0.998
494492.814	6084293.222	39.403	230	231	231	231	-0.224	0.974	0.014
494492.976	6084293.197	40.487	232	233	233	233	0.529	0.846	-0.064
494491.284	6084292.954	39.051	191	191	191	191	-0.015	-0.015	-0.999
494492.410	6084292.982	39.314	215	215	215	215	-0.075	-0.015	0.997
494492.990	6084293.183	40.233	246	246	246	246	0.580	0.814	-0.012

The point cloud data acquired during the initial scan in the environment of the third floor of the *Sqveras* office building was georeferenced to a global coordinate system. All other point cloud models obtained both on the first floor of the *Sqveras* office building and on the residential building *Piliamiestis AI* were not georeferenced and remained in the local coordinate system. In the case of a georeferenced point cloud model, the x, y, z coordinates of each data point were expressed in thousandths and millionths, as previously shown in Table 28.

Meanwhile, in the Open3D module, such large values are represented as concise decimal values, as shown in Table 29. The coordinates of the remaining point cloud data, including those produced from IFC models, were expressed in small units. Such significant spatial separation of the source and target data increased the computational complexity and posed some challenges for use in the *Open3D* module (Figure 58).

Table 29. Representation of *Sqveras* 3rd floor scan data in *Open3D* module

3D spatial coordinates of the points, meters		
x	y	z
[[4.94492729e+05	6.08429319e+06	3.96308530e+01]
[4.94491434e+05	6.08429296e+06	3.90528530e+01]
[4.94492683e+05	6.08429314e+06	4.03238530e+01]
[4.94491071e+05	6.08429325e+06	3.98048530e+01]
[4.94492028e+05	6.08429279e+06	3.90458530e+01]
[4.94492197e+05	6.08429290e+06	3.93108530e+01]
[4.94492317e+05	6.08429316e+06	3.90558530e+01]
[4.94492815e+05	6.08429322e+06	3.94038530e+01]
[4.94492977e+05	6.08429320e+06	4.04878530e+01]
[4.94491285e+05	6.08429295e+06	3.90518530e+01]
[4.94492411e+05	6.08429298e+06	3.93148530e+01]
[4.94492991e+05	6.08429318e+06	4.02338530e+01]]

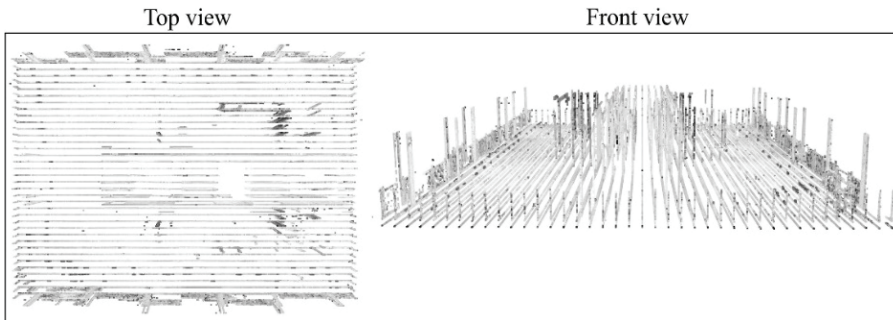


Fig. 58. *Sqveras* 3rd floor georeferenced point cloud data in *Open3D* module

It was concluded that the coordinates were too large for the Open3D module to handle and needed to be converted to smaller units. To address this issue, the georeferenced data was transformed to zero-origin coordinates. The coordinate transformation of the *Sqveras* 3rd floor scan data was performed by finding the minimum value of the x, y, and z column of the georeferenced scan data and subtracting that value from the coordinates of each column, as shown in Table 30.

Table 30. Transformation of *Sqveras* 3rd floor scan data coordinates to zero origin

Min Values::: 494490.875861 6084290.780026 38.665853		
To zero origin:		
x	y	z
[[1.853	2.406	0.965]
[0.558	2.179	0.387]
[1.807	2.361	1.658]
[0.195	2.465	1.139]
[1.152	2.010	0.380]
[1.321	2.116	0.645]
[1.441	2.382	0.390]
[1.939	2.442	0.738]
[2.101	2.417	1.822]
[0.409	2.174	0.386]
[1.535	2.202	0.649]
[2.115	2.403	1.568]]

After coordinate transformation, the source point cloud and the target point cloud were spatially located close to each other, and the point cloud model was correctly represented in the *Open3D* module. The results of the transformation of the georeferenced coordinates of the third floor of *Sqveras* are shown in Figure 59.

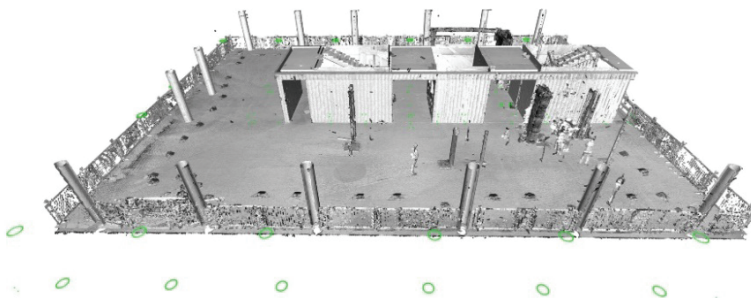


Fig. 59. Spatial location of the source point cloud model compared to the target point cloud data after the transformation of the georeferenced data into zero-origin coordinates

As previously mentioned, all of the point cloud models used in the experiment, with the exception of the *Sqveras* 3rd floor data, were not georeferenced. This implies that this point cloud data was in a local coordinate system, which was provided directly by the laser scanner. In practical applications, IFC building models are typically designed without georeferencing to global coordinates, often by utilizing a zero-coordinate system. During the experiment, the alignment of the initial data set, which had been georeferenced beforehand, it was observed that the source and target point cloud models were significantly distant from each other. As a result, additional measures were required to transform the coordinates of the georeferenced point cloud to the zero-origin. Meanwhile, since the laser scans obtained in the *Piliamiestis A1* project and the 1st floor of the *Sqveras* building were processed in the local coordinates, the transformation of the coordinates to the zero origin was not necessary in the alignment process, since the coordinates of the

source and the target point clouds were not far apart and were spatially located close to each other. However, in the experiment, the transformation of the coordinates to the zero origin was performed so that to minimize the distance (as shown in Figures 60 and 61).

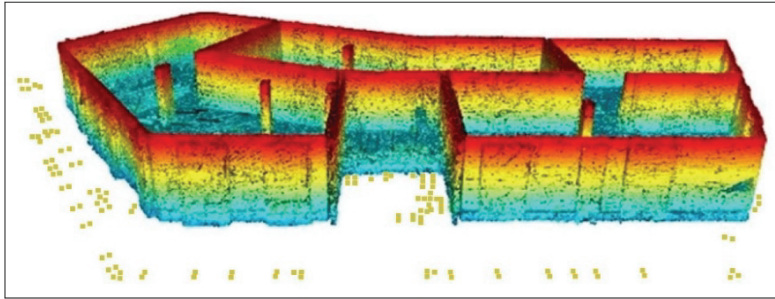


Fig. 60. Spatial location of *Piliamiestis A1* point cloud data after coordinate transformation to zero origin

Sqveras: 1st floor (FARO Focus S70)

Sqveras: 1st floor (Leica BKL360)

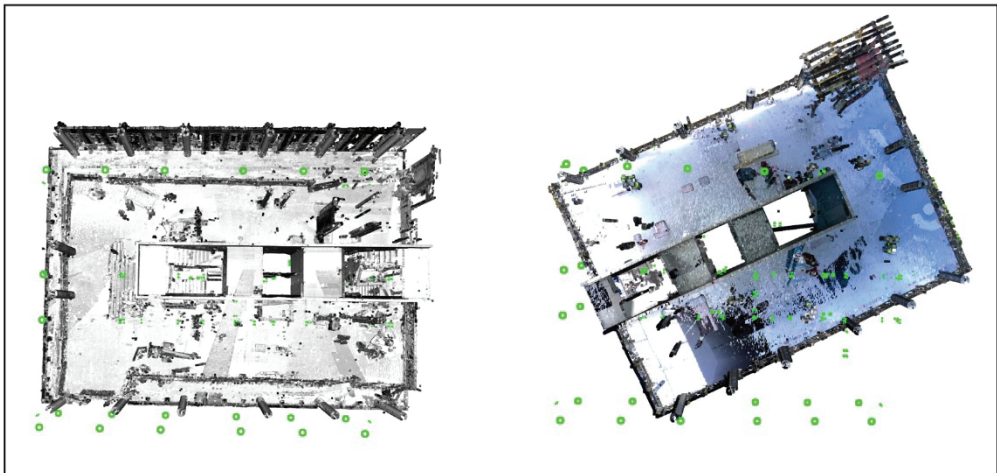


Fig. 61. Spatial location of *Sqveras* 1st floor point cloud data after coordinate transformation to zero origin. The data obtained by using *FARO Focus* laser scanner was not that far aligned, and the data obtained by using *Leica* laser scanner was not aligned at all

Initially, the source point cloud and the target point cloud were roughly aligned by selecting three pairs of reference points. The selection of reference points had to be done manually by the user. Once the rough alignment had been completed, the ICP method was then automatically applied to perform the final refinement by applying the resulting transformation matrix to the source point cloud. However, the performance of the alignment process was greatly influenced by the selection of the distance threshold, where the modification of its value yielded different outcomes. In this case, a threshold distance of 3 cm was used for the final ICP alignment.

The outcomes of the initial alignment, after selecting three correspondences, demonstrated reasonably well-aligned models. Point-to-plane and point-to-point ICP

approaches were compared during the testing phase, with superior alignment results achieved when using the point-to-point ICP method. Hence, an algorithm based on point-to-point ICP was employed in order to minimize the disparity between the two point clouds, which resulted in an improved alignment accuracy of approximately 0.021 m RMSE. The alignment results of the data sets used in the experiment, when using three user-selected reference points and the ICP point-to-point method, are presented in Figures 62–65.

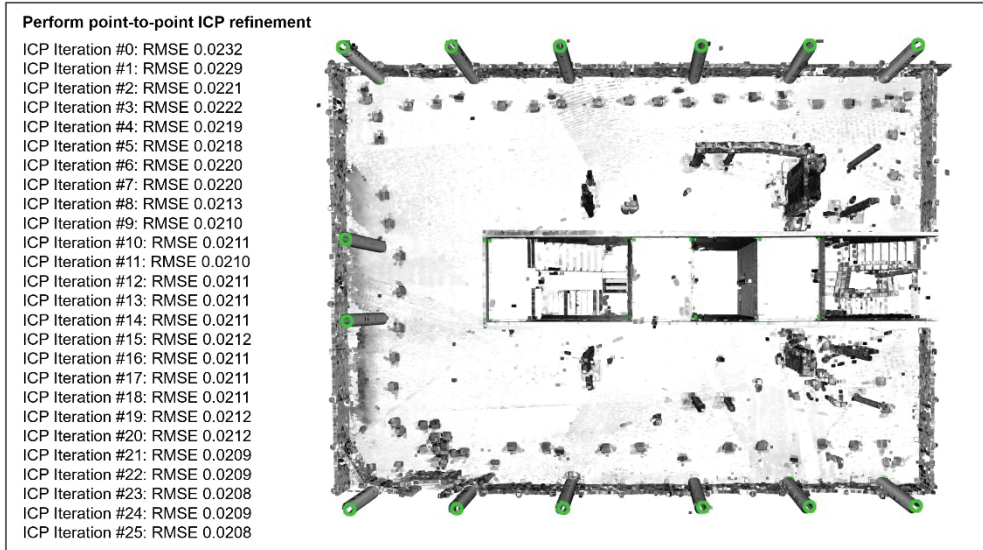


Fig. 62. Alignment results: *Sqveras 3rd floor (FARO Focus S70)*

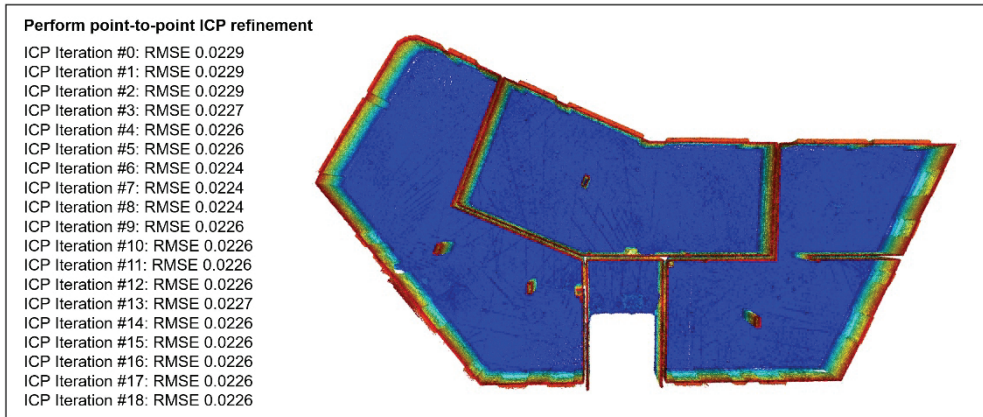


Fig. 63. Alignment results: *Piliamiestis A1 (ZEB-GO mobile laser scanner)*

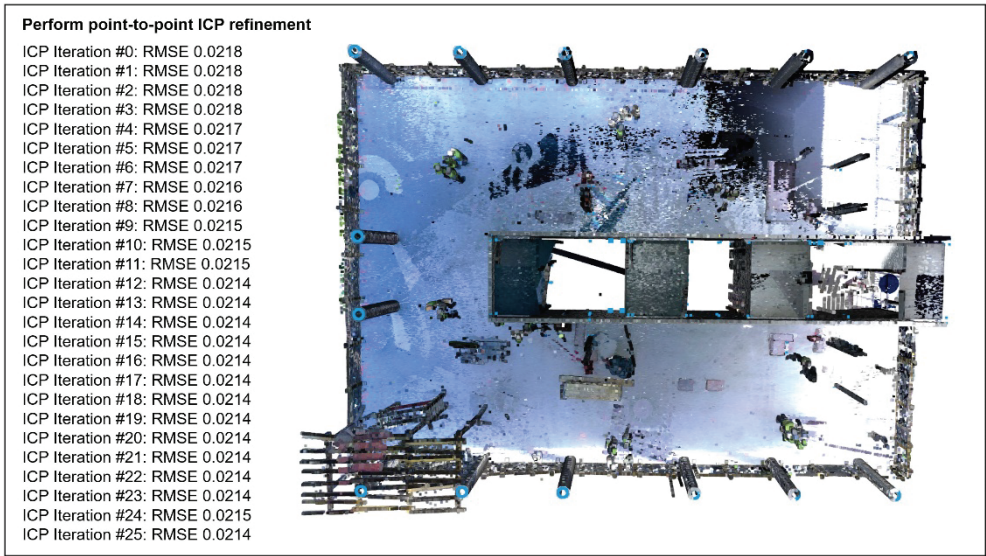


Fig. 64. Alignment results: *Sqveras* 1st floor (*Leica BLK360*)

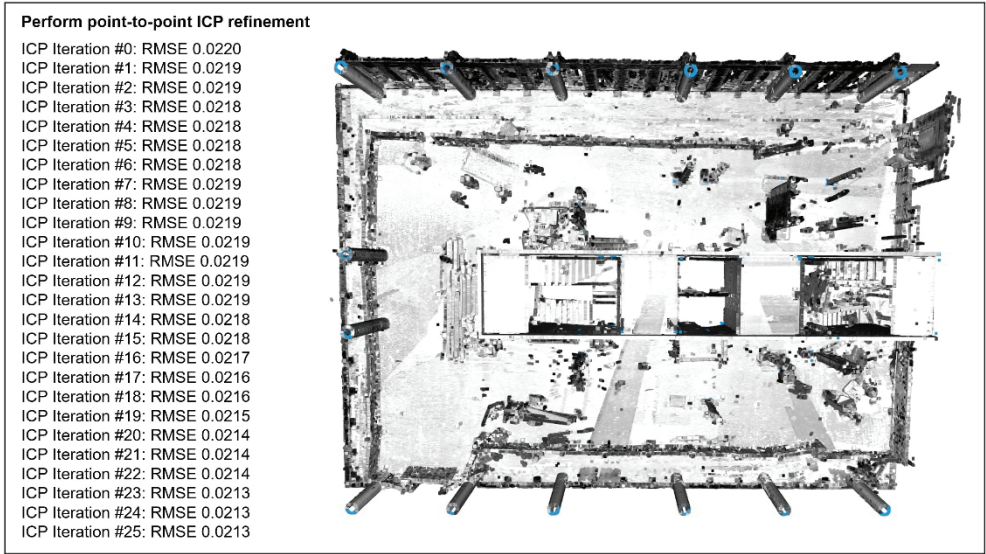


Fig. 65. Alignment results: *Sqveras* 1st floor (*FARO Focus S70*)

3.5.2. Evaluation of object detection

The methodology proposed in this research focused on automatic detection of vertical structures, such as walls and columns. Six data sets consisting of the as-built point cloud data and the corresponding as-designed IFC model were analyzed. For both the first and the third floor datasets of the *Sqveras* building, the IFC models were designed identically, with each consisting of 25 vertical objects which were tested to evaluate the proposed methodology. Meanwhile, in the *Piliamestis A1*

dataset, the IFC model consisted of 38 vertical objects which were used for the object detection test.

Another important criterion for IFC object detection in a point cloud was the successful detection of objects under the real construction conditions where the scanned scenes were occluded, or the scan data was of low quality. Accordingly, the object detection approach was based on defined parameters, which allowed flexibility in the presence of inaccurate or incomplete scan data. First, in order to determine whether an object was present in the point cloud, the faces composing the current IFC object were found. Thus, each face of the wall (a cube rectangle) has two faces (two triangles) whose vertices were extracted, and the plane equation of the current face was found. Then, the perpendicular distance from each point cloud point to the face plane was calculated, and the plane was constrained to consider only the point that was inside the limit of the plane. The result was the number of points which belonged to each face determined with a threshold of 0.5, the area of the face, and 0 or 1, where '1' indicated that the face contained enough points. A face was considered complete if there were at least 400 points per square meter that belonged to that face, as shown in Figure 53. Since each object had multiple faces, if at least 60% of the faces were marked as complete, then the object was marked as detected. These parameters allowed the successful automated identification of built and not built objects in the point cloud, even when the scan was performed in a cluttered environment, and the scan data was of a low quality.

First, the method was evaluated by using datasets 1 and 2, where the scanning environment was free of occlusion. Dataset 1 contained relatively high-quality scan data acquired on the third floor of the *Sqveras* building. Meanwhile, in dataset 2, the point cloud data was obtained with a laser scanner with much lower accuracy parameters in the *Pilamiestis AI* building. The initial object detection test with these datasets was successful, with all objects detected and identified as built. The green color in Figure 66 indicates that all objects have been detected.

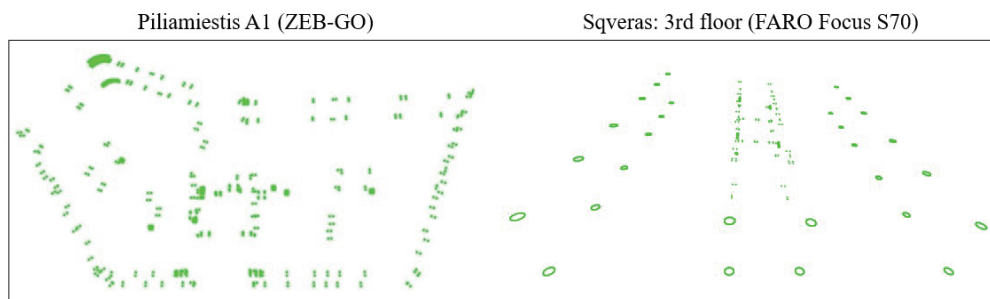


Fig. 66. Objects marked in green are detected and identified as built

In addition, the results were presented in an automated monitoring report that lists 0's and 1's along with the global IDs of the objects defined in the IFC model. In the report, '0' means that the object was not detected in the point cloud and is not built, while '1' means that the object was detected and has already been built. The report results for datasets '1' and '2' are shown in Table 31.

Table 31. Automated tracking report listing 0's and 1's along with global IDs

No.	Piliamiestis A1		Sqveras 3 rd floor	
	Object ID	Built/ Not built	Object ID	Built/ Not built
1	1csl aXPmL9cenLNaPHhfDm	1	0xiLmjZqXDvv7s6AzqDEoM	1
2	1csl aXPmL9cenLNaPHhfDo	1	0xiLmjZqXDvv7s6AzqDEoK	1
3	1csl aXPmL9cenLNaPHhfDq	1	0xiLmjZqXDvv7s6AzqDEoI	1
4	1csl aXPmL9cenLNaPHhfDs	1	0xiLmjZqXDvv7s6AzqDEoG	1
5	1csl aXPmL9cenLNaPHhfDt	1	0xiLmjZqXDvv7s6AzqDEoU	1
6	1csl aXPmL9cenLNaPHhfDe	1	0xiLmjZqXDvv7s6AzqDEoS	1
7	1csl aXPmL9cenLNaPHhfDf	1	0xiLmjZqXDvv7s6AzqDEoQ	1
8	1csl aXPmL9cenLNaPHhfDg	1	0xiLmjZqXDvv7s6AzqDEoO	1
9	1csl aXPmL9cenLNaPHhfDh	1	0xiLmjZqXDvv7s6AzqDEoc	1
10	1csl aXPmL9cenLNaPHhfDi	1	0xiLmjZqXDvv7s6AzqDEoa	1
11	1csl aXPmL9cenLNaPHhfDj	1	0xiLmjZqXDvv7s6AzqDEoY	1
12	1csl aXPmL9cenLNaPHhfDk	1	0xiLmjZqXDvv7s6AzqDEoW	1
13	1csl aXPmL9cenLNaPHhfDl	1	0xiLmjZqXDvv7s6AzqDEgf	1
14	1csl aXPmL9cenLNaPHhfDW	1	0xiLmjZqXDvv7s6AzqDEgt	1
15	1csl aXPmL9cenLNaPHhfDX	1	0xiLmjZqXDvv7s6AzqDFXm	1
16	1csl aXPmL9cenLNaPHhfDY	1	0xiLmjZqXDvv7s6AzqDFX	1
17	1csl aXPmL9cenLNaPHhfDZ	1	0xiLmjZqXDvv7s6AzqDFXy	1
18	1csl aXPmL9cenLNaPHhfDa	1	0xiLmjZqXDvv7s6AzqDFXw	1
19	1csl aXPmL9cenLNaPHhfDb	1	0xiLmjZqXDvv7s6AzqDFXu	1
20	1csl aXPmL9cenLNaPHhfDc	1	0xiLmjZqXDvv7s6AzqDFXv	1
21	1csl aXPmL9cenLNaPHhfDd	1	0xiLmjZqXDvv7s6AzqDFW7	1
22	1csl aXPmL9cenLNaPHhfDO	1	0xiLmjZqXDvv7s6AzqDFW4	1
23	1csl aXPmL9cenLNaPHhfDP	1	0xiLmjZqXDvv7s6AzqDFW2	1
24	1csl aXPmL9cenLNaPHhfDQ	1	0xiLmjZqXDvv7s6AzqDFW3	1
25	1csl aXPmL9cenLNaPHhfDR	1	0xiLmjZqXDvv7s6AzqDFW0	1
26	1csl aXPmL9cenLNaPHhfDS	1		
27	1csl aXPmL9cenLNaPHhfDT	1		
28	1csl aXPmL9cenLNaPHhfDU	1		
29	1csl aXPmL9cenLNaPHhfDV	1		
30	1csl aXPmL9cenLNaPHhfDG	1		
31	1csl aXPmL9cenLNaPHhfDH	1		
32	1csl aXPmL9cenLNaPHhfDI	1		
33	1csl aXPmL9cenLNaPHhfDJ	1		
34	1csl aXPmL9cenLNaPHhfDK	1		
35	1csl aXPmL9cenLNaPHhfDF	1		
36	1csl aXPmL9cenLNaPHhfD1	1		
37	1csl aXPmL9cenLNaPHhfD3	1		
38	1csl aXPmL9cenLNaPHhfD5	1		

Since the objects in the point cloud were identified by comparing the point cloud data to the IFC model, it was important to identify which object was actually detected. In addition to producing a report with a list of 0's and 1's and a

visualization, the global IDs allowed identifying which object from the IFC model was detected (as shown in Figure 67).

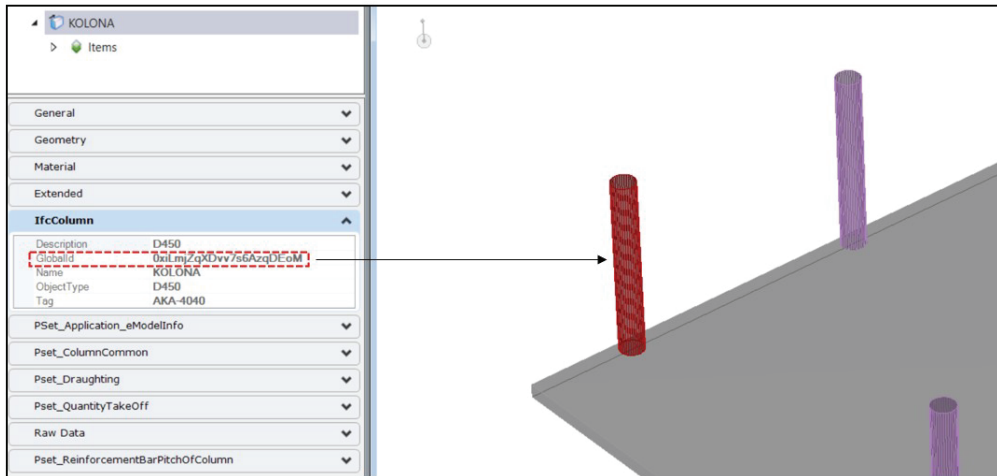


Fig. 67. Global ID of a specific IFC object in *Bentley Descartes* software

During the experiment with datasets 1 and 2, all the objects were detected successfully. The next step was to evaluate how the method is able to detect the missing objects in the point cloud. To accomplish this, several objects were removed from the point cloud models. In this way, it was simulated that the objects were not built in reality. One wall and two columns were removed from the point cloud model belonging to dataset 1, and the resulting point cloud model was assigned to dataset 3. Meanwhile, two walls and two columns were removed from the point cloud model belonging to dataset 2, and this model was assigned to dataset 4. The objects removed from the point clouds are shown in Figure 68.

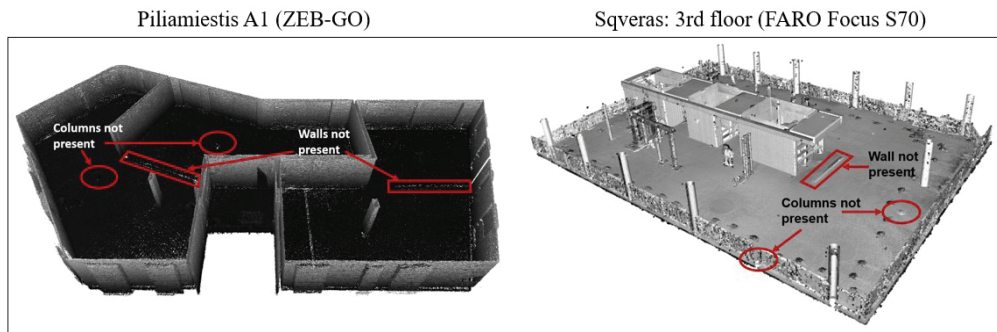


Fig. 68. Method evaluation by removing objects in point cloud data

In this case, the objects missing from the point cloud compared to the IFC model were identified as not built. The object detection results are shown in Figure 69, where the detected objects are marked in green, and the undetected objects that were identified as unbuilt are marked in blue.

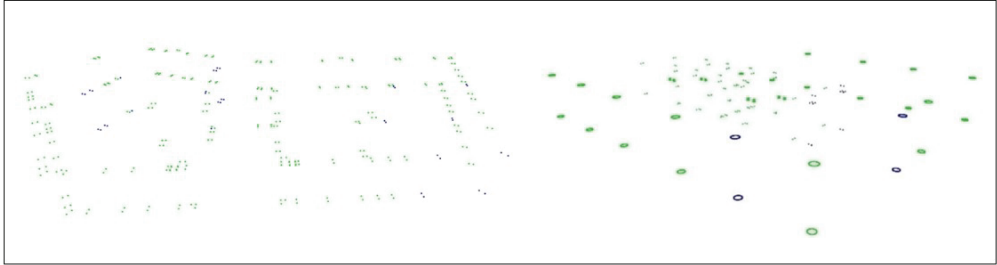


Fig. 69. Object detection in datasets 3 and 4 when there were missing objects in the point cloud

In some cases, the obtained results can be difficult to visually analyze by looking only at the IFC extracted vertices. To facilitate progress tracking, the proposed methodology allows the integration of both source and target point clouds for additional visual analysis which provides superior understanding of the current situation. The integration of the as-built point cloud and the point cloud obtained by extracting vertices from IFC objects is shown in Figure 70. This integration can facilitate the evaluation of the current progress.

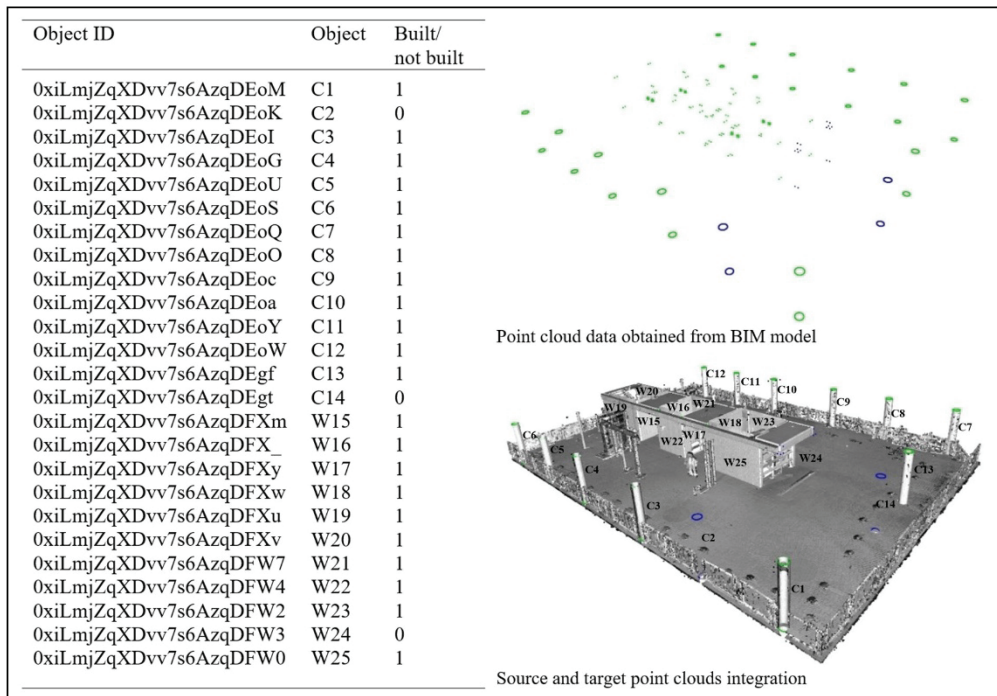


Fig. 70. Integration of source and target point cloud data: the case of *Sqveras* 3rd floor where two columns and one wall were removed

Up to this point in the experiment, the proposed method was able to correctly detect and identify built and unbuilt objects in the point cloud when the environment was not cluttered. However, in construction, the environment is constantly changing,

and in practice it is difficult to perform scanning without various interferences, which can lead to incompletely scanned surfaces and, consequently, to a lower data quality. Therefore, the next step was to evaluate the object detection method in a cluttered environment. In this case, the methodology was evaluated using by datasets 5 and 6, where the data was captured with a particular focus on cluttered environments. Dataset 5 contained a point cloud acquired with a *FARO Focus* laser scanner on the first floor of the *Sqveras* building. Dataset 6, meanwhile, contained a point cloud acquired at the same location by using a *Leica BLK360* laser scanner with lower accuracy parameters. In addition to the environment being cluttered with construction materials and the presence of other obstacles, such as formwork or scaffolding, no effort was made to perform a high-quality scan. The aforementioned conditions contributed to the displacement and duplication of some columns and incompletely scanned objects in the resulting cloud model. Such conditions partially reflected the real environment during the construction process. Also, at this stage of the experiment, most of the redundant points were not removed and remained in the point cloud models for further evaluation. The obtained point cloud reflecting these conditions is shown in Figure 71.

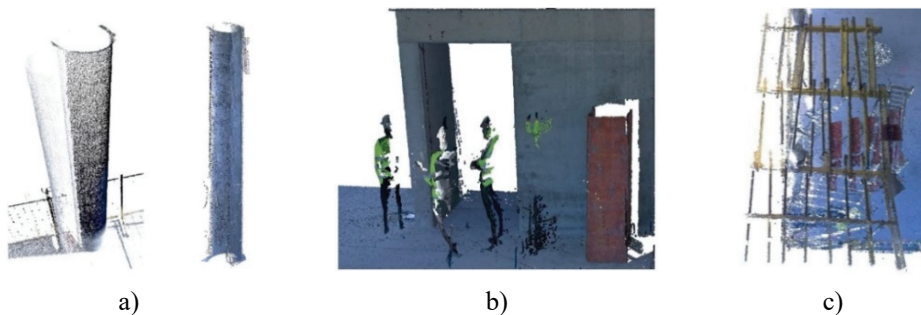


Fig. 71. Example of the resulting point cloud in a cluttered environment: a) several columns were displaced and duplicated and had incompletely scanned surfaces; b) an obstruction caused a hole in the scanned surface, and redundant points were not removed; c) formwork was installed above the column, there were scaffolding and other items nearby

Despite the aforementioned challenges, the proposed method was able to correctly detect IFC objects in datasets 5 and 6. The results of object detection in a cluttered construction environment are presented in Table 32.

Table 32. Object detection in cluttered construction environment

No.	<i>Sqveras</i> 1 st floor	Dataset 5	Dataset 6
	Object ID	Built/Not built	Built/Not built
1	0xiLmjZqXDvv7s6AzqDEpm	1	1
2	0xiLmjZqXDvv7s6AzqDEp	1	1
3	0xiLmjZqXDvv7s6AzqDEpy	1	1
4	0xiLmjZqXDvv7s6AzqDEpw	1	1
5	0xiLmjZqXDvv7s6AzqDEpu	1	1
6	0xiLmjZqXDvv7s6AzqDEo6	1	1
7	0xiLmjZqXDvv7s6AzqDEo4	1	1
8	0xiLmjZqXDvv7s6AzqDEo2	1	1

9	0xiLmjZqXDvv7s6AzqDEo0	1	1
10	0xiLmjZqXDvv7s6AzqDEoE	1	1
11	0xiLmjZqXDvv7s6AzqDEoC	1	1
12	0xiLmjZqXDvv7s6AzqDEoA	1	1
13	0xiLmjZqXDvv7s6AzqDEgr	1	1
14	0xiLmjZqXDvv7s6AzqDEgp	1	1
15	0xiLmjZqXDvv7s6AzqDFXQ	1	1
16	0xiLmjZqXDvv7s6AzqDFXO	1	1
17	0xiLmjZqXDvv7s6AzqDFXc	1	1
18	0xiLmjZqXDvv7s6AzqDFXa	1	1
19	0xiLmjZqXDvv7s6AzqDFXY	1	1
20	0xiLmjZqXDvv7s6AzqDFXZ	1	1
21	0xiLmjZqXDvv7s6AzqDFXX	1	1
22	0xiLmjZqXDvv7s6AzqDFXk	1	1
23	0xiLmjZqXDvv7s6AzqDFXi	1	1
24	0xiLmjZqXDvv7s6AzqDFXj	1	1
25	0xiLmjZqXDvv7s6AzqDFXg	1	1

The results of object detection tests carried out up to this stage of the experiment are presented in Table 33.

Table 33. Object detection results for all datasets

Obj. No.	Objects detected/not detected					
	Dataset 1	Dataset 2	Dataset 3	Dataset 4	Dataset 5	Dataset 6
1	1	1	1	1	1	1
2	1	1	0	1	1	1
3	1	1	1	1	1	1
4	1	1	1	1	1	1
5	1	1	1	1	1	1
6	1	1	1	1	1	1
7	1	1	1	1	1	1
8	1	1	1	1	1	1
9	1	1	1	1	1	1
10	1	1	1	1	1	1
11	1	1	1	1	1	1
12	1	1	1	0	1	1
13	1	1	1	1	1	1
14	1	1	0	1	1	1
15	1	1	1	1	1	1
16	1	1	1	1	1	1
17	1	1	1	1	1	1
18	1	1	1	1	1	1
19	1	1	1	1	1	1
20	1	1	1	1	1	1
21	1	1	1	1	1	1
22	1	1	1	1	1	1
23	1	1	1	1	1	1
24	1	1	0	1	1	1

25	1	1	1	1	1	1
26		1		1		
27		1		1		
28		1		1		
29		1		1		
30		1		0		
31		1		1		
32		1		1		
33		1		0		
34		1		1		
35		1		1		
36		1		0		
37		1		0		
38		1		1		

In the results presented in Table 33, all the detected objects in the point cloud were marked as ‘1’, whereas not detected objects were marked as ‘0’. All objects specifically removed in point clouds in datasets 3 and 4 were marked as not detected. The results for all the six datasets showed that the objects were detected with minimal error. One object was incorrectly identified in dataset 4, as an existing object was marked as not detected. All the other objects analyzed in the experiment were correctly identified.

3.5.3. Optimization

One of the optimization measures in this study was the processing of one triangle per face as previously described in Chapter 3.4.3. This optimization methodology was implemented from the beginning of the experiment and was used in all tests, thus reducing the computational demand by half.

Since laser-scanned point clouds consist of a large amount of data that is often redundant, another important aspect to improve the efficiency of the whole process was data reduction. To reduce the amount of data, a downsampling method using a 5 cm voxel size was applied after the object detection methodology had been validated in the main tests. After applying downsampling, the point cloud models were reduced by 91–96% (as shown in Table 34), which proportionally increased the computational efficiency.

Table 34. Point cloud (PC) data reduction information

Point cloud data	Original PC (number of points)	Downsampled PC (number of points)
SQVERAS 3 rd floor (FARO Focus S70)	9451351	834551
PILIAMIESTIS A1 (ZEB-GO)	12510712	1236999
SQVERAS 1 st floor (FARO Focus S70)	13882774	641578
SQVERAS 1 st floor (Leica BLK360)	12990132	532111

After downsampling the point cloud data, the point density decreased, which resulted in a degraded surface appearance (as shown in Figure 72). Also, a decrease in the density of points can affect the detection of small objects. However, in this

study, small objects were not examined, and therefore no additional challenges arose in this particular field.

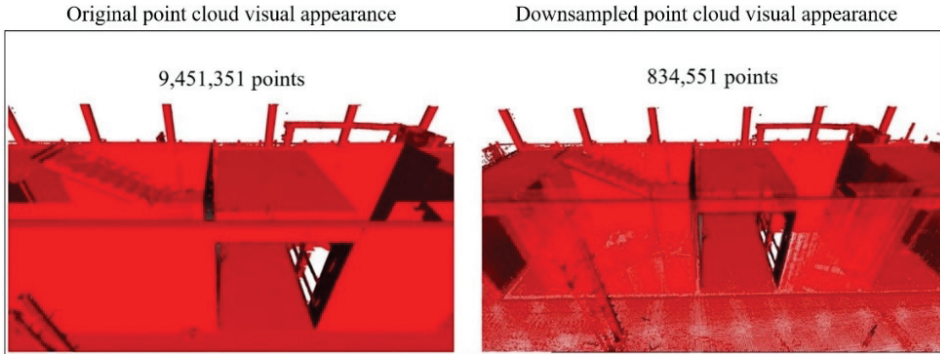


Fig. 72. Example of original and downsampled point cloud data

Data reduction was not observed to affect the alignment process, as the obtained alignment results were approximately 0.021 m RMSE, similar to the results obtained before applying downsampling. However, although the computational efficiency increased after the downsampling process, the proposed object detection method failed to avoid object detection errors in some cases. All objects were correctly detected in the *Sqveras* 3rd floor and *Piliamiestis AI* datasets. However, challenges arose with the detection of objects on the first floor of *Sqveras* building, where the environment was considered cluttered, and the data quality was lower. In this case, two existing columns were not detected in the point cloud model obtained with the *FARO Focus* laser scanner, as shown in Figure 73. However, all the walls were detected correctly in this phase of the experiment (Figure 74).

Matrix result: [1, 1, 1, 1, 1, 1, 1, 1, 1, 1, 1, 0, 0].

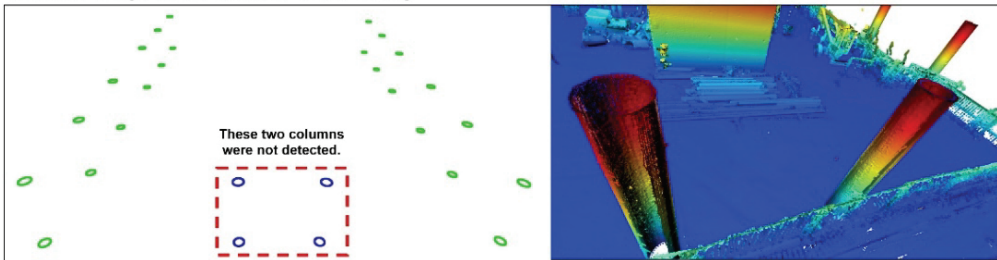


Fig. 73. The last two columns were not detected in the point cloud obtained with the *FARO Focus* laser scanner on the first floor of the *Sqveras* building

Matrix result: [1, 1, 1, 1, 1, 1, 1, 1, 1, 1, 1].

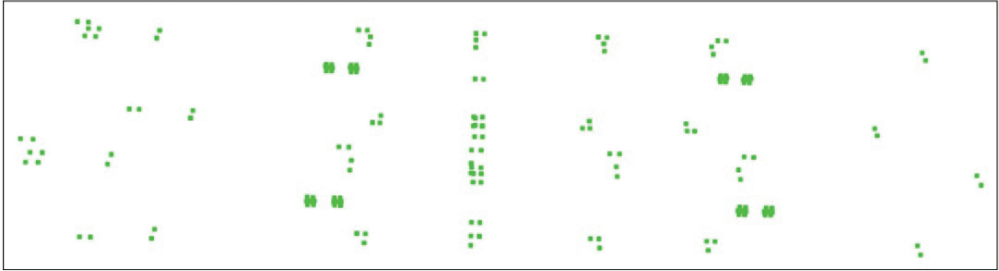


Fig. 74. There are no blue dots in the results visualization, which means that, after applying downsampling, all walls were detected

Meanwhile, in the point cloud model obtained with a *Leica BLK360* laser scanner, three existing columns and two existing walls were not detected after data downsampling had been applied, as shown in Figures 75–77.

Matrix result: [0, 1, 1, 1, 1, 1, 0, 0, 1, 1, 1, 1, 1].

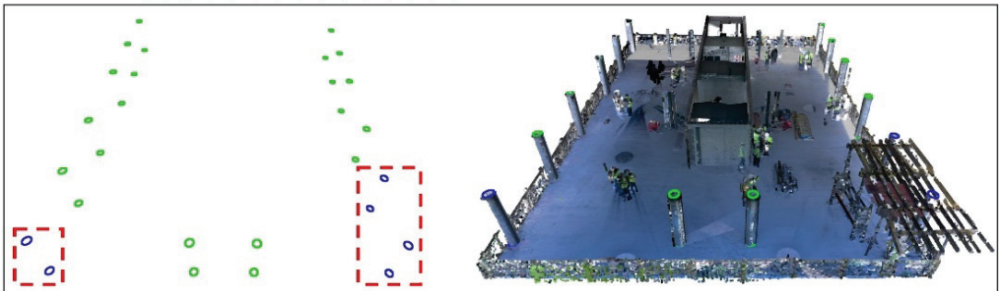


Fig. 75. Columns 1, 7 and 8 were not detected in the point cloud obtained with the *Leica BLK360* laser scanner on the first floor of the *Sqveras* building

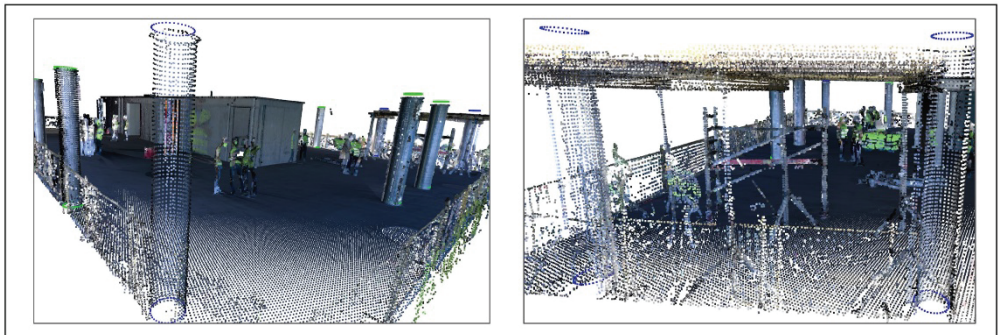


Fig. 76. On the left side, the undetected column No. 1 is shown, whereas, on the right side, columns Nos. 7 and 8 went undetected

Matrix result: [1, 1, 1, 1, 1, 1, 1, 1, 0, 1, 0].

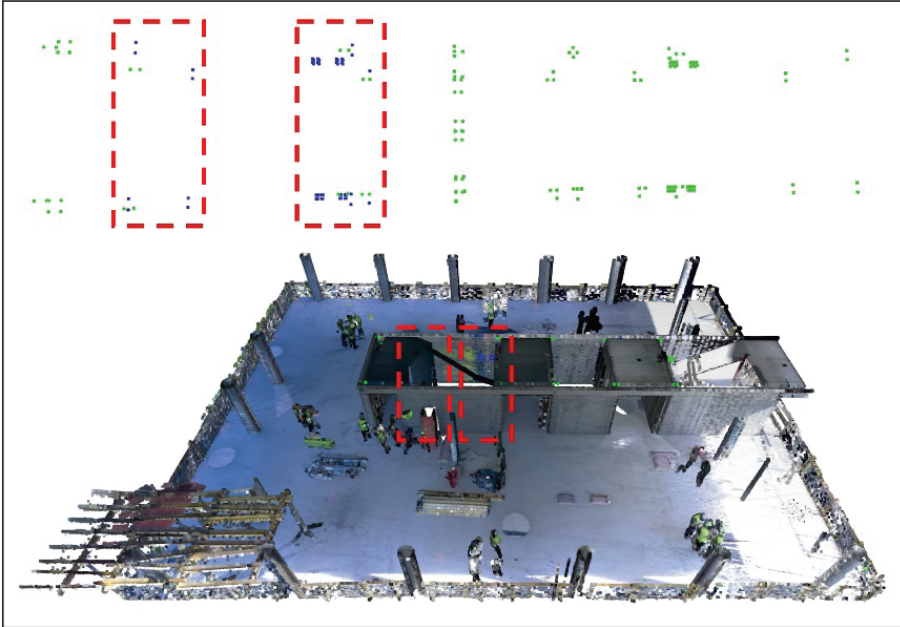


Fig. 77. Walls Nos. 9 and 11 were not detected

The results showed that the reduced point density had a negative effect on the detection of objects that had been previously successfully detected. However, it was observed that point clouds in which all the objects were successfully detected were considered as high-quality data, or the scanning was performed in an unobstructed field of view. Object detection challenges arose in those reduced point clouds that were considered to be of a lower quality, such as where object surfaces were incompletely captured due to various obstacles. Apparently, reducing the point density when part of the surface had already been incompletely scanned due to interference in the cluttered environment resulted in insufficient data to determine the relationship of the points to the faces of IFC objects. A summary of object detection test results after applying the downsampling is presented in Table 35.

Table 35. Object detection results for all datasets after applying downsampling

Obj. No.	Objects detected/not detected after applying downsampling			
	Dataset 1	Dataset 2	Dataset 5	Dataset 6
1	1	1	1	0
2	1	1	0	1
3	1	1	1	1
4	1	1	1	1
5	1	1	1	1
6	1	1	1	1
7	1	1	1	1
8	1	1	1	1

9	1	1	1	1
10	1	1	1	1
11	1	1	1	0
12	1	1	1	0
13	1	1	0	1
14	1	1	0	1
15	1	1	1	1
16	1	1	1	1
17	1	1	1	1
18	1	1	1	1
19	1	1	1	1
20	1	1	1	1
21	1	1	1	1
22	1	1	1	1
23	1	1	1	0
24	1	1	1	1
25	1	1	1	0
26		1		
27		1		
28		1		
29		1		
30		1		
31		1		
32		1		
33		1		
34		1		
35		1		
36		1		
37		1		
38		1		

3.6. Chapter Conclusions

1. The proposed construction progress monitoring method was based on the automated detection of objects in the point cloud by comparing the point cloud data with the IFC model. Data alignment was based on vertex extraction of IFC objects, which allowed the resulting point cloud of IFC vertices to be aligned with the as-built point cloud obtained by laser scanning. The object detection process involved determining the relationship between the existing points and IFC objects faces by computing the plane equation.
2. In order to perform the construction monitoring task, experiments were conducted under different construction conditions. The geometry of the structural objects was captured by using three laser scanners with accuracy parameters ranging from 1 to 30 mm, including static and mobile scanning workflows. The initial object detection methodology was developed by using scan data obtained in an orderly environment, and then the methodology was verified with the scan data obtained in a cluttered environment, which reflected the real situation in the daily construction process.

3. The evaluation of the proposed methodology focused on the effectiveness of data alignment and whether objects in the point cloud were correctly identified as built or as not built under different construction conditions compared to the IFC model. During the experiment, after performing three tests and evaluating 6 datasets, approximately 99% of the objects were correctly detected. However, the presented method cannot estimate deviations or determine whether the object has been built correctly. An object is considered built if at least 60% of the faces of the IFC object have a relationship with the points of the as-built point cloud according to the defined parameters. Therefore, theoretically, if the object is not yet built, but its completion is at least 60%, it could be identified as built.
4. A downsampling method was applied to optimize the object detection process, thus reducing the amount of data by 91–96%, and, as a result, the computational efficiency increased proportionally. With this approach, the object detection task was greatly influenced by the quality of the scanned data and the scanning environment. In cases where the scan data was of a lower quality and the scan was performed in a cluttered environment, several objects were incorrectly identified. However, in point clouds obtained by scanning in an orderly environment with an unobstructed field of view, all the objects were detected correctly.

4. RESULTS AND DISCUSSION

This Chapter summarizes the results obtained from the experiments conducted during the earthwork construction and structural construction phases. Chapter 4.1 presents the impact of progress monitoring automation on the traditional approaches and highlights the benefits of applying 3D point clouds to automate the monitoring process by using UAV-based photogrammetry and laser scanning technologies. Chapter 4.2 presents the main limitations which were determined during the experiments.

Several studies have been conducted to evaluate the accuracy and efficiency of different point cloud-based technologies, such as mobile and terrestrial laser scanning [102, 103, 104]. The accuracy of UAV-based photogrammetry using different configurations of GCPs, camera settings, and data processing schemes has been analyzed in [89, 90, 91]. In recent years, several studies have been conducted examining the RTK and PPK workflows of UAV-based photogrammetry [202, 203]. There have also been several studies comparing the most popular photogrammetry software packages, such as *Agisoft Metashape*, *Pix4D*, *Bentley ContextCapture*, and others [89, 204, 205]. Based on previous studies, comparison of software packages or evaluation of the accuracy of each method was beyond the scope of this study. The results are presented to fill research gaps by comparing different workflows in terms of accuracy, reliability, and time approaches as they influence the traditional nature of work. Accuracy is evaluated in terms of how accurately a method can identify objects and estimate quantities compared to the traditional approaches as a reference.

4.1. Impact of Automation on Monitoring Processes

In this thesis, the impact of automation on monitoring processes is evaluated from several aspects. First, the data accuracy of point cloud-based technologies was evaluated in comparison with the results obtained by the traditional approaches. In both experiments, data acquisition workflows were tested under real construction conditions. Secondly, the time and cost aspects of automated approaches were considered. Then, the output data and automation quality aspects of both experimental results were analyzed. Finally, health and safety factors were considered based on a comparison of workflows between the automated and traditional approaches. A representation of the aggregated results of both experiments is shown in Figure 78. The construction phase consists of various categories of work. Therefore, different technologies and workflows had to be applied to monitor the progress. However, the data obtained by both methods, which is used for the analysis of automated progress monitoring processes, is expressed in the point cloud format.

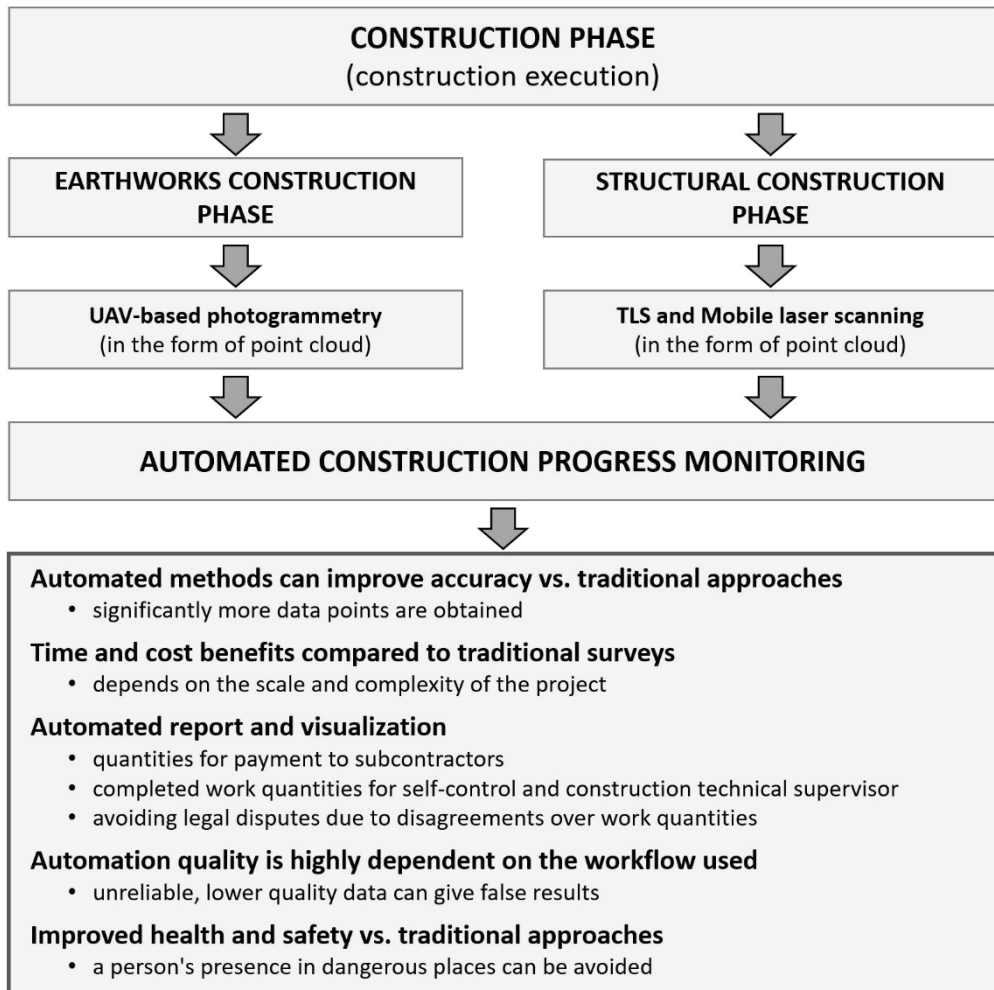


Fig. 78. Outcome of automated progress monitoring

A summary of the comparison of all the technologies examined in the thesis is schematically shown in Figure 79. The results of the methodologies used in the experiments are compared with the traditional approach, which serves as a reference line. The equipment cost, data acquisition and processing time efficiency, and other comparative results are shown as approximations. The cost of the units has been estimated based on preliminary information based on the initial verbal offers from vendors. The data acquisition and processing times using the traditional methods are based on the experience and information provided by professional surveyors. The accuracy and reliability of UAV-based technologies have been evaluated through experiments. The accuracy of laser scanning was evaluated according to the technical specifications of the device as declared by the manufacturer, and the data quality was evaluated according to the amount of noise obtained in the data, the population of points per m^3 , and the correspondence to the geometry of the BIM model, as well as the overall visual assessment. The reliability of the workflows was

evaluated based on how smoothly the data was obtained and how many and what errors occurred during each experiment with respect to the accuracy and quality of the final data.

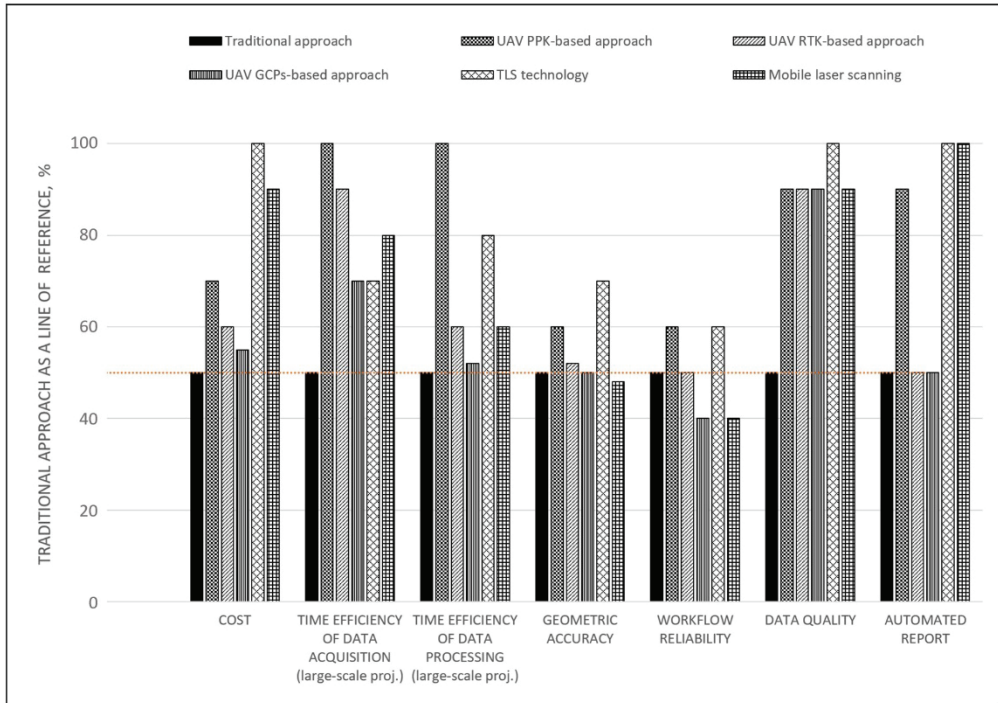


Fig. 79. Comparison of automated construction monitoring technologies compared to the traditional approach

4.1.1. Accuracy

The accuracy of the automated construction progress monitoring methods was evaluated considering the results obtained by the traditional approaches under real construction conditions. The accuracy of the earthworks control was evaluated by the quantities obtained in comparison with the quantities obtained by the traditional methods. When measuring more than 10000 m³ of soil, the results obtained by the traditional method differed from the results obtained by automated methods from 1.96% to 4.67%. The problem here is that, in practice, for this type of work, the traditional methods rely on a GNSS receiver which can incur an error of several centimeters. The traditional method can measure a point more precisely if there is vegetation in a certain area, but it is unrealistic to collect so many data points compared to the point cloud-based technology. During the experiment, 1008 points were acquired when using a GNSS receiver, while millions of x, y, z data points were acquired by UAV-based photogrammetry. A much larger number of data points can improve the overall accuracy of the model. The mesh surfaces obtained from photogrammetric models and *Civil 3D* software were superimposed and compared. Three random cross-sections were made in stockpiles No. 3, No. 15, and No. 16. The locations of the cuts are shown in Figure 13. In the cross-sections, the

differences between the UAV data obtained from 74 m and 100 m heights against those of the ground level survey data were compared. As Figure 80 shows, with a GNSS receiver, a data point is captured at the bottom and top of the stockpile. In practice, it is difficult to capture a sufficient amount of data points to accurately reproduce the surface curvature. The cross-sections showed that the differences between UAV data obtained from different altitudes varied by approximately 0.04–0.08 m in some locations. However, the difference between the photogrammetric surfaces and the surface measured with the GNSS receiver reached up to 0.26–0.89 m in some places.

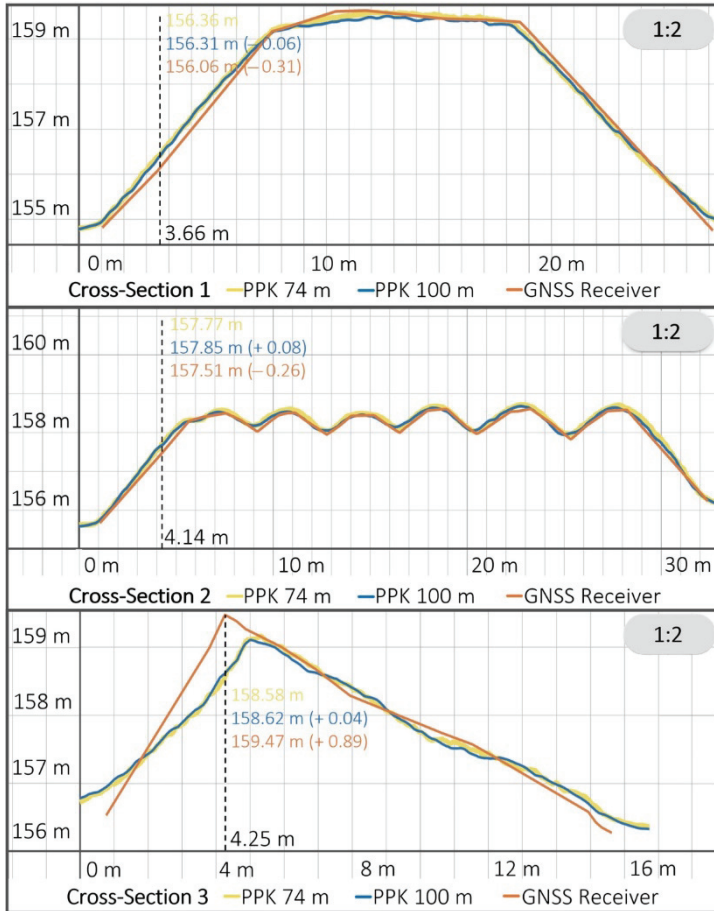


Fig. 80. Cross-sections of random stockpiles

The use of point cloud-based technologies in building construction also results in a significantly larger amount of x, y, z data points, which can improve the accuracy. However, in this case, the geometric accuracy was not evaluated. The accuracy of the monitoring process was evaluated based on how accurately the method was able to automatically identify built and not built structural objects compared to the associated IFC model. The results obtained during the experiment showed that the presented method correctly identified approximately 99 percent of

the objects. In general, the methods investigated in both experiments were evaluated according to how accurately the amounts of work performed were estimated.

4.1.2. Time and cost benefits

When automating the monitoring of construction progress, it is fundamentally important to consider the benefits this process can provide in terms of time and cost. The UAV-based technology is a relatively inexpensive solution which can provide tangible benefits depending on the scale of the project. An industrial unmanned aerial system for earthworks survey can cost from approximately 5000 Euros upwards. In this case, such a system was used. An additional similar contribution to the price may be the software, which also depends on the workflow used. However, when using UAV-based technologies, significantly more data can be captured in significantly less time compared to the traditional approach (Figure 81). When evaluating the area of 5549.55 m² measured in the traditional way during the experiment, the same area was measured approximately six times faster when using the UAV-based approach. With an increase of the area, the UAV-based method becomes significantly more efficient.

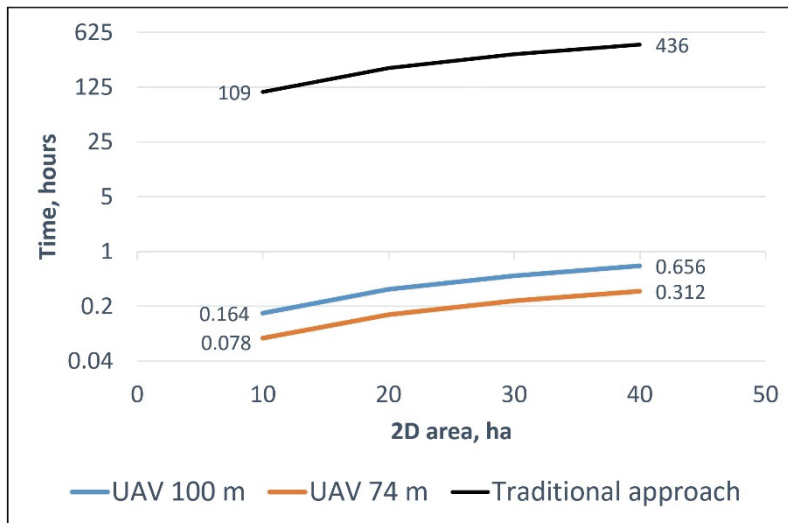


Fig. 81. Data acquisition time of automated vs. traditional approaches

However, it should be considered that, when flying a UAV, preparation is required for setting up the control points, and the preparation time depends on the workflow used. During the experiment, the most reliable results were obtained when using the PPK workflow. However, this workflow requires the installation of at least one known control point, which must be activated and immobilized for at least 45 minutes. Other workflows require several ground control points, which must be installed at appropriate distances and at the edges of the surveyed site. In any case, the minimum set-up and flight time can take about one hour, so the time efficiency of the UAV-based technology during the experiment was determined only for construction sites larger than 925 m² (Figure 82).

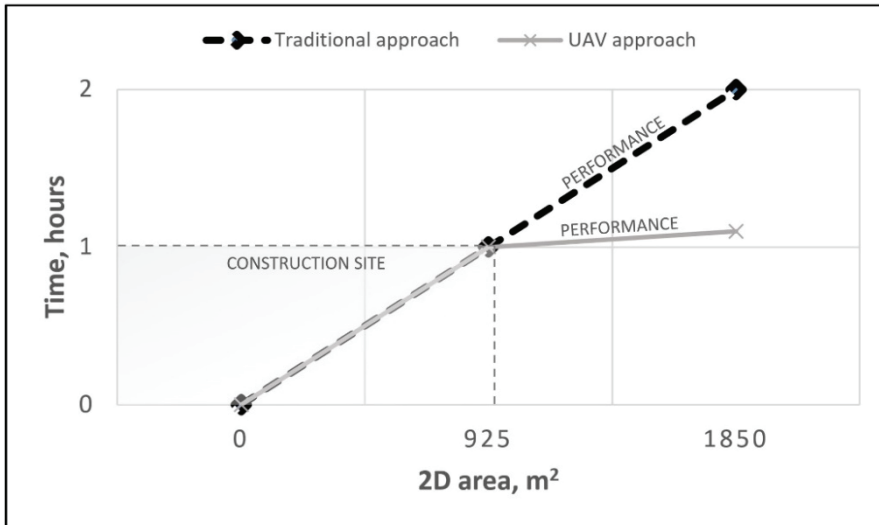


Fig. 82. Efficiency in relation to the scale of project

In addition, the efficiency of data acquisition can be affected by the expertise of the person flying the UAV, otherwise known as the remote pilot. An experienced remote pilot can reduce the data acquisition time by optimizing the flight planning and execution, as well as by ensuring the data quality and regulatory compliance. Capturing high-quality images is critical to the accuracy of the photogrammetric model. Poorly captured images can adversely affect the data accuracy and may require a re-flight. In favorable weather conditions and when implementing uncomplicated flights, the remote pilot's competencies are not so significant. However, it is very important to note that the complexity of the surveyed area, the difference in terrain heights, and adverse weather conditions have a significant impact on the flight safety, data acquisition time, and data quality. The experience of the remote pilot is especially important for obtaining data under these conditions.

The laser scanning technologies needed to monitor the construction progress of a building are significantly more expensive. The approximate prices of the 3D laser scanners used in the experiment range from 20 to 70 thousand Euros. The price depends on the technical parameters of the devices, such as the ability to achieve millimeter-level accuracy. However, there are many occlusions in the construction environment, and a lot of noise is obtained in the scan data, so the accuracy parameters do not necessarily play the most important role in the proposed methodology. The results of the experiment showed that the developed methodology can successfully identify objects by using laser scanners with accuracy parameters from 1 to 30 mm, which allows a wider choice of devices in terms of price.

However, there are more important factors to consider when monitoring the progress in a real construction environment, such as occlusion and data acquisition efficiency. Static scanners can provide more accurate data, but they were found to be quite time-consuming during the experiments. Mobile laser scanning was more time-efficient in capturing data, especially with regard to obstacle avoidance. The experimental study was conducted as part of a construction project and was not

compared to the traditional approach. However, it is assumed that, in a large-scale project or in hard-to-reach areas, the laser scanning technology can be a more time-efficient and cost-effective approach to data capturing compared against the traditional method, depending on the construction conditions. One argument is that laser scanning can produce a large amount of accurate data that can then be automatically integrated into an IFC model with minimal manual steps, thereby saving time-consuming manual calculation of quantities.

4.1.3. Report and visualization

A major advantage of automated construction progress monitoring is that the completed work report is generated automatically. The reports indicate the quantities of work performed and provide a visualization which helps to determine the location and what work has been done or not done yet, and capture the current situation at a certain point in time. An example of an earthworks control report is shown in Figure 83, and an example of a building construction progress monitoring report is shown in Figure 84.

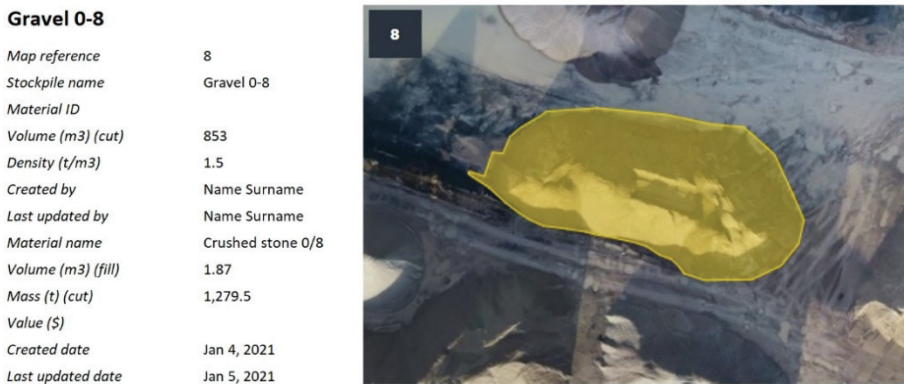


Fig. 83. Example of visualization and report of earthworks control

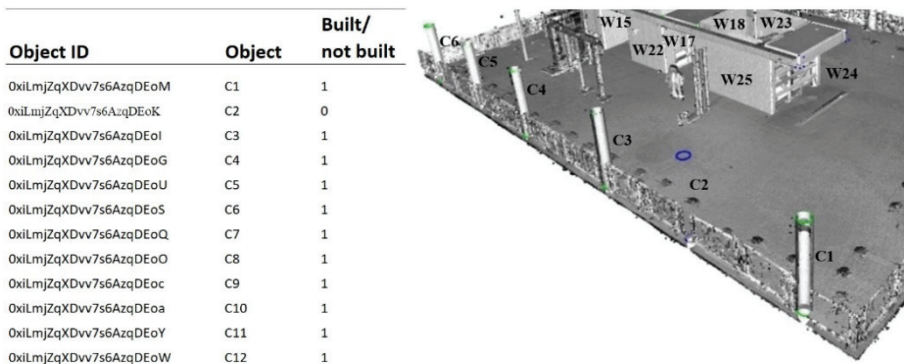


Fig. 84. Example of visualization and report of structural construction progress monitoring

In the case of automated earthwork control, the report was generated by using a commercial solution. In this case, several manual steps are required, such as setting the name of the material or its properties. Then, by using elementary tools,

such as polyline, the desired area for quantity calculation is marked, and the report is generated automatically. One of the advantages of this earthwork control system is that the platform is cloud-based, and stakeholder(s) can perform the calculations themselves without the need for the intervention of a surveyor. During practical experiments, it was determined that such an automated system helps construction managers to perform self-control, to control the quantities and quality of subcontractors' work, or submit invoices for payment based on the report.

The automated monitoring system for building construction was developed during this thesis without the use of commercial solutions. Minimal commercial software intervention was required only for input data preparation, and improvements are still needed to test the method in practice. However, the developed automated monitoring system offers great potential for practical use as it was able to automatically identify structural objects from the scanned data from occlusive construction environment. The system automatically provides a report with the identified objects, while also automatically providing the ID of each object extracted from the IFC file and delivering a visualization of the as-planned and as-built models integration. As with the control of earthworks, in this case, it is also possible to perform self-control by controlling the quantities of work performed, or to submit invoices for payment based on an automatically generated report.

Both in the case of the earthworks phase and in the case of the structural construction phase, the reports visually present the as-is situation in relation to the date, thus reducing the possibility of disagreements about the quantities of work performed.

4.1.4. Automation quality

The quality of automation of both UAV-based photogrammetry and laser scanning technologies can be sufficiently influenced by the quality of the data obtained. During the experiments, it was observed that the data quality was influenced by the parameters of the devices and the workflow used. For example, when flying the UAV at an altitude of 100 m, the data was captured faster compared to the flight at a lower altitude, but the quality of the obtained data was lower, which resulted in less accurate calculations of the work performed. In the case of laser scanning, the data was obtained faster with a mobile scanner, but capturing data by using this approach requires more expertise, the scanning range of the device is more limited, and the accuracy parameters are lower compared to other static scanners used in the experiment. All this affected the quality of the data, as a result of which, an object was incorrectly identified during the test.

During the earthworks phase, the data are usually assigned to a certain common coordinate system, and the accuracy of the results is highly dependent on the correct alignment of the data sets. Although the earthworks control system is automated and greatly facilitates the work of construction managers and other interested parties, manual steps are still required to perform measurements or data alignment corrections if the quality of data has been affected by external factors. In building construction, IFC models are usually assigned to the zero-coordinate system, which is different from the data obtained by laser scanning. Therefore, in this case, the automation process requires additional manual intervention so that to

roughly align the datasets. After uploading the data into the developed system, apart from this manual intervention, the entire object detection process was fully automated.

4.1.5. Health and safety

The experiments have shown that health- and safety-related challenges in the construction progress monitoring process can be avoided by using UAVs or laser scanners. The traditional way of measuring the earth's surface involved climbing steep slopes and loose stockpiles, the height of which reached several meters. The GCP-based UAV approach also posed some safety-related challenges, as control points must be located at appropriate distances and within the borders of the measured area. However, with RTK- or PPK-based UAV approaches, only a few control points were required, and, in the case of the PPK workflow, only one known point was used as a control point. Such solutions allowed relatively safe and fast capturing of the reality data compared to the traditional method of measuring with a GNSS receiver. In addition, with a reality model, construction managers can assess hazardous locations, thus preventing accidents in advance. Meanwhile, during the building construction monitoring process, the terrestrial laser scanner was placed at 16 locations to capture the as-is data of the entire 600 m² area. This helped to avoid excessive walking in occluded areas. In this case, the construction environment was not particularly dangerous. However, in complex projects with high ceilings or hard-to-reach areas, it could significantly improve health and safety in terms of as-is data capture.

4.2. Limitations

UAV-based photogrammetry and laser scanning technologies are used in the construction sector for 3D mapping, terrain and object modelling, and this offers the potential to automate the process of monitoring the progress during the construction phase. However, these technologies still suffer from some common limitations that need to be considered.

First, the accuracy of both photogrammetry and laser scanning-based approaches is affected by factors such as weather conditions or equipment quality. During the experiments, the accuracy and reliability of the data was also affected by the choice of the workflow to be used. For example, in earthworks construction, the most reliable data was obtained by using the PPK workflow, while, in the structural construction experiment, the most reliable data was obtained by using TLS high technical parameters. However, high-quality laser scanning equipment can be prohibitively expensive. In some cases, the cost of high-quality unmanned aerial systems, including software, can also be high. Data processing requires significant processing power and can be time-consuming, especially when working with large data sets. In this study, a cloud-based technology was used for the photogrammetric approach, which helped avoid the need for a highly powered computer, but this solution resulted in a higher cost. TLS data processing required the use of third-party software for data conversion and pre-processing. Also, to speed up the calculation process, the amount of TLS point cloud data was optimized by reducing the number of points, which affected the accuracy of object identification in the case when the

data quality was lower. Both UAV-based photogrammetry and TLS data quality can be affected by environmental factors, such as vegetation, shadows, and changes in the light conditions, and therefore require a certain level of skill and experience to use these technologies effectively. In addition, in UAV applications, the data quality may be affected by atmospheric conditions and other external factors which are out of human control, such as the effect of ionospheric and tropospheric refraction, which may cause the distance to deviate from its true value or the geometry of the satellite at the time of data collection. Figure 85 shows an example of a cycle slip error from satellites.

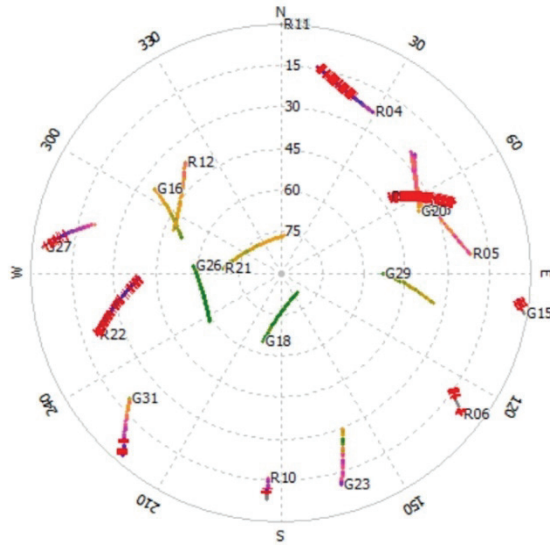


Fig. 85. Multiple cycle slips from satellites (image from <https://www.propelleraero.com/support team>)

Furthermore, while UAVs can improve the construction site safety, the unmanned vehicle itself is a potentially dangerous device, and, in a loss-of-control scenario, the speed at which a remotely piloted aircraft descends from an altitude of approximately 60 m and reaches its terminal velocity is much higher than the determined acceptable values, which may cause unacceptably serious injuries [206]. At an altitude of 60 m, the *DJI Phantom 4 RTK* aircraft would have an estimated terminal velocity of 36 m/s on impact and a kinetic energy of about 900 Joules, which could cause fatal injuries [207]. For safety reasons, (ES) 2019/247 regulation has been issued in Europe. It restricts the possibility of unmanned aerial vehicles flying over uninvolved persons [208]. This limitation significantly complicates effective data collection, as it is practically difficult to achieve that no people remain in the construction site during the working hours.

4.3. Chapter Conclusions

1. Earthworks and building construction progress monitoring use different methodologies, but both methodologies are based on 3D point cloud applications.

The results obtained during the experiments showed that the use of point cloud technologies can improve the data accuracy and capture the data efficiently in terms of time, as thousands of data points are measured in one second, and the density of the obtained points allows for much more accurate reproduction of the surface area compared to the traditional approaches.

2. Experiments have shown that the quality of both UAV-based photogrammetry and laser scanning data affects the quality of automation. Meanwhile, the data quality is influenced by the chosen data capture technique and the technical parameters of the equipment in use. In the case of the UAV approach, when capturing data by using a lower image resolution, the results of the calculated work quantities differed by 1.08–2.12% from those obtained when capturing data with a higher resolution. Meanwhile, when scanning with a laser scanner of lower-level parameters, the object was incorrectly identified. In both cases, the data quality suffered as a result of speeding up data acquisition.
3. The UAV-based photogrammetry and laser scanning technologies explored in this thesis involve a sufficiently high level of automation and are capable of providing automated reports of work quantities, but both methods suffer from several limitations in terms of the data acquisition efficiency. In the case of a UAV-based approach, the effectiveness of data capturing is limited by no-fly zones, permit-to-fly procedures, and safety considerations that prevent overflying people not involved in the flight operation. Meanwhile, the time efficiency of laser scanning data acquisition must be balanced with the quality of the data obtained, especially in terms of the accuracy and population of data points per cubic meter. Scanning with a static laser scanner usually produces higher quality data, but it is also a slower data acquisition process.

5. GENERAL CONCLUSIONS

1. The literature review shows a significant interest among researchers in the topic of automated construction progress monitoring using 3D point cloud technologies, such as photogrammetry and laser scanning. Previous studies have shown that collecting data and updating schedules can take 20–30% of the time each day, and ineffective construction progress monitoring causes more than 53% of construction projects to fall behind schedule. However, the construction phase consists of different categories of work, such as earthworks construction, structural construction, MEP, finishing works, etc., and thus different methodologies have to be applied to automate the monitoring process. 3D point cloud technologies offer the greatest practical value for civil works and structural construction monitoring. It has been found that, in terms of data acquisition, it is most effective to apply UAV-based photogrammetry for earthworks construction, and laser scanning technology for structural construction. The main challenges have been identified, such as the automated alignment of IFC and point cloud models, particularly in the presence of noise and outliers in the captured data, and automatic object detection in occluded environments where the surface of objects cannot be fully scanned. Various methods have been proposed by researchers, but the challenges of reliable and effective practical application under real construction conditions are still being addressed.
2. During the earthworks control experiment, three different UAV-based photogrammetry workflows were investigated, such as GCPs-based, RTK and PPK approaches and compared with the traditional method involving the use of a GNSS receiver. In an area of 5549.55 m², data was obtained by UAVs 83% faster than when measuring with the traditional method using a GNSS receiver. The difference in the vertical reference points between the analyzed methods did not exceed the RMSE value of 4 cm, and, in most cases, it was less than 3 cm. The PPK method was found to provide the most time-efficient and reliable results in terms of the accuracy and error rate and had a significant impact on the efficiency of earthwork quantity estimation. However, due to the relatively high cost and workflow specificity, automated technologies can improve the efficiency of construction progress monitoring in large-scale projects. During the experiment, it was found that the UAV-based method gains time efficiency from a project scale of 925 m². As technology advances, gathering data with drones can become faster and make the whole progress monitoring process even more efficient.
3. Practical experiments have shown that, in many cases, site supervisors and managers do not need a surveyor on site, as they can quickly estimate volumes by themselves. This technology replaces the need for calculations of trucks and gives better accuracy and reliability of the earth quantity control, including the control of the subcontractors' work. To reduce the possibility of mistakes, to plan the quantities, and to perform quality control, LandXML and .dfx designs are efficiently used for ground levelling and other operations, when the traditional

method would take much longer, and some control operations may be impossible to complete.

4. During the structural construction experiment, a methodology for the automated detection of existing objects based on the assigned IFC model was developed, which allowed for the automated alignment of point cloud and IFC models in the presence of noisy and biased scan data, and the successful automatic detection of objects when their surfaces were not fully scanned:
 - a) the geometry of the building structures was captured by using three 3D laser scanners with different technical parameters. Two static laser scanners with a declared accuracy of 1 mm and 4–7 mm and one mobile laser scanner with a declared accuracy of 10–30 mm were used. As-is data was collected in an orderly environment with no obstructions in the line of sight and also in an occluded construction environment to reflect a real construction scene.
 - b) after manual pre-processing of the obtained data, an automated alignment process of IFC and point cloud models was developed based on the ICP algorithm. This process allowed the data to be aligned with an accuracy of 2.1 cm RMSE, which was sufficient to correctly identify the objects. To unify the structure of the data, the vertices of the elements were extracted from the IFC, thus obtaining a point cloud extracted from the IFC. The only manual intervention required for data alignment was the selection of three pairs of reference points in both point cloud models.
 - c) a methodology for automatic object detection was developed which allows extracting IFC data, calculating the plane equation of faces, and estimating the distance from a point to a plane. During the experimental test, out of 176 evaluated construction objects, 99.4% were correctly identified, including in the occluded construction environment, when the surface of the objects was incompletely scanned, or the obtained data was of poor quality. After optimizing the object detection process, the amount of data was reduced by 91–96%. In this case, 92.9% of the 113 assessed objects were correctly identified. Therefore, it becomes evident that the quality of the data has a significant impact on the automation process.
5. UAV photogrammetry and laser scanning technologies can provide reasonably accurate data and reduce labor and material costs for large-scale projects compared to the traditional methods, such as the use of a GNSS receiver or a total station. With constantly updated construction data, it is possible to effectively control the scope of work, identify the potential problems or delays, and take action to keep the project on schedule and avoid additional costs. Automatically generated reports combined with visualization can help avoid disputes that can end in financial losses. Data collection during the experiments required continuous manual intervention, and, in the case of laser scanning, data acquisition was not as time-efficient as compared to the UAV approach. For small-scale construction projects, these technologies can be prohibitively expensive and inefficient.
6. Based on the results of the research, several aspects are recommended for construction companies planning to implement UAV-based photogrammetry or

3D laser scanning for construction progress monitoring. First, companies need a strategic and holistic approach, because practice shows that innovative tools get adopted rather slowly. Investment should be considered as a potential long-term cost saving by controlling the quantities and quality of the work performed and the possibility of ensuring sustainable competitiveness. The price of the laser scanners used in the research ranges from 20000 to 70000 Euros. The UAV system would require a further investment of around 5000 Euros. However, before investing, it is important to assess the limitations of the technology, such as reflective surfaces, complex geometries, occluded environment, weather effects, and compliance with the regulatory rules for UAV flights. In addition, it should be considered that not all software solutions have the height system LAS07, which is widely used in Lithuania, installed. Successful use of these technologies requires training programs for employees and reliable software solutions, the price ranges of which can vary from 5000 to 20000 Euros.

6. FURTHER WORK

Large-scale land surface capture by using UAV-based photogrammetry is an efficient process compared to the traditional methods using GNSS receivers. Although the data acquisition is automated, it still requires human intervention during the flight. Also, in smaller-scale construction sites, data acquisition by using drones becomes inefficient due to the preparation-to-flight time. The development of an autonomous data acquisition system could reduce the need for human intervention and could make the progress monitoring process more efficient in smaller-scale construction projects.

In order to obtain accurate, high-quality data, indoor laser scanning is also a relatively time-consuming process which requires constant manual intervention. The methodology proposed in the thesis allows successful automatic identification of construction objects even with lower-quality scan data. This can contribute to improving the effectiveness of progress monitoring through the data acquisition process.

Although the objectives of the thesis have been achieved, the proposed automated construction progress monitoring methodology still suffers from several limitations. For example, small faces in an IFC object usually do not have an associated point cloud and therefore cannot be detected. Also, while the alignment process is seamless, minimal manual intervention is still required. Fully automating the alignment process could be an area to explore. A further direction of research could be based on the improvement of the aforementioned limitations, and the experiments should be carried out on a larger scale by analyzing the whole building instead of a part of it.

7. SANTRAUKA

Tyrimo aktualumas

Statybos pramonė vaidina svarbų vaidmenį bet kurios šalies ekonomikoje, tačiau pastaruosius dešimtmečius šis sektorius buvo vienas mažiausiai skaitmenintų. Statybos pramonės transformacija per skaitmeninimą buvo apibrėžiama terminu Statyba 4.0, kuris skatino diegti naujas skaitmenines technologijas ir praktiką, kad pagerintų statybos projektų efektyvumą, kokybę ir tvarumą. Kadangi dėl didėjančio pasaulio gyventojų skaičiaus ir klimato kaitos didėja būsto [1] ir infrastruktūros [2] poreikis, statybų pramonė turi pritaikyti naują praktiką ir naujas darbo metodikas, kad galėtų toliau remti žmogaus veiklą tvaresniu ir veiksmingesniu būdu.

Nepaisant sparčios statybos pramonės skaitmeninimo, skaitmeninimo pažanga įvairiose šalyse buvo nevienalytė. Pavyzdžiui, Šiaurės ir Vakarų Europos šalys žengia į priekį greičiau nei Vidurio ar Rytų Europos šalys. Skaitmenindama statybų sektorių, Europa siekia naudoti pažangias technologijas, tokias kaip statinio informacinis modeliavimas (BIM), bepiločių orlaivių (BO) ir lazerinio skenavimo technologijos, kartu su mašininu mokymusi ir kompiuterija, kad būtų pagerintas statybos procesų efektyvumas, sumažintas atliekų kiekis ir būtų pagerintas bendras našumas. Be to, skaitmeninimas gali padaryti projektinius sprendimus skaidresnius, padėti išspręsti sudėtingas problemas siekiant aukštesnių tvarumo standartų, skatinti inovacijas ir padidinti saugumą [3, 4].

Pastarąjį dešimtmetį skaitmeninių inovacijų dėmesio centre buvo BIM diegimas, tačiau lygiagrečiai augo ir tokių technologijų, kaip bepiločių orlaivių fotogrametrija ir lazerinis skenavimas, svarba. Šios technologijos leidžia tiksliau išmatuoti kiekius ir nustatyti galimas atliekas. Tokiu būdu galima efektyviau panaudoti medžiagas ir sumažinti poveikį aplinkai, taip pagerinant statybos tvarumą. Statybų procesui stebėti gali būti naudojamos lazerinio skenavimo technologijos, kurios gali padėti išvengti klaidų ir užtikrinti, kad statybos projektas būtų vykdomas pagal planą. Tai gali padėti sumažinti pakartotinio darbo poreikį ir sumažinti laiką bei išteklius. Bepiločiai orlaiviai gali būti naudojami statybvietėse, siekiant pagerinti statybos eigos stebėjimo efektyvumą, nustatyti galimus rizikos veiksnius ir pagerinti kokybės kontrolę bei saugos priemones.

Statybos eigos stebėjimas yra svarbi projekto valdymo sudedamoji dalis, padedanti laiku identifikuoti ir spręsti problemas, kurių gali iškilti statybos proceso metu. Įvairių pramonės šakų statybos įmonės 3D lazerinį skenavimą ir fotogrametriją praktikoje taiko įvairiais tikslais. Situacijai įvertinti skenuojami tiltai, keliai ir kiti infrastruktūros objektai, pastatų konstrukcijos, apleistos teritorijos. Taikymas apima topografinius matavimus, kelio dangos ir šaligatvių profiliavimą, tūrio skaičiavimus, tiltų pažeidimų įvertinimus ir kt. Šios metodikos taikomos apžiūrint pastatų, apleistų teritorijų ir infrastruktūros esamą būklę prieš projektuojant, o vėliau tos pačios vietos yra iš naujo fiksuojamos pažangai stebėti ir analizuoti.

Norint stebėti statybos eigą, bepiločių orlaivių fotogrametrija plačiai naudojama žemės darbų kiekių kontrolei, o lazerinis skenavimas dažniau

naudojamas pastatų statybos projektuose. Nors dėl technologijų pažangos šios technologijos vis dažniau naudojamos statybos pažangai stebėti, tačiau taip pat yra susiduriama ir su tam tikrais iššūkiais. Tai apima nepasitikėjimą naujomis technologijomis, integracijos su kitomis technologijomis, pavyzdžiui, BIM, sudėtingumą ir nepakankamą automatizavimo lygį. Dėl nuolatinių pokyčių statybos aikštelėse susidaro sudėtingos sąlygos gauti kokybiškus duomenis. Automatizuotos statybų pažangos stebėjimo metodikos analizė ir tobulinimas, išsprendžiant minėtus iššūkius, galėtų pagerinti stebėjimo proceso efektyvumą ir taip pagerinti statybų sektoriaus įvairių bei prisidėti prie europinių statybos skaitmeninimo tikslų įgyvendinimo.

Tyrimų objektas

Šiame darbe tiriamas fotogrametrijos ir lazerinio skenavimo technologijų naudojimas statybos etape. Nagrinėjamas šių technologijų taikymas žemės darbų ir pastato konstrukcijų statybos pažangai stebėti.

Tyrimo tikslas

Šiuo tyrimu siekiama pritaikyti fotogrametrijos ir lazerinio skenavimo metodus statybos pažangai stebėti nuo žemės darbų valdymo iki pastato konstrukcijų stebėjimo ir pasiūlyti stebėjimo proceso automatizavimo metodiką, apimančią statinio informacinio modelio ir lazerinio skenavimo duomenų integravimą.

Tyrimo uždaviniai

Norint pasiekti tikslą sukurti automatizuotą statybos eigos stebėjimo metodiką, buvo nustatyti keli konkretūs uždaviniai:

1. Išanalizuoti esamą literatūrą ir ištirti duomenų gavimo priemones, technologijas ir metodus, naudojamus statybos eigai stebėti.
2. Atlikti eksperimentus ir išanalizuoti įvairias bepiločių orlaivių fotogrametrijos darbo eigas bei pateikti stebėjimus, lyginančius skirtingų metodų efektyvumą ir patikimumą žemės darbų eigai stebėti.
3. Užfiksuoti erdvinius pastato konstrukcijų duomenis statybinėje aplinkoje naudojant įvairius lazerinio skenavimo būdus ir iš gautų duomenų sukurti bandomuosius duomenų rinkinius.
4. Sukurti 3D taškų debesies duomenų ir atitinkamo BIM modelio sulygiavimo ir integravimo metodiką, naudojant skaitmeninį duomenų standartą-formatą (IFC).
5. Sukurti automatizuotą statomų objektų stebėjimo procesą palyginant skenavimo duomenis su projektiniu 3D modeliu, ypatingą dėmesį skiriant objektų aptikimui realioje statybos aplinkoje.

Tyrimo metodologija

Norint pasiekti šiuos tikslus, būtina suvokti BIM technologijos sampratą, erdvinių duomenų gavimo technologijas, šių technologijų integravimo galimybes bei iššūkius statybos eigos stebėjimo kontekste. Šiam tikslui pasiekti buvo atlikta išsami literatūros analizė.

Remiantis literatūros apžvalgos išvadomis bei praktiniais pastebėjimais buvo nustatyta, kad fotogrametrijos taikymas yra efektyvesnis žemės darbų eigai stebėti, o lazerinio skenavimo technologijos praktikoje daugiau taikomos pastato statybos etape. Atsižvelgiant į tai, baigiamajame darbe buvo atliekami du eksperimentai: pažangos stebėjimas žemės darbų etape ir pažangos stebėjimas pastato statybos etape.

Bepiločių orlaivių fotogrametrija turi įvairias darbo eigas ir metodikas, kurios gali nulemti pažangos stebėjimo efektyvumą ir patikimumą. Siekiant nustatyti darbo eigos poveikį žemės darbų eigos stebėjimui, buvo atlikti eksperimentiniai bandymai naudojant tris skirtingas metodikas, kurios taip pat buvo palygintos su tradiciniu metodu.

Pastato statybos etape buvo tiriamas lazerinio skenavimo technologijų taikymas pažangai stebėti. Naudojant lazerinio skenavimo būdu gautus duomenis, buvo sukurta metodika, leidžianti integruoti IFC ir 3D taškų debesies duomenis bei automatiškai aptikti pastato objektus 3D taškų debesyje pagal atitinkamą IFC modelį.

Mokslinis naujumas

Tyrimo naujumas pagrįstas fotogrametrijos ir lazerinio skenavimo technologijų taikymu automatizuotai statybos eigos stebėsenai nuolat kintančioje aplinkoje:

1. Tyrime nustatytas pažangių realaus laiko kinematinės ir vėlesnio koordinatinių patikslinimo bepiločių orlaivių fotogrametrijos metodų tikslumas ir patikimumas, kurie buvo palyginti su įprastine praktika naudojant antžeminį GNSS imtuvą.
2. Pasiūlytas naujas metodas, kuris integruoja lazerinio skenavimo duomenis su IFC modeliu, leidžia automatiškai aptikti 3D taškų debesyje esančius objektus lyginant su IFC faile esančiais objektais.
3. Objektų aptikimo procesas, sukurtas apskaičiuojant kiekvieno IFC elemento paviršiaus plokštumos lygtį ir nustatant ryšį tarp taško ir IFC objekto, leidžia identifikuoti nevisiškai nuskenuotus objektus 3D taškų debesyje.

Ginamieji teiginiai

1. Statybos pažangos stebėjimo procese automatizuotos bepiločių orlaivių fotogrametrinės darbo eigos užtikrina didelio masto projektų, kurių plotas didesnis nei 925 m², efektyvumą, palyginti su tradiciniais metodais, tikslumo, patikimumo ir laiko požiūriu.
2. IFC ir 3D taškų debesies duomenų integravimo procesas, išfiltruojant IFC elementų viršūnes, užtikrina duomenų sulygiavimo ir automatinio statybos objektų aptikimo galimybę 3D taškų debesyje, lyginant su pateiktu IFC modeliu.
3. Pasiūlytas metodas leidžia išfiltruoti IFC duomenis, apskaičiuoti objekto kiekvieno paviršiaus plokštuminę lygtį ir atlikti atstumo nuo taško iki plokštumos įvertinimą, kas leidžia automatiškai aptikti pastato objektus realioje statybos aplinkoje, kai paviršius yra ne iki galo nuskenuotas arba gauti duomenys yra nekokybiški.

Praktinė tyrimo reikšmė

Siūloma metodika gali pagerinti statybos eigos stebėjimo efektyvumą užtikrinant, kad būtų prieinama naujausia ir patikima informacija, padedanti priimti sprendimus, reikalingus projekto tikslams pasiekti laiku ir neviršijant biudžeto, taip sutaupant laiko ir sąnaudų. Šio proceso automatizavimas galėtų prisidėti prie europinių statybos sektoriaus skaitmeninimo tikslų, sumažinant darbo ir laiko poreikį, taip pagerinant bendrą statybiečių saugą ir bendrą statybos procesų efektyvumą.

7.1. LITERATŪROS APŽVALGA

Ši skyrių sudaro literatūros apžvalga šiame darbe nagrinėjamosiomis temomis. Tolimesnei baigiamojai darbo eigai reikalingos BIM, erdviųjų duomenų fiksavimo technologijų ir šių technologijų panaudojimo galimybių statybos eigos stebėjimo procese išmanymas. Pirmiausia apžvelgiami pagrindiniai BIM aspektai, nes ši technologija yra statybų skaitmeninimo pagrindas ir gali būti neatsiejama fotogrametrijos ir lazerinio skenavimo technologijų dalis, automatizuojant statybos eigos stebėjimą. Toliau apžvelgiamos statybos eigos stebėjimo metodikos žemės darbų ir pastato statybos etapuose, daugiausia dėmesio skiriant fotogrametrijos ir lazerinio skenavimo technologijų taikymui. Šios technologijos vystėsi lygiagrečiai su BIM ir kartu atlieka svarbų vaidmenį automatizuojant statybos eigos stebėjimo procesą.

7.1.1. Statybos pažangos stebėjimo technikų apžvalga

Pramonės varomoji jėga tradiciškai buvo pagrįsta laiku, sąnaudomis ir kokybe. Be to, pramonės šakos, įskaitant statybų sektorių, susiduria su griežtesniais tvarumo reikalavimais. BIM buvo sukurtas kaip bendradarbiavimo procesas, siekiant sumažinti atliekų kiekį, pagerinti efektyvumą ir optimizuoti statybos projekto valdymą per visą projekto gyvavimo ciklą [5, 6]. BIM apima tokius procesus, kaip koordinavimas ir dalijimasis naujausia informacija tarp projekto dalyvių, įvairių projektavimo disciplinų koordinavimas, kiekių ir sąnaudų kontrolė, saugos problemų fiksavimas ir analizė ir kt. [12].

1994 m., siekiant patenkinti pramonės BIM sąveikos poreikius, buvo pradėtas vystyti atvirų duomenų modelio standartas IFC [13]. IFC yra atviras ir standartizuotas skaitmeninis aprašymas, skirtas keistis duomenimis, kad būtų užtikrintas efektyvus BIM procesas [14]. Nors IFC tikslas yra duomenų sąveika tarp skirtingos BIM programinės įrangos [17], tačiau būtent čia kyla problemų. Keičiantis ir dalijantis duomenimis dažnai prarandami duomenys, pavyzdžiui, trūksta objektų arba neteisingai pavaizduota jų geometrija.

Statybų valdymo srityje BIM vaidina svarbų vaidmenį per visą projekto gyvavimo ciklą. Pavyzdžiui, esamų sąlygų 3D modelio kūrimas naudojant BIM programinę įrangą ir lazerinį skenavimą, fotogrametriją ar kitus matavimo metodus gali suteikti apčiuopiamos naudos, pavyzdžiui, pateikti aplinkos duomenis būsimam naudojimui, padėti ateityje modeliuoti ir koordinuoti 3D dizainą ir tiksliai atvaizduoti atliktus darbus [22]. BIM ir kitų technologijų, tokių kaip fotogrametrija ir 3D lazerinis skenavimas, integravimas gali smarkiai išplėsti šių technologijų taikymo ribas.

Kadangi statybos projektai tampa sudėtingesni, statybos eigos stebėjimo efektyvumas tampa labai svarbus projekto valdymui, o tam savo ruožtu reikia laiku gauti tikslios informacijos [73, 74]. Nors pažangiosios technologijos yra prieinamos daugumai statybos įmonių, tradiciniai metodai, tokie kaip vizualinė apžiūra ar kasdinių meistro ataskaitų naudojimas, vis dar dažnai naudojami pažangai stebėti ir šiandien, o tai užima daug laiko ir didina klaidų tikimybę [77, 78]. Duomenų rinkimas ir grafikų atnaujinimas pagal esamas statybos sąlygas gali užtrukti 20–30 % laiko kiekvieną dieną [79]. Neefektyvus statybų eigos stebėjimas iš dalies yra

atsakingas už tai, kad daugiau nei 53 % statybos projektų atsilieka nuo grafiko, o daugiau nei 66 % – viršija biudžetą [80]. Norint, kad pažangos stebėjimas būtų efektyvus, reikia automatizuoti šį procesą, o naudojant vien BIM technologiją automatizavimo procesas bus apribotas, nes pirmiausia reikia efektyviai surinkti duomenis. Statybietės duomenys 3D taškų debesies formatu gali būti efektyviai gaunami naudojant lazerinio skenavimo ar fotogrametrijos technologijas ir taip padidinti pažangos stebėjimo proceso efektyvumą [81–84]. Pavyzdžiui, duomenys, gauti naudojant 3D lazerinį skaitytuvą, gali būti integruoti į atitinkamo statinio informacinį modelį ir palyginti tarpusavyje, kad būtų aptikti nukrypimai [85]. Tačiau efektyvų šių technologijų naudojimą riboja neišspręsti iššūkiai, susiję su statybos objektais, kuriuos užstoja statybinės medžiagos, mechanizmai, kita įranga; taip pat ir 3D taškų debesies tankis ar perteklinių taškų filtravimas [105, 106].

Žemės darbų kontrolė yra svarbus veiksnys, į kurį būtina atsižvelgti, norint įvertinti optimalią statybos kainą statybvietėje, ir yra svarbus nuo inžinerinių konstrukcijų projektavimo iki statybos etapo [114]. Per pastaruosius 30 metų žemės darbų stebėjimo procesai labai pasikeitė nuo įprastinių metodų naudojant nusėdimo plokšteles ir matuoklius [115] iki 3D taškinių debesų taikymo. Duomenų, gautų naudojant bepiločių orlaivių fotogrametriją, lygis nėra prastesnis už duomenis, renkamius naudojant tradicinius metodus, tokius kaip GNSS imtuvo naudojimas ant žemės, tačiau bepiločiais orlaiviais per dieną galima įveikti iki 30 kartų didesnę atstumą. Todėl ši technologija yra pagrindinė priemonė stebint žemės darbų pažangą didelės apimties projektuose [127]. Bepiločių orlaivių fotogrametrijos efektyvumas ypač išryškėja skaičiuojant žemės darbų apimtį arba stebint konkrečias nuošliaužų rizikos zonas [128, 129]. Moon ir kt. [87] palygino bepiločių orlaivių fotogrametrijos metodą su antžemine lazerinio skenavimo technologija žemės darbams. Atliktame tyrime duomenų gavimo laikas naudojant bepiločių orlaivių fotogrametriją buvo keturis kartus trumpesnis, palyginti su antžeminiu lazeriniu skenavimu, ir nors fotogrametrijos tikslumas buvo mažesnis, jo pakako žemės darbų kontrolei užtikrinti. Statybų pramonė šiandien naudoja įvairias bepiločių orlaivių fotogrametrijos darbo eigas, tačiau trūksta tyrimų, kaip jie sąveikauja tarpusavyje, ypač praktiniu požiūriu.

Statybos žemės darbų eigos stebėjimas dažnai apima tik tūrių skaičiavimą, todėl yra gana paprastas procesas. Pastatų konstrukcijų stebėjimas reikalauja daugiau pastangų, nes 3D taškų debesyje reikia identifikuoti įvairius pastato elementus, lyginant 3D taškų debesies duomenis su atitinkamu BIM modeliu [116]. Automatizuojant statybos eigos stebėjimą, svarbu atsižvelgti į pastato duomenų gavimą, gautų duomenų sulgyjamumą su BIM modeliu ir integravimą į vieną modelį [138, 139]. Lazerinis skenavimas laikomas viena tiksliausių ir efektyviausių geometrinių duomenų fiksavimo technologijų pastato statybos aplinkoje, ypač kai kalbama apie 3D taškų debesies integravimą su BIM [72]. Šio tipo duomenims sulgyti galima naudoti gerai žinomą klasikinį ICP metodą [141, 142]. Tačiau, pavyzdžiui, IFC modelio ir 3D taškų debesies duomenų lygiavimas kelia papildomų iššūkių, nes duomenys yra skirtingų failų struktūrų. Sulgydavus duomenis, kitas svarbus etapas yra automatinis objektų aptikimas. Yra keli galimi šio proceso vykdymo variantai, pavyzdžiui, 3D taškų debesies palyginimas su BIM modeliu

[155, 156] arba 3D taškų debesies konvertavimas į BIM modelį [157, 158]. Pastarasis variantas yra sudėtingesnis, nes paprastai reikia skaidyti į segmentus ir klasifikuoti 3D taškų debesies elementus, todėl dažnai reikia taikyti mašininį mokymąsi, gilųjį mokymąsi ir kitus sudėtingus metodus [159, 160, 161]. Nors objektų aptikimo 3D taškų debesyje metodai yra perspektyvūs, jie vis dar reikalauja reikšmingo rankinio įsikišimo ir yra jautrūs duomenų „triukšmui“ ir kokybei, kuriai labai didelę įtaką daro įvairūs trukdžiai, esantys statybos aplinkoje [165].

7.1.2. Pažangos stebėjimo metodų nustatymas

Šiame baigiamajame darbe nagrinėjama statybos darbų pažangos stebėseną statybos etape. Norint efektyviai valdyti sudėtingus statybos projektus, pagal statybos procesą būtina juos suskirstyti į etapus. Kadangi statybos etapas apima visus su statybos vykdymu susijusius aspektus, šį etapą galima suskirstyti į kelias darbų kategorijas, priklausomai nuo darbų pobūdžio. Bendrai kaip pagrindinius statybos vykdymo etapus galima įvardinti šias darbų kategorijas: 1) žemės darbai, 2) konstrukcijų statyba, 3) mechanika, elektra ir santelchnika ir 4) užbaigimo darbai [192, 193].

Yra kelios skirtingos duomenų gavimo technologijos, kurios gali būti naudojamos automatizuotam statybų eigos stebėjimui, pavyzdžiui, geografinė informacinė sistema (GIS), globali padėties nustatymo sistema (GPS), brūkšniniai kodai, radijo dažnio identifikavimas (RFID), lazerinis skenavimas, fotogrametrija, videogrametrija ir kt. Tačiau visas šias technologijas galima suskirstyti į keturias pagrindines kategorijas, tokias kaip lazerinis skenavimas, nuotraukos, vaizdo įrašai ir sekimas bei jutimas [105].

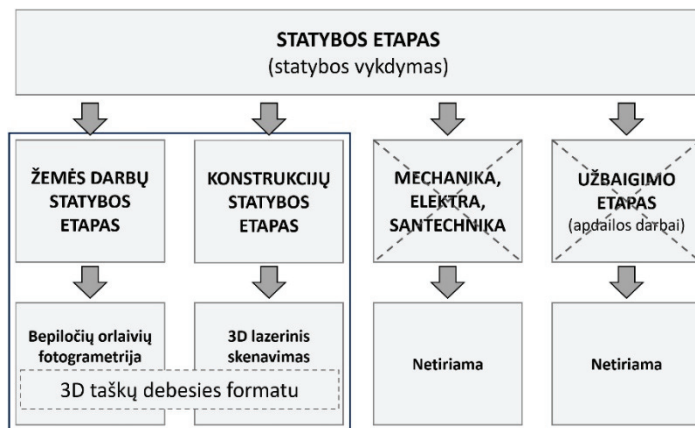
Videogrametrijos būdu gautiems rezultatams didelę įtaką turi tokie faktoriai, kaip vaizdo kameros kokybė, vaizdo kokybė, apšvietimo sąlygos ir kiti faktoriai, o pats metodas neužtikrina pakankamo tikslumo, palyginti su lazeriniu skenavimu ar fotogrametrija [194, 195].

Sekimo ir jutimo technologija, tokia kaip RFID, sutaupo daugiau laiko, palyginti su tradicine vizualine apžiūra, tačiau ji yra gana brangi ir turi problemų. Pavyzdžiui, RFID sistemos nėra labai tikslios ir objektų atpažinimo problemų kyla, jei vienu metu reikia aptikti kelias žymas. Be to, trukdžių sukelia tam tikros medžiagos, tokios kaip metalas ir betonas [196, 197].

Statybos darbams stebėti fotogrametrija yra ekonomišką ir efektyvų būdą gauti pakankamai tikslius 3D taškų debesies duomenis [137], kuris efektyviausiai gali būti pritaikytas žemės darbų valdymo srityje. O lazerinis skenavimas laikomas vienu patikimiausių metodų tikslumui užtikrinti [72] ir todėl jo taikymas didžiausią naudą turi pastato statybos etape.

Kalbant apie duomenų rinkimą, didžiausią praktinę naudą statybos pažangos stebėjimo efektyvumui gerinti turi fotogrametrija ir lazerinis skenavimas 3D taškų debesies formatu. Iš praktinės pusės, šios technologijos gali būti efektyviai taikomos žemės darbų valdymui ir pastato konstrukcijų statyboje. Tačiau šių technologijų taikymas mechanikos, elektros ir santelchnikos darbams bei apdailos darbams yra labai ribotas ir gali duoti mažai praktinės naudos. Todėl, atsižvelgiant į praktinį pritaikymą, eksperimentiniai tyrimai šiame baigiamajame darbe apsiribojo bepiločių

orlaivių fotogrametrijos metodais žemės darbų eigos stebėsenai ir lazerinio skenavimo metodais pastato konstrukcijų pažangai stebėti (kaip parodyta 86 pav.).



86 pav. Eksperimentų metodika ir apimtis

Remiantis anksčiau paskelbtais tyrimais, šiame darbe nagrinėjamas automatizuotas statybos eigos stebėjimas naudojant BO fotogrametrijos ir 3D lazerinio skenavimo metodus statybos etape. Ankstesniuose tyrimuose buvo analizuojami įvairūs BO fotogrametrijos metodai, tokie kaip PPK ir RTK, tačiau trūksta tyrimų apie šių technologijų praktinį pritaikymą ir palyginimą su tradiciniais metodais. Todėl šiame darbe nagrinėjamos pažangios fotogrametrijos darbo eigos ir naudojami pramonėje plačiai naudojami bepiločiai orlaiviai, siekiant įvertinti skirtingų darbo eigų veikimą ir palyginti poveikį tradiciniam darbo pobūdžiui realiomis statybos sąlygomis. Kita vertus, pastatų statyboje pagrindiniai iššūkiai kyla dėl nuolat kintančios aplinkos, nes tokiomis sąlygomis nuskenuoti visą objekto paviršių yra sudėtinga. BIM ir 3D taškų debesies integravimas pažangai stebėti taip pat yra plačiai tyrinėjama sritis. Remiantis ankstesniuose tyrimuose minėtais iššūkiais, baigiamajame darbe kuriama metodika, leidžianti sulygiuoti ir integruoti skenavimo duomenis su IFC modeliu ir automatiškai identifikuoti objektus 3D taškų debesyje, kai objektų paviršius nėra iki galo nuskenuotas.

7.2. TAIKYMAS ŽEMĖS DARBŲ STATYBOJE

Šiame darbe analizuojamas bepiločių orlaivių fotogrametrijos ir 3D lazerinio skenavimo taikymas automatizuotai statybos eigos stebėsenai. Šių technologijų darbo eigos, metodai, įrankiai ir praktinis pritaikymas skiriasi, jos yra naudojamos skirtingų tipų darbams stebėti. Dėl minėtų priežasčių eksperimentinio tyrimo objektai, metodai ir priemonės aprašomi atskiruose skyriuose. Tokia struktūra turėtų padėti skaitytojui lengviau suprasti aprašomus tyrimus. 7.2 skyriuje pristatomas bepiločių orlaivių fotogrametrijos taikymas žemės darbų eigos stebėsenai. 7.3 skyriuje pristatoma pastato statybos eigos stebėjimo metodika, taikant 3D lazerinį skenavimą ir BIM technologijas.

7.2.1. Tiriamojo objekto aprašymas

Remiantis literatūros apžvalgos išvadomis, BO fotogrametrija statybose gali būti veiksmingai taikoma stebint žemės darbų eigą. Šiuo atveju tyrimo objektas buvo 36 ha karjeras Lietuvoje, Trakų rajono savivaldybėje, kuriame buvo maždaug iki 5 m aukščio žvyro ir skaldos atsargos (87 pav.). Šio tyrimo objekto pasirinkimui įtakos turėjo gana didelė objekto apimtis ir tai, kad atliekant bandymus jis nebuvo eksportuotas. Tai leido įvertinti duomenų gavimo efektyvumą ir tikslumą.



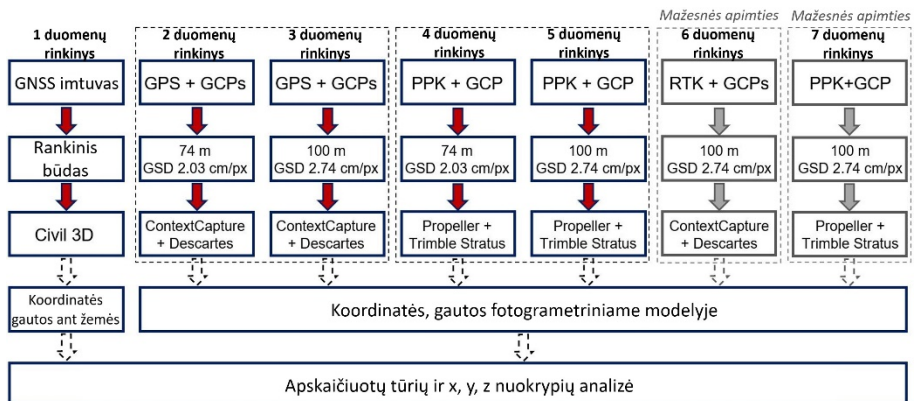
87 pav. Eksperimentinio tyrimo vietos fotogrametrinis modelis, gautas naudojant Bentley ContextCapture programinę įrangą

7.2.2. Metodai ir įrankiai

Šiame eksperimente nagrinėjamos trys skirtingos automatizuoto duomenų gavimo darbo eigos naudojant bepiločių orlaivių fotogrametriją. Šios darbo eigos buvo palygintos tarpusavyje ir su dabartinėje praktikoje vis dar naudojamu tradiciniu metodu, kai duomenys gaunami rankiniu būdu, naudojant GNSS-RTK imtuvą.

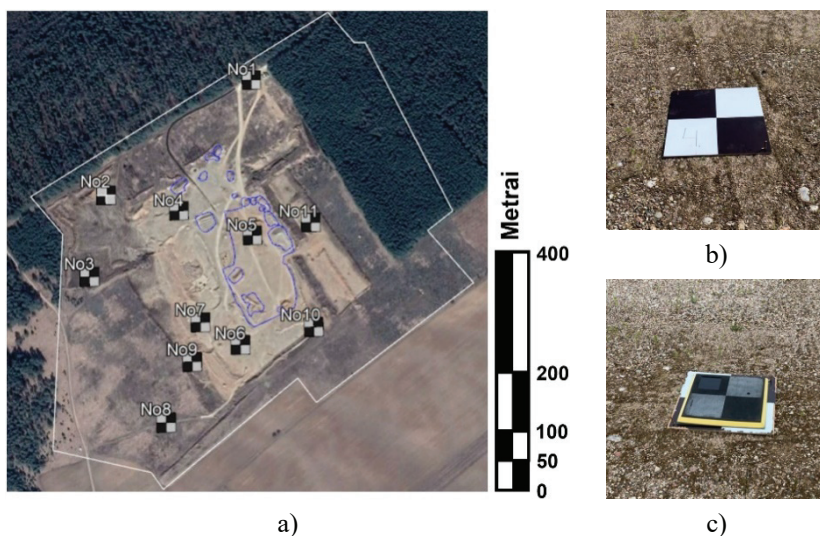
Pirma, matavimai buvo atlikti tradiciniu metodu, kuris vėliau buvo naudojamas kaip automatizuotų metodų vertinimo pagrindas. Duomenų apdorojimas šiuo atveju buvo atliktas Autodesk Civil3D programine įranga. O automatizuotam duomenų rinkimui buvo naudojami bepiločių orlaivių fotogrametriniai metodai, tokie kaip žemės kontroliniais taškais (ŽKT) pagrįsta darbo eiga, kinematinio apdorojimo realiuoju laiku (RTK) ir kinematinio apdorojimo, kai duomenų apdorojimas vyksta vėliau (PPK), metodai. Kiekvienas bepiločių orlaivių

fotogrametrijos metodus buvo analizuojamas atliekant po du skrydžius 74 ir 100 m aukštyje. Užfiksuojant duomenis iš mažesnio aukščio gaunami išsamesni vaizdai, tačiau dėl įvairių kliūčių, tokių kaip kranai, aukšti pastatai ar elektros stulpai, skrydžiai iš mažesnio aukščio gali būti nesaugūs, o duomenų gavimo ir apdorojimo procesas labai pailgėja ir gali būti neefektyvus. Atsižvelgiant į gamintojų rekomendacijas ir taikymo praktikas, optimalus duomenų gavimo aukštis paprastai svyruoja nuo 70 iki 100 m virš žemės lygio. Eksperimento metu fiksuojant vaizdus iš 74 m aukščio, fizinis vieno pikselio vaizde dydis, atitinkantis tikrąjį žemės paviršių (GSD), buvo 2,03 cm/px, o fiksuojant vaizdus iš 100 m aukščio – 2,74 cm/px. Duomenys, gauti naudojant RTK ir ŽKT pagrįstas darbo eigas, buvo apdoroti naudojant Bentley ContextCapture programinę įrangą, o tolesnė duomenų analizė atlikta Bentley Descartes programine įranga. PPK darbo eigos metu gauti duomenys buvo apdorojami ir analizuojami Trimble Stratus ir Propeller platformoje. Eksperimentinį tyrimą sudarė septyni duomenų rinkiniai, kurie buvo analizuojami lyginant kontrolinių taškų tikslumą ir išmatuotų žemės tūrių įvertinimą, atsižvelgiant į žemės darbų valdymo proceso efektyvumą ir duomenų patikimumą. Eksperimento schema parodyta 88 pav.



88 pav. Eksperimentinio tyrimo schema

Kontroliniai taškai naudojami fotogrametrinio modelio masteliui nustatyti ir turi esminės įtakos modelio tikslumui. Eksperimento metu buvo panaudota 11 žymeklių, kurie buvo naudojami kaip žemės kontroliniai taškai masteliui nustatyti ir modelio tikslumui įvertinti. Tiriamos teritorijos ribos ir kontrolinių taškų išdėstymas parodytas 89 pav., a. Žemės tūrio analizė buvo atlikta mėlyna spalva pažymėtose ribose. Eksperimente buvo naudojami 0,6 × 0,6 m kontroliniai taškai, pagaminti iš faneros su juodai baltu šaškių lentos raštu (89 pav., b). Be to, taikant PPK metodą buvo naudojami Propeller Aeropoint 1.0 išmanieji kontroliniai taškai, kurie tarnavo kaip bazinės stotys (89 pav., c).



89 pav. Bandymo aikštelės schema ir kontroliniai taškai: a) aikštelės ribos ir kontrolinių taškų išdėstymo schema (mėlynose ribose buvo atlikta žemės tūrių analizė), b) savadarbis kontrolinis taškas, c) AeroPoint 1.0 bazinė stotis

Žemės paviršiaus duomenims gauti buvo naudojamas Trimble GNSS-RTK imtuvas ir trys DJI Phantom 4 serijos bepiločiai orlaiviai. Praktikoje GNSS imtuvas dažniausiai naudojamas žemės darbų matavimams statybose, kai nereikalaujamas milimetrinis tikslumas. DJI Phantom 4 RTK yra vieni populiariausių bepiločių orlaivių, naudojamų statybų pramonėje geodeziniais tikslais. Eksperimente taip pat buvo išbandytas bepilotis orlaivis DJI Phantom 4 PRO, kuriame nėra įmontuotos RTK technologijos ir kurio kaina yra maždaug tris kartus mažesnė nei DJI Phantom 4 RTK. Eksperimente naudoti matavimo prietaisai pateikti 36 lentelėje.

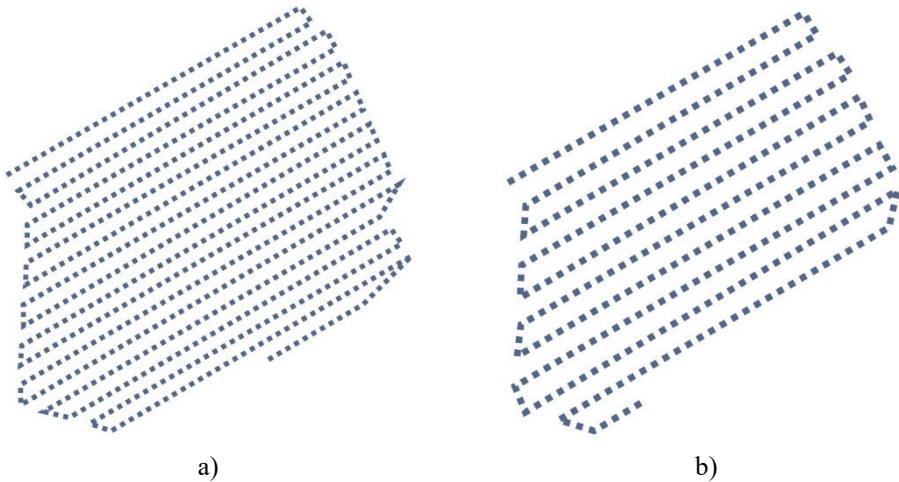
36 lentelė. Eksperimente naudojama duomenų gavimo įranga

Nr	Įrenginys	Pavadinimas	Pagrindinės savybės
1	GNSS imtuvas	Trimble SPS985	RTK
2	Bepilotis orlaivis	DJI Phantom 4 RTK	Integruota RTK technologija, 20 MP kamera, mechaninis užrakto greitis
3	Bepilotis orlaivis	DJI Phantom 4 RTK	Integruota RTK technologija (RTK išjungtas), 20 MP kamera, mechaninis užrakto greitis
4	Bepilotis orlaivis	DJI Phantom 4 Pro	Pasaulinė padėties nustatymo sistema, 20 MP kamera, mechaninis užrakto greitis

7.2.3. Duomenų gavimo darbo eigos

Kiekviena eksperimente analizuota bepiločių orlaivių fotogrametrijos darbo eiga buvo išbandyta naudojant tuos pačius skrydžio ir fotoaparato nustatymus. Optimalūs skrydžio parametrai buvo nustatyti remiantis ankstesniais tyrimais [89, 90] ir praktine patirtimi. Visi skrydžio planai buvo nustatyti pagal 2D fotogrametrijos modelį (90 pav.), fotografuojant 90° kampu. Vaizdų fiksavimas

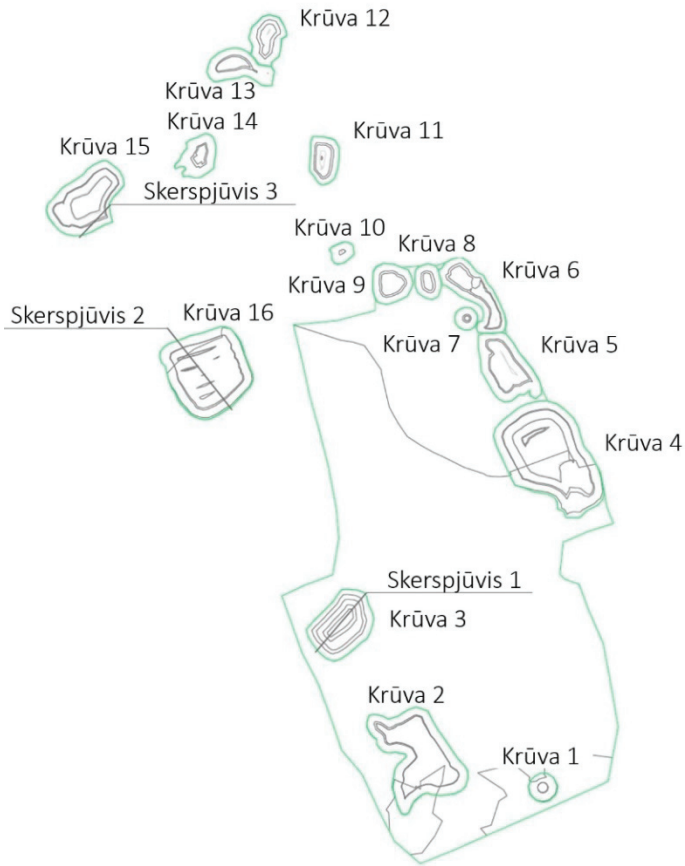
buvo nustatytas 80% priekiniam persidengimui ir 70% šoniniam persidengimui. Bepiločių orlaivių skrydžio greitis buvo 5,8 m/s. Skrydžiai buvo vykdomi vasarą saulėtomis sąlygomis, todėl pakako nustatyti automatinį fotografavimo režimą. Kiti fotoaparato nustatymai: jutiklio plotis 13,2 mm, jutiklio aukštis 8 mm, židinio nuotolis 8,8 mm, vaizdo plotis 5472 pikseliai ir aukštis 3648 pikseliai. Papildomas mažesnio masto tyrimas buvo atliktas žiemos metu. Eksperimentų metu karjeras buvo neaktyvus.



90 pav. 2D fotogrametrijos skrydžių planai: a) 74 m aukštyje, b) 100 m aukštyje

Šiame eksperimente matavimai pirmiausia buvo atlikti naudojant Trimble SPS985 GNSS imtuvą. Ši matavimo sistema naudojo Lietuvos padėties nustatymo sistemą (LitPOS), kuri yra pasaulinės navigacinės palydovinės sistemos infrastruktūra Lietuvai. Visą Lietuvos teritoriją apėmė 26 LitPOS GNSS nuolatinės atskaitos stotys, kurios teikė realiu laiku apskaičiuotus ir ištaisytą klaidų duomenis iš GNSS palydovų [200].

Matavimai GNSS imtuvu buvo atliekami rankiniu būdu, matuojant taškus kas 1–15 m. Tokiu būdu buvo išmatuotas 5549,55 m² plotas, užfiksuojant 1108 x, y, z duomenų taškus. Išmatuotame plote buvo 16 įvairaus dydžio atsargų krūvų (91 pav.), kurių apimtys svyravo nuo mažiau nei 100 m³ iki daugiau nei 3000 m³ ir bendras tūris viršijo 10000 m³. 91 paveiksle taip pat pavaizduotos atsitiktinės skerspjūvių vietos, kuriose bus vertinamas fotogrametrinių duomenų ir rankinių matavimų tikslumas.



91 pav. Žemės atsargų krūvos tūriui įvertinti ir atsitiktinės skerspjūvių vietos

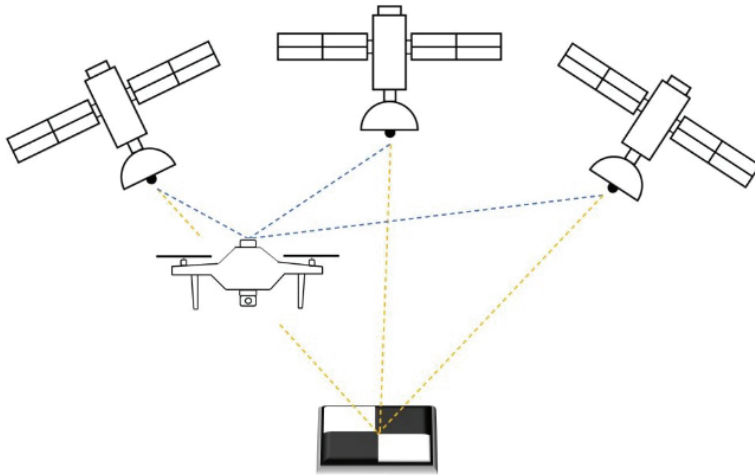
Visi horizontalūs x , y matavimai buvo atlikti Europos naftos tyrimų grupės (EPSG) projekcijoje 3346–Lietuvos koordinatų sistemoje (LKS94). Vertikalūs matavimai buvo atlikti Lietuvos valstybinėje aukščių sistemoje (LAS07) naudojant Lietuvos teritorinį geoido modelį (LIT15G). Tose pačiose koordinatų sistemose buvo atliekami ir bepiločių orlaivių fotogrametriniai tyrimai.

Šiame eksperimento etape žemės paviršiui užfiksuoti buvo naudojamas bepilotis orlaivis DJI Phantom 4 PRO. Šiuose orlaiviuose nėra integruotos GNSS RTK antenos, leidžiančios sistemai tiesiogiai geografiškai žymėti padėties koordinatas. Įmontuoti GPS įrenginiai nėra labai tikslūs ir gali turėti maždaug 3–9 m nukrypimus nuo faktinės x , y , z vietos. Šiuo atveju žemės kontrolinių taškų išdėstymas yra ypač svarbus tikslumui užtikrinti, nes bepiločiais orlaiviais gaunamus vaizdus reikia sulygiuoti su žemės paviršiumi.

Bepiločiai orlaiviai su integruotu RTK moduliu skiriasi nuo įprastų orlaivių, tokių kaip DJI Phantom 4 PRO, nes RTK technologija leidžia tiksliai sekti jų padėtis ir įrašyti GPS informaciją kinematinio apdorojimo realiuoju laiku metu. Naudojant šią technologiją, orlaivis įrašo GPS informaciją ir pažymi vaizdus geografinėmis žymomis, įrašydamas GPS vietą vaizdo centre. Taikant RTK metodą, galima naudoti mažiau žemės kontrolinių taškų, nes ant žemės esanti bazinė stotis siunčia

neapdorotus GPS duomenis į orlaivį, taip nustatydamą jo padėtį bazinės stoties atžvilgiu. Šiame eksperimento etape DJI Phantom 4 RTK bepilotis orlaivis buvo naudojamas duomenims užfiksuoti, o orlaivio radijo valdiklis su LitPOS tinklo RTK paslauga buvo naudojamas kaip bazinė stotis analizuojant RTK darbo eigą.

Pagrindinis skirtumas tarp RTK ir PPK metodų yra duomenų apdorojimo eiga. Naudojant PPK darbo eigą, bepilotio orlaivio GPS įrenginys geografiškai pažymi kiekvieno vaizdo x, y, z koordinatas, o bazinė stotis įrašo padėties duomenis su tikslesne trianguliacija, kaip parodyta 92 pav.



92 pav. PPK darbo eiga GPS informacijai įrašyti

Kaip ir naudojant RTK metodą, PPK darbo eigai analizuoti taip pat buvo naudojamas DJI Phantom 4 RTK orlaivis. Vienintelis skrydžio nustatymų skirtumas, palyginti su RTK darbo eiga, buvo tas, kad RTK režimas buvo išjungtas.

7.2.4. Fotogrametrinių duomenų apdorojimas

Gautų 3D taškų debesies duomenų apdorojimas ir analizė buvo atlikta naudojant šiuolaikinius programinius sprendimus. Pirmiausia buvo apdorojami tradicinės darbo eigos duomenys, o tada gautas paviršiaus modelis buvo importuotas į fotogrametrinę programinę įrangą tikslumo analizei ir palyginimui. GNSS imtuvu gauti duomenys buvo naudojami kaip pagrindas vertinant fotogrametrinių modelių tikslumą.

Žemės kontroliniais taškais pagrįstas metodas reikalauja pakankamo šių taškų skaičiaus. Fotogrametriniams duomenims apdoroti buvo naudojamos skirtingos ŽKT išdėstymo schemas, siekiant nustatyti, kokią įtaką jų skaičius turi fotogrametrinio modelio tikslumui. Duomenų apdorojimo metu žemės kontroliniai taškai buvo priskirti tam tikram skaičiui žinomų taškų, kurie anksčiau buvo išmatuoti GNSS imtuvu, o likę žinomi taškai buvo naudojami kaip patikrinimo taškai (PT). Buvo naudojamos trys kontrolinių taškų išdėstymo konfigūracijos: 8 ŽKT ir 3 PT, 6 ŽKT ir 5 PT bei 5 ŽKT ir 6 PT. Žemės kontroliniai taškai buvo naudojami

fotogrametrinio modelio tikslumui užtikrinti, o gautam tikslumui patikrinti buvo naudojami patikros taškai.

RTK metodo duomenų apdorojimo procedūra iš esmės buvo tokia pati, kaip žemės kontroliniais taškais pagrįsto metodo. Tačiau, naudojant RTK metodą, fotogrametriniam modeliui sugeneruoti pakanka mažiau žemės kontrolinių taškų. Todėl šiuo atveju buvo naudojamos dvi išdėstymo konfigūracijos, naudojant 5 ŽKT ir 3 PT bei 3 ŽKT ir 5 PT. Dėl žmogiškos klaidos renkant duomenis dalis ploto nebuvo užfiksuota, todėl bendrą kontrolinių taškų išdėstymo schemą šiuo atveju sudarė 8 žinomi taškai vietoj 11.

PPK darbo eigos atveju fotogrametriniam modeliui sugeneruoti buvo naudojama viena Aeropoint bazinė stotis, kuri duomenų apdorojimo proceso metu buvo pasirinkta kaip žemės kontrolinis taškas. Šiuo atveju kontrolinių taškų išdėstymo schema buvo 1 ŽKT ir 10 PT.

Eksperimente analizuotų metodų tikslumas buvo įvertintas lyginant skaičiuojamuosius žemės atsargų tūrius ir kontrolinių taškų x, y, z koordinačių nuokrypius. Pirmiausia tūrio skaičiavimai ir kontrolinių taškų matavimai buvo atlikti tradiciniu metodu, naudojant GNSS imtuvą. Tada buvo sugeneruoti fotogrametriniai modeliai ir apskaičiuoti tų pačių atsargų tūriai bei palyginami žinomų taškų koordinačių nuokrypiai.

7.2.5. Eksperimentiniai žemės darbų valdymo rezultatai

Tūrio įvertinimas buvo analizuojamas tiriant 16 įvairaus dydžio žemės krūvų. Pirmiausia analizuojamos žemės krūvos buvo išmatuotos naudojant Trimble GNSS imtuvą, o jų tūris apskaičiuotas naudojant Civil3D programinę įrangą. Bendras 16 krūvų tūris sudarė 10532,18 m³.

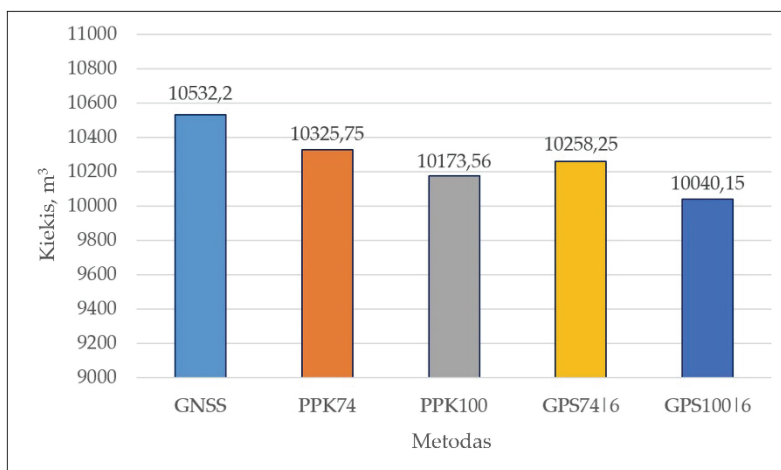
Apskaičiavus tūrius GNSS imtuvu, tose pačiose ribose buvo apskaičiuoti tūriai fotogrametriniuose modeliuose. Analizuojant žemės kontroliniais taškais pagrįstu metodu gautus duomenis buvo panaudotos trys kontrolinių taškų išdėstymo schemas. Duomenys, apdoroti naudojant 5 ŽKT ir 6 PT bei 8 ŽKT ir 3 PT išdėstymo schemas, parodė nenuoseklius arba reikšmingus nukrypimus nuo GNSS imtuvo matavimų. Patikimiausi rezultatai buvo gauti naudojant 6 ŽKT ir 5 PT išdėstymo schemą. Šis fotogrametrinis modelis buvo toliau naudojamas tūrio analizei, o likę modeliai buvo pašalinti iš tolimesnių skaičiavimų.

RTK metodu fiksuojant žemės paviršių iš 74 m aukščio, RTK signalas buvo trumpam dingęs, todėl gauti duomenys tapo nepatikimi ir buvo atmesti iš tolimesnės analizės. O renkant duomenis iš 100 m aukščio dėl skrydžio planavimo klaidos buvo užfiksuotas ne visas plotas. Dėl šių priežasčių RTK metodas buvo toliau tiriamas mažesniu mastu, analizuojant penkias žemės krūvas, kurių bendras tūris sudarė apytiksliai 3800 m³. 37 lentelėje pateiktas kiekvienos žemės krūvos tūrio, gauto visais eksperimente nagrinėtais metodais, palyginimas.

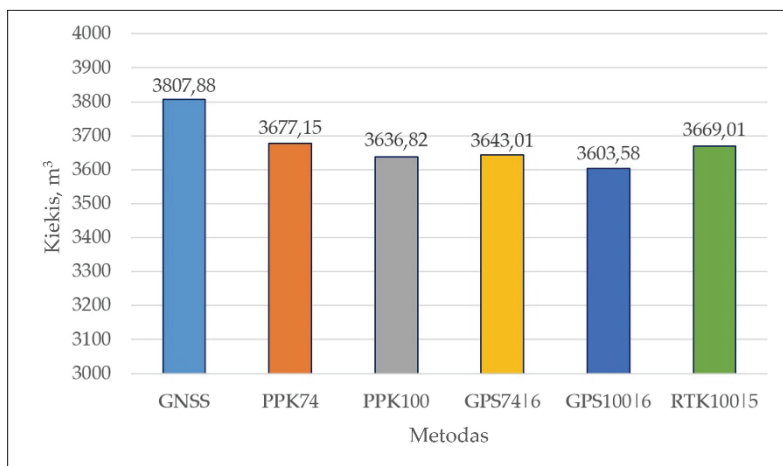
37 lentelė. Žemės krūvų tūrio palyginimas

Nr.	GNSS įmtuvos	PPK metodas		6 ŽKT pagrįstas metodas		RTK metodas
	Žemės lygis, m ³	74 metrai, m ³	100 metrų, m ³	74 metrai, m ³	100 metrų, m ³	100 metrų, m ³
1	91,95	96,95	94,57	95,09	94,95	–
2	1407,86	1285,00	1254,00	1280,17	1273,18	–
3	832,19	791,00	775,00	797,65	791,79	800,72
4	3046,91	3210,00	3187,00	3119,22	3003,53	–
5	623,28	598,00	582,00	650,09	639,56	–
6	475,50	421,00	413,00	430,66	411,46	–
7	48,22	51,65	49,17	50,80	49,10	–
8	115,73	117,00	114,00	114,65	114,44	–
9	242,96	239,00	236,00	236,13	229,00	237,29
10	36,21	35,15	32,82	36,35	36,00	35,31
11	255,40	236,00	230,00	226,56	223,05	–
12	228,59	210,00	194,00	219,38	219,19	–
13	255,57	266,00	266,00	267,28	253,86	–
14	175,31	157,00	153,00	161,34	154,25	–
15	1185,39	1101,00	1094,00	1060,42	1053,92	1068,88
16	1511,13	1511,00	1499,00	1512,46	1492,87	1526,81

Išnagrinėjus kiekvienos krūvos tūrį atskirai, koreliacijos tarp skirtingais metodais gautų rezultatų nebuvo nustatyta. 93 ir 94 pav. parodytas kiekvienu metodu gautų bendrų kiekių palyginimas.



93 pav. Bendras 16 krūvų tūrio palyginimas



94 pav. Bendras 5 krūvų tūrio palyginimas

Tradiciniu metodu apskaičiuoti kiekiai nuo fotogrametrinių metodų skyrėsi 1,96–4,67% lyginant šešiolikos krūvų tūrį, ir 3,43–5,36% lyginant penkių krūvų tūrius. Lyginant fotogrametrinių metodų rezultatus, visos apimties tyrime kiekiai skyrėsi 0,65–2,76%, o mažos apimties tyrime – 0,17–2%. Lyginant fotogrametrinius metodus, buvo pastebėta koreliacija tarp apskaičiuotų rezultatų ir duomenų gavimo aukščio, tačiau bendras skirtumas neviršijo 1,44% vidurkio.

Kontrolinių taškų tikslumas buvo įvertintas lyginant fotogrametriniuose modeliuose gautų x , y , z koordinatų nuokrypį nuo GNSS imtuvu gautų matavimų. Buvo išmatuota ir palyginta 11 kontrolinių taškų. Kadangi RTK metodas užfiksavo mažesnę plotą ir ne visi žinomi taškai buvo įtraukti į fotogrametrinį modelį, todėl šio metodo tikslumas buvo įvertintas palyginus 8 kontrolinius taškus. Taip pat buvo atliktas papildomas mažesnio masto tyrimas žiemos metu, naudojant PPK darbo eigą. Šiuo atveju buvo panaudoti 5 kontroliniai taškai, kurie GNSS imtuvu buvo pakartotinai išmatuoti kitose, su ankstesniais matavimais nesusijusiose vietose. Fotogrametriniais metodais gautų x , y , z matavimų nuokrypiai, lyginant su GNSS imtuvo matavimais, buvo apskaičiuoti naudojant vidutinės kvadratinės paklaidos (RMSE) statistinį metodą. RMSE reikšmės buvo gautos pakėlus kvadratu skirtumus tarp įprastai išmatuotų ir fotogrametriniu būdu išmatuotų taškų, juos sudėjus ir padalijus iš panaudotų taškų skaičiaus bei apskaičiavus gauto rezultato kvadratinę šaknį:

$$RMSE = \sqrt{\frac{\sum(y_i - y_p)^2}{n}}, \quad (1)$$

čia: y_i yra tikroji kiekvieno žemės kontrolinio taško vertė, išmatuota GNSS imtuvu; y_p yra numatoma atitinkamų žemės kontrolinių taškų vertė, išmatuota fotogrametriniame modelyje; n yra bendras žemės kontrolinių taškų skaičius.

Žemės kontroliniais taškais pagrįsto ir PPK metodų x , y , z nuokrypčių rezultatai vertinant 11 žinomų taškų pateikti 38 ir 39 lentelėse.

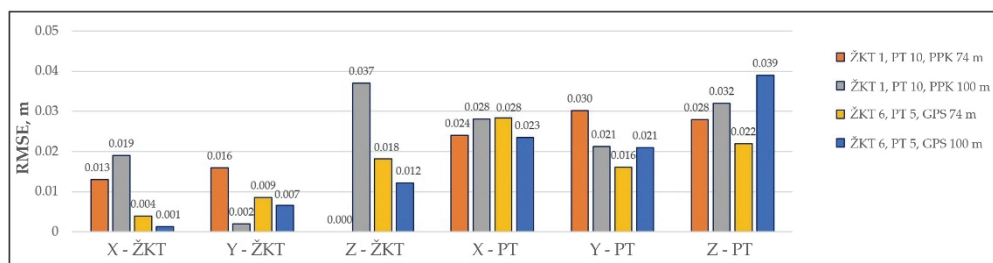
38 lentelė. RMSE nuokrypiai 11 kontrolinių taškų

Metodas	X, m	Y, m	Z, m
5 ŽKT ir 6 PT GPS 74 m	0,017	0,017	0,434
5 ŽKT ir 6 PT GPS 100 m	0,026	0,011	0,256
6 ŽKT ir 5 PT GPS 74 m	0,018	0,020	0,050
6 ŽKT ir 5 PT GPS 100 m	0,015	0,014	0,030
8 ŽKT ir 3 PT GPS 74 m	0,010	0,010	0,047
8 ŽKT ir 3 PT GPS 100 m	0,010	0,009	0,021
1 ŽKT ir 10 PT PPK 74 m	0,023	0,028	0,026
1 ŽKT ir 10 PT PPK 100 m	0,026	0,024	0,038

39 lentelė. RMSE nuokrypiai vertinant žemės kontrolinius taškus ir patikros taškus

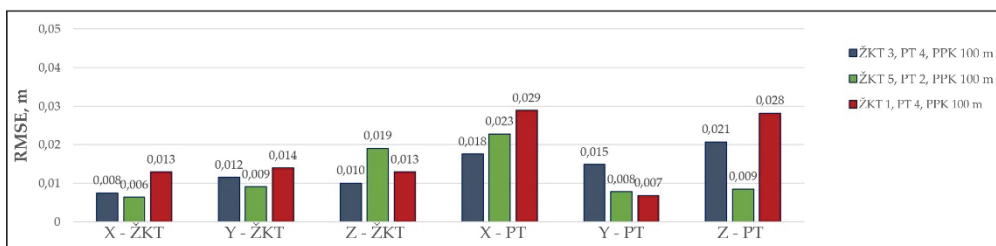
Metodas	ŽKT			PT		
	X, m	Y, m	Z, m	X, m	Y, m	Z, m
5 ŽKT ir 6 PT GPS 74 m	0,008	0,018	0,237	0,023	0,017	0,547
5 ŽKT ir 6 PT GPS 100 m	0,004	0,003	0,022	0,035	0,015	0,346
6 ŽKT ir 5 PT GPS 74 m	0,040	0,09	0,018	0,026	0,028	0,071
6 ŽKT ir 5 PT GPS 100 m	0,010	0,07	0,012	0,022	0,020	0,043
8 ŽKT ir 3 PT GPS 74 m	0,005	0,008	0,016	0,018	0,014	0,085
8 ŽKT ir 3 PT GPS 100 m	0,007	0,009	0,023	0,016	0,008	0,014
1 ŽKT ir 10 PT PPK 74 m	0,013	0,016	0,000	0,023	0,029	0,028
1 ŽKT ir 10 PT PPK 100 m	0,019	0,002	0,037	0,027	0,025	0,038

Analizuojant rezultatus taikant kontroliniais taškais pagrįstą metodą, buvo pastebėti reikšmingi z reikšmių nuokrypiai. Išanalizavus vertikalinių atskaitos taškų rezultatus, pastebėta, kad dažniausiai didesnis nuokrypis buvo taške Nr. 8. Taip galėjo būti dėl to, kad šis taškas buvo įrengtas tiriamosios zonos pakraštyje ir žolėtoje vietoje. Todėl taškas Nr. 8 buvo pašalintas iš tolimesnės analizės. Tačiau taip pat buvo pastebėta, kad ŽKT pagrįsto metodo, naudojant 5 ŽKT ir 6 PT bei 8 ŽKT ir 3 PT taškų išdėstymo schemas, nukrypimai buvo nenuspėjami ir kai kuriais atvejais labai reikšmingi. Todėl šios išdėstymo schemas toliau nebuvo analizuojamos. Atlikus pataisymus gauti rezultatai pateikti 95 pav.



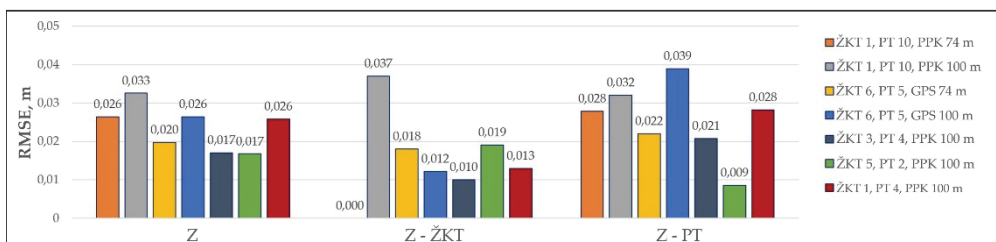
95 pav. PPK ir ŽKT pagrįstų metodų RMSE nuokrypiai

Analizuojant RTK metodą, vienas kontrolinis taškas taip pat buvo tiriamos teritorijos pakraštyje ir turėjo reikšmingą nuokrypį. RMSE nuokrypių rezultatai pašalinus šį tašką kartu su PPK metodo rezultatais žiemos metu parodyti 96 pav.



96 pav. RTK ir PPK metodų RMSE nuokrypiai mažos apimties tyrimuose

Visų analizuojamų metodų vertikaliųjų atskaitos taškų analizės rezultatai pateikti 97 pav.



97 pav. Visų analizuotų metodų vertikaliųjų atskaitos taškų rezultatų palyginimas

Tradiciniu būdu naudojant GNSS imtuvą, norint išmatuoti 5549,55 m² plotą, prirėkė maždaug 6 valandų. Bepiločiams orlaiviams iš 100 m aukščio užfiksuoti 36 ha plotą prirėkė 17 minučių, o iš 74 m aukščio – 37 minučių. Skrydžio aukštis turėjo nedidelį poveikį duomenų tikslumui, tačiau turėjo reikšmingos įtakos skrydžio laikui ir duomenų dydžiui. Skrydžio laikas 74 m aukštyje užtruko 54% ilgiau, o gautų duomenų kiekis buvo 55% didesnis, palyginti su skrydžiu 100 m aukštyje. Tačiau, įvertinus pasirošimo skrydžiui laiką, duomenų gavimo laikas pailgėjo iki maždaug 1 valandos. 0,55 ha ploto duomenų gavimo efektyvumo palyginimas pateiktas 40 lentelėje.

40 lentelė. Duomenų gavimo efektyvumas 0,55 ha plote

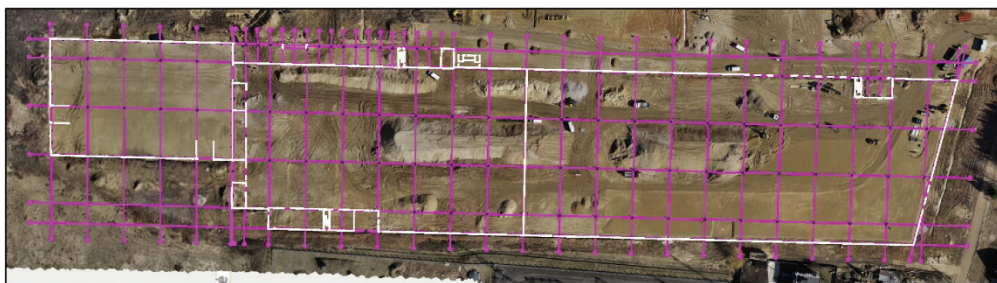
Duomenų gavimo metodas	Tiriamas plotas	Duomenų gavimo aukštis	Duomenų gavimo laikas	Išmatuotų taškų skaičius
GNSS-RTK imtuvas	0,55 ha	Žemės lygis	6 val.	1108
BO fotogrametrija	0,55 ha	74 m	1 val.	Milijonai
BO fotogrametrija	0,55 ha	100 m	1 val.	Milijonai

Eksperimente naudojamų bepiločių orlaivių rekomenduojama darbinė temperatūra yra nuo 0 iki +40 °C. Esant žemai temperatūrai, akumulatorius gali greičiau išsikrauti, tačiau duomenų gavimo greičiui temperatūra nurodytame diapazone įtakos neturi. Eksperimente naudojamo GNSS imtuvo darbinė temperatūra gamintojo techninėse specifikacijose nurodyta nuo –40 iki +65 °C, tačiau reikia atkreipti dėmesį, kad nurodyta GNSS imtuvo akumulatoriaus darbinė temperatūra yra iki –20 °C. Duomenų gavimo laikui, naudojant BO fotogrametrijos metodus, labai didelę įtaką turi apšvietimas ir skrydžio aukštis. Esant debesuotam orui ar skrydžio aukščio apribojimams, duomenų gavimas gali užtrukti daug ilgiau,

nes fotogrametrijos procesui reikalingos aukštos kokybės nuotraukos. Be to, bepiločio orlaivio naudoti nerekomenduojama lyjant, esant rūkui ar vėjo greičiui viršijant 10 m/s.

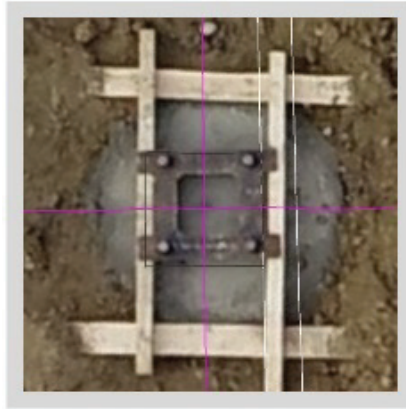
Kadangi PPK darbo eigos analizės rezultatai parodė metodo patikimumą, technologija toliau buvo išbandyta realiame pramoninio pastato statybos projekte. Statybos aikštelė Kaune užėmė apytiksliai 16 ha plotą. Į projektą buvo įtraukta gamyklos statyba, kur taip pat reikėjo atlikti nemažai žemės darbų. Šiame projekte, remiantis eksperimentinių tyrimų rezultatais, užteko tik vienos Aeropoint bazinės stoties, kuri buvo naudojama kaip žemės kontrolinis taškas.

Siekiant efektyviai stebėti žemės darbų eigą, skrydžiai buvo vykdomi nepertraukiamai kartą ar du per savaitę per visą statybos etapą, kol buvo atliekami žemės darbai. Gavus fotogrametrinį modelį, pirmiausia ašys ir pastato ribos buvo importuotos į fotogrametrinį modelį CAD formatu, kaip parodyta 98 pav. Tai padėjo planuoti ir sekti darbų eigą.



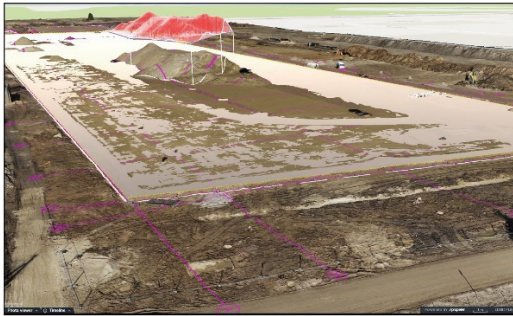
98 pav. Ašys ir pastato ribos importuotos į fotogrametrinį modelį

Fotogrametrinio modelio x ir y tikslumas buvo įvertintas vizualiai lyginant projektinius brėžinius LKS94 koordinacių sistemoje, užkeliant juos ant fotogrametrinio modelio. Pavyzdžiui, ašys buvo eksportuotos iš projektinių CAD brėžinių ir įkeltos į Propeller platformą palyginimui. Kadangi CAD brėžiniai ir fotogrametrinis modelis buvo toje pačioje koordinacių sistemoje, buvo galima palyginti atliktus darbus fotogrametriniame modelyje su projektiniais brėžiniais. 99 pav. pateiktame pavyzdyje vizualiai buvo įvertinta kolonos įrengimo vieta. Fotogrametriniame modelyje CAD ašių susikirtimo centras vizualiai atitiko įrengtos kolonos centrą. Taip galima vizualiai įsitikinti, ar fotogrametrinis modelis yra teisingai sulygiuotas x ir y koordinacių sistemoje ir kartu stebėti darbų eigą bei kontroliuoti konstrukcijų įrengimo darbus.

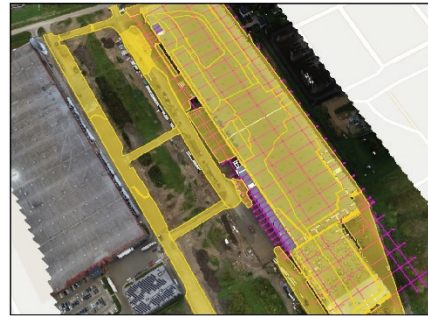


99 pav. Vizualinis x, y tikslumo įvertinimas

Žemės darbų metu fotogrametriniai modeliai buvo naudojami įvairiems tikslams. Pavyzdžiui, realybės modelis su projektiniu paviršiumi padėjo kontroliuoti žemės lygiavimo darbų eigą (100 pav., a). Be to, šis metodas nuolatos buvo naudojamas planuojant ir kontroliuojant žemės darbų apimtį (100 pav., b).



a)



b)

100 pav. Praktinio panaudojimo būdai: a) vykdomų darbų stebėjimas lyginant su projektiniu paviršiumi, b) žemės darbų apimčių kontrolė

7.3. TAIKYMAS PASTATO KONSTRUKCIJŲ STATYBOJE

7.3.1. Tiriamojo objekto aprašymas

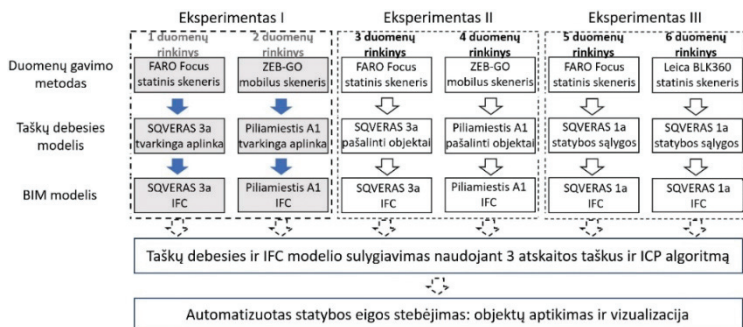
3D lazerinis skenavimas paprastai naudojamas pastatų statybose arba ten, kur reikalingas milimetrinis tikslumas. Statant pastatus dažniausiai naudojami IFC modeliai, pagal kuriuos atliekami statybos darbai ir stebima jų eiga. Siekiant sukurti statybos stebėjimo automatizavimo metodiką, eksperimentui buvo atrinkti du pastatai su IFC modeliu. Skenavimas buvo atliktas biurų pastato Sqveras ir gyvenamojo namo Piliamiestis A1 statybos projektuose. Šie objektai tyrimui pasirinkti, nes reprezentavo tipinę statybų aplinką, todėl sukurta metodika būtų lengviau pritaikoma praktikoje.

Sqveras pastate lazerinis skenavimas buvo atliktas pirmame ir trečiame aukštuose. Abiejuose aukštuose konstrukcijos buvo monolitinės, grindų plotas apie 600 m², konstrukcijos standartinės – kolonos, sijos, sienos. Trečiame aukšte pastato konstrukcijos buvo aiškiai matomos, neuždengtos statybinėmis medžiagomis ar kita statybine technika. Pirmame aukšte virš kolonų buvo įrengti klojiniai, šalia stovėjo pastoliai ir kiti objektai, kai kurių konstrukcijų paviršiai buvo užstatyti statybinėmis medžiagomis.

Skenavimo metu Piliamiestis A1 pastate statybos darbai nebuvo vykdomi, aplinka buvo švari, be kliūčių. Skenuojamos konstrukcijos buvo mūrinės ir monolitinės, sudarytos iš perdangos plokščių, sienų ir sijų. Bendras grindų plotas užėmė 450 m².

7.3.2. Metodai ir įrankiai

Šiame eksperimentiniame tyrime nagrinėjamas 3D taškų debesies, gauto iš lazerinių skenerių jutiklių, pritaikymas statybos eigai stebėti, automatiškai identifikuojant IFC objektus 3D taškų debesyje. Tyrimo metodika susideda iš trijų eksperimentų, atliekamų skirtingomis sąlygomis. Eksperimentų metu buvo analizuojami šeši duomenų rinkiniai, kurių kiekvienas susideda iš 3D taškų debesies duomenų ir IFC failo, atitinkančio nuskenuotą vietą. Eksperimentinio tyrimo schema pateikta 101 pav.



101 pav. Eksperimentinio tyrimo schema

Pastato konstrukcijų geometrijai užfiksuoti buvo naudojami statiniai lazeriniai skeneriai FARO Focus S ir Leica BLK360 bei rankinis lazerinis skeneris ZEB-GO. Šie įrenginiai skiriasi techniniais parametrais, tokiais kaip nuskaitymo diapazonas,

skenavimo greitis, tikslumas ir kt. Tyrime buvo atsižvelgta į gamintojo deklaruojamus parametrus ir tolesnis tikslumo vertinimas nebuvo atliktas. Pagrindiniai naudojamų prietaisų techniniai parametrai pateikti 41 lentelėje.

41 lentelė. Pagrindiniai eksperimente naudotų lazerinių skenerių parametrai

Lazerinio skenerio pavadinimas	Prietaiso tipas	Nuskaitymo tikslumas	Nuskaitymo diapazonas	Skenavimo greitis, taškai per sekundę
FARO Focus S70	Statinis / TLS	1 mm	70 m	1000000
Leica BLK360	Statinis / TLS	4 mm (10 m)	60 m	360000
		7 mm (20 m)		
ZEB-GO & ZEB-DL2600 duomenų kaupiklis	Mobilusis / rankinis	10–30 mm	30 m	43000

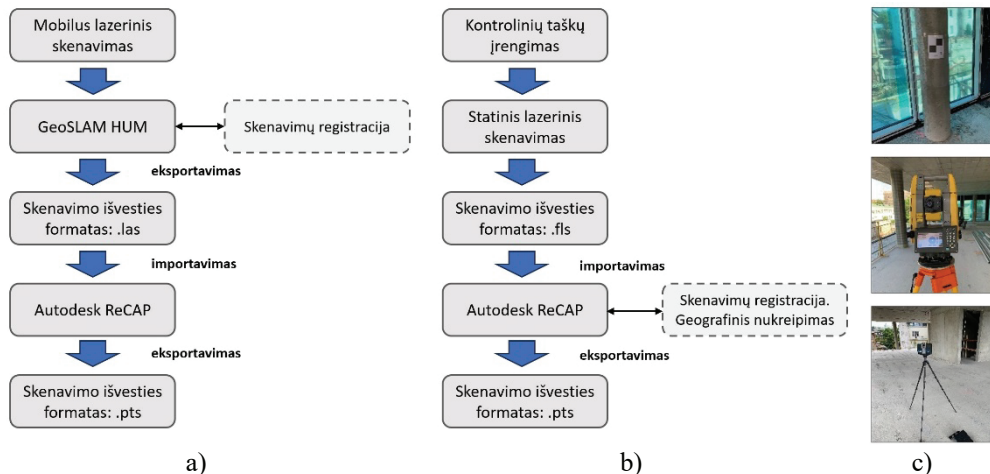
Pirmiausia duomenys buvo gauti palyginti tvarkingoje statybų aplinkoje, naudojant aukštos kokybės lazerinį skenerį FARO Focus. Deklaruojamas šio lazerinio skenerio tikslumas siekė iki 1 mm ir buvo didžiausias tarp šiame eksperimente naudotų skenerių. Todėl šiuo skeneriu tvarkingoje aplinkoje gauti duomenys buvo panaudoti kuriant pirminę automatizuotą objektų aptikimo metodiką. Mobiliojo lazerinio skaitytuvo ZEB-GO gauti duomenys taip pat buvo gauti palyginti tvarkingoje aplinkoje ir naudojami objektų aptikimo procesui patikrinti. Gavus sėkmingus rezultatus, iš šio 3D taškų debesies buvo pašalinta keletas objektų, siekiant įvertinti, ar sukurtas procesas sėkmingai identifikuoja nesamus objektus. Galiausiai skenavimas buvo atliktas su aukštos kokybės FARO Focus skeneriu ir žemesnės specifikacijos, tačiau gerokai pigesniu Leica BLK360 skeneriu statybos aplinkoje, kurioje buvo įvairių trukdžių tinkamai užfiksuoti konstrukcijų paviršius. Kiekvieną duomenų rinkinį sudarė lazerinio skenerio 3D taškų debesies duomenys ir atitinkamas IFC modelis.

7.3.3. Duomenų gavimo darbo eigos

Eksperimentinio tyrimo metu skenavimas buvo atliktas naudojant tris skirtingų techninių specifikacijų lazerinius skenerius. Pirma, skenavimas buvo atliktas tvarkingoje aplinkoje, Sqveras pastato trečiame aukšte ir Piliamiestis A1 statybos projekte. Čia konstrukcijos buvo aiškiai matomos matymo linijoje. Šiuo atveju Sqveras pastate skenuojant buvo naudojamas lazerinis skeneris FARO Focus, o Piliamiestis A1 pastate – rankinis lazerinis skeneris ZEB-GO. Vėliau skenavimas buvo atliktas Sqveras pastato pirmame aukšte, kur dalis konstrukcijų buvo užstatytos įvairiomis statybinėmis medžiagomis ir įranga. Čia buvo naudojami lazeriniai skeneriai FARO Focus ir Leica BLK360.

Pagrindinis dėmesys buvo skiriamas kokybiškiems duomenims gauti trečiame Sqveras pastato aukšte, nes šie duomenys buvo skirti metodikai kurti. Pirmiausia ant sienų ir kolonų buvo įrengti septyni kontroliniai taškai. Kontroliniai taškai buvo padaryti spausdinant juodai baltą šaškių lentos raštą ant A4 formato popieriaus lapo. Naudojant šiuos kontrolinius taškus ir TOPCON GT serijos robotizuotą padėties nustatymo sistemą, taškų debesies modelis buvo geografiškai nukreiptas į LKS94 koordinacių sistemą ir LAS07 aukščio sistemą. Viso aukšto aplinkos skenavimas

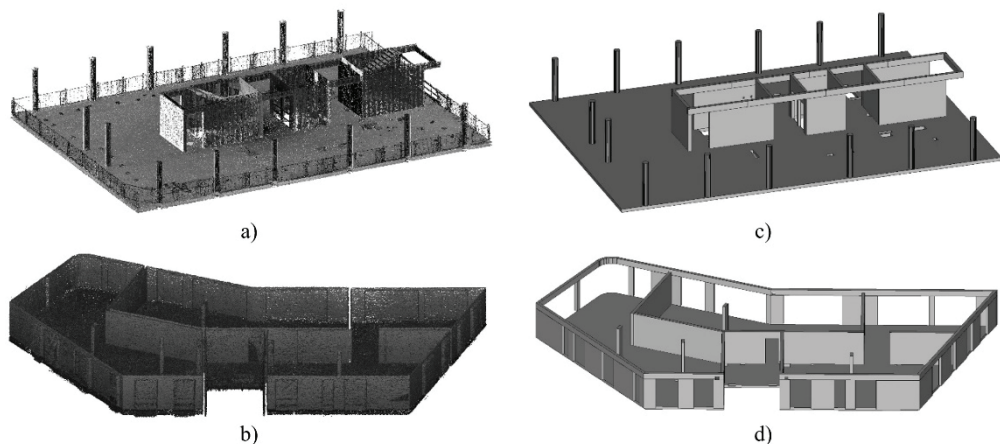
buvo atliktas iš šešiolikos skenavimo vietų. Sqveras pastato pirmame aukšte ir Piliamiestis A1 pastate 3D taškų debesis nebuvo geografiškai nukreiptas ir toliau buvo analizuojamas vietinėje koordinacių sistemoje. Duomenų gavimo ir išankstinio apdorojimo darbo eiga bei naudojama įranga pateikta 102 pav.



102 pav. Duomenų gavimo darbo eiga: a) mobilus lazerinis skenavimas, b) statinis lazerinis skenavimas, c) kontrolinis taškas, TOPCON GT serijos robotizuotas tacheometras ir FARO Focus lazerinis skeneris

7.3.4. Duomenų apdorojimas

Pagrindinis tyrimo tikslas buvo automatizuotas vertikalinių objektų, tokių kaip sienos ir kolonos, aptikimas 3D taškų debesyje, lyginant taškinio debesies geometriją su IFC modeliu. 3D taškų debesis modeliai buvo iš anksto apdoroti Autodesek ReCap programine įranga pašalinant perteklinius taškus, o geresniam vizualizavimui buvo pašalinta viršutinė perdangos plokštė (103 pav.). Informacija apie 3D taškų debesis modelius pateikta 42 lentelėje. Atitinkamai IFC modeliai buvo supaprastinti pašalinant perteklinius elementus ir elementų mazgus ir paliekant tik nuskenuotos srities modelį be lubų plokštumos (103 pav.). Modeliai buvo sukurti Tekla Structures 2017 programine įranga ir eksportuoti IFC formatu, pasirinkus IFC2X3 schemą su numatytais nustatymais. Nereikalingi IFC modelio elementai buvo pašalinti Simplebim 8.2 SR1 programine įranga.



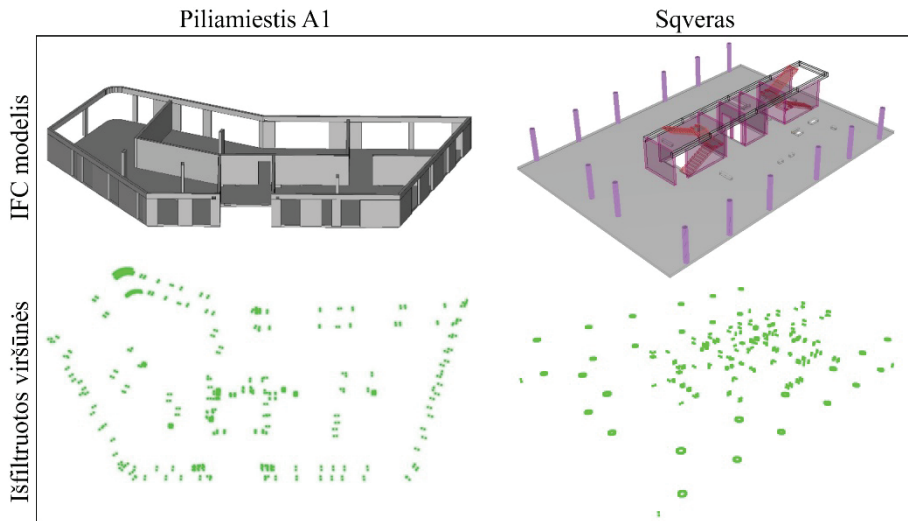
103 pav. IFC ir 3D taškų debesies modeliai paruošti tolesnei analizei: a) Sqveras pastato 3D taškų debesies modelis, b) Piliamiestis A1 3D taškų debesies modelis, c) Sqveras pastato IFC modelis, d) Piliamiestis A1 IFC modelis

42 lentelė. Informacija apie 3D taškų debesies modelius

3D taškų debesies modelis	Vidutinė taškų populiacija, taškai per m ³	Taškų skaičius	Duomenų dydis, mb
SQVERAS trečias aukštas (FARO Focus S70)	1438,78	9451351	758
PILIAMIESTIS A1 (ZEB-GO)	521,48	12510712	677
SQVERAS pirmas aukštas (FARO Focus S70)	2211,69	13882774	1007
SQVERAS pirmas aukštas (Leica BLK360)	726,60	12990132	903

Norint atlikti pastatytų ir nepastatytų objektų aptikimo procesą, pirmiausia reikėjo sulygiuoti duomenų modelius. Tačiau IFC ir 3D taškų debesies failai turi skirtingas duomenų struktūras, kurios nėra tiesiogiai palyginamos. Pavyzdžiui, IFC failuose yra pastato elementų (pvz., plokščių, sijų, sienų, kolonų) sąrašas, kuriame kiekvienas elementas apibūdinamas jo savybėmis, pavyzdžiui, viršūnėmis, linijomis, paviršiais ir jų erdvinėmis koordinatėmis (x, y, z). O 3D taškų debesies failuose yra taškų rinkinys, atspindintis skenavimo metu užfiksuotų objektų geometriją. Prie šių duomenų taškų pateikiamos jų erdvinės koordinatės, tačiau šie taškai neturi informacijos apie semantinį atvaizdavimą.

Norint atlikti duomenų sulygiavimą, pirmiausia iš IFC failo esančių objektų buvo išfiltruotos viršūnės. Šio proceso metu buvo gauta IFC modelio 3D taškų debesies versija, kaip parodyta 104 pav.

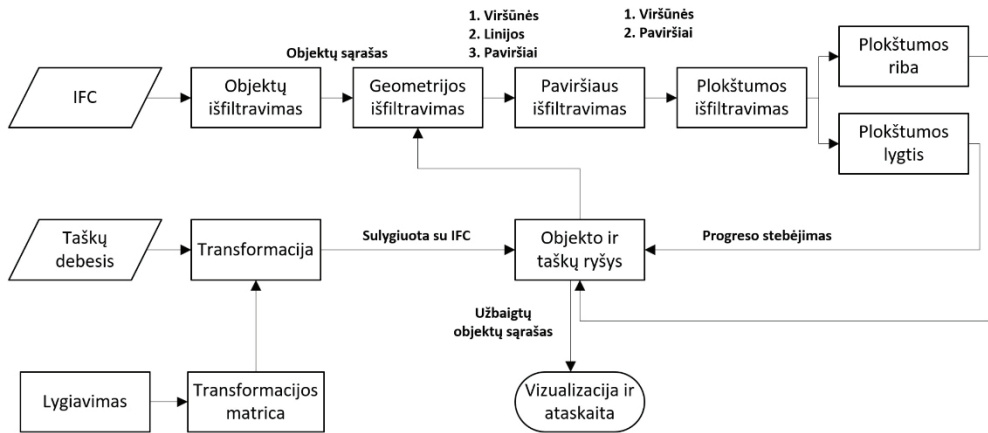


104 pav. 3D taškų debesies versija, gauta išfiltravus IFC elementų viršūnes

Gavus 3D taškų debesį iš IFC objektų viršūnių, buvo inicijuojamas duomenų lygiavimo procesas. Duomenims sulygiuoti buvo pritaikytas gerai žinomas iteracinio artimiausio taško (ICP) algoritmas. ICP algoritmas veikia su dviem skirtingais 3D taškų debesų rinkiniais, kur vienas laikomas šaltinio 3D taškų debesiu, o kitas – tiksliniu 3D taškiniu debesiu. Šiame kontekste šaltinio 3D taškų debesis atitiko duomenis, gautus iš lazerinių skenerių jutiklių, o tikslinis 3D taškų debesis atitiko 3D taškų debesį, sukurtą iš išfiltruotų IFC elementų viršūnių.

Norint gauti tikslius transformacijos parametrus taškų debesims sulygiuoti, prieš tai reikia atlikti apytikslį sulygiavimą. ICP daro prielaidą, kad taškų debesis jau yra apytiksliai sulygiuoti, ir siekia rasti standžią transformaciją, kuri geriausiai patikslina lygiavimą. Algoritmas apytiksliai suderina atitikmenis kartotiniu būdu, ieškodamas artimiausio atstumo tarp taškų ir taip pagerindamas išlygiavimą kiekviename žingsnyje. Paprastai duomenų lygiavimas naudojant ICP metodą priklauso tik nuo 3D taškų debesies informacijos. Šiame tyrime, norint pradėti lygiavimo procesą, reikėjo vartotojo įvesties, pasirenkant tris atskaitos taškų poras šaltinio ir tikslinių 3D taškų debesų modeliuose. Tai užtikrino pakankamai tikslų ir efektyvų lygiavimo procesą.

Sulygiavus duomenis buvo pradėtas procesas, skirtas automatiškai palyginti faktinę konstrukciją su projektiniu modeliu, siekiant identifikuoti pastatytus ir nepastatytus objektus. Automatizuotas objektų aptikimo procesas parodytas 105 pav.

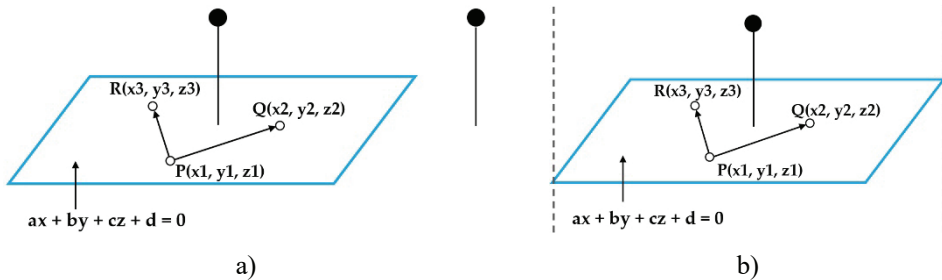


105 pav. Automatizuotas objektų aptikimo procesas

Kaip parodyta 105 pav., visas procesas susideda iš kelių užduočių. Siekiant nustatyti, koks objektas buvo identifikuotas taškų debesyje, buvo atliktas IFC objektų išfiltravimo procesas. Šiame etape buvo išfiltruoti IFC objektų identifikatoriai. Geometrijos išfiltravimo procese buvo išfiltruoti pagrindiniai IFC objektų atributai, tokie kaip viršūnės, linijos ir objektų paviršių plokštumos. IFC failuose kiekvieno elemento paviršiaus plokštuma turi ryšį tarp viršūnių, todėl objekto paviršiaus išfiltravimo procese buvo išfiltruota tik objektų paviršiaus plokštumos ir viršūnių informacija. Plokštumos išfiltravimo procese buvo identifikuojama, kuriai plokštumai, būtent (x, y) , (x, z) arba (y, z) , priklauso kiekviena objekto paviršiaus plokštuma. Siekiant nustatyti, ar 3D taškų debesyje esantis objektas yra pastatytas lyginant su IFC modeliu, buvo taikoma metodika, kuri palygino, kiek taškų 3D taškų debesyje buvo arti kiekvieno IFC objekto paviršiaus. Ši užduotis žinoma kaip atstumo nuo taško iki plokštumos įvertinimas. Norint apskaičiuoti atstumą nuo taško iki plokštumos, reikėjo apskaičiuoti paviršiaus plokštumos lygtį. IFC objekto paviršiai pavaizduoti kaip trikampiai, o tai supaprastino plokštumos lygties skaičiavimą, nes reikėjo tik trijų taškų:

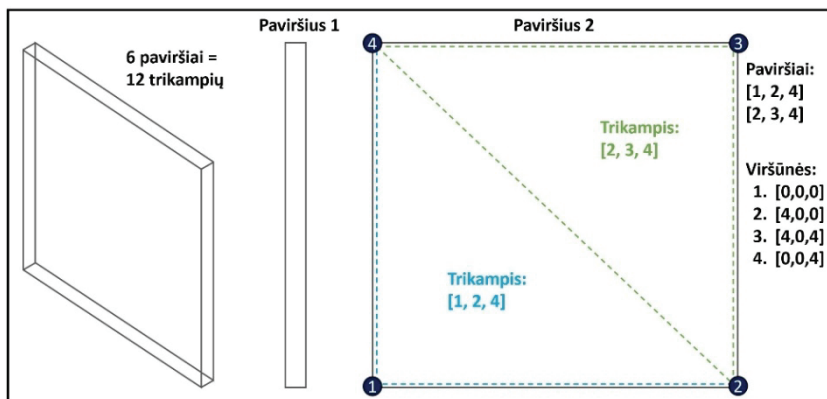
$$ax + by + cz + d = 0, \quad (2)$$

čia: x, y, z yra koordinatės, apibrėžiančios bet kurį 3D erdvės tašką; a, b ir c yra koeficientai, vaizduojantys normalųjį plokštumos vektorius; d yra pastovus narys ir jis įtakoja plokštumos padėtį 3D erdvėje normalaus vektoriaus kryptimi. Lygtis vaizduoja 3D plokštumą Dekarto koordinatinių sistemoje. Vektorius (a, b, c) yra statmenas plokštumai, o jo kryptis lemia plokštumos orientaciją. Žinodami a, b, c ir d reikšmes, galime apibūdinti 3D plokštumą ir jos ryšį su kitais aplinkos subjektais. Ši lygtis buvo naudojama plokštumai pritaikyti prie 3D taškų rinkinio. Atstumas nuo taškų iki plokštumos buvo apskaičiuotas naudojant plokštumos lygtį, apimančią visus taškus, neatsižvelgiant į tai, ar jie patenka į konkrečias plokštumos ribas (kaip parodyta 106 pav., a). Todėl procesas apėmė taškų, esančių už plokštumos ribų, atmetimą (kaip parodyta 106 pav., b).



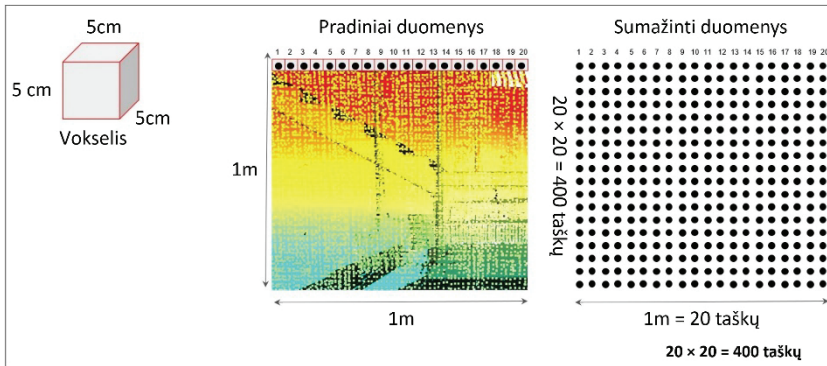
106 pav. Plokštumos riba: a) atstumo iki visų taškų skaičiavimas, b) taškų, esančių už plokštumos, atmetimas

Remiantis 107 pav. pavaizduotu sienos pavyzdžiu, buvo nustatyta, kad kiekvienas IFC objekto paviršius buvo sudarytas iš dviejų trikampių, kurie sudaro tinklą, o visa siena buvo sudaryta iš 6 paviršių, kuriuos sudarė 12 trikampių. Eksperimento metu buvo pastebėta, kad, nustatant ryšį tarp taškų ir IFC objekto paviršiaus, vienodas taškų skaičius buvo susietas su trikampaiais, priklausančiais tam pačiam paviršiui. Siekiant optimizuoti procesą, ryšys tarp IFC objekto paviršiaus ir 3D taškų debesies taškų buvo nustatytas apdorojant po vieną trikampį kiekvienam paviršiui.



107 pav. IFC objekto paviršiaus informacija, vaizduojama kaip ryšys tarp viršūnių

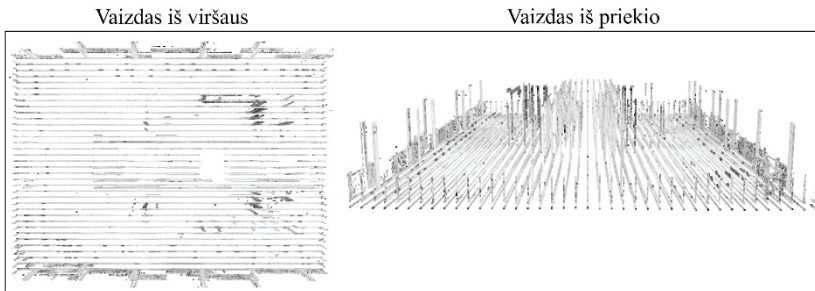
Be to, dirbant su 3D taškų debesimis kyla tam tikrų iššūkių dėl didelio duomenų kiekio. Šiame tyrime 3D taškų debesies duomenų dydis buvo sumažintas naudojant Open3D teikiamą funkciją (`open3d.geometry.voxel_down_sample`). Open3D yra Python biblioteka, skirta 3D duomenims apdoroti. Duomenų mažinimo funkcija (*angl. Downsampling*) Open3D bibliotekoje naudojama 3D taškų debesiui sumažinti naudojant vokselių tinklą. Šis metodas naudojamas siekiant sumažinti 3D taškų debesų tankį, kartu išsaugant bendrą duomenų struktūrą. Taškų skaičiaus sumažinimo procesas buvo atliktas naudojant 5 cm vokselio dydį (108 pav.). Vokselio dydis yra parametras, apibrėžiantis vokselių tinklo, naudojamo duomenims mažinti, dydį. Taškai tame pačiame vokselėje sumažinami iki vieno taško.



108 pav. Taškų sumažinimo procesas naudojant 5 cm vokselio dydį

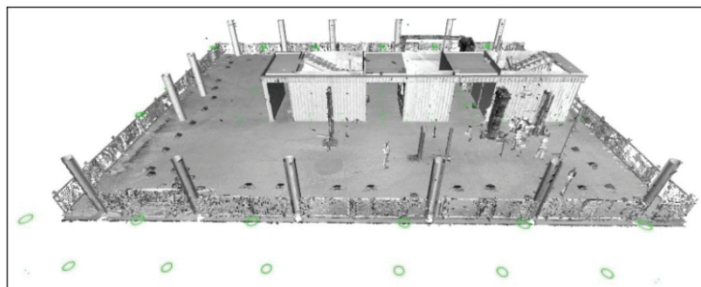
7.3.5. Statybos objektų stebėjimo eksperimentiniai rezultatai

Geografiškai nukreipto 3D taškų debesies atveju kiekvieno duomenų taško x , y , z koordinatės buvo išreikštos tūkstantosiomis ir milijoninėmis dalimis. O likusių 3D taškų debesies modelių ir visų IFC modelių koordinatės buvo išreikštos mažais vienetais. Toks reikšmingas šaltinio ir tikslinių duomenų erdvinis atskyrimas padidino skaičiavimo sudėtingumą ir sukėlė tam tikrų iššūkių naudojant Open3D modulį (109 pav.).



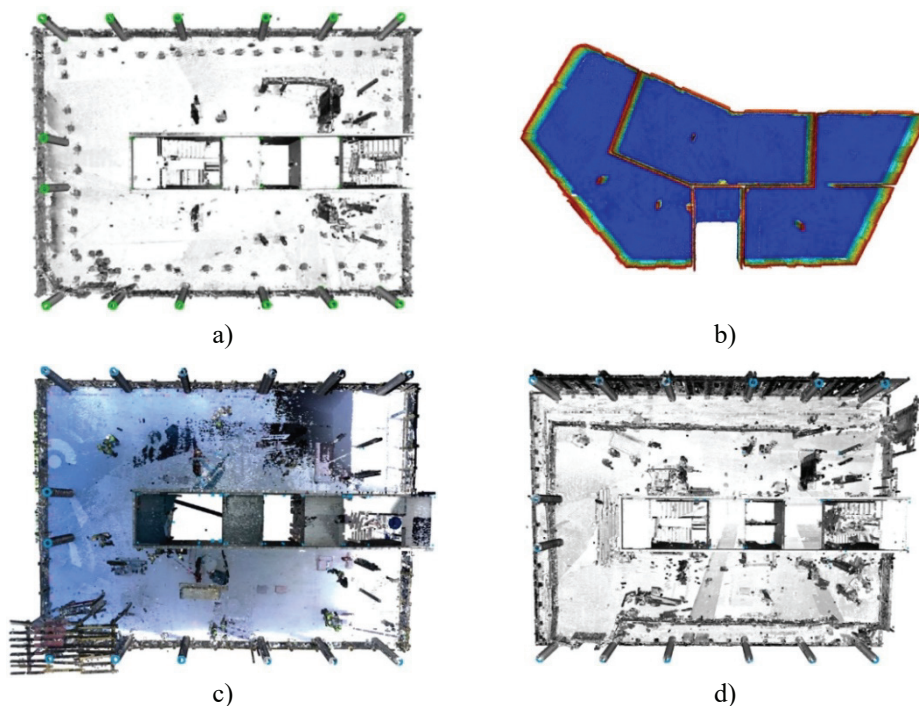
109 pav. Sqveras trečiojo aukšto geografiškai nukreiptas 3D taškų debesies modelis Open3D modulyje

Buvo padaryta išvada, kad koordinatės buvo per didelės, todėl jos buvo transformuotos į nulines kilmės koordinatas. Koordinačių transformacija buvo atlikta surandant minimalią nuskenuotų duomenų stulpelio x , y ir z reikšmę ir atimant tą reikšmę iš kiekvieno stulpelio koordinatė. Po koordinatė transformacijos šaltinio ir tikslinio 3D taškų debesies modeliai buvo arti vienas kito, o 3D taškų debesies modelis buvo teisingai pavaizduotas Open3D modulyje, kaip parodyta pavyzdyje 110 pav.



110 pav. Erdvinė šaltinio ir tikslinio 3D taškų debesies vieta po koordinacių transformacijos

Iš pradžių šaltinio ir tikslinio 3D taškų debesies modeliai buvo apytiksliai sulygiuoti pasirinkus tris atskaitos taškų poras, kurie buvo pasirinkti rankiniu būdu. Kai apytikslis lygiavimas buvo baigtas, ICP metodas buvo automatiškai pritaikytas galutiniam lygiavimui atlikti, taikant gautą transformacijos matricą šaltinio 3D taškų debesyje. Šis procesas patikslino pradinio lygiavimo rezultatus. Šiuo atveju galutiniam ICP išlygiavimui buvo naudojamas 3 cm slenksčio atstumas. Po pradinio ir galutinio lygiavimo visais atvejais duomenų sulygiavimo tikslumas siekė apytiksliai 0,021 m RMSE. Sulygiuoti 3D taškų debesies modeliai pateikti 111 pav.



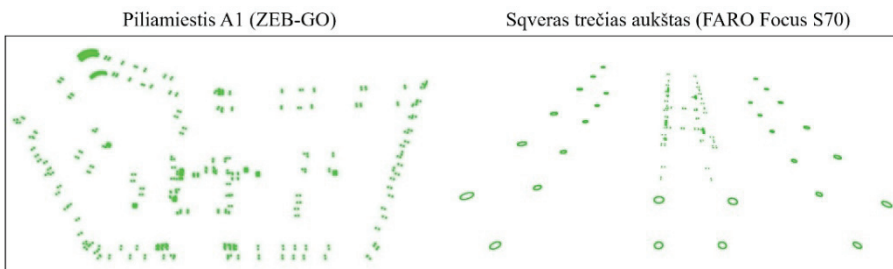
111 pav. Sulygiavimo rezultatai: a) Sqveras trečias aukštas, b) Piliamiestis A1, c) Sqveras pirmas aukštas (Leica BLK360), d) Sqveras pirmas aukštas (FARO Focus S70)

Svarbus objektų aptikimo vertinimo kriterijus buvo sėkmingas objektų aptikimas realiomis statybos sąlygomis, kai skenuojamoje aplinkoje yra įvairių trukdžių, neleidžiančių gerai nuskenuoti objektų paviršiaus. Tokioje aplinkoje

skenavimo duomenys gali būti prastos kokybės. Todėl objektų aptikimo metodikoje buvo apibrėžti parametrai, kurie suteikė lankstumo identifikuojant objektus, kai skenavimo duomenys buvo netikslūs arba neišsamūs.

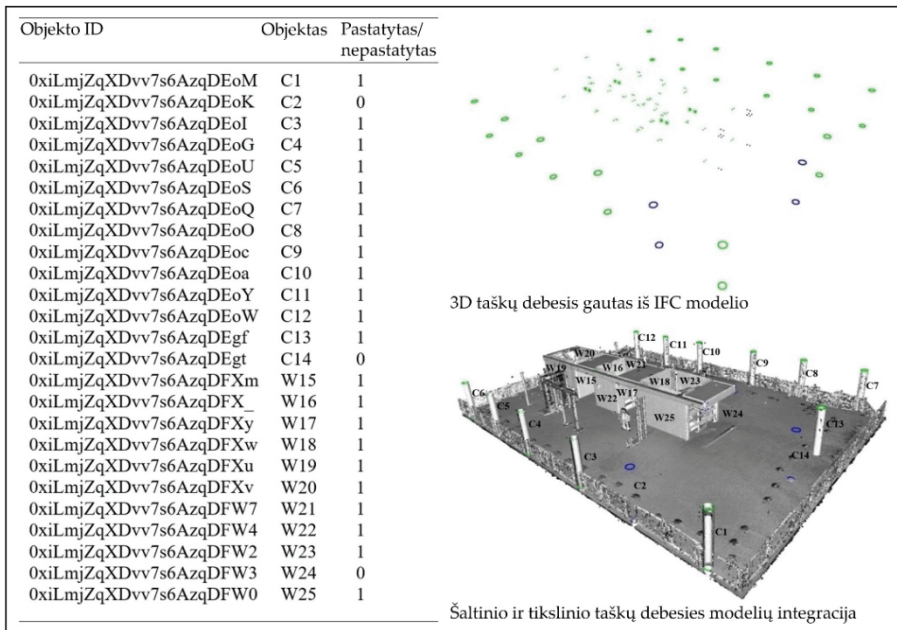
Pirmiausia, norint nustatyti, ar 3D taškų debesyje yra IFC objektas, buvo surasti paviršiai, sudarantys dabartinį IFC objektą. Taigi, kiekvienas stačiakampės sienos paviršius turi du paviršius (du trikampus), kurių viršūnės buvo išskirtos, ir buvo rasta paviršiaus plokštumos lygtis. Tada buvo apskaičiuotas statmenas atstumas nuo kiekvieno 3D taškų debesies taško iki paviršiaus plokštumos. Taškai, kurie buvo už plokštumos ribų, buvo atmesti. Rezultatas buvo taškų, priklausančių kiekvienam paviršiui, skaičius pagal 0,5 slenkstį. 3D taškų debesies duomenų mažinimo procesas sumažino taškų skaičių iki 400 vienam kvadratiniam metrui. Todėl, norint nuspręsti, ar 3D taškų debesyje yra objektas, pirmiausia buvo apskaičiuotas kiekvieno IFC objekto paviršiaus plotas ir paviršiai pažymėti kaip užbaigti, jei jų kvadratiniam metre buvo bent 400 taškų, kaip parodyta 108 pav. Kiekvienas objektas turėjo kelis paviršius ir buvo pažymėtas kaip aptiktas, jei bent 60% paviršių buvo pažymėti kaip aptikti. Šie parametrai leido sėkmingai automatizuotai identifikuoti pastatytus ir nepastatytus objektus 3D taškų debesyje, net kai skenavimas buvo atliktas įvairių trukdžių turinčioje statybos aplinkoje ir kai skenavimo duomenys buvo laikomi prastos kokybės, t. y. taškų debesies modelyje nuskenuoti objektai buvo pasislinkę ir dubliuoti, nevysiškai nuskenuotas paviršius, nepašalinti pertekliniai taškai.

Iš pradžių metodas buvo įvertintas naudojant 1 ir 2 duomenų rinkinius, kur skenavimo aplinka buvo tvarkinga ir be trukdžių. Pradinis objektų aptikimo bandymas naudojant šiuos duomenų rinkinius buvo sėkmingas, visi objektai buvo aptikti ir teisingai identifikuoti kaip pastatyti. Žalia spalva 112 pav. rodo, kad visi objektai buvo aptikti.



112 pav. Objektai pažymėti žaliai buvo identifikuoti kaip pastatyti

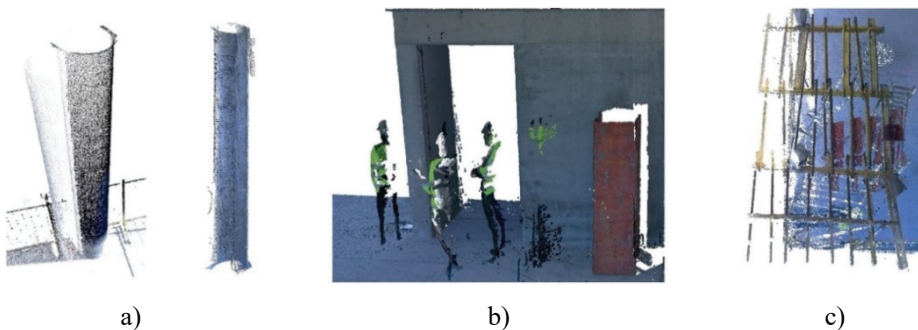
Kai objektai buvo sėkmingai aptikti, kitas žingsnis buvo įvertinti, kaip metodas gali aptikti 3D taškų debesyje nesamus objektus. Iš 3D taškų debesies modelio, priklausančio 1 duomenų rinkiniui, buvo pašalinta viena siena ir dvi kolonos, o iš 2 duomenų rinkiniui priklausančio 3D taškų debesies modelio buvo pašalintos dvi sienos ir dvi kolonos. Be vaizdinių rezultatų, metodas pateikia automatizuotą rezultatų ataskaitą, kurioje yra 0 ir 1 skaičių sąrašas kartu su objektų ID, kaip parodyta 113 pav.



113 pav. Rezultatų ataskaitos pavyzdys

Kaip parodyta 113 pav., neaptikti objektai buvo identifikuojami kaip nepastatyti ir pažymėti mėlyna spalva. Ataskaitoje 0 reiškia, kad objektas nebuvo aptiktas 3D taškų debesyje ir identifikuojamas kaip nepastatytas, o 1 reiškia, kad objektas buvo aptiktas ir identifikuojamas kaip jau pastatytas. Automatiškai išgaunant globalius objektų ID iš IFC modelio, buvo galima tiksliai nustatyti, kuris objektas buvo aptiktas arba neaptiktas.

Kitas žingsnis buvo objekto aptikimo metodo įvertinimas statybinėje aplinkoje, kur buvo įvairių kliūčių atlikti kokybišką nuskaitymą, kaip parodyta 114 pav.



114 pav. 3D taškų debesis modelis atspindintis sudėtingą statybos aplinką: a) kelios kolonos buvo pasislinkusios ir susidubliavusios, b) dėl kliūčių nuskenuotame paviršiuje atsirado skylė, c) virš kolonų buvo sumontuoti klojiniai

Objektų aptikimo bandymų, atliktų iki šio eksperimento etapo, rezultatai pateikti 115 pav.

Objekto numeris	1	2	3	4	5	6	7	8	9	10	11	12	13	14	15	16	17	18	19	20	21	22	23	24	25	26	27	28	29	30	31	32	33	34	35	36	37	38		
Aptikti/neaptikti objektai																																								
1 duomenų rinkinys	1	1	1	1	1	1	1	1	1	1	1	1	1	1	1	1	1	1	1	1	1	1	1	1	1	1	1	1	1	1	1	1	1	1	1	1	1	1	1	
2 duomenų rinkinys	1	1	1	1	1	1	1	1	1	1	1	1	1	1	1	1	1	1	1	1	1	1	1	1	1	1	1	1	1	1	1	1	1	1	1	1	1	1	1	1
3 duomenų rinkinys	1	0	1	1	1	1	1	1	1	1	1	1	1	1	0	1	1	1	1	1	1	1	1	1	1	1	0	1												
4 duomenų rinkinys	1	1	1	1	1	1	1	1	1	1	1	0	1	1	1	1	1	1	1	1	1	1	1	1	1	1	1	1	1	1	0	1	1	0	1	1	0	0	1	
5 duomenų rinkinys	1	1	1	1	1	1	1	1	1	1	1	1	1	1	1	1	1	1	1	1	1	1	1	1	1	1	1	1	1	1	1	1	1	1	1	1	1	1	1	1
6 duomenų rinkinys	1	1	1	1	1	1	1	1	1	1	1	1	1	1	1	1	1	1	1	1	1	1	1	1	1	1	1	1	1	1	1	1	1	1	1	1	1	1	1	1

115 pav. Visų duomenų rinkinių objektų aptikimo rezultatai

Pateiktuose rezultatuose 3D taškų debesyje aptikti objektai buvo pažymėti kaip 1, o neaptikti kaip 0. 3 ir 4 duomenų rinkinių 3D taškų debesies modeliuose pašalinti objektai buvo pažymėti kaip neaptikti. Visų šešių duomenų rinkinių rezultatai parodė, kad objektai buvo aptikti su minimalia klaida. Vienas objektas buvo neteisingai identifikuotas 4 duomenų rinkinyje, nes esamas objektas buvo pažymėtas kaip neaptiktas. Visi kiti eksperimente analizuoti objektai buvo identifikuoti teisingai.

Viena iš optimizavimo priemonių šiame tyrime buvo vieno trikampio apdorojimas kiekviename paviršiuje, kaip aprašyta 7.3.4 skyriuje. Ši optimizavimo metodika buvo įdiegta nuo eksperimento pradžios ir buvo naudojama visuose bandymuose, todėl skaičiavimo poreikis sumažėjo perpus.

Siekiant sumažinti duomenų kiekį, buvo pritaikytas Downsampling sumažinimo metodas, naudojant 5 cm vokselio dydį. Pritaikius šį metodą, 3D taškų debesų modeliai sumažėjo 91–96% (kaip parodyta 43 lentelėje), o tai proporcingai padidino skaičiavimo efektyvumą.

43 lentelė. 3D taškų debesies modelių informacija

3D taškų debesies modelis	Nesumažinto modelio taškų skaičius	Sumažinto modelio taškų skaičius
SQVERAS trečias aukštas (FARO Focus S70)	9451351	834551
PILIAMIESTIS A1 (ZEB-GO)	12510712	1236999
SQVERAS pirmas aukštas (FARO Focus S70)	13882774	641578
SQVERAS pirmas aukštas (Leica BLK360)	12990132	532111

Nebuvo pastebėta, kad duomenų sumažinimas būtų turėjęs įtakos duomenų lygiavimo procesui. Po sumažinimo sulygiavimo tikslumas siekė apytiksliai 0,021 m RMSE ir buvo panašus į rezultatus, gautus prieš pritaikant duomenų sumažinimo metodiką. Po 3D taškų debesies modelių sumažinimo skaičiavimo efektyvumas reikšmingai padidėjo, tačiau ne visi objektai buvo identifikuoti teisingai. Visi objektai buvo teisingai aptikti Sqvero trečio aukšto ir Piliamiestis A1 duomenų rinkiniuose. Tačiau iššūkių aptinkant objektus kilo pirmame Sqveras pastato aukšte,

kur skenavimo aplinka buvo laikoma sudėtinga, o duomenų kokybė buvo prastesnė. Rezultatai po 3D taškų debesies modelių sumažinimo pateikti 116 pav.

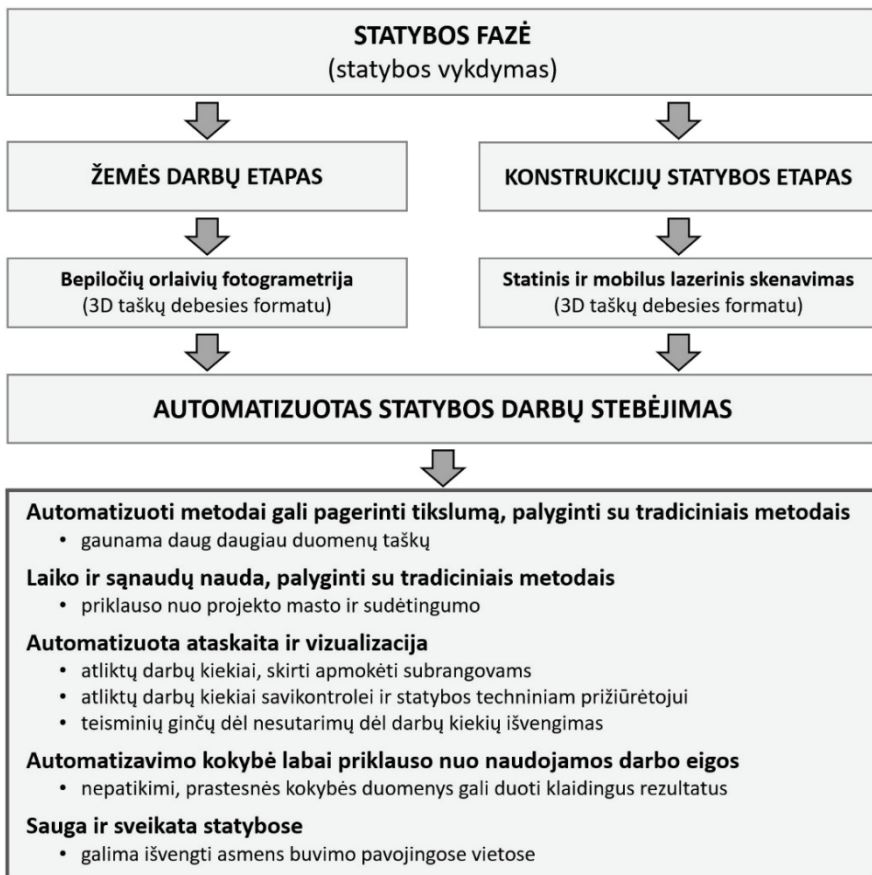
Objekto numeris	1	2	3	4	5	6	7	8	9	10	11	12	13	14	15	16	17	18	19	20	21	22	23	24	25	26	27	28	29	30	31	32	33	34	35	36	37	38	
Aptikti/ncaptikti objektai po duomenų sumažinimo																																							
1 duomenų rinkinys	1	1	1	1	1	1	1	1	1	1	1	1	1	1	1	1	1	1	1	1	1	1	1	1	1	1	1	1	1	1	1	1	1	1	1	1	1	1	
2 duomenų rinkinys	1	1	1	1	1	1	1	1	1	1	1	1	1	1	1	1	1	1	1	1	1	1	1	1	1	1	1	1	1	1	1	1	1	1	1	1	1	1	1
5 duomenų rinkinys	1	1	1	1	1	1	1	1	1	1	1	1	1	0	0	1	1	1	1	1	1	1	1	1	1	1	1	1	1	1	1	1	1	1	1	1	1	1	1
6 duomenų rinkinys	0	1	1	1	1	1	1	1	1	1	1	1	0	0	1	1	1	1	1	1	1	1	1	1	1	1	0	1	0	1	1	1	1	1	1	1	1	1	

116 pav. Objektų aptikimo rezultatai po duomenų sumažinimo

7.4. REZULTATAI IR DISKUSIJOS

7.4.1. Automatizavimo įtaka stebėjimo procesams

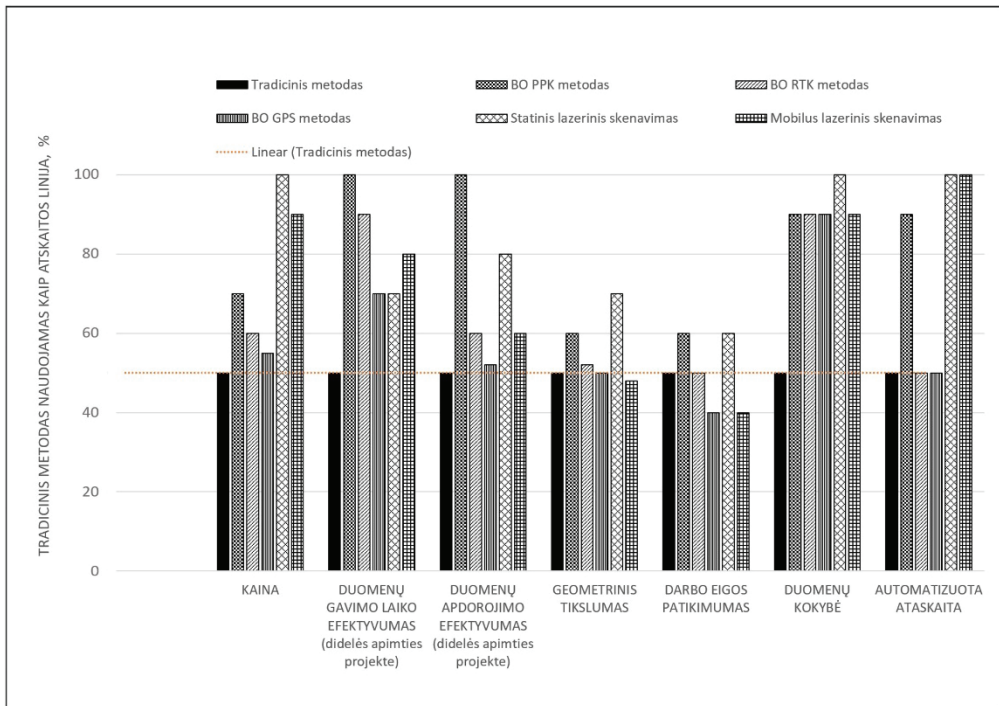
Šiame darbe automatizavimo įtaka statybos darbų stebėjimo procesams buvo vertinama keliais aspektais. Pirmiausia buvo įvertintas 3D taškų debesies duomenų tikslumas, lyginant su tradiciniais metodais gautais rezultatais. Abiejuose eksperimentuose duomenų gavimo darbo eigos buvo išbandytos realiomis statybos sąlygomis. Antra, buvo atsižvelgta į analizuotų metodų laiko ir sąnaudų aspektus. Tada buvo analizuojami abiejų eksperimentinių rezultatų išvesties duomenys ir automatizavimo kokybės aspektai. Galiausiai buvo atsižvelgta į sveikatos ir saugos veiksnius. Eksperimentiniuose tyrimuose nagrinėjami rezultatai schematiškai pateikti 117 pav. Statybos etapą sudaro keletas darbų kategorijų. Todėl pažangai stebėti reikėjo taikyti skirtingas technologijas ir darbo eigas. Tačiau abu metodai paremti 3D taškų debesies technologijomis.



117 pav. Automatizavimo įtaka statybos darbų pažangos stebėjimui

Visų darbe nagrinėtų technologijų palyginimas schematiškai pateiktas 118 pav. Eksperimentuose naudotų metodikų rezultatai buvo lyginami su tradiciniu metodu gautais rezultatais, kurie buvo naudojami kaip atskaitos linija. Įrangos kaina,

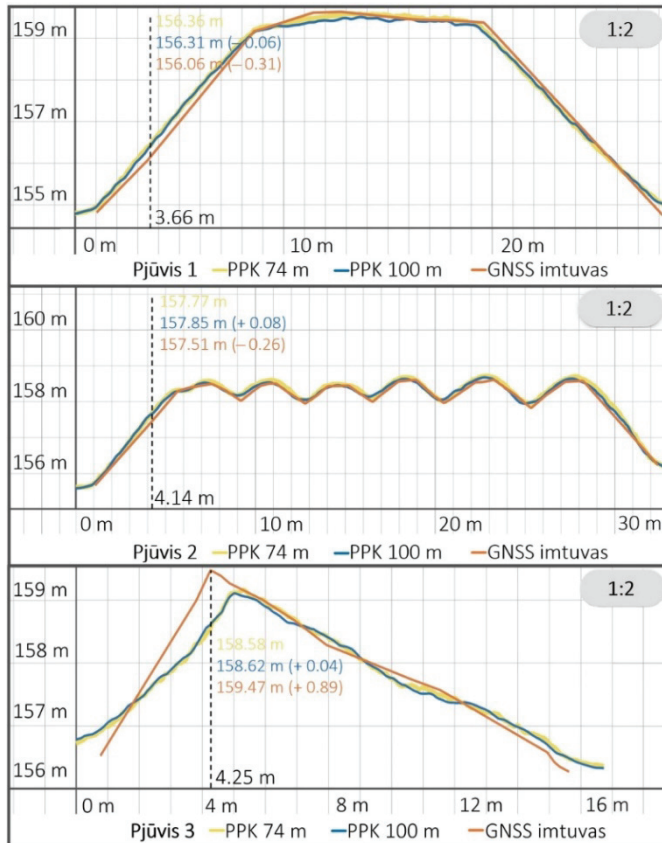
duomenų gavimo ir apdorojimo laiko efektyvumas bei kiti lyginamieji rezultatai pateikiami kaip apytiksliai. Įrenginių kaina buvo apskaičiuota remiantis preliminarine informacija, paremta pirminiais pardavėjų pasiūlymais. Duomenų gavimo ir apdorojimo laikas tradiciniais metodais buvo pagrįstas profesionalių geodezininkų pateikta informacija. Bepiločių orlaivių fotogrametrijos tikslumas ir patikimumas buvo įvertintas atliekant eksperimentus. Lazerinio skenavimo tikslumas buvo vertinamas pagal gamintojo deklaruotas įrenginio technines specifikacijas, o duomenų kokybė – pagal gautą triukšmo kiekį duomenyse, taškų populiaciją ir atitiktį BIM modelio geometrijai. Darbo eigų patikimumas buvo vertinamas pagal tai, kaip sklandžiai buvo gauti duomenys ir kiek bei kokių klaidų įvyko kiekvieno eksperimento metu, atsižvelgiant į galutinių duomenų tikslumą ir kokybę.



118 pav. Automatizuotų statybos eigos stebėjimo technologijų palyginimas su tradiciniu metodu

Automatizuotų statybos eigos stebėjimo metodų tikslumas buvo įvertintas realiuose statybos projektuose. Žemės darbų kontrolės tikslumas buvo įvertintas lyginant įprastu būdu gautus kiekius su automatizuotais metodais gautais kiekiais. Išmatavus daugiau nei 10000 m³ žemės tūrio, tradiciniu metodu gauti rezultatai skyrėsi nuo automatizuotomis metodikomis gautų rezultatų nuo 1,96 iki 4,67 proc. Eksperimento metu naudojant GNSS imtuvą buvo gauti 1008 taškai, o naudojant bepiločių orlaivių fotogrametriją, buvo gauti milijonai x, y, z duomenų taškų. Daug didesnis duomenų taškų skaičius gali pagerinti bendrą modelio tikslumą. Fotogrametriniai paviršiai ir GNSS imtuvu išmatuoti paviršiai buvo palyginti tarpusavyje. Analizuojamose žemės krūvose Nr. 3, Nr. 15, ir Nr. 16 buvo padaryti

trys atsitiktiniai skerspjūviai. Skerspjūvių vietos parodytos 91 pav. Kaip parodyta 119 pav., naudojant GNSS imtuvą, duomenų taškai buvo fiksuojami krūvos apačioje ir viršuje. Praktikoje yra sunku užfiksuoti pakankamai duomenų taškų, kad būtų galima tiksliai atkartoti paviršiaus kreivumą. Skerspjūviai parodė, kad skirtumai tarp bepiločių orlaivių fotogrametrinių duomenų, gautų iš skirtingų aukščių, kai kuriose vietose skyrėsi maždaug 0,04–0,08 m. Tačiau skirtumas tarp fotogrametrinių paviršių ir GNSS imtuvu išmatuoto paviršiaus vietomis siekė iki 0,26–0,89 m.

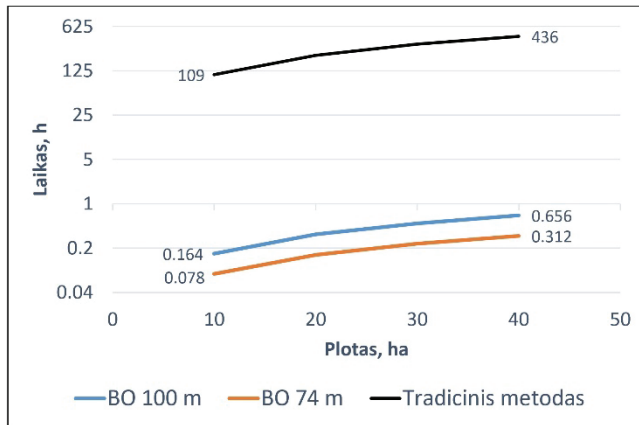


119 pav. Atsitiktinių žemės krūvų pjūviai

Naudojant 3D taškų debesis technologijas pastatų statyboje taip pat gaunamas daug didesnis x, y, z duomenų taškų skaičius, palyginti su įprastiniais metodais. Tačiau šiuo atveju geometrinis tikslumas nebuvo įvertintas. Statybos pažangos stebėsenos tikslumas buvo įvertintas pagal tai, kaip tiksliai metodas sugebėjo automatiškai identifikuoti pastatytus ir nepastatytus konstrukcinius objektus. Eksperimento metu gauti rezultatai parodė, kad pateiktas metodas teisingai identifikavo apytiksliai 99% objektų. Abiejuose eksperimentuose tirti metodai buvo vertinami pagal tai, kaip tiksliai buvo įvertinti atliktų darbų kiekiai.

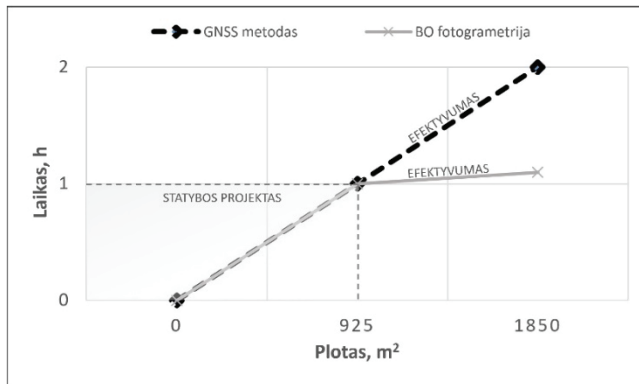
Bepiločių orlaivių fotogrametrija yra palyginti nebrangus sprendimas, galintis suteikti apčiuopiamos naudos, priklausomai nuo projekto masto. Naudojant šias technologijas per daug trumpesnę laiką galima užfiksuoti daug daugiau duomenų,

palyginti su tradiciniu metodu (120 pav.). Vertinant eksperimento metu tradiciniu būdu išmatuotą 5549,55 m² plotą, naudojant bepiločių orlaivių fotogrametriją, tas pats plotas buvo išmatuotas maždaug šešis kartus greičiau. Didėjant plotui, bepiločių orlaivių fotogrametrijos metodai tampa daug efektyvesni.



120 pav. BO fotogrametrijos ir tradicinio metodo duomenų gavimo laikas

Tačiau reikia atsižvelgti į tai, kad, skraidinant bepilotį orlaivį, reikia įvertinti pasiruošimo skrydžiui laiką bei kitus aspektus, kurie priklauso nuo konkrečios darbo eigos. Įvertinus tai, duomenų gavimas naudojant visas BO fotogrametrijos darbo eigas užtruko apie vieną valandą. Todėl BO fotogrametrijos laiko efektyvumas eksperimento metu buvo nustatytas tik didesnėse nei 925 m² statybvietėse (121 pav.).



121 pav. Efektyvumas atsižvelgiant į projekto mastą

Be to, duomenų gavimo efektyvumui įtakos gali turėti ir bepilotį orlaivių skraidančio asmens (nuotolinio piloto) kompetencija. Patyręs nuotolinis pilotas gali sutrumpinti duomenų gavimo laiką optimizuodamas visus skrydžio veiklos aspektus – nuo planavimo ir vykdymo iki duomenų kokybės ir taisyklių laikymosi užtikrinimo. Fotogrametrinio modelio tikslumui labai svarbu užfiksuoti aukštos kokybės vaizdus. Dėl prastai užfiksuotų vaizdų gali prireikti pakartotinai atlikti skrydį. Esant palankioms oro sąlygoms ir nesudėtingiems skrydžiams, nuotolinio

piloto kompetencijos nėra tokios reikšmingos. Tačiau labai svarbu pažymėti, kad tiriamos teritorijos sudėtingumas, reljefo aukščių skirtumas, prastos oro sąlygos turi didelę įtaką skrydžių saugai, duomenų rinkimo laikui ir duomenų kokybei. Nuotolinio piloto patirtis yra ypač svarbi norint saugiai ir efektyviai gauti duomenis tokiomis sąlygomis.

Pastato statybos eigai stebėti reikalingos lazerinio skenavimo technologijos yra daug brangesnės. Kaina turi įtakos techniniams prietaisų parametrams, pavyzdžiui, galimybei pasiekti milimetro tikslumą. Statiniai lazeriniai skeneriai gali pateikti tikslesnius duomenis, tačiau eksperimentų metu duomenų rinkimas užtruko gana daug laiko. Mobilusis lazerinis skeneris buvo efektyvesnis renkant duomenis, ypač siekiant išvengti kliūčių. Tačiau daroma prielaida, kad sudėtinguose, didelio masto projektuose, kur sunkiai pasiekiamos vietos, lazerinio skenavimo technologija gali būti efektyvesnis duomenų gavimo būdas, palyginti su tradiciniu metodu.

Didelis automatizuoto statybos eigos stebėjimo privalumas yra tai, kad atliktų darbų ataskaita generuojama automatiškai. Ataskaitose nurodomi atliktų darbų kiekiai ir pateikiama vizualizacija, padedanti nustatyti vietą, kokie darbai buvo atlikti ar neatlikti, bei užfiksuoti esamą situaciją tam tikru momentu. Tai sumažina nesutarimų galimybę dėl atliktų darbų kiekių ir kokybės.

Nagrinėjamų technologijų automatizavimo kokybei pakankamai įtakos turėjo gautų duomenų kokybė. O duomenų kokybei įtakos turėjo įrenginių parametrai ir naudojama darbo eiga. Žemės darbų eigos stebėjimas vykdomas lyginant duomenis, gautus toje pačioje koordinačių sistemoje, todėl jų tikslumas labai priklauso nuo to, kaip tiksliai toje pačioje koordinačių sistemoje sulygiuoti atskiri duomenys. Statybos darbų eigos stebėjimo atveju IFC modelis ir 3D taškų debesis turi skirtingas koordinates, todėl, norint sulygtinti šiuos duomenis, reikalingas papildomas veiksmas, kuriam reikia rankinio įsikišimo.

Eksperimentai parodė, kad su sveikata ir sauga susijusių iššūkių statybos eigos stebėjimo procese buvo galima išvengti naudojant bepiločius orlaivius ir lazerinius skenerius, nes buvo išvengta kopimo į stačius šlaitus ir buvimo kitose nesaugiose vietose. Be to, naudodamiesi realybės modeliu, statybų vadovai gali įvertinti pavojingas zonas ir taip iš anksto užkirsti kelią nelaimingiems atsitikimams.

7.4.2. Technologijų apribojimai

Tiek fotogrametrijos, tiek lazerinio skenavimo metodų tikslumą veikia tokie veiksniai, kaip oro sąlygos, skenuojamų paviršių savybės, įrangos kokybė ir kt. Eksperimentų metu duomenų tikslumui ir patikimumui įtakos turėjo naudojamos darbo eigos pasirinkimas. Pavyzdžiui, žemės darbų statyboje patikimiausi duomenys buvo gauti naudojant PPK darbo eigą, o pastato statybos eksperimente patikimiausi duomenys buvo gauti skenavimą atliekant tvarkingoje aplinkoje naudojant aukštas techninius parametrus turintį statinį lazerinį skenerį. Tačiau aukštos kokybės lazerinio skenavimo įranga gali būti brangi. Aukštos kokybės bepiločių orlaivių sistemų, įskaitant programinę įrangą, kaina taip pat gali būti didelė. Duomenų apdorojimas reikalauja didelės apdorojimo galios ir gali užtrukti daug laiko, ypač dirbant su dideliais duomenų kiekiais. PPK darbo eigos atveju tai efektyviai išsprendė debesų technologija, tačiau šis sprendimas lėmė didesnes išlaidas.

7.5. IŠVADOS

1. Literatūros apžvalga rodo didelį mokslininkų susidomėjimą statybos darbų eigos automatizavimo tema, taikant 3D taškų debesies technologijas, tokias kaip fotogrametrija ir lazerinis skenavimas. Tyrimai parodė, kad duomenų rinkimas ir grafikų atnaujinimas kiekvieną dieną gali užtrukti 20–30% laiko, o dėl neefektyvaus statybos eigos stebėjimo daugiau nei 53% statybos projektų atsilieka nuo grafiko. Tačiau statybos etapas susideda iš skirtingų darbų kategorijų, tokių kaip žemės darbų statyba, konstrukcijų statyba, mechaniniai, elektros ir santchnikos darbai, apdailos darbai ir kt., todėl stebėjimo procesui automatizuoti tenka taikyti skirtingas metodikas. 3D taškų debesies technologijos turi didžiausią praktinę vertę žemės darbams ir pastato konstrukcijų statybų stebėjimui. Nustatyta, kad, duomenų gavimo požiūriu, efektyviausia žemės darbų statybai taikyti bepiločių orlaivių fotogrametrija, o konstrukcijų statybai – lazerinio skenavimo technologija. Mokslininkai pasiūlė įvairius statybos eigos stebėjimo automatizavimo metodus, tačiau patikimo ir efektyvaus praktinio pritaikymo iššūkiai nuolat kintančioje statybų aplinkoje vis dar sprendžiami.
2. Žemės darbų eigos stebėjimo eksperimento metu buvo ištirtos trys skirtingos BO fotogrametrijos darbo eigos, tokios kaip RTK, PPK ir GPS metodas, paremtas žemės kontroliniais taškais, ir palygintos su tradiciniu metodu naudojant GNSS imtuvą. 5549,55 m² plote duomenys bepiločiais orlaiviais gauti 83% greičiau nei matuojant tradiciniu metodu naudojant GNSS imtuvą. Vertikalių atskaitos taškų skirtumas tarp analizuojamų metodų neviršijo 4 cm RMSE vertės ir daugeliu atvejų buvo mažesnis nei 3 cm. Nustatyta, kad PPK metodas turėjo reikšmingos įtakos žemės darbų kiekio įvertinimo efektyvumui, atsižvelgiant į rezultatų tikslumą ir klaidų dažnumą. Tačiau dėl gana didelių sąnaudų ir darbo eigos specifikos automatizuotos technologijos gali pagerinti statybos eigos stebėjimo efektyvumą tik didesnės apimties projektuose. Eksperimento metu buvo nustatytas BO fotogrametrijos efektyvumas statybos projektuose, kurių plotas didesnis nei 925 m². Tobulėjant technologijoms, duomenų rinkimas naudojant BO gali tapti tik dar efektyvesnis.
3. Praktiniai eksperimentai parodė, kad, naudojant fotogrametrijos technologijas, daugeliu atvejų statybos vadovams nereikėjo geodezininko pagalbos, nes jie patys galėjo greitai įvertinti apimtį, o tai sutaupė daug laiko. Ši technologija pakeičia sunkvežimių skaičiavimų poreikį ir užtikrina didesnį žemės kiekio kontrolės tikslumą ir patikimumą, įskaitant subrangovų darbo kontrolę. Siekiant sumažinti klaidų galimybę, planuoti kiekius, atlikti kokybės kontrolę, LandXML ir .dfx projektiniai paviršiai efektyviai buvo naudojami žemės išlyginimui, tūriui įvertinti ir kitoms operacijoms, kai tradiciniu būdu tai užtruktų daug ilgiau ir kai kurios valdymo operacijos gali likti neatliktos.
4. Konstrukcijų statybos eksperimento metu buvo sukurta esamų objektų automatinio aptikimo metodika pagal priskirtą IFC modelį:
 - a) pastato konstrukcijų geometrija buvo užfiksuota naudojant tris skirtingų techninių parametrų 3D lazerinius skenerius. Buvo naudojami du statiniai lazeriniai skeneriai, kurių deklaruojamas tikslumas siekė 1 mm ir 4–7 mm, ir

- vienas mobilusis lazerinis skeneris, kurio deklaruojamas tikslumas 10–30 mm. Duomenys buvo renkami tvarkingoje aplinkoje be kliūčių matymo linijoje ir aplinkoje su įvairiais trukdžiais, kad atspindėtų realią statybos aplinką;
- b) rankiniu būdu iš anksto apdorojus gautus duomenis, naudojant ICP algoritmą buvo sukurtas automatizuotas IFC ir 3D taškų debesies sulygiavimo procesas. Šis procesas leido sulygiuoti duomenis 2,1 cm RMSE tikslumu, kurio pakako teisingai identifikuoti objektus. Siekiant suvienodinti duomenų struktūrą, iš IFC elementų buvo išfiltruotos viršūnės ir taip gauta IFC 3D taškų debesies versija. Vienintelis rankinis įsikišimas, reikalingas duomenims sulygiuoti, buvo trijų atskaitos taškų porų parinkimas abiejuose 3D taškų debesies modeliuose;
 - c) sukurta automatinio objektų aptikimo metodika, leidžianti išgauti IFC duomenis, apskaičiuoti paviršių plokštuminę lygtį ir įvertinti atstumą nuo taško iki plokštumos. Eksperimentinio bandymo metu iš 176 vertintų statybos objektų 99,4% buvo teisingai identifikuoti, įskaitant sudėtingoje statybos aplinkoje, kai objektų paviršius buvo nevysišškai nuskenuotas arba gauti duomenys buvo nekokybiški. Optimizavus objektų aptikimo procesą, duomenų kiekis sumažėjo 91–96%. Šiuo atveju iš 113 vertintų objektų buvo teisingai identifikuoti 92,9%. Todėl duomenų kokybė turi didelę įtaką automatizavimo procesui.
5. BO fotogrametrijos ir lazerinio skenavimo technologijos gali pateikti pakankamai tikslius duomenis ir sumažinti didelio masto projektų darbo ir medžiagų sąnaudas, palyginti su tradiciniais metodais, tokiais kaip GNSS imtuvai ar tacheometras. Turint nuolat atnaujinamus statybos duomenis, galima efektyviai kontroliuoti darbų apimtį, identifikuoti galimas problemas ar vėlavimus bei imtis veiksmų, kad projektas vyktų pagal grafiką ir būtų išvengta papildomų išlaidų. Automatiškai generuojamos ataskaitos kartu su vizualizacija gali padėti išvengti ginčų, kurie gali baigtis finansiniais nuostoliais. Renkant duomenis eksperimentų metu reikėjo nuolatinio rankinio įsikišimo, o lazerinio skenavimo atveju duomenų gavimas nebuvo toks efektyvus laiko atžvilgiu, palyginti su BO fotogrametrija. Mažos apimties statybos projektams šios technologijos gali būti per brangios ir neefektyvios.
 6. Remiantis tyrimo rezultatais, statybos įmonėms, planuojančioms diegti BO fotogrametriją arba 3D lazerinį skenavimą statybos eigai stebėti, rekomenduojama atsižvelgti į keletą aspektų. Pirma, įmonėms reikia strateginio ir holistinio požiūrio, nes praktika rodo, kad inovatyvūs įrankiai į procesus diegiami gana lėtai. Investicija turėtų būti vertinama kaip galimas ilgalaikis kaštų taupymas kontroliuojant atliekamų darbų kiekius ir kokybę bei galimybę užtikrinti tvarų konkurencingumą. Tyrime naudotų lazerinių skenerių kaina svyruoja nuo 20 000 iki 70 000 eurų. BO sistemai reikėtų investuoti apie 5 000 eurų. Tačiau prieš investuojant svarbu įvertinti technologijų apribojimus, tokius kaip atspindintys paviršiai, sudėtingos geometrijos, užstatyta aplinka, oro sąlygų poveikis ir UAV skrydžių reglamentavimo taisyklių laikymasis. Be to, reikia atsižvelgti į tai, kad ne visuose programiniuose sprendimuose yra įdiegta

Lietuvoje plačiai naudojama aukščių sistema LAS07. Norint sėkmingai naudoti šias technologijas, reikalingos darbuotojų mokymo programos ir patikimi programiniai sprendimai, kurių kaina gali svyruoti nuo 5 000 iki 20 000 eurų.

REFERENCES

1. EUROPEAN COMMISSION. *Building permits for residential building in the EU on the rise in 2021* [online]. 2022 [accessed 1 August 2023]. Available from: <https://ec.europa.eu/eurostat/cache/digpub/housing/bloc-3b.html?lang=en>
2. MCKINSEY. *Accelerating sustainable infrastructure: An investor's perspective* [online]. 16 September 2021 [accessed 1 August 2023]. Available from: <https://www.mckinsey.com/capabilities/operations/our-insights/accelerating-sustainable-infrastructure-an-investors-perspective>
3. EUROPEAN COMMISSION. *Transition pathway for construction* [online]. 14 March 2023 [accessed 1 August 2023]. Available from: <https://ec.europa.eu/docsroom/documents/53854>
4. EUROPEAN CONSTRUCTION INDUSTRY FEDERATION. *Smarter construction, stronger economy, inclusive society: The European construction industry manifesto for digitalisation* [online]. 2018 [accessed 1 August 2023]. Available from: <https://www.fiec.eu/library/manifestos/joint-manifesto-digitalisation-construction-industry>
5. AL HATTAB, Malak. The dynamic evolution of synergies between BIM and sustainability: A text mining and network theory approach. *Journal of Building Engineering* [online]. 2021, Vol. 37, pp. 102159 [accessed 19 February 2023]. Available from: <https://doi.org/10.1016/j.jobbe.2021.102159>
6. AZHAR, Salman. Building Information Modeling (BIM): Trends, Benefits, Risks, and Challenges for the AEC Industry. *Leadership and Management in Engineering* [online]. 2011, Vol. 11, no. 3, pp. 241–252 [accessed 19 February 2023]. Available from: [https://doi.org/10.1061/\(ASCE\)LM.1943-5630.0000127](https://doi.org/10.1061/(ASCE)LM.1943-5630.0000127)
7. THOMSON, Charles Patrick Hugo. *From Point Cloud to Building Information Model*. Doctoral thesis [online]. University College London, London, UK, 2016 [accessed 19 February 2023]. Available from: <https://discovery.ucl.ac.uk/id/eprint/1485847>
8. GRILO, António and JARDIM-GONCALVES, Ricardo. Value proposition on interoperability of BIM and collaborative working environments. *Automation in Construction* [online]. 2010, Vol. 19, no. 5, pp. 522–530 [accessed 19 February 2023]. Available from: <https://doi.org/10.1016/j.autcon.2009.11.003>
9. YALCINKAYA, Mehmet and SINGH, Vishal. Patterns and trends in Building Information Modeling (BIM) research: A Latent Semantic Analysis. *Automation in Construction* [online]. 2015, Vol. 59, pp. 68–80 [accessed 19 February 2023]. Available from: <https://doi.org/10.1016/j.autcon.2015.07.012>
10. KHEMLANI, Lachmi. *AEC Tech News #90* [online]. 2003 [accessed 20 February 2023]. Available from: <https://www.cadalyst.com/aec/news/aec-tech-news-90-jan-29-2003-3797>
11. MCARTHUR, J.J. A Building Information Management (BIM) Framework and Supporting Case Study for Existing Building Operations, Maintenance and Sustainability. *Procedia Engineering* [online]. 2015, Vol. 118, pp. 1104–1111 [accessed 20 February 2023]. Available from: <https://doi.org/10.1016/j.proeng.2015.08.450>
12. FAZLI, Abdulsame, FATHI, Sajad, ENFERADI, Mohammad Hadi, FAZLI, Mayram and FATHI, Behrooz. Appraising Effectiveness of Building Information Management (BIM) in Project Management. *Procedia Technology* [online]. 2014, Vol. 16, pp. 1116–1125 [accessed 20 February 2023]. Available from: <https://doi.org/10.1016/j.protcy.2014.10.126>

13. LAAKSO, Mikael and KIVINIEMI, Arto. The IFC standard: A review of history, development, and standardization. *Journal of Information Technology in Construction* [online]. 2012, Vol. 17, pp. 134–161 [accessed 21 February 2023]. Available from: https://www.itcon.org/papers/2012_9.content.01913.pdf
14. *BuildingSMART International* [online]. 2023 [accessed 21 February 2023]. Available from: <https://www.buildingsmart.org>
15. CLEMEN, Christian and GRÜNDIG, Lothar. The Industry Foundation Classes (IFC) – Ready for Indoor Cadastre? In: *Proceedings of XXIII International FIG Congress* [online], 8–13 October 2006, Munich, Vol 18 [accessed 22 February 2023]. Available from: https://www.fig.net/resources/proceedings/fig_proceedings/fig2006/papers/ts48/ts48_01_clemen_gruendig_0414.pdf
16. XUE, Weirui, WANG, Yaowu and MAN, Qingpeng. Research on information models for the construction schedule management based on the IFC standard. *Journal of Industrial Engineering and Management* [online]. 2015, Vol. 8, no. 3, pp. 615–635 [accessed 22 February 2023]. Available from: <http://dx.doi.org/10.3926/jiem.1283>
17. ZHANG, Le and ISSA, Raja R A. Development of IFC-based Construction Industry Ontology for Information Retrieval from IFC Models. In: *EG-ICE Workshop* [online], 6 July 2011, University of Twente, The Netherlands [accessed 23 February 2023]. Available from: <https://www.researchgate.net/publication/267857855>
18. LAI, Huahui and DENG, Xueyuan. Interoperability analysis of IFC-based data exchange between heterogeneous BIM software. *Journal of Civil Engineering and Management* [online]. 2018, Vol. 24, no. 7, pp. 537–555 [accessed 23 February 2023]. Available from: <https://doi.org/10.3846/jcem.2018.6132>
19. FLEMING, Quentin W and KOPPELMAN, Joel M. Integrated project development teams: another fad ... or a permanent change. *International Journal of Project Management* [online]. 1996, Vol. 14, no. 3, pp. 163–168 [accessed 23 February 2023]. Available from: [https://doi.org/10.1016/0263-7863\(95\)00068-2](https://doi.org/10.1016/0263-7863(95)00068-2)
20. GLICK, Scott. IPD and BIM: Benefits and Opportunities for Regulatory Agencies. In: *Proceedings of 45th Associated Schools of Construction National Conference* [online], 2 April 2009, University of Florida, Gainesville, Florida [accessed 24 February 2023]. Available from: <http://ascpro0.ascweb.org/archives/cd/2009/paper/CPGT172002009.pdf>
21. BRYDE, David, BROQUETAS, Martí and VOLM, Jürgen Marc. The project benefits of Building Information Modelling (BIM). *International Journal of Project Management* [online]. 2013, Vol. 31, no. 7, pp. 971–980 [accessed 24 February 2023]. Available from: <https://doi.org/10.1016/j.ijproman.2012.12.001>
22. PENNSTATE COLLEGE OF ENGINEERING. *BIM uses* [online]. [Accessed 28 February 2023]. Available from: <https://bim.psu.edu/uses/>
23. MORENO BAZÁN, Ángela, ALBERTI, Marcos G., ARCOS ÁLVAREZ, Antonio and TRIGUEROS, Jesús Alonso. New Perspectives for BIM Usage in Transportation Infrastructure Projects. *Applied Sciences* [online]. 2020, Vol. 10, no. 20, pp. 7072 [accessed 28 February 2023]. Available from: <https://doi.org/10.3390/app10207072>
24. BRADLEY, Alex, LI, Haijiang, LARK, Robert and DUNN, Simon. BIM for infrastructure: An overall review and constructor perspective. *Automation in Construction* [online]. 2016, Vol. 71, pp. 139–152 [accessed 28 February 2023]. Available from: <https://doi.org/10.1016/j.autcon.2016.08.019>
25. LIU, Qingjuana and CAO, Jialin. Application Research on Engineering Cost Management Based on BIM. *Procedia Computer Science* [online]. 2021, Vol. 183,

- pp. 720–723 [accessed 28 February 2023]. Available from: <https://doi.org/10.1016/j.procs.2021.02.120>
26. BIANCARDO, Salvatore Antonio, GESUALDI, Michele, SAVASTANO, Davide, INTIGNANO, Mattia, HENKE, Ilaria and PAGLIARA, Francesca. An innovative framework for integrating Cost-Benefit Analysis (CBA) within Building Information Modeling (BIM). *Socio-Economic Planning Sciences* [online]. 2023, Vol. 85, pp. 101495 [accessed 28 February 2023]. Available from: <https://doi.org/10.1016/j.seps.2022.101495>
 27. CANTISANI, Giuseppe, PANESSO, Juan David Correa, DEL SERRONE, Giulia, DI MASCIÒ, Paola, GENTILE, Guido, LOPRENCIPE, Giuseppe and MORETTI, Laura. Re-design of a road node with 7D BIM: Geometrical, environmental and microsimulation approaches to implement a benefit-cost analysis between alternatives. *Automation in Construction* [online]. 2022, Vol. 135, pp. 104133 [accessed 1 March 2023]. Available from: <https://doi.org/10.1016/j.autcon.2022.104133>
 28. BARLISH, Kristen and SULLIVAN, Kenneth. How to measure the benefits of BIM — A case study approach. *Automation in Construction* [online]. 2012, Vol. 24, pp. 149–159 [accessed 1 March 2023]. Available from: <https://doi.org/10.1016/j.autcon.2012.02.008>
 29. ZHOU, Ying, DING, Lieyun, WANG, Xiangyu, TRUIJENS, Martijn and LUO, Hanbin. Applicability of 4D modeling for resource allocation in mega liquefied natural gas plant construction. *Automation in Construction* [online]. 2015, Vol. 50, pp. 50–63 [accessed 1 March 2023]. Available from: <https://doi.org/10.1016/j.autcon.2014.10.016>
 30. BORTOLINI, Rafaela, FORMOSO, Carlos Torres and VIANA, Daniela D. Site logistics planning and control for engineer-to-order prefabricated building systems using BIM 4D modeling. *Automation in Construction* [online]. 2019, Vol. 98, pp. 248–264 [accessed 1 March 2023]. Available from: <https://doi.org/10.1016/j.autcon.2018.11.031>
 31. TAK, Ala Nekouvaght, TAGHADDOS, Hosein, MOUSAEI, Ali, BOLOURANI, Anahita and HERMANN, Ulrich. BIM-based 4D mobile crane simulation and onsite operation management. *Automation in Construction* [online]. 2021, Vol. 128, pp. 103766 [accessed 1 March 2023]. Available from: <https://doi.org/10.1016/j.autcon.2021.103766>
 32. PATEL, Arpit, SHELAKE, Abhaysinha and YADHAV, Adinath. Sustainable construction by using novel frameworks using BIM, LEED, and Lean methods. In: *Materials Today: Proceedings* [online], 2023 [accessed 1 March 2023]. Available from: <https://doi.org/10.1016/j.matpr.2023.02.238>
 33. EBOLOR, Alexander, AGARWAL, Nivedita and BREM, Alexander. Sustainable development in the construction industry: The role of frugal innovation. *Journal of Cleaner Production* [online]. 2022, Vol. 380, pp. 134922 [accessed 2 March 2023]. Available from: <https://doi.org/10.1016/j.jclepro.2022.134922>
 34. WANG, Yuhong. Sustainability in Construction Education. *Journal of Professional Issues in Engineering Education and Practice* [online]. 2009, Vol. 135, no. 1, pp. 21–30 [accessed 2 March 2023]. Available from: [https://doi.org/10.1061/\(ASCE\)1052-3928\(2009\)135:1\(21\)](https://doi.org/10.1061/(ASCE)1052-3928(2009)135:1(21))
 35. KANG, Kai, BESKLUBOVA, Svetlana, DAI, Yaqi and ZHONG, Ray Y. Building demolition waste management through smart BIM: A case study in Hong Kong. *Waste Management* [online]. 2022, Vol. 143, pp. 69–83 [accessed 2 March 2023]. Available from: <https://doi.org/10.1016/j.wasman.2022.02.027>

36. GUERRA, Beatriz C., LEITE, Fernanda and FAUST, Kasey M. 4D-BIM to enhance construction waste reuse and recycle planning: Case studies on concrete and drywall waste streams. *Waste Management* [online]. 2020, Vol. 116, pp. 79–90 [accessed 2 March 2023]. Available from: <https://doi.org/10.1016/j.wasman.2020.07.035>
37. CONDOTTA, Massimiliano and SCANAGATTA, Chiara. BIM-based method to inform operation and maintenance phases through a simplified procedure. *Journal of Building Engineering* [online]. 2023, Vol. 65, pp. 105730 [accessed 2 March 2023]. Available from: <https://doi.org/10.1016/j.jobe.2022.105730>
38. DEMIRDÖĞEN, Gökhan, İŞIK, Zeynep and ARAYICI, Yusuf. BIM-based big data analytic system for healthcare facility management. *Journal of Building Engineering* [online]. 2023, Vol. 64, pp. 105713 [accessed 2 March 2023]. Available from: <https://doi.org/10.1016/j.jobe.2022.105713>
39. SALZANO, Antonio, PARISI, Claudia Mariaserena, ACAMPA, Giovanna and NICOLELLA, Maurizio. Existing assets maintenance management: Optimizing maintenance procedures and costs through BIM tools. *Automation in Construction* [online]. 2023, Vol. 149, pp. 104788 [accessed 3 March 2023]. Available from: <https://doi.org/10.1016/j.autcon.2023.104788>
40. LEYGONIE, Romain, MOTAMEDI, Ali and IORDANOVA, Ivanka. Development of quality improvement procedures and tools for facility management BIM. *Developments in the Built Environment* [online]. 2022, Vol. 11, pp. 100075 [accessed 3 March 2023]. Available from: <https://doi.org/10.1016/j.dibe.2022.100075>
41. LI, Lingzhi, YUAN, Jingfeng, TANG, Meiling, XU, Zhao, XU, Wei and CHENG, Yusi. Developing a BIM-enabled building lifecycle management system for owners: Architecture and case scenario. *Automation in Construction* [online]. 2021, Vol. 129, pp. 103814 [accessed 3 March 2023]. Available from: <https://doi.org/10.1016/j.autcon.2021.103814>
42. LAINE, Tuomas, HÄNNINEN, Reijo and KAROLA, Antti. Benefits of BIM in the thermal performance management. In: *Proceedings of building simulation* [online], 3 September 2007, Beijing, China, pp. 1455–1461 [accessed 3 March 2023]. Available from: <https://www.aivc.org/resource/benefits-bim-thermal-performance-management>
43. OLAWUMI, Timothy O. and CHAN, Daniel W.M. Identifying and prioritizing the benefits of integrating BIM and sustainability practices in construction projects: A Delphi survey of international experts. *Sustainable Cities and Society* [online]. 2018, Vol. 40, pp. 16–27 [accessed 3 March 2023]. Available from: <https://doi.org/10.1016/j.scs.2018.03.033>
44. ATTARAN, Mohsen and CELIK, Bilge Gokhan. Digital Twin: Benefits, use cases, challenges, and opportunities. *Decision Analytics Journal* [online]. 2023, Vol. 6, pp. 100165 [accessed 4 March 2023]. Available from: <https://doi.org/10.1016/j.dajour.2023.100165>
45. PANYA, David Stephen, KIM, Taehoon and CHOO, Seungyeon. An interactive design change methodology using a BIM-based Virtual Reality and Augmented Reality. *Journal of Building Engineering* [online]. 2023, Vol. 68, pp. 106030 [accessed 4 March 2023]. Available from: <https://doi.org/10.1016/j.jobe.2023.106030>
46. SINGH, Vishal. BIM Ecosystem Research: What, Why and How? Framing the Directions for a Holistic View of BIM. In: *13th IFIP WG 5.1 International Conference on Product Lifecycle Management (PLM16)* [online], 11–13 July 2016, Columbia, SC, United States, pp. 433–442 [accessed 5 March 2023]. Available from: https://doi.org/10.1007/978-3-319-54660-5_39
47. YILMAZ, Gokcen, AKCAMETE, Asli and DEMIRORS, Onur. BIM-CAREM: Assessing the BIM capabilities of design, construction and facilities management

- processes in the construction industry. *Computers in Industry* [online]. 2023, Vol. 147, pp. 103861 [accessed 5 March 2023]. Available from: <https://doi.org/10.1016/j.compind.2023.103861>
48. EUROPEAN COMMISSION. *European Construction Sector Observatory – Trend Paper – Building Information Modelling in the EU construction sector* [online]. 19 March 2019 [accessed 8 March 2023]. Available from: <https://ec.europa.eu/docsroom/documents/34518/>
 49. SAKA, Abdullahi B., CHAN, Daniel W.M. and WUNI, Ibrahim Y. Knowledge-based decision support for BIM adoption by small and medium-sized enterprises in developing economies. *Automation in Construction* [online]. 2022, Vol. 141, pp. 104407 [accessed 8 March 2023]. Available from: <https://doi.org/10.1016/j.autcon.2022.104407>
 50. VIDALAKIS, Christos, ABANDA, Fonbeyin Henry and OTI, Akponanabofa Henry. BIM adoption and implementation: focusing on SMEs. *Construction Innovation* [online]. 2020, Vol. 20, no. 1, pp. 128–147 [accessed 8 March 2023]. Available from: <https://doi.org/10.1108/CI-09-2018-0076>
 51. WONG, Andy K. D., WONG, Francis K. W. and NADEEM, Abid. Attributes of Building Information Modelling Implementations in Various Countries. *Architectural Engineering and Design Management* [online]. 2010, Vol. 6, no. 4, pp. 288–302 [accessed 8 March 2023]. Available from: <https://doi.org/10.3763/aedm.2010.IDDS6>
 52. ULLAH, Kaleem, LILL, Irene and WITT, Emlyn. An Overview of BIM Adoption in the Construction Industry: Benefits and Barriers. In: *10th Nordic conference on construction economics and organization* [online], 1 May 2019, Bingley, Vol. 2, pp. 297–303 [accessed 8 March 2023]. Available from: <https://doi.org/10.1108/S2516-285320190000002052>
 53. JUNG, Wooyoung and LEE, Ghang. The Status of Bim Adoption on Six Continents. *International Journal of Civil and Environmental Engineering* [online]. 2015, Vol. 9, no. 5, pp. 512–516 [accessed 9 March 2023]. Available from: <https://doi.org/10.5281/zenodo.1100430>
 54. GEORGIADOU, Maria Christina. An overview of benefits and challenges of building information modelling (BIM) adoption in UK residential projects. *Construction Innovation* [online]. 2019, Vol. 19, no. 3, pp. 298–320 [accessed 9 March 2023]. Available from: <https://doi.org/10.1108/CI-04-2017-0030>
 55. MARTIN, Pierre, BELADJINE, Djaoued and BEDDIAR, Karim. Evolution within the maturity concept of BIM. *WIT Transactions on the Built Environment* [online]. 2019, Vol. 192, pp. 131–142 [accessed 9 March 2023]. Available from: <https://doi.org/10.2495/BIM190121>
 56. HONG, Ying, HAMMAD, Ahmed W.A., SEPASGOZAR, Samad and AKBARNEZHAD, Ali. BIM adoption model for small and medium construction organisations in Australia. *Engineering, Construction and Architectural Management* [online]. 2019, Vol. 26, no. 2, pp. 154–183 [accessed 9 March 2023]. Available from: <https://doi.org/10.1108/ECAM-04-2017-0064>
 57. NEWTON, Kym and CHILESHE, Nicholas. Awareness, usage and benefits of building information modelling (bim) adoption—the case of the south Australian construction organisations. In: *Smith, S.D (Ed) Procs 28th Annual ARCOM Conference* [online], 3–5 September 2012, Edinburgh, UK, Association of Researchers in Construction Management, Vol. 3, pp. 12 [accessed 9 March 2023]. Available from: https://www.arcom.ac.uk/-docs/proceedings/ar2012-0003-0012_Newton_Chileshe.pdf
 58. GIRGINKAYA AKDAG, Suzan and MAQSOOD, Uzair. A roadmap for BIM adoption and implementation in developing countries: the Pakistan case. *Archnet-*

- IJAR: International Journal of Architectural Research* [online]. 2020, Vol. 14, no. 1, pp. 112–132 [accessed 9 March 2023]. Available from: <https://doi.org/10.1108/ARCH-04-2019-0081>
59. HERR, Christiane M. and FISCHER, Thomas. BIM adoption across the Chinese AEC industries: An extended BIM adoption model. *Journal of Computational Design and Engineering* [online]. 2019, Vol. 6, no. 2, pp. 173–178 [accessed 9 March 2023]. Available from: <https://doi.org/10.1016/j.jcde.2018.06.001>
 60. CHENG, Jack C.P. and LU, Qiqi. A review of the efforts and roles of the public sector for BIM adoption worldwide. *Journal of Information Technology in Construction (ITcon)* [online]. 2015, Vol. 20, no. 27, pp. 442–478 [accessed 10 March 2023]. Available from: <https://www.itcon.org/2015/27>
 61. CHAREF, Rabia, EMMITT, Stephen, ALAKA, Hafiz and FOUCHAL, Farid. Building Information Modelling adoption in the European Union: An overview. *Journal of Building Engineering* [online]. 2019, Vol. 25, pp. 100777 [accessed 10 March 2023]. Available from: <https://doi.org/10.1016/j.jobe.2019.100777>
 62. GUREVICH, Ury and SACKS, Rafael. Longitudinal Study of BIM Adoption by Public Construction Clients. *Journal of Management in Engineering* [online]. 2020, Vol. 36, no. 4, pp. 05020008 [accessed 10 March 2023]. Available from: [https://doi.org/10.1061/\(ASCE\)ME.1943-5479.0000797](https://doi.org/10.1061/(ASCE)ME.1943-5479.0000797)
 63. Directive 2014/24/EU of the European Parliament and of the Council of 26 February 2014 on public procurement and repealing Directive 2004/18/EC. *Official Journal of the European Union* [online]. 26 February 2014 [accessed 13 March 2023]. Available from: <http://data.europa.eu/eli/dir/2014/24/oj>
 64. THE ECONOMIST. *The construction industry's productivity problem* [online]. 17 August 2017 [accessed 13 March 2023]. Available from: <https://www.economist.com/leaders/2017/08/17/the-construction-industrys-productivity-problem>
 65. ADEMCI, Ensar and GUNDES, Selin. Review of Studies on BIM Adoption in AEC Industry. In: *5th International Project and Construction Management Conference (IPCMC) Proceedings* [online], 16–18 November 2018, N. Cyprus, pp. 1046–1055 [accessed 13 March 2023]. Available from: <https://ssrn.com/abstract=3615107>
 66. LIETUVOS RESPUBLIKOS APLINKOS MINISTERIJA. *Statyba 4.0* [online]. 2023 [accessed 14 March 2023]. Available from: <https://statyba40.lt>
 67. LIETUVOS RESPUBLIKOS VYRIAUSYBĖ. *Nutarimas dėl reikalavimų ir (arba) kriterijų dėl statinio informacinio modeliavimo metodų taikymo Nr. 1061* [online]. TAR, 14 December 2021, No. 25772 [accessed 14 March 2023]. Available from: <https://www.e-tar.lt/portal/en/legalAct/cfcdflb05cb111eca9ac839120d251c4>
 68. IBRAHIM, Hilfie Safwan, HASHIM, Norfashiha and AHMAD JAMAL, Khairool Aizat. The Potential Benefits of Building Information Modelling (BIM) in Construction Industry. In: *IOP Conference Series: Earth and Environmental Science* [online], 1 November 2019, Vol. 385, no. 1, pp. 012047 [accessed 14 March 2023]. Available from: <https://iopscience.iop.org/article/10.1088/1755-1315/385/1/012047/pdf>
 69. WALASEK, Dariusz and BARSZCZ, Arkadiusz. Analysis of the Adoption Rate of Building Information Modeling [BIM] and its Return on Investment [ROI]. *Procedia Engineering* [online]. 2017, Vol. 172, pp. 1227–1234 [accessed 15 March 2023]. Available from: <https://doi.org/10.1016/j.proeng.2017.02.144>
 70. CHAN, Daniel W.M., OLAWUMI, Timothy O. and HO, Alfred M.L. Perceived benefits of and barriers to Building Information Modelling (BIM) implementation in construction: The case of Hong Kong. *Journal of Building Engineering* [online]. 2019,

Vol. 25, pp. 100764 [accessed 15 March 2023]. Available from:

<https://doi.org/10.1016/j.jobe.2019.100764>

71. XU, Jiang. Research on Application of BIM 5D Technology in Central Grand Project. *Procedia Engineering* [online]. 2017, Vol. 174, pp. 600–610 [accessed 15 March 2023]. Available from: <https://doi.org/10.1016/j.proeng.2017.01.194>
72. LIU, Jingbin, XU, Dong, HYYPPA, Juha and LIANG, Yifan. A Survey of Applications with Combined BIM and 3D Laser Scanning in the Life Cycle of Buildings. *IEEE Journal of Selected Topics in Applied Earth Observations and Remote Sensing* [online]. 2021, Vol. 14, pp. 5627–5637 [accessed 16 March 2023]. Available from: <https://ieeexplore.ieee.org/abstract/document/9387090>
73. ARDITI, David and GUNAYDIN, H Murat. Total quality management in the construction process. *International Journal of Project Management* [online]. 1997, Vol. 15, no. 4, pp. 235–243 [accessed 16 March 2023]. Available from: [https://doi.org/10.1016/S0263-7863\(96\)00076-2](https://doi.org/10.1016/S0263-7863(96)00076-2)
74. GIEL, B. and ISSA, R. R. A. Using Laser Scanning to Access the Accuracy of As-Built BIM. In: *International Workshop on Computing in Civil Engineering* [online], 16 June 2011, Miami, Florida, United States, pp. 665–672 [accessed 17 March 2023]. Available from: [https://doi.org/10.1061/41182\(416\)82](https://doi.org/10.1061/41182(416)82)
75. NAVON, R. Research in automated measurement of project performance indicators. *Automation in Construction* [online]. 2007, Vol. 16, no. 2, pp. 176–188 [accessed 17 March 2023]. Available from: <https://doi.org/10.1016/j.autcon.2006.03.003>
76. KIM, Changmin, SON, Hyojoo and KIM, Changwan. Automated construction progress measurement using a 4D building information model and 3D data. *Automation in Construction* [online]. 2013, Vol. 31, pp. 75–82 [accessed 17 March 2023]. Available from: <https://doi.org/10.1016/j.autcon.2012.11.041>
77. TURKAN, Yelda, BOSCHE, Frederic, HAAS, Carl T. and HAAS, Ralph. Automated progress tracking using 4D schedule and 3D sensing technologies. *Automation in Construction* [online]. 2012, Vol. 22, pp. 414–421 [accessed 17 March 2023]. Available from: <https://doi.org/10.1016/j.autcon.2011.10.003>
78. ABD-ELMAABOUD, Ahmed M, EL-TOKHEY, Mohamed E, RAGHEB, Ahmed E and MOGAHED, Yasser M. Comparative Assessment of Terrestrial Laser Scanner Against Traditional Surveying Methods. *International Journal of Engineering and Applied Sciences* [online]. 2019, Vol. 6, no. 4, pp. 79–84 [accessed 17 March 2023]. Available from: <https://www.researchgate.net/publication/338149924>
79. ASADI, Khashayar, RAMSHANKAR, Hariharan, NOGHABAEI, Mojtaba and HAN, Kevin. Real-Time Image Localization and Registration with BIM Using Perspective Alignment for Indoor Monitoring of Construction. *Journal of Computing in Civil Engineering* [online]. 2019, Vol. 33, no. 5, pp. 04019031 [accessed 17 March 2023]. Available from: [https://doi.org/10.1061/\(ASCE\)CP.1943-5487.0000847](https://doi.org/10.1061/(ASCE)CP.1943-5487.0000847)
80. HAN, Kevin, DEGOL, Joseph and GOLPARVAR-FARD, Mani. Geometry- and Appearance-Based Reasoning of Construction Progress Monitoring. *Journal of Construction Engineering and Management* [online]. 2018, Vol. 144, no. 2, pp. 04017110 [accessed 17 March 2023]. Available from: [https://doi.org/10.1061/\(ASCE\)CO.1943-7862.0001428](https://doi.org/10.1061/(ASCE)CO.1943-7862.0001428)
81. WANG, Chao, CHO, Yong K. and KIM, Changwan. Automatic BIM component extraction from point clouds of existing buildings for sustainability applications. *Automation in Construction* [online]. 2015, Vol. 56, pp. 1–13 [accessed 18 March 2023]. Available from: <https://doi.org/10.1016/j.autcon.2015.04.001>
82. DU, Jia-Chong and TENG, Hung-Chao. 3D laser scanning and GPS technology for landslide earthwork volume estimation. *Automation in Construction* [online]. 2007,

- Vol. 16, no. 5, pp. 657–663 [accessed 18 March 2023]. Available from: <https://doi.org/10.1016/j.autcon.2006.11.002>
83. KWON, Soonwook, PARK, Jae-Woo, MOON, Daeyoon, JUNG, Suwan and PARK, Heesung. Smart Merging Method for Hybrid Point Cloud Data using UAV and LIDAR in Earthwork Construction. *Procedia Engineering* [online]. 2017, Vol. 196, pp. 21–28 [accessed 18 March 2023]. Available from: <https://doi.org/10.1016/j.proeng.2017.07.168>
 84. UNGER, J., REICH, M. and HEIPKE, C. UAV-based photogrammetry: monitoring of a building zone. *The International Archives of the Photogrammetry, Remote Sensing and Spatial Information Sciences* [online]. 2014, Vol. XL–5, pp. 601–606 [accessed 18 March 2023]. Available from: <https://doi.org/10.5194/isprsarchives-XL-5-601-2014>
 85. HERGUNSEL, Mehmet F. *Benefits of building information modeling for construction managers and BIM based scheduling*. Master's thesis [online]. Worcester Polytechnic Institute, 2011 [accessed 21 March 2023]. Available from: <https://digitalcommons.wpi.edu/etd-theses/230>
 86. REBOLJ, Danijel, PUČKO, Zoran, BABIĆ, Nenad Čuš, BIZJAK, Marko and MONGUS, Domen. Point cloud quality requirements for Scan-vs-BIM based automated construction progress monitoring. *Automation in Construction* [online]. 2017, Vol. 84, pp. 323–334 [accessed 22 March 2023]. Available from: <https://doi.org/10.1016/j.autcon.2017.09.021>
 87. MOON, Daeyoon, CHUNG, Suwan, KWON, Soonwook, SEO, Jongwon and SHIN, Joonghwan. Comparison and utilization of point cloud generated from photogrammetry and laser scanning: 3D world model for smart heavy equipment planning. *Automation in Construction* [online]. 2019, Vol. 98, pp. 322–331 [accessed 22 March 2023]. Available from: <https://doi.org/10.1016/j.autcon.2018.07.020>
 88. HELLMUTH, René, WEHNER, Florian and GIANNAKIDIS, Alexandros. Datasets of captured images of three different devices for photogrammetry calculation comparison and integration into a laserscan point cloud of a built environment. *Data in Brief* [online]. 2020, Vol. 33, pp. 106321 [accessed 22 March 2023]. Available from: <https://doi.org/10.1016/j.dib.2020.106321>
 89. CASELLA, Vittorio, CHIABRANDO, Filiberto, FRANZINI, Marica and MANZINO, Ambrogio Maria. Accuracy Assessment of a UAV Block by Different Software Packages, Processing Schemes and Validation Strategies. *ISPRS International Journal of Geo-Information* [online]. 2020, Vol. 9, no. 3, pp. 164 [accessed 22 March 2023]. Available from: <https://doi.org/10.3390/ijgi9030164>
 90. SANZ-ABLANEDO, Enoc, CHANDLER, Jim, RODRÍGUEZ-PÉREZ, José and ORDÓÑEZ, Celestino. Accuracy of Unmanned Aerial Vehicle (UAV) and SfM Photogrammetry Survey as a Function of the Number and Location of Ground Control Points Used. *Remote Sensing* [online]. 2018, Vol. 10, no. 10, pp. 1606 [accessed 22 March 2023]. Available from: <https://doi.org/10.3390/rs10101606>
 91. MARTÍNEZ-CARRICONDO, Patricio, AGÜERA-VEGA, Francisco, CARVAJAL-RAMÍREZ, Fernando, MESAS-CARRASCOSA, Francisco-Javier, GARCÍA-FERRER, Alfonso and PÉREZ-PORRAS, Fernando-Juan. Assessment of UAV-photogrammetric mapping accuracy based on variation of ground control points. *International Journal of Applied Earth Observation and Geoinformation* [online]. 2018, Vol. 72, pp. 1–10 [accessed 22 March 2023]. Available from: <https://doi.org/10.1016/j.jag.2018.05.015>
 92. CRYDERMAN, Chris, MAH, S. Bill and SHUFLETOSKI, Aaron. Evaluation of UAV Photogrammetric Accuracy for Mapping and Earthworks Computations.

- Geomatica* [online]. 2014, Vol. 68, no. 4, pp. 309–317 [accessed 22 March 2023]. Available from: <https://doi.org/10.5623/cig2014-405>
93. AKTURK, Emre and ALTUNEL, Arif Oguz. Accuracy assessment of a low-cost UAV derived digital elevation model (DEM) in a highly broken and vegetated terrain. *Measurement* [online]. 2019, Vol. 136, pp. 382–386 [accessed 22 March 2023]. Available from: <https://doi.org/10.1016/j.measurement.2018.12.101>
 94. ALFIO, Vincenzo Saverio, COSTANTINO, Domenica and PEPE, Massimiliano. Influence of Image TIFF Format and JPEG Compression Level in the Accuracy of the 3D Model and Quality of the Orthophoto in UAV Photogrammetry. *Journal of Imaging* [online]. 2020, Vol. 6, no. 5, pp. 30 [accessed 3 April 2023]. Available from: <https://doi.org/10.3390/jimaging6050030>
 95. O'CONNOR, James, SMITH, Mike and JAMES, Mike R. Impact of image compression on Structure from Motion photogrammetry. *Geophysical Research Abstracts* [online]. 2019, Vol. 21, pp. 1–1, EGU2019-15523 [accessed 3 April 2023]. Available from: <https://meetingorganizer.copernicus.org/EGU2019/EGU2019-15523.pdf>
 96. MARTINEZ, Jhonattan G., ALBEAINO, Gilles, GHEISARI, Masoud, VOLKMANN, Walter and ALARCÓN, Luis F. UAS Point Cloud Accuracy Assessment Using Structure from Motion–Based Photogrammetry and PPK Georeferencing Technique for Building Surveying Applications. *Journal of Computing in Civil Engineering* [online]. 2021, Vol. 35, no. 1, pp. 05020004 [accessed 3 April 2023]. Available from: [https://doi.org/10.1061/\(ASCE\)CP.1943-5487.0000936](https://doi.org/10.1061/(ASCE)CP.1943-5487.0000936)
 97. DAI, Fei and LU, Ming. Assessing the Accuracy of Applying Photogrammetry to Take Geometric Measurements on Building Products. *Journal of Construction Engineering and Management* [online]. 2010, Vol. 136, no. 2, pp. 242–250 [accessed 3 April 2023]. Available from: [https://doi.org/10.1061/\(ASCE\)CO.1943-7862.0000114](https://doi.org/10.1061/(ASCE)CO.1943-7862.0000114)
 98. NOCERINO, Erica, MENNA, Fabio, REMONDINO, Fabio and SALERI, Renato. Accuracy and block deformation analysis in automatic UAV and terrestrial photogrammetry – lesson learnt –. *ISPRS Annals of the Photogrammetry, Remote Sensing and Spatial Information Sciences* [online]. 2013, Vol. II-5/W1, pp. 203–208 [accessed 3 April 2023]. Available from: <https://doi.org/10.5194/isprsannals-II-5-W1-203-2013>
 99. KORUMAZ, Saadet Armağan GÜLEÇ. Terrestrial Laser Scanning with Potentials and Limitations for Archaeological Documentation: a Case Study of the Çatalhöyük. *Advanced LiDAR* [online]. 2021, Vol. 1, no. 1, pp. 32–38 [accessed 4 April 2023]. Available from: <https://publish.mersin.edu.tr/index.php/lidar/article/view/59/32>
 100. EL-DIN FAWZY, Hossam. 3D laser scanning and close-range photogrammetry for buildings documentation: A hybrid technique towards a better accuracy. *Alexandria Engineering Journal* [online]. 2019, Vol. 58, no. 4, pp. 1191–1204 [accessed 4 April 2023]. Available from: <https://doi.org/10.1016/j.aej.2019.10.003>
 101. BAUWENS, Sébastien, BARTHOLOMEUS, Harm, CALDERS, Kim and LEJEUNE, Philippe. Forest Inventory with Terrestrial LiDAR: A Comparison of Static and Hand-Held Mobile Laser Scanning. *Forests* [online]. 2016, Vol. 7, no. 12, pp. 127 [accessed 4 April 2023]. Available from: <https://doi.org/10.3390/f7060127>
 102. THOMSON, C., APOSTOLOPOULOS, G., BACKES, D. and BOEHM, J. Mobile Laser Scanning for Indoor Modelling. *ISPRS Annals of the Photogrammetry, Remote Sensing and Spatial Information Sciences* [online]. 2013, Vol. II-5/W2, pp. 289–293 [accessed 4 April 2023]. Available from: <https://doi.org/10.5194/isprsannals-II-5-W2-289-2013>

103. LEHTOLA, Ville, KAARTINEN, Harri, NÜCHTER, Andreas, KAIJALUOTO, Risto, KUKKO, Antero, LITKEY, Paula, HONKAVAARA, Eija, ROSNELL, Tomi, VAAJA, Matti, VIRTANEN, Juho-Pekka, KURKELA, Matti, EL ISSAOUI, Aimad, ZHU, Lingli, JAAKKOLA, Anttoni and HYYPPÄ, Juha. Comparison of the Selected State-Of-The-Art 3D Indoor Scanning and Point Cloud Generation Methods. *Remote Sensing* [online]. 2017, Vol. 9, no. 8, pp. 796 [accessed 4 April 2023]. Available from: <https://doi.org/10.3390/rs9080796>
104. TRZECIAK, Maciej Piotr and BRILAKIS, Ioannis. Comparison of accuracy and density of static and mobile laser scanners. In: *2021 European Conference on Computing in Construction* [online], 26 July 2021, pp. 197–203 [accessed 4 April 2023]. Available from: <https://doi.org/10.35490/ec3.2021.183>
105. HANNAN QURESHI, Abdul, ALALOUL, Wesam Salah, WING, Wong Kai, SAAD, Syed, AMMAD, Syed and MUSARAT, Muhammad Ali. Factors impacting the implementation process of automated construction progress monitoring. *Ain Shams Engineering Journal* [online]. 2022, Vol. 13, no. 6, pp. 101808 [accessed 4 April 2023]. Available from: <https://doi.org/10.1016/j.asej.2022.101808>
106. IBRAHIMKHIL, Mohammad Hashim, SHEN, Xuesong, BARATI, Khalegh and WANG, Cynthia Changxin. Dynamic Progress Monitoring of Masonry Construction through Mobile SLAM Mapping and As-Built Modeling. *Buildings* [online]. 2023, Vol. 13, no. 4, pp. 930 [accessed 4 April 2023]. Available from: <https://doi.org/10.3390/buildings13040930>
107. OMAR, Tarek and NEHDI, Moncef L. Data acquisition technologies for construction progress tracking. *Automation in Construction* [online]. 2016, Vol. 70, pp. 143–155 [accessed 5 April 2023]. Available from: <https://doi.org/10.1016/j.autcon.2016.06.016>
108. REJA, Varun Kumar, BHADANIYA, Parth, VARGHESE, Koshy and HA, Quang Phuc. Vision-Based Progress Monitoring of Building Structures Using Point-Intensity Approach. In: *Proceedings of the 38th International Symposium on Automation and Robotics in Construction* [online], 2 November 2021, Dubai, UAE, pp. 349–356 [accessed 5 April 2023]. Available from: <https://doi.org/10.22260/ISARC2021/0049>
109. ZHANG, Chengyi and ARDITI, David. Automated progress control using laser scanning technology. *Automation in Construction* [online]. 2013, Vol. 36, pp. 108–116 [accessed 5 April 2023]. Available from: <https://doi.org/10.1016/j.autcon.2013.08.012>
110. GOLPARVAR-FARD, Mani, PEÑA-MORA, Feniosky and SAVARESE, Silvio. Automated Progress Monitoring Using Unordered Daily Construction Photographs and IFC-Based Building Information Models. *Journal of Computing in Civil Engineering* [online]. 2015, Vol. 29, no. 1, pp. 04014025 [accessed 5 April 2023]. Available from: [https://doi.org/10.1061/\(ASCE\)CP.1943-5487.0000205](https://doi.org/10.1061/(ASCE)CP.1943-5487.0000205)
111. ELQASABY, Ahmed R., ALQAHTANI, Fahad K. and ALHEYF, Mohammed. Automated Schedule and Cost Control Using 3D Sensing Technologies. *Applied Sciences* [online]. 2023, Vol. 13, no. 2, pp. 783 [accessed 6 April 2023]. Available from: <https://doi.org/10.3390/app13020783>
112. PUČKO, Zoran, ŠUMAN, Nataša and REBOLJ, Danijel. Automated continuous construction progress monitoring using multiple workplace real time 3D scans. *Advanced Engineering Informatics* [online]. 2018, Vol. 38, pp. 27–40 [accessed 6 April 2023]. Available from: <https://doi.org/10.1016/j.aei.2018.06.001>
113. BRAUN, Alex, TUTTAS, Sebastian, BORRMANN, André and STILLA, Uwe. Improving progress monitoring by fusing point clouds, semantic data and computer vision. *Automation in Construction* [online]. 2020, Vol. 116, pp. 103210 [accessed 6 April 2023]. Available from: <https://doi.org/10.1016/j.autcon.2020.103210>

114. KIM, Sewon and KIM, YoungSeok. Development and Evaluation of High-precision Earth-work Calculating System using Drone Survey. *Journal of the Korean Geosynthetics Society* [online]. 2019, Vol. 18, no. 4, pp. 87–95 [accessed 11 April 2023]. Available from: <https://doi.org/10.12814/jkgss.2019.18.4.087>
115. VCS, Au and S. Buttling. Application of instrumentation to the monitoring of ground treatment on an earthworks contract. *International Journal of Rock Mechanics and Mining Sciences & Geomechanics Abstracts* [online]. 1991, Vol. 28, no. 2–3, pp. A108 [accessed 11 April 2023]. Available from: [https://doi.org/10.1016/0148-9062\(91\)92539-B](https://doi.org/10.1016/0148-9062(91)92539-B)
116. WANG, Qian and KIM, Min-Koo. Applications of 3D point cloud data in the construction industry: A fifteen-year review from 2004 to 2018. *Advanced Engineering Informatics* [online]. 2019, Vol. 39, pp. 306–319 [accessed 11 April 2023]. Available from: <https://doi.org/10.1016/j.aei.2019.02.007>
117. CHAE, Myung Jin, LEE, Gyu Won, KIM, Jung Yoel, PARK, Jae Woo and CHO, Moon Young. A 3D surface modeling system for intelligent excavation system. *Automation in Construction* [online]. 2011, Vol. 20, no. 7, pp. 808–817 [accessed 11 April 2023]. Available from: <https://doi.org/10.1016/j.autcon.2011.02.003>
118. KWON, Soonwook, LEE, Mina, LEE, Moonju, LEE, Sukhan and LEE, Junbok. Development of optimized point cloud merging algorithms for accurate processing to create earthwork site models. *Automation in Construction* [online]. 2013, Vol. 35, pp. 618–624 [accessed 11 April 2023]. Available from: <https://doi.org/10.1016/j.autcon.2013.01.004>
119. AL-HANBALI, Nedal, HUTTON, Joe, MOSTAFA, Mohamed Mr and HILL, Richmond. Mobile Mapping for Earthwork Monitoring: A Case Study on the Convergence of Photogrammetry with Advanced Positioning Techniques for Maximum Productivity and Accuracy. In: *Proceedings of 52nd Photogrammetric Week* [online], 7–11 September 2009, University of Stuttgart, Germany [accessed 11 April 2023]. Available from: <https://phowo.ifp.uni-stuttgart.de/publications/phowo09/210Al-Hanbali.pdf>
120. KIM, Jeonghwan, LEE, Soomin, SEO, Jongwon, LEE, Dong-Eun and CHOI, Hee Seon. The Integration of Earthwork Design Review and Planning Using UAV-Based Point Cloud and BIM. *Applied Sciences* [online]. 2021, Vol. 11, no. 8, pp. 3435 [accessed 12 April 2023]. Available from: <https://doi.org/10.3390/app11083435>
121. CHO, Sun Il, LIM, Jae Hyoung, LIM, Soo Bong and YUN, Hee Cheon. A Study on DEM-based Automatic Calculation of Earthwork Volume for BIM Application. *Journal of the Korean Society of Surveying, Geodesy, Photogrammetry and Cartography* [online]. 2020, Vol. 38, no. 2, pp. 131–140 [accessed 12 April 2023]. Available from: <https://doi.org/10.7848/ksgpc.2020.38.2.131>
122. YOU, Ke, DING, Lieyun, ZHOU, Cheng, DOU, Quanli, WANG, Xuepeng and HU, Bin. 5G-based earthwork monitoring system for an unmanned bulldozer. *Automation in Construction* [online]. 2021, Vol. 131, pp. 103891 [accessed 12 April 2023]. Available from: <https://doi.org/10.1016/j.autcon.2021.103891>
123. NAGHSHBANDI, Seyedeh Neda, VARGA, Liz and HU, Yukun. Technology capabilities for an automated and connected earthwork roadmap. *Construction Innovation* [online]. 2022, Vol. 22, no. 4, pp. 768–788 [accessed 12 April 2023]. Available from: <https://doi.org/10.1108/CI-02-2021-0022>
124. NAGHSHBANDI, S. Neda, VARGA, Liz and HU, Yukun. Components of a Technology Roadmap for Automated Excavation. In: *International Conference on Energy, Ecology and Environment (ICEEE 2019)* [online], 23–26 July 2019,

- Stavanger, Norway [accessed 12 April 2023]. Available from: <https://www.researchgate.net/publication/336930851>
125. ROGAGE, Kay, MAHAMED, Elham, BRILAKIS, Ioannis and KASSEM, Mohamad. Beyond digital shadows: Digital Twin used for monitoring earthwork operation in large infrastructure projects. *AI in Civil Engineering* [online]. 2022, Vol. 1, no. 1, pp. 7 [accessed 12 April 2023]. Available from: <https://doi.org/10.1007/s43503-022-00009-5>
 126. KAMARI, Mirsalar and HAM, Youngjib. Vision-based volumetric measurements via deep learning-based point cloud segmentation for material management in jobsites. *Automation in Construction* [online]. 2021, Vol. 121, pp. 103430 [accessed 13 April 2023]. Available from: <https://doi.org/10.1016/j.autcon.2020.103430>
 127. BROWN, Andy. *The sky's the limit: the latest in drone technology* [online]. 10 March 2023 [accessed 13 April 2023]. Available from: <https://www.constructiontechnology.media/news/the-sky-s-the-limit-the-latest-in-drone-technology/8026985.article>
 128. DAAKIR, M., PIERROT-DESEILLIGNY, M., BOSSER, P., PICHARD, F. and THOM, C. UAV onboard photogrammetry and GPS positioning for earthworks. *The International Archives of the Photogrammetry, Remote Sensing and Spatial Information Sciences* [online]. 2015, Vol. XL-3/W3, pp. 293–298 [accessed 13 April 2023]. Available from: <https://doi.org/10.5194/isprsarchives-XL-3-W3-293-2015>
 129. JULGE, Kalev, ELLMANN, Artu and KÖÖK, Romet. Unmanned Aerial Vehicle Surveying for Monitoring Road Construction Earthworks. *The Baltic Journal of Road and Bridge Engineering* [online]. 2019, Vol. 14, no. 1, pp. 1–17 [accessed 13 April 2023]. Available from: <https://doi.org/10.7250/bjrbe.2019-14.430>
 130. CHO, Jin-Woo, LEE, Jae-Kang and PARK, Jisoo. Large-Scale Earthwork Progress Digitalization Practices Using Series of 3D Models Generated from UAS Images. *Drones* [online]. 2021, Vol. 5, no. 4, pp. 147 [accessed 13 April 2023]. Available from: <https://doi.org/10.3390/drones5040147>
 131. LEE, Kirim and LEE, Won Hee. Earthwork Volume Calculation, 3D Model Generation, and Comparative Evaluation Using Vertical and High-Oblique Images Acquired by Unmanned Aerial Vehicles. *Aerospace* [online]. 2022, Vol. 9, no. 10, pp. 606 [accessed 13 April 2023]. Available from: <https://doi.org/10.3390/aerospace9100606>
 132. LEE, Suk Bae, SONG, Mihwa, KIM, Sukgu and WON, Jae-Ho. Change Monitoring at Expressway Infrastructure Construction Sites Using Drone. *Sensors and Materials* [online]. 2020, Vol. 32, no. 11, pp. 3923–3933 [accessed 13 April 2023]. Available from: <https://doi.org/10.18494/SAM.2020.2971>
 133. AKGUL, Mustafa, YURTSEVEN, Huseyin, GULCI, Sercan and AKAY, Abdullah E. Evaluation of UAV- and GNSS-Based DEMs for Earthwork Volume. *Arabian Journal for Science and Engineering* [online]. 2018, Vol. 43, no. 4, pp. 1893–1909 [accessed 13 April 2023]. Available from: <https://doi.org/10.1007/s13369-017-2811-9>
 134. SEONG, Jonghyeun, CHO, Sun Il, XU, Chunxu and YUN, Hee Cheon. UAV Utilization for Efficient Estimation of Earthwork Volume Based on DEM. *Journal of the Korean Society of Surveying, Geodesy, Photogrammetry and Cartography* [online]. 2021, Vol. 39, no. 5, pp. 279–288 [accessed 14 April 2023]. Available from: <https://doi.org/10.7848/ksgpc.2021.39.5.279>
 135. KAVALLIAUSKAS, Paulius, ŽIDANA VIČIUS, Daumantas and JURELIONIS, Andrius. Geometric Accuracy of 3D Reality Mesh Utilization for BIM-Based Earthwork Quantity Estimation Workflows. *ISPRS International Journal of Geo-*

- Information [online]. 2021, Vol. 10, no. 6, pp. 399 [accessed 14 April 2023]. Available from: <https://doi.org/10.3390/ijgi10060399>
136. PARK, Joon Kyu and JUNG, Kap Yong. Accuracy Evaluation of Earthwork Volume Calculation According to Terrain Model Generation Method. *Journal of the Korean Society of Surveying, Geodesy, Photogrammetry and Cartography* [online]. 2021, Vol. 39, no. 1, pp. 47–54 [accessed 14 April 2023]. Available from: <https://doi.org/10.7848/ksgpc.2021.39.1.47>
 137. ALALOUL, Wesam Salah, QURESHI, Abdul Hannan, MUSARAT, Muhammad Ali and SAAD, Syed. Evolution of close-range detection and data acquisition technologies towards automation in construction progress monitoring. *Journal of Building Engineering* [online]. 2021, Vol. 43, pp. 102877 [accessed 18 April 2023]. Available from: <https://doi.org/10.1016/j.job.2021.102877>
 138. BOSCHÉ, Frédéric. Automated recognition of 3D CAD model objects in laser scans and calculation of as-built dimensions for dimensional compliance control in construction. *Advanced Engineering Informatics* [online]. 2010, Vol. 24, no. 1, pp. 107–118 [accessed 18 April 2023]. Available from: <https://doi.org/10.1016/j.aei.2009.08.006>
 139. KAVALIAUSKAS, Paulius, FERNANDEZ, Jaime B., MCGUINNESS, Kevin and JURELIONIS, Andrius. Automation of Construction Progress Monitoring by Integrating 3D Point Cloud Data with an IFC-Based BIM Model. *Buildings* [online]. 2022, Vol. 12, no. 10, pp. 1754 [accessed 18 April 2023]. Available from: <https://doi.org/10.3390/buildings12101754>
 140. MASOOD, Mustafa K., AIKALA, Antti, SEPPÄNEN, Olli and SINGH, Vishal. Multi-Building Extraction and Alignment for As-Built Point Clouds: A Case Study with Crane Cameras. *Frontiers in Built Environment* [online]. 2020, Vol. 6, pp. 581295 [accessed 20 April 2023]. Available from: <https://doi.org/10.3389/fbuil.2020.581295>
 141. BESL, Paul J. and MCKAY, Neil D. Method for registration of 3-D shapes. In: *SPIE, Sensor fusion IV: control paradigms and data structures* [online], 30 April 1992, Boston, MA, United States, Vol. 1611, pp. 586–606, [accessed 20 April 2023]. Available from: <https://doi.org/10.1117/12.57955>
 142. CHEN, Junjie, LI, Shuai and LU, Weisheng. Align to locate: Registering photogrammetric point clouds to BIM for robust indoor localization. *Building and Environment* [online]. 2022, Vol. 209, pp. 108675 [accessed 20 April 2023]. Available from: <https://doi.org/10.1016/j.buildenv.2021.108675>
 143. BOUAZIZ, Sofien, TAGLIASACCHI, Andrea and PAULY, Mark. Sparse Iterative Closest Point. In: *Computer Graphics Forum* [online], 19 August 2013, Oxford, UK, Vol. 32, no. 5, pp. 113–123 [accessed 21 April 2023]. Available from: <https://doi.org/10.1111/cgf.12178>
 144. MAVRIDIS, Pavlos, ANDREADIS, Anthousis and PAPAIOANNOU, Georgios. Efficient Sparse ICP. *Computer Aided Geometric Design* [online]. 2015, Vol. 35–36, pp. 16–26 [accessed 21 April 2023]. Available from: <https://doi.org/10.1016/j.cagd.2015.03.022>
 145. YANG, Jiaolong, LI, Hongdong and JIA, Yunde. Go-ICP: Solving 3D Registration Efficiently and Globally Optimally. In: *Proceedings of the IEEE International Conference on Computer Vision 2013* [online], 1–8 December 2013, Sydney, Australia, pp. 1457–1464 [accessed 21 April 2023]. Available from: <https://doi.org/10.1109/ICCV.2013.184>
 146. FONTANA, Simone, CATTANEO, Daniele, BALLARDINI, Augusto L., VAGHI, Matteo and SORRENTI, Domenico G. A benchmark for point clouds registration

- algorithms. *Robotics and Autonomous Systems* [online]. 2021, Vol. 140, pp. 103734 [accessed 24 April 2023]. Available from: <https://doi.org/10.1016/j.robot.2021.103734>
147. HE, Ying, LIANG, Bin, YANG, Jun, LI, Shunzhi and HE, Jin. An Iterative Closest Points Algorithm for Registration of 3D Laser Scanner Point Clouds with Geometric Features. *Sensors* [online]. 2017, Vol. 17, no. 8, pp. 1862 [accessed 24 April 2023]. Available from: <https://doi.org/10.3390/s17081862>
 148. BOSCHÉ, Frédéric. Plane-based registration of construction laser scans with 3D/4D building models. *Advanced Engineering Informatics* [online]. 2012, Vol. 26, no. 1, pp. 90–102 [accessed 24 April 2023]. Available from: <https://doi.org/10.1016/j.aei.2011.08.009>
 149. BUENO, Martín, BOSCHÉ, Frédéric, GONZÁLEZ-JORGE, Higinio, MARTÍNEZ-SÁNCHEZ, Joaquín and ARIAS, Pedro. 4-Plane congruent sets for automatic registration of as-is 3D point clouds with 3D BIM models. *Automation in Construction* [online]. 2018, Vol. 89, pp. 120–134 [accessed 24 April 2023]. Available from: <https://doi.org/10.1016/j.autcon.2018.01.014>
 150. SOILÁN, Mario, JUSTO, Andrés, SÁNCHEZ-RODRÍGUEZ, Ana and RIVEIRO, Belén. 3D Point Cloud to BIM: Semi-Automated Framework to Define IFC Alignment Entities from MLS-Acquired LiDAR Data of Highway Roads. *Remote Sensing* [online]. 2020, Vol. 12, no. 14, pp. 2301 [accessed 24 April 2023]. Available from: <https://doi.org/10.3390/rs12142301>
 151. HUANG, Rong, XU, Yusheng, YAO, Wei, HOEGNER, Ludwig and STILLA, Uwe. Robust global registration of point clouds by closed-form solution in the frequency domain. *ISPRS Journal of Photogrammetry and Remote Sensing* [online]. 2021, Vol. 171, pp. 310–329 [accessed 24 April 2023]. Available from: <https://doi.org/10.1016/j.isprsjprs.2020.11.014>
 152. KAISER, Tim, CLEMEN, Christian and MAAS, Hans-Gerd. Automatic co-registration of photogrammetric point clouds with digital building models. *Automation in Construction* [online]. 2022, Vol. 134, pp. 104098 [accessed 24 March 2023]. Available from: <https://doi.org/10.1016/j.autcon.2021.104098>
 153. TURKAN, Yelda, BOSCHE, Frederic, HAAS, Carl T. and HAAS, Ralph. Towards automated progress tracking of erection of concrete structures. In: *Proceedings of the 6th International Conference on Innovation in Architecture, Engineering & Construction (AEC'10)* [online], 9–11 June 2010, State College, Pennsylvania, USA [accessed 24 April 2023]. Available from: <https://www.researchgate.net/publication/260639255>
 154. KRIJNEN, Thomas and BEETZ, Jakob. An IFC schema extension and binary serialization format to efficiently integrate point cloud data into building models. *Advanced Engineering Informatics* [online]. 2017, Vol. 33, pp. 473–490 [accessed 25 April 2023]. Available from: <https://doi.org/10.1016/j.aei.2017.03.008>
 155. CHEN, Jingdao and CHO, Yong K. Point-to-point Comparison Method for Automated Scan-vs-BIM Deviation Detection. In: *Proceedings of the 17th International Conference on Computing in Civil and Building Engineering* [online], 4–7 June 2018, Tampere, Finland [accessed 26 April 2023]. Available from: <https://www.researchgate.net/profile/Jingdao-Chen/publication/325813565>
 156. BOSCHÉ, Frédéric, AHMED, Mahmoud, TURKAN, Yelda, HAAS, Carl T. and HAAS, Ralph. The value of integrating Scan-to-BIM and Scan-vs-BIM techniques for construction monitoring using laser scanning and BIM: The case of cylindrical MEP components. *Automation in Construction* [online]. 2015, Vol. 49, pp. 201–213 [accessed 26 April 2023]. Available from: <https://doi.org/10.1016/j.autcon.2014.05.014>

157. CUI, Yang, LI, Qingquan, YANG, Bisheng, XIAO, Wen, CHEN, Chi and DONG, Zhen. Automatic 3-D Reconstruction of Indoor Environment With Mobile Laser Scanning Point Clouds. *IEEE Journal of Selected Topics in Applied Earth Observations and Remote Sensing* [online]. 2019, Vol. 12, no. 8, pp. 3117–3130 [accessed 26 April 2023]. Available from: <https://doi.org/10.1109/JSTARS.2019.2918937>
158. OCHMANN, Sebastian, VOCK, Richard and KLEIN, Reinhard. Automatic reconstruction of fully volumetric 3D building models from oriented point clouds. *ISPRS Journal of Photogrammetry and Remote Sensing* [online]. 2019, Vol. 151, pp. 251–262 [accessed 26 April 2023]. Available from: <https://doi.org/10.1016/j.isprsjprs.2019.03.017>
159. TRAN, Ha and KHOSHELHAM, Kourosh. Procedural Reconstruction of 3D Indoor Models from Lidar Data Using Reversible Jump Markov Chain Monte Carlo. *Remote Sensing* [online]. 2020, Vol. 12, no. 5, pp. 838 [accessed 26 April 2023]. Available from: <https://doi.org/10.3390/rs12050838>
160. CHEN, Jingdao, KIRA, Zsolt and CHO, Yong K. Deep Learning Approach to Point Cloud Scene Understanding for Automated Scan to 3D Reconstruction. *Journal of Computing in Civil Engineering* [online]. 2019, Vol. 33, no. 4, pp. 04019027 [accessed 26 April 2023]. Available from: [https://doi.org/10.1061/\(ASCE\)CP.1943-5487.0000842](https://doi.org/10.1061/(ASCE)CP.1943-5487.0000842)
161. MA, Jong Won, CZERNIAWSKI, Thomas and LEITE, Fernanda. Semantic segmentation of point clouds of building interiors with deep learning: Augmenting training datasets with synthetic BIM-based point clouds. *Automation in Construction* [online]. 2020, Vol. 113, pp. 103144 [accessed 26 April 2023]. Available from: <https://doi.org/10.1016/j.autcon.2020.103144>
162. MAHAMI, Hadi, NASIRZADEH, Farnad, HOSSEININAVEH AHMADABADIAN, Ali and NAHAVANDI, Saeid. Automated Progress Controlling and Monitoring Using Daily Site Images and Building Information Modelling. *Buildings* [online]. 2019, Vol. 9, no. 3, pp. 70 [accessed 26 April 2023]. Available from: <https://doi.org/10.3390/buildings9030070>
163. MACHER, Hélène, LANDES, Tania and GRUSSENMEYER, Pierre. From Point Clouds to Building Information Models: 3D Semi-Automatic Reconstruction of Indoors of Existing Buildings. *Applied Sciences* [online]. 2017, Vol. 7, no. 10, pp. 1030 [accessed 26 April 2023]. Available from: <https://doi.org/10.3390/app7101030>
164. BASSIER, M., KLEIN, R., VAN GENECHTEN, B. and VERGAUWEN, M. IFC wall reconstruction from unstructured point clouds. *ISPRS Annals of the Photogrammetry, Remote Sensing and Spatial Information Sciences* [online]. 2018, Vol. IV–2, pp. 33–39 [accessed 26 April 2023]. Available from: <https://doi.org/10.5194/isprs-annals-IV-2-33-2018>
165. WANG, Qian, GUO, Jingjing and KIM, Min-Koo. An Application Oriented Scan-to-BIM Framework. *Remote Sensing* [online]. 2019, Vol. 11, no. 3, pp. 365 [accessed 26 April 2023]. Available from: <https://doi.org/10.3390/rs11030365>
166. BARICZOVÁ, Gabriela, ERDÉLYI, Ján, HONTI, Richard and TOMEK, Lukáš. Wall Structure Geometry Verification Using TLS Data and BIM Model. *Applied Sciences* [online]. 2021, Vol. 11, no. 24, pp. 11804 [accessed 26 April 2023]. Available from: <https://doi.org/10.3390/app112411804>
167. ERDÉLYI, Ján, HONTI, Richard, FUNTÍK, Tomáš, MAYER, Pavol and MADIEV, Aset. Verification of Building Structures Using Point Clouds and Building Information

- Models. *Buildings* [online]. 2022, Vol. 12, no. 12, pp. 2218–11804 [accessed 27 April 2023]. Available from: <https://doi.org/10.3390/buildings12122218>
168. MEYER, Theresa, BRUNN, Ansgar and STILLA, Uwe. Change detection for indoor construction progress monitoring based on BIM, point clouds and uncertainties. *Automation in Construction* [online]. 2022, Vol. 141, pp. 104442 [accessed 27 April 2023]. Available from: <https://doi.org/10.1016/j.autcon.2022.104442>
 169. TUTTAS, S., BRAUN, A., BORRMANN, A. and STILLA, U. Validation of BIM components by photogrammetric point clouds for construction site monitoring. *ISPRS Annals of the Photogrammetry, Remote Sensing and Spatial Information Sciences* [online]. 2015, Vol. II-3/W4, pp. 231–237 [accessed 27 April 2023]. Available from: <https://doi.org/10.5194/isprsannals-II-3-W4-231-2015>
 170. TUTTAS, Sebastian, BRAUN, Alexander, BORRMANN, André and STILLA, Uwe. Acquisition and Consecutive Registration of Photogrammetric Point Clouds for Construction Progress Monitoring Using a 4D BIM. *PGF – Journal of Photogrammetry, Remote Sensing and Geoinformation Science* [online]. 2017, Vol. 85, no. 1, pp. 3–15 [accessed 27 April 2023]. Available from: <https://doi.org/10.1007/s41064-016-0002-z>
 171. MEYER, Theresa, BRUNN, Ansgar and STILLA, Uwe. Geometric BIM verification of indoor construction sites by photogrammetric point clouds and evidence theory. *ISPRS Journal of Photogrammetry and Remote Sensing* [online]. 2023, Vol. 195, pp. 432–445 [accessed 27 April 2023]. Available from: <https://doi.org/10.1016/j.isprsjprs.2022.12.014>
 172. ANWAR, Naveed, IZHAR, Muhammad Amir and NAJAM, Fawad Ahmed. Construction Monitoring and Reporting using Drones and Unmanned Aerial Vehicles (UAVs). In: *The Tenth International Conference on Construction in the 21st Century (CITC-10)* [online], 2–4 July 2018, Colombo, Sri Lanka [accessed 29 April 2023]. Available from: <https://www.researchgate.net/publication/326264559>
 173. QU, Tengting, ZANG, Wei, PENG, Zhenwei, LIU, Jun, LI, Weiwei, ZHU, Yun, ZHANG, Bin and WANG, Yongsheng. Construction Site Monitoring Using UAV Oblique Photogrammetry and BIM Technologies. In: *Proceedings of the 22nd CAADRIA Conference* [online], 5–8 April 2017, Suzhou, China, pp. 655–662 [accessed 29 April 2023]. Available from: <https://doi.org/10.52842/conf.caadria.2017.655>
 174. YANG, Liu, CHENG, Jack C.P. and WANG, Qian. Semi-automated generation of parametric BIM for steel structures based on terrestrial laser scanning data. *Automation in Construction* [online]. 2020, Vol. 112, pp. 103037 [accessed 1 May 2023]. Available from: <https://doi.org/10.1016/j.autcon.2019.103037>
 175. WANG, Boyu, YIN, Chao, LUO, Han, CHENG, Jack C.P. and WANG, Qian. Fully automated generation of parametric BIM for MEP scenes based on terrestrial laser scanning data. *Automation in Construction* [online]. 2021, Vol. 125, pp. [accessed 1 May 2023]. Available from: <https://doi.org/10.1016/j.autcon.2021.103615>
 176. RAUSCH, Christopher and HAAS, Carl. Automated shape and pose updating of building information model elements from 3D point clouds. *Automation in Construction* [online]. 2021, Vol. 124, pp. 103561 [accessed 1 May 2023]. Available from: <https://doi.org/10.1016/j.autcon.2021.103561>
 177. REJA, Varun Kumar, VARGHESE, Koshy and HA, Quang Phuc. Computer vision-based construction progress monitoring. *Automation in Construction* [online]. 2022, Vol. 138, pp. [accessed 1 May 2023]. Available from: <https://doi.org/10.1016/j.autcon.2022.104245>

178. WEI, Wei, LU, Yujie, ZHONG, Tao, LI, Peixian and LIU, Bo. Integrated vision-based automated progress monitoring of indoor construction using mask region-based convolutional neural networks and BIM. *Automation in Construction* [online]. 2022, Vol. 140, pp. 104327 [accessed 1 May 2023]. Available from: <https://doi.org/10.1016/j.autcon.2022.104327>
179. A.S., Greeshma and EDAYADIYIL, Jeena B. Automated progress monitoring of construction projects using Machine learning and image processing approach. *Materials Today: Proceedings* [online]. 2022, Vol. 65, pp. 554–563 [accessed 1 May 2023]. Available from: <https://doi.org/10.1016/j.matpr.2022.03.137>
180. GORDON, Matthew, BATALLÉ, Anna, DE WOLF, Catherine, SOLLAZZO, Aldo, DUBOR, Alexandre and WANG, Tong. Automating building element detection for deconstruction planning and material reuse: A case study. *Automation in Construction* [online]. 2023, Vol. 146, pp [accessed 1 May 2023]. Available from: <https://doi.org/10.1016/j.autcon.2022.104697>
181. LEI FAN and ATKINSON, P. M. Accuracy of Digital Elevation Models Derived from Terrestrial Laser Scanning Data. *IEEE Geoscience and Remote Sensing Letters* [online]. 2015, Vol. 12, no. 9, pp. 1923–1927 [accessed 1 May 2023]. Available from: <https://doi.org/10.1109/LGRS.2015.2438394>
182. BRAUN, Alex and BORRMANN, André. Combining inverse photogrammetry and BIM for automated labeling of construction site images for machine learning. *Automation in Construction* [online]. 2019, Vol. 106, pp. 102879 [accessed 1 May 2023]. Available from: <https://doi.org/10.1016/j.autcon.2019.102879>
183. EKANAYAKE, Biyanka, WONG, Johnny Kwok-Wai, FINI, Alireza Ahmadian Fard and SMITH, Peter. Computer vision-based interior construction progress monitoring: A literature review and future research directions. *Automation in Construction* [online]. 2021, Vol. 127, pp. 103705 [accessed 1 May 2023]. Available from: <https://doi.org/10.1016/j.autcon.2021.103705>
184. ROMERO-JARÉN, R. and ARRANZ, J.J. Automatic segmentation and classification of BIM elements from point clouds. *Automation in Construction* [online]. 2021, Vol. 124, pp. 103576 [accessed 2 May 2023]. Available from: <https://doi.org/10.1016/j.autcon.2021.103576>
185. POUX, Florent and BILLEN, Roland. Voxel-based 3D Point Cloud Semantic Segmentation: Unsupervised Geometric and Relationship Featuring vs Deep Learning Methods. *ISPRS International Journal of Geo-Information* [online]. 2019, Vol. 8, no. 5, pp. 213 [accessed 2 May 2023]. Available from: <https://doi.org/10.3390/ijgi8050213>
186. JI, Ankang, ZHOU, Yunxiang, ZHANG, Limao, TIONG, Robert L.K. and XUE, Xiaolong. Semi-supervised learning-based point cloud network for segmentation of 3D tunnel scenes. *Automation in Construction* [online]. 2023, Vol. 146, pp. 104668 [accessed 2 May 2023]. Available from: <https://doi.org/10.1016/j.autcon.2022.104668>
187. YANG, Xiaofei, DEL REY CASTILLO, Enrique, ZOU, Yang and WOTHERSPOON, Liam. Semantic segmentation of bridge point clouds with a synthetic data augmentation strategy and graph-structured deep metric learning. *Automation in Construction* [online]. 2023, Vol. 150, pp. 104838 [accessed 2 May 2023]. Available from: <https://doi.org/10.1016/j.autcon.2023.104838>
188. ZHANG, Min, KADAM, Pranav, LIU, Shan and KUO, C.-C. Jay. GSIP: Green Semantic Segmentation of Large-Scale Indoor Point Clouds. *Pattern Recognition Letters* [online]. 2022, Vol. 164, pp. 9–15 [accessed 2 May 2023]. Available from: <https://doi.org/10.1016/j.patrec.2022.10.014>

189. JABAR, Izatul laili, ISMAIL, Faridah and MUSTAFA, Arniatul Aiza. Issues in Managing Construction Phase of IBS Projects. *Procedia - Social and Behavioral Sciences* [online]. 2013, Vol. 101, pp. 81–89 [accessed 4 May 2023]. Available from: <https://doi.org/10.1016/j.sbspro.2013.07.181>
190. SARVARI, Hadi, CHAN, Daniel W. M., RAKHSHANIFAR, Mansooreh, BANAITIENE, Nerija and BANAITIS, Audrius. Evaluating the Impact of Building Information Modeling (BIM) on Mass House Building Projects. *Buildings* [online]. 2020, Vol. 10, no. 2, pp. 35 [accessed 4 May 2023]. Available from: <https://doi.org/10.3390/buildings10020035>
191. KOLAEI, Ali Zabihi, HEDAYATI, Erfan, KHANZADI, Mostafa and AMIRI, Gholamreza Ghodrati. Challenges and opportunities of augmented reality during the construction phase. *Automation in Construction* [online]. 2022, Vol. 143, pp. 104586 [accessed 4 May 2023]. Available from: <https://doi.org/10.1016/j.autcon.2022.104586>
192. TRILLO CABELLO, Antonio, MARTÍNEZ-ROJAS, María, CARRILLO-CASTRILLO, Jesús A. and RUBIO-ROMERO, Juan Carlos. Occupational accident analysis according to professionals of different construction phases using association rules. *Safety Science* [online]. 2021, Vol. 144, pp. 105457 [accessed 4 May 2023]. Available from: <https://doi.org/10.1016/j.ssci.2021.105457>
193. NICOLETTI, Vanni, AREZZO, Davide, CARBONARI, Sandro and GARA, Fabrizio. Dynamic monitoring of buildings as a diagnostic tool during construction phases. *Journal of Building Engineering* [online]. 2022, Vol. 46, pp. 103764 [accessed 4 May 2023]. Available from: <https://doi.org/10.1016/j.jobe.2021.103764>
194. BRILAKIS, Ioannis, FATHI, Habib and RASHIDI, Abbas. Progressive 3D reconstruction of infrastructure with videogrammetry. *Automation in Construction* [online]. 2011, Vol. 20, no. 7, pp. 884–895 pp. 103764 [accessed 5 May 2023]. Available from: <https://doi.org/10.1016/j.autcon.2011.03.005>
195. DAI, Fei, RASHIDI, Abbas, BRILAKIS, Ioannis and VELA, Patricio. Comparison of Image-Based and Time-of-Flight-Based Technologies for Three-Dimensional Reconstruction of Infrastructure. *Journal of Construction Engineering and Management* [online]. 2013, Vol. 139, no. 1, pp. 69–79 [accessed 5 May 2023]. Available from: [https://doi.org/10.1061/\(ASCE\)CO.1943-7862.0000565](https://doi.org/10.1061/(ASCE)CO.1943-7862.0000565)
196. VALERO, Enrique and ADÁN, Antonio. Integration of RFID with other technologies in construction. *Measurement* [online]. 2016, Vol. 94, pp. 614–620 [accessed 5 May 2023]. Available from: <https://doi.org/10.1016/j.measurement.2016.08.037>
197. ATHERINIS, Daniel, BAKOWSKI, Benjamin, VELCEK, Mathew and MOON, Sungkon. Developing and Laboratory Testing a Smart System for Automated Falsework Inspection in Construction. *Journal of Construction Engineering and Management* [online]. 2018, Vol. 144, no. 3, pp. 04017119 [accessed 5 May 2023]. Available from: [https://doi.org/10.1061/\(ASCE\)CO.1943-7862.0001439](https://doi.org/10.1061/(ASCE)CO.1943-7862.0001439)
198. DENG, Hui, HONG, Hao, LUO, Dehuan, DENG, Yichuan and SU, Cheng. Automatic Indoor Construction Process Monitoring for Tiles Based on BIM and Computer Vision. *Journal of Construction Engineering and Management* [online]. 2020, Vol. 146, no. 1, pp. 04019095 [accessed 8 May 2023]. Available from: [https://doi.org/10.1061/\(ASCE\)CO.1943-7862.0001744](https://doi.org/10.1061/(ASCE)CO.1943-7862.0001744)
199. KAVALIAUSKAS, Paulius and JURELIONIS, Andrius. 3D reality mesh utilization for BIM-based earthwork quality estimations. In: *Proceedings of 1st International Scientific Conference, Advanced Construction and Architecture* [online], 23–25 September 2020, Kaunas, Lithuania, [accessed 10 May 2023]. Available from: <https://doi.org/10.5755/e01.2669-1922.2020>

200. PARSELIUNAS, Eimuntas, BUGA, Arunas, MAROZAS, Leonardas, PETNIUNAS, Marius and URBANAS, Saulius. Litpos - A Part of EUPOS ®. Geodesy and Cartography [online]. 2008, Vol. 34, no. 2, pp. 50–57 [accessed 01 June 2023]. Available from: <https://doi.org/10.3846/1392-1541.2008.34.50-57>
201. KAVALIAUSKAS, Paulius, FERNANDEZ, Jaime B., MCGUINNESS, Kevin and JURELIONIS, Andrius. Integrating BIM and 3D Point Cloud Data for Construction Monitoring Automation. In: *3rd Baltic Conference of Young Researchers in Architecture, Landscape Architecture, Urbanism and Civil Engineering*, 24 November 2022, Kaunas, Lithuania.
202. TADDIA, Yuri, STECCHI, Francesco and PELLEGRINELLI, Alberto. Coastal Mapping Using DJI Phantom 4 RTK in Post-Processing Kinematic Mode. *Drones* [online]. 2020, Vol. 4, no. 2, pp. 9 [accessed 15 May 2023]. Available from: <https://doi.org/10.3390/drones4020009>
203. FORLANI, Gianfranco, DALL'ASTA, Elisa, DIOTRI, Fabrizio, CELLA, Umberto Morra di, RONCELLA, Riccardo and SANTISE, Marina. Quality Assessment of DSMs Produced from UAV Flights Georeferenced with On-Board RTK Positioning. *Remote Sensing* [online]. 2018, Vol. 10, no. 2, pp. 311 [accessed 15 May 2023]. Available from: <https://doi.org/10.3390/rs10020311>
204. LEWIŃSKA, Paulina, GŁOWACKI, Oskar, MOSKALIK, Mateusz and SMITH, William A.P. Evaluation of structure-from-motion for analysis of small-scale glacier dynamics. *Measurement* [online]. 2021, Vol. 168, pp. 108327 [accessed 15 May 2023]. Available from: <https://doi.org/10.1016/j.measurement.2020.108327>
205. KINGSLAND, Kaitlyn. Comparative analysis of digital photogrammetry software for cultural heritage. *Digital Applications in Archaeology and Cultural Heritage* [online]. 2020, Vol. 18, pp. e00157 [accessed 15 May 2023]. Available from: <https://doi.org/10.1016/j.daach.2020.e00157>
206. MONASH UNIVERSITY. Human injury model for small unmanned aircraft impacts. *Authority, Civil Aviation Safety* [online]. 2013, Melbourne, Australia [accessed 18 May 2023]. Available from: <https://auntypru.com/wp-content/uploads/2016/10/f164491.pdf>
207. *AAIB Bulletin: DJI Phantom 4 RTK AAIB-27058* [online]. 2021 [accessed 18 May 2023]. Available from: https://assets.publishing.service.gov.uk/media/609cf2d98fa8f56a39f36210/DJI_Phantom_4_RTK_UAS_reg_N-A_06-21.pdf
208. Commission implementing regulation (EU) 2019/947. *Official Journal of the European Union* [online]. 24 May 2019 [accessed 18 May 2023]. Available from: http://data.europa.eu/eli/reg_impl/2019/947/oj

CURRICULUM VITAE

Personal information

Paulius Kavaliauskas was born on January 20, 1983 in Kaunas, Lithuania.

Email: pa.kavaliauskas@gmail.com, pa.kavaliauskas@ktu.edu

Education:

- | | |
|-------------|---|
| 2004 – 2009 | Bachelor's degree of Civil Engineering at Kaunas University of Technology. |
| 2016 – 2018 | Master's degree of Building Construction Technology at Kaunas University of Technology. |
| 2018 – 2023 | Doctoral studies of Civil Engineering at Kaunas University of Technology. |

List of publications on the dissertation topic:

1. Kavaliauskas, Paulius; Fernandez, Jaime B; McGuinness, Kevin; Jurelionis, Andrius. Automation of Construction Progress Monitoring by Integrating 3D Point Cloud Data with an IFC-Based BIM Model // Buildings (Basel). ISSN: 2075-5309. EISSN: 2075-5309. 2022, vol. 12, No. 10, p. 1754. DOI: 10.3390/buildings12101754 [Science Citation Index Expanded (Web of Science); Scopus; Inspec].
2. Kavaliauskas, Paulius; Židanavičius, Daumantas; Jurelionis, Andrius. Geometric Accuracy of 3D Reality Mesh Utilization for BIM-Based Earthwork Quantity Estimation Workflows // ISPRS international journal of geo-information. ISSN: 2220-9964. EISSN: 2220-9964. 2021, vol. 10, No. 6, p. 399. DOI: 10.3390/ijgi10060399 [Science Citation Index Expanded (Web of Science); Scopus; GeoRef, PubAg].

List of international scientific conferences:

1. Kavaliauskas, Paulius. Integrating BIM and 3D Point Cloud Data for Construction Monitoring Automation // 3rd Baltic Conference of Young Researchers in Architecture, Landscape Architecture, 24 November 2022, Kaunas.
2. Kavaliauskas, Paulius; Jurelionis, Andrius. 3D Reality Mesh Utilization for BIM-Based Earthwork Quality Estimations // Advanced Construction and Architecture: Proceedings of the 1st international scientific conference, 23–25 September 2020, Kaunas, Lithuania. Kaunas: Technologija. ISSN: 2669-1922. 2020, p. 82. DOI: 10.5755/e01.2669-1922.2020.

ACKNOWLEDGMENT

In a work of such a scope, there was more than one person whom the author would like to thank for their contribution.

First and foremost, I would like to thank my scientific supervisor Andrius Jurelionis for introducing me to the topic of this thesis, guiding and supporting me in the development of research ideas. Andrius supported me and gave me advice during the entire process of the thesis.

Second, I would like to thank the academic partners at Dublin City University, in particular, Jaime B. Fernández, for their valuable insights and contribution in shaping and achieving the objectives of the experimental research.

I am very grateful to *UAB YIT Lietuva* for providing access to the construction facilities, technical equipment, and data necessary for this study. This significantly contributed to the practical value of the experimental research conducted in the thesis.

I would also like to thank the industrial partners *Bentley Systems* for financial support and discussions on the thesis topic. Special thanks go to David G. Robertson, Director – University Partnerships for his support and encouragement in entering this interdisciplinary topic which was new to me at the time.

Apart from my colleagues and partners from the academic and industrial environment, my parents wholeheartedly supported me throughout the dissertation process. Their support and continuous encouragement greatly contributed to this dissertation.

I especially want to thank my wife Rūta for her patience and faith in me, without which this thesis would not have been possible.

UDK 69:004.9+528.7](043.3)

SL344. 2024-03-22, 24,25 leidyb. apsk. I. Tiražas 14 egz. Užsakymas 51.
Išleido Kauno technologijos universitetas, K. Donelaičio g. 73, 44249 Kaunas
Spausdino leidyklos „Technologija“ spaustuvė, Studentų g. 54, 51424 Kaunas

